Professorship of Regenerative Energy Systems
TUM School of Engineering and Design
Technical University of Munich

Techno-Economic Assessment of H_2-based Power-to-X Plants integrated into a Pulp Mill

Doctoral Thesis

Daniel Klüh

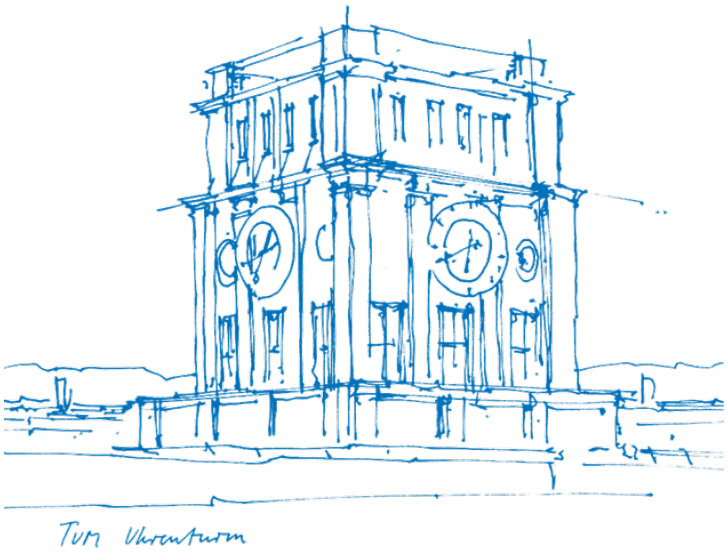

Techno-Economic Assessment of H_2-based Power-to-X Plants integrated into a Pulp Mill

Doctoral Thesis

Daniel Klüh

Technische Universität München
TUM School of Engineering and Design

Techno-Economic Assessment of H_2-based Power-to-X Plants integrated into a Pulp Mill

Daniel Martin Klüh

Vollständiger Abdruck der von der TUM School of Engineering and Design der Technischen Universität München zur Erlangung eines

Doktors der Ingenieurwssenschaften (Dr.-Ing.)

genehmigten Dissertation.

Vorsitz: Prof. Dr.-Ing. Hartmut Spliethoff

Prüfende der Dissertation:

1. Prof. Dr.-Ing. Matthias Gaderer
2. Asst. Prof. Dr. Kristian Melin
3. Prof. Dr.-Ing. Harald Klein

Die Dissertation wurde am 13.02.2024 bei der Technischen Universität München eingereicht und durch die TUM School of Engineering and Design am 28.10.2024 angenommen.

Acknowledgement

This thesis has been realized during my time as a research assistant at the Professorship of Regenerative Energy Systems at the Campus Straubing for Biotechnology and Sustainability of the Technical University of Munich for 5 years and 2 months. With the submission of the thesis, this journey comes to an end.

No money, no funny! This thesis would not have been possible without public funding by the Federal Ministry for Economic Affairs and Climate Action. Thanks to the Ministry for providing the financial means for this project.

First and foremost, I would like to express my gratitude to my doctoral advisor, Prof. Dr.-Ing. Matthias Gaderer. I would like to extend my sincere thanks to Kristian Melin, PhD for being the second examiner. Thanks also for the other collaborative work we did together and for giving me the possibility for the research stay in Finland. Thirdly, I would like to thank Prof. Dr.-Ing. Harald Klein for being the third examiner. Lastly, another thanks goes out to Prof. Dr.-Ing. Hartmut Spliethoff for presiding over the examination.

Another big thanks goes out to Zellstoff Stendal namely Knut Bader, Sabine Teucke, Frank Wegener and the other involved employees for supporting me with data for my research, insights into the pulp mill processes and laboratory analysis. The visits to the pulp mill especially during the planned maintenance stops were really inspiring seeing all the equipment from the inside. For the laboratory analysis at the university I would like to thank Marlit Köstler for assisting with the laboratory work and for performing the density measurements. Additionally, a big thank goes out to my brother for performing the adsorption and precipitation experiments.

The best office should not be unmentioned with different office mates over the years: Bernhard, Basti and Lingga. You accompanied me through this journey and made it more pleasant and fun. The good times I had with Basti and Yusheng during the many field trips to various power plants for measurements will always stay in my mind.

But the biggest thank goes out to my family and friends. You helped me a lot to also see the other things in life than my dissertation and to also enjoy other things in life. Thanks to my roommates for letting me occupy our pressboard dining table on which this thesis was mostly written. Thanks to my girlfriend for supporting me during the difficult phases.

Another thank you goes out to the brewery Phil&Eddy's who supplied me with high quality and locally produced beer. Your beer is awesome!

Publicly funded research results are meant to be available to everybody. This thesis is therefore written in English and published online. The results are meant to contribute to a more sustainable development of this world. All required information to understand and reproduced the results should be available in this thesis.
If you have any more questions, please reach out to me. You will find a way to contact me.

Abstract

A reduction of greenhouse gas emissions are necessary to reduce the impact of human greenhouse gas emissions on the climate. Renewable fuels and chemicals are needed for reducing fossil resource use and CO_2 emissions. One possible option is the utilization of biomass, CO_2 and renewable electricity as new raw materials. This thesis investigates the integration of processes into a pulp mill for the production of chemicals and fuels based on H_2 which is derived from water electrolysis. Furthermore, different processes for the supply of the lime kiln with green fuels are investigated. A process simulation software was used to generate the mass and energy balances of the investigated processes. With the data, the processes are evaluated in terms of cost, efficiency and CO_2 emissions. Special focus is on the integration with the pulp mill based on the exchange of material and energy streams. Furthermore, lab and pilot lab experiments were performed on the purification of methanol derived from the Power-to-Methanol process and the methanol containing side stream of the pulp mill.

The most promising Power-to-X product with lowest price and emissions in comparison to the fossil equivalent is hydrogen peroxide. Other promising products are methanol and acetic acid. The levelized cost are found to be 535 - 705 €t_{H2O2}, 1207 - 1500 t_{MeOH} and 1065 - 1386 t_{AA}. The integration with the pulp mill generally shows a small increase of the utilities in comparison to the processed amounts in the pulp mill. The O_2 demand of the pulp mill can be covered in almost all cases. The integration can lead to a decrease or increase of electricity generation onsite mostly depending on the effect of heat integration, process cooling and O_2 supply. Purge streams can effectively be used to decrease the fossil fuel use in the lime kiln. The CO_2 abatement cost are negative for H_2O_2 at -542 or -165 €/t CO_2 for the 50 and 150 MW_{el} plant. The abatement cost of acetic acid and methanol (50 MW_{el} plant) are in the range of 300 to 400 €/t CO_2. The highest abatement cost above 1000 €/t CO_2 are found for some FT processes and SNG for the 50 MW_{el} plants. The increase in pulp selling price for enumeration of the PtX products with market prices leads to an increase of the pulp price of roughly -120 to almost 200 €/ADt.

The decarbonization and defossilization of the lime kiln is investigated for 10 different cases utilizing biomass, CO_2 or H_2 for the production of the fuel for the lime kiln. The H_2 based routes show the tremendously higher cost than the biomass based routes. The available biomass should be used in the lime kiln for the substitution of fossil fuels instead of being burnt for electricity production. The impact on the pulp selling price is in the range of 9 to 165 €/ADt. The milled wood combustion and combustion of producer gas from air blown biomass gasification are in terms of economics and emissions the most promising options with abatement cost of 46 €/t CO_2 and 179 €/t CO_2.

The combined purification of methanol allows the valorization of the available methanol stream in the pulp mill together with the methanol stream from a Power-to-Methanol plant. Simulations confirm that a combined purification is possible for larger Power-to-Methanol plants without prepurification. For smaller plant sized a prepurification is necessary to reach the required purities. The rectification experiments cannot confirm the results obtained by simulation. Experiments on the selective removal of sulphur or nitrogen compounds with activated carbon or the precipitation with Fe(II) ions from the methanol stream derived from the pulping process is possible but most likely not economical.

The results show that pulp mills are good sites for the integration of the investigated routes which is due to the availability of green electricity and biomass, and due to the available low carbon infrastructure. However, the assessment is site specific and has to be assessed for every pulp mill in detail. Especially the choice of the type of process needs to be tailored for every pulp mill.

Key words: Pulp mill, Techno-economic assessment, Power-to-X, Hydrogen, Renewable fuels and chemicals, CO_2 capture, biomass gasification, decarbonization, lime kiln

Abbreviations

AA	Acetic acid
AC	Activated carbon
ADt	Air dried ton
AEL	Alkaline electrolyser
AEMEL	Anion exchange membrane electrolyser
AFT	Adiabatic flame temperature
AHQ	Anthrahydroquinone
AQ	Anthraquinone
ASF	Anderson-Schulz-Flory
B	Bottom product
BC	Base case
BLG	Black liquor gasification
CAPEX	Capital expenditures
CCU	Carbon capture and utilisation
CCS	Carbon capture and storage
CE	Carbon efficiency
CEPCI	Chemical engineering plant index
CL	Closed loop
CO_2 AC	CO_2 abatement cost
D	Distillate (Top product)
DME	Dimethyl ether
DMS	Dimethyl sulfide
FC	Foul condensate
FO	Fuel oil
FT	Fischer Tropsch
GHG	Greenhouse gas
HE	Hydrogen efficiency
HP	High pressure
HTFT	High temperature Fischer Tropsch
IGCC	Integrated gasification combined cycle
KPI	Key performance indicator
LTFT	Low temperature Fischer Tropsch
LP	Low pressure
MEA	Monoethanolamine
MeOH	Methanol
MP	Medium pressure
N	Nitrogen
NCG	Non condensable gas
NG	Natural gas
NGCC	Natural gas combined cycle
NRTL	Non random two liquid

ODT	Oven dry ton
OL	Open loop
OPEX	Operating expenditures
PEMEL	Polymer electrolyte membrane electrolyser
PG	Producer gas
P&ID	Process and instrumentation diagram
PSA	Pressure swing adsorption
PtMeOH	Power-to-Methanol
PtX	Power-to-X
RWGS	Reverse water gas shift
S	Sulphur
SG	Syngas
SNG	Synthetic natural gas
SOEL	Solide oxide electrolyser
SOG	Stripper off gas
TRL	Technology readiness level
VLE	Vapor liquid equilibrium
W	Wood residues

List of Symbols

Variable	Description	Typical unit
α	Chain growth probability	%
ACC	Annualized capital cost	M€/a
AF	Annuity factor	-
β	Selectivity exponential parameter	-
$\dot{B}$	Bottom product mass flow	kg/h
C	Cost	€/MWh or €/t
c	Concentration	mol/l or bar/bar
c_p	Isobaric specific heat capacity	J kg^{-1} K^{-1}
$\dot{D}$	Distillate mass flow	kg/h
D:F	Distillate to feed ratio	kg/kg or mol/mol
E	Plate efficiency	%
e	Annual emissions	t CO_2/a
ΔE_α	Selectivity activation energy difference	J mol^{-1}
EF	Emission factor	kg CO_2/MWh or t CO_2/t
$\dot{F}$	Feed mass flow	kg/h
FCI	Fixed capital investment	M€
FL	Flame length	m
H	Enthalpy	J
h	Enthalpy / Height	kJ/kg / m
HETP	Height equivalent to a theoretical plate	m
HR	Heat rate	GJ/t CaO
IR	Interest rate	%
IPP	Increase in pulp price	€/ADt
k_α	Selectivity constant	-
k_D	Rate constant	kmol m^{-2} c^{-1} atm^{-1}
$\dot{L}$	Liquid mass flow	kg/h
LCOP	Levelized cost of product (also with product names)	€/t or €/MWh
LHV	Lower heating value	MJ/kg
$\dot{m}$	Mass flow	kg/h
N_{np}	Number of nonparticulate processing steps	-
N_{OL}	Number of operators per shift	-
n	Number of plates/carbon atoms	-
OPEX	Operating expenditures	M€/a
Δp	Pressure difference	mbar
PL	Plant life time	a
P	Power	MW_{el} or MW_{th}

Variable	Description	Typical unit
P_e	Equilibrium dissociation pressure	atm
q	Liquid mole fraction of feed	mol %
R	Gas constant	J mol^{-1} K^{-1}
R_D	Reaction rate	kmol m^{-2} s^{-1}
R_L	Reflux ratio	kg/kg
S	Capacity / Size	kW, m, m^2
T	Temperature	K or °C
TAC	Total annual cost	M€/a
$\dot{V}$	Vapor mass flow	kg/h
W	Work	MW
w	Mass fraction	wt. %
x	Mole fraction in liquid	mol %
y	Mole fraction in vapor	mol %

Contents

List of Figures

List of Tables

1 Introduction

The reduction of greenhouse gas (GHG) emissions is an important task to limit climate change and its harmful impact on the Earth. Leaders, organizations and governments call for action to cut GHG emissions. However, not much progress is made so far. Figure 1.1 shows the annual change of GHG emissions in the world. Obviously, GHG emissions are increasing for most years. The most effective instruments capable of reducing emissions in the last years are pandemics (in 2020) and economic crisis like the on in 2009. Not included are other factors influencing the GHG emissions like the increasing population or the change in living standards.

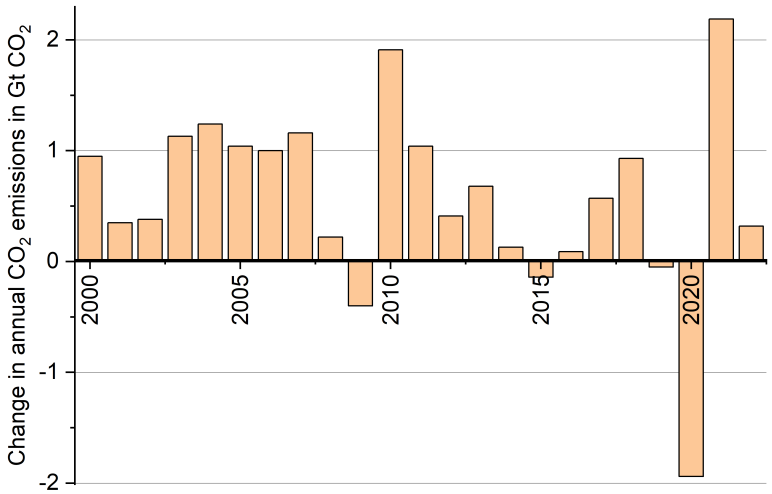

Figure 1.1 Worldwide change in annual GHG emissions from energy combustion and industrial processes [1]

The most important GHG is CO_2 which derives from the combustion of fossil carbonaceous resources. Therefore, defossilization, meaning the replacement of fossil resources by renewable ones, is one important measure to lower the GHG emissions of our energy system. The consequence of defossilization is the decarbonization which means the reduction of GHG emissions. Both concepts are closely related. For both concepts Power-to-X (PtX) technologies are a possible measure to reach a decarbonized and defossilized energy system. In this thesis, PtX is used to describe a process that converts electricity to hydrogen (H_2) in a first step. In a following conversion step, H_2 is converted into a fuel or chemical. The major raw materials for the processes are electricity from renewable sources and CO_2 as carbon source if needed. The replacement of fossil fuels and chemicals with sustainably produced PtX products enables the decarbonization of sectors like transportation or chemical industry.

Integrating the production of chemicals with pulp mills has been investigated already for more processes than PtX. In 1995, different processes were investigated for the integration with a pulp mill [3]. The production of sulfuric acid in pulp mills is an established and commercially available process for the utilization in pulp mills. Furthermore, recovering the available methanol stream is also an established technology. The production of chemicals and fuels via the Power-to-X routes are extensively investigated. However, the integration with pulp mills is a rather new idea and was first investigated by Jannasch et al. [4]. Further concepts of the integration are described for Fischer Tropsch syncrude [5] or methanol [6].

In this thesis, the focus is on the in-depth analysis of integrating the production routes in an exemplary pulp mill. Stay tuned if you want to know why such Power-to-X plants are a perfect match for being integrated into a pulp mill.

1.1 Benefits of integrating Power-to-X plants in pulp mills

The motivation for integrating PtX plants in pulp mills are briefly teasered here. The integration provides environmental, economical and technical benefits. Most of the named points are valid for both, integrated (pulp production integrated with paper production) and non-integrated pulp mills. However, integrated pulp mills might suffer from a lower availability of heat and electricity meaning that additional energy needs to be imported. The following list highlights some key aspects illustrating that pulp mills are beneficial sites for PtX plant:

- Steadily available green electricity:
  A non-integrated pulp mill is a net electricity exporter. All the electricity is produced by steam generated in the bark and recovery boiler. Thus, the electricity has a very low carbon footprint if biomass is supplied from a sustainably managed source. The low carbon electricity is also constantly available making it possible to reach high full load hours of the electrolysis which improves the economics of this process.

- Availability of biogenic CO_2:
  The CO_2 released by combustion of biomass in the recovery boiler and the bark boiler, and the process related CO_2 emissions from the lime kiln are of biogenic origin. The origin of energy related CO_2 emissions in the lime kiln depend on the used fuel. Pulp mills are very large point sources for biogenic CO_2 present in the flue gases. The utilization of biogenic CO_2 as feedstock compared to fossil CO_2 offers the benefit of closing the carbon cycle. The CO_2 which was fixed by the tree and released during combustion in the pulp mill is converted into a fuel or chemical which will eventually be released as CO_2 to the atmosphere from which it was fixed before during the tree growth. Pulp mills are large point sources for biogenic CO_2 which can be exploited. Other point sources for biogenic CO_2 are generally smaller like for example wood fired power plants, biogas plants or waste incineration plants.

- Combustion of purge streams in the lime kiln:
  All PtX processes with recycle stream need a purge stream to avoid the accumulation of impurities in the system. The purge stream contains combustable gases that can be used in the lime kiln to substitute fossil fuels. Furthermore, concepts dedicated to the production of fuels and chemical at the same time as supplying combustible gases to the lime kiln can be developed.

- Onsite utilization of O_2 from electrolysis:
  In a pulp mill O_2 is needed for pulp bleaching. Therefore, the O_2 produced in the electrolysis can be used onsite. Surplus O_2 can be sold, mixed with the combustion air for the incineration processes or used in the waste water treatment plant.

- Onsite utilization of Power-to-X products:
  Hydrogen peroxide is used in pulp bleaching. If produced onsite, it can be used directly without further purification saving cost and energy in the purification step. Furthermore, methanol is needed for the production of ClO_2 (bleaching agent in the pulp mill). With these two PtX products, the pulp mill can increase its self-sufficiency.

- Heat integration:
  PtX plants are chemical plants that need utilities for operation. One purpose of utilities is to provide heating or cooling to process steps. The heating and cooling demand of the PtX plant can be coupled with the pulp mills steam system to either produce more valuable steam for electricity generation or to receive steam with low carbon emissions from the pulp mill.

– Methanol:
  Methanol is already produced as by-product in pulp mills. This methanol stream can be integrated in a Power-to-Methanol plant. In most mills, this methanol stream is currently not explicitly valorized for sale. Therefore, an investment in a PtMeOH plant would also be able to recover the unused methanol stream.

Besides these aspects, one could think of more beneficial points for the integration like necessary infrastructure (for example waste water treatment plant, fire brigade, ...). Therefore, compared to greenfield or integration with other types of industries, as for example cement, chemicals or paper, pulp mills are superior for integration as they are sites with a low carbon infrastructure readily available for the integration of a PtX plant.

1.2 Aim and objective of this thesis

The thesis investigates various pulp mill integrated PtX processes and also biomass based routes to reduce GHG emissions and produce sustainable fuels and chemicals. The processes are integrated into the pulp mill by connecting the mass and energy flows of the PtX plant with the pulp mill.

The first part is concerned with the simulation and integration of H_2 based production processes towards fuels or chemicals. With the generated mass and energy balances, the processes are evaluated based on technical, economic and environmental parameters. The second part focuses on the decarbonization of the lime kiln by the utilization of waste biomass available from the pulp mill and electricity for H_2 production which can be further converted to fuels. The processes are simulated to gain mass and energy balances. Based on the data, the process options are compared with technical, economic and environmental parameters. Thirdly, the combined purification of methanol from CO_2 hydrogenation and methanol as by-product from the pulping process is experimentally investigated in the lab and pilot lab with suitable experimental setups. The experiments are carried out with real samples from the pulp mill to validate the models of the process simulation. Besides rectification, adsorption with activated carbon is used to remove impurities from the methanol stream.

1.3 Thesis outline

The thesis is divided into 8 Chapters. Chapter 2 describes the technology background and introduces the reader to the most important concepts and technologies touched upon in the later parts. Major topics are the production of H_2, CO_2 capture, and processes for the production of fuels and chemicals based on H_2. Additionally, pulp production and other production routes of fuels and chemicals in pulp mills are discussed. In Chapter 3, the tools and methods used for evaluating the processes are described including environmental, economic and technical assessment, and modeling tools. Chapter 4 deals with the process simulations for different production routes of chemicals and fuels. Based on the process models, the paths are assessed in terms of economic, environmental and technical performance, and integration with the pulp mill. Furthermore, the routes are compared with each other. Chapter 5 is concerned with the decarbonization and defossilization of the lime kiln. Different fuels for supplying heat to the lime kiln are modeled and assessed. Based on process simulations, the concepts are evaluated to find the most cost efficient and environmentally friendly solution. The purification of methanol is presented in Chapter 6. The results are based on experimental as well as simulation work. The goal is to find the optimal integration of the foul condensate stream from the pulp mill with a Power-to-Methanol plant. Chapter 7 comprises the discussion on the applicability of the presented concepts to other type of pulp mills and industries. In the conclusion (Chapter 8), the results are summarized on a higher level assessing the overarching picture of integrating Power-to-X processes in pulp mills.

2 Technology background and literature review

This chapter reviews the state of technology and introduces the reader to the relevant concepts and knowledge needed for understanding the following chapters.

2.1 Pulp production

Pulp mills based on the sulphate process will be the focus of this thesis. The other relevant process for chemical pulp production is the sulphite process. Due to the importance of sulphite pulp mills in Germany, the tranferability of the concepts for sulphate pulp mills towards sulphite pulp mills are discussed in 7.1. Sulphite pulp mills account for less than 6 % of the total chemical pulp production in Europe (2020) [7]. However, the role of sulphite pulp mills is more important in Germany (see Table 7.1). Sulphate pulp has the benefit of producing stronger pulp compared to sulphite pulp [8]. Furthermore, the regeneration of energy and chemicals is more efficient [8]. The wood species that can be used for sulphite pulping are limited [8].

Figure 2.1 shows the processes flow diagram of the sulphate process which consists of two chemical recycling loops: for sodium and for calcium. The first step is wood debarking. After chipping, the wood chips are fed into the digester where they are impregnated with steam. After that the cooking liquor is added. The cooking process can either be a continous or a batch process. After cooking, pulp and black liquor are separated. The pulp is screened, washed, bleached, dried and finally packaged in case of a stand alone mill. The water content of black liquor is reduced in the evaporation plant. In the recovery boiler, the black liquor is combusted to generate energy for the facilities and to recover the pulping chemicals. The pulping chemicals accumulate as smelt at the bottom of the boiler. The smelt is contacted with water and yields the green liquor.

The second chemical recycling loop is concerned with the calcium recycle. In the lime kiln, calcium carbonate is reacted under high temperature to calcium oxide and CO_2 as depicted in Equation 2.1.

$$CaCO_3 \longrightarrow CaO + CO_2 \tag{2.1}$$

In the caustification step, CaO is reacted to calcium hydroxide as shown in the following equation:

$$CaO + H_2O \longrightarrow Ca(OH)_2 \tag{2.2}$$

The calcium hydroxide is mixed with the green liquor and undergoes the reaction as shown in Equation 2.3. After filtration, the solids are returned to the lime kiln, while the solution is transformed into what is referred to as white liquor. The white liquor is ready for use in the cooking process again.

$$Ca(OH)_2 + Na_2CO_3 \longrightarrow CaCO_3 + 2\,NaOH \tag{2.3}$$

Aside from the lime kiln, there are two other primary sources of CO_2 in a pulp mill: the recovery boiler and the bark boiler. Since the lime kiln is typically powered by fossil fuels, such as natural gas, it stands as the sole source of fossil CO_2 emissions within a pulp mill.

The processes in sulphite pulp mills are similar to the ones in the sulphate pulp mill. The major difference is the use of an acidic bisulphite cooking solution based on MgO and SO_2 and a single recycle loop for pulping chemicals so that no additional equipment like lime kiln are necessary. Figure A.2 in the Appendix shows the process flow diagram of the sulphite pulping process.

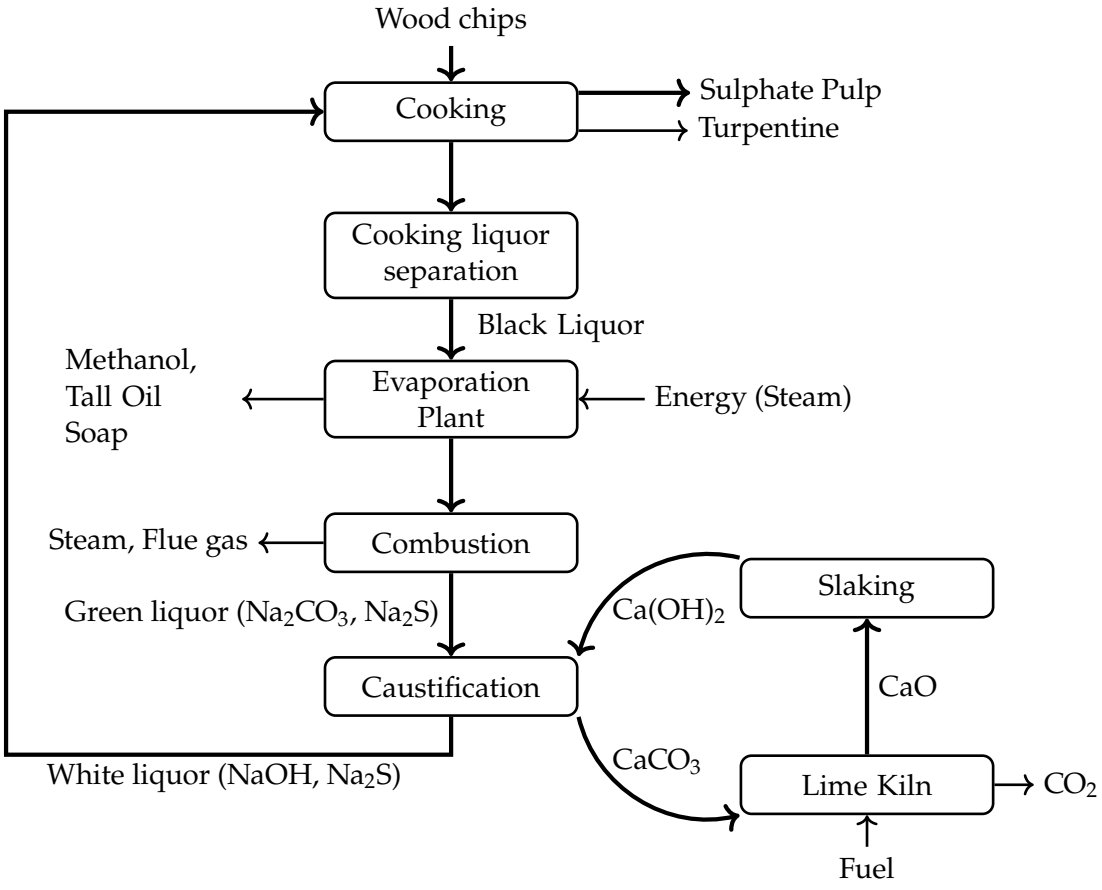

Figure 2.1 Flow diagram of the sulphate pulping process with two cycles for chemical recycling [9]

2.1.1 Methanol from pulping

Volatile organic compounds released during the cooking process are a side stream collected in the evaporation plant. It contains several components like alcohols (methanol), acids (formic acid, acetic acid), ketones (acetone), terpenes (α-pinene, β-pinene) and sulphur containing compounds (dimethyl sulfide, dimethyl disulfide) [10]. In the evaporation plant, methanol (MeOH) which is produced during the cooking process is separated together with water and other volatile compounds from the black liquor. The light volatile components are collected as foul condensate (FC) and are usually stripped yielding stripper off gases (SOG). MeOH formation in hardwood pulp mills (up to 15 kg/ODT pulp) is usually higher than in softwood pulp mills (7.3 kg/ODT pulp) [11].

The majority of MeOH is formed by demethylation of xylan. A smaller share is produced by demethylation of lignin. Both reaction need hydroxyl ions. The reaction mechanism is a bimolecular nucleophilic substitution S_N2 [12]. The following reaction shows the demethylation of a methoxyl group as occurring during the cooking process.

$$R{-}OCH_3 + NaOH \longrightarrow CH_3OH + R{-}ONa \tag{2.4}$$

2.1.2 Alternative fuels in lime kiln

The rotary lime kiln of a sulphate pulp mill converts calcium carbonate into calcium oxide according to Equation 2.1. The process is endothermic and requires high temperatures. The heat rate required in the lime kiln is between 5 and 8 GJ/t CaO [13]. Lime kilns are in most pulp mills the last source for fossil CO_2 if fossil fuels are burnt in the kiln. In a worldwide survey, 36 % and 33 % of the lime kilns are fired with natural gas or fuel oil [13].

Ideas to use renewable fuels substituting fossil fuels in the lime kiln are discussed in literature [14, 15, 16]. Potential biofuels are evaluated for cofiring [17]. The main drivers to use alternative fuels are lower energy cost and the utilization of renewable energy sources [13]. Furthermore, the goal to reduce fossil CO_2 emissions can be reached. In the following list major green fuels are discussed. One major difficulty with biomass based fuels is the introduction of non-process elements to the calcium loop. Non-process elements cause problems in the lime kiln and other parts of the pulp mill [18]. A higher purge stream in the calcium loop can reduce the load of non-process elements. Alternative fuels do also influence the thermal energy requirement of the lime kiln leading to a higher or lower thermal power input to the lime kiln [17].

- Producer gas:
  Biomass is gasified with air in a circulating fluidized bed gasifier to yield a syngas with lower heating value (3 - 12 MJ/kg) compared to natural gas [14, 15]. Therefore, a higher mass flow is required to supply the amount of heat needed leading possibly to overloading of the flue gas treatment system and to higher flow velocities in the kiln causing dusting [14]. Additionally, non-process elements are introduced to the lime cycle [14]. However, most non-process elements are separated with ash from the gasifier and in the dust collection system after the lime kiln consequently not causing substantial problems [15, 19]. Taillon et al. provide a detailed process description of an air-blown gasification unit for lime kiln supply [19].

- Pulverized wood:
  Biomass is dried to a moisture content of 5-8 % before grinding [20]. The powder (size: 1-3 mm) is fed to the kiln with a special powder burner [15, 20]. Non-process elements are more challenging in pulverized wood combustion than in producer gas combustion as all non-process elements are directly introduced to the lime kiln [15].

- H_2:
  H_2 can be produced via water electrolysis. According to the opinion from the industry and based on a withdrawn patent, the maximum amount of H_2 addition to the lime kiln should not

exceed 50 % of the required thermal energy [21]. H_2 co-firing can be easily implemented and is already performed in lime kilns at Stora Enso Oulu, Finland and UPM Fray Bentos, Uruguay [15].

- MeOH:
  MeOH is a by-product of the pulping process that can be recovered as described in 2.8.1. Since the available amount is limited, MeOH can only cover 10 - 15 % of the fuel input to the lime kiln [16].
- Lignin:
  Lignin can be separated from black liquor as discussed in section 2.8.2. The combustion of lignin has been demonstrated in pilot and commercial scale for 100 % lignin as fuel [16].
- Bio-coal or bio-char:
  Solid fuel derived from biomass can be produced by a variety of processes like torrefaction, hydrothermal carbonization or pyrolysis [15].
- Bio-oil:
  Bio-oils (for example: vegetable oil, animal fat, glycerin or pyrolysis oil) are already used in lime kilns [15].
- Turpentine:
  Turpentine is collected in the condensate at the evaporator plant together with MeOH. Turpentine is fired at some lime kilns and can account for roughly 10 % of the thermal energy requirement [16].
- Biomethane:
  Imported or onsite produced biomethane (for example from sludge treatment) can be used similarly to natural gas [22, 23, 24].

Kuparinen and Vakkilainen investigated the influence of alternative fuels (H_2, producer gas, torrified biomass, lignin and pulverized wood) from a system level [25]. The sensitivity of the biomass based concepts on electricity price is very low and shows breakeven prices for replacing fossil fuels of below 25 $/MWh [25]. For H_2, the breakeven price is extremely sensitive to the electricity price [25].

The lime kiln can also be replaced completely by an electrically driven plasma calcination process. This technology is offered by LimeArc Process AB [26]. In the calcination reactor, the lime is contacted with a CO_2 based plasma [27]. For electricity prices below 42 or 53 €/MWh, the plasma based process is more cost efficient than the conventional process. The process allows for the capture of biogenic CO_2 leading to capture cost between 36 and 60 €/t CO_2.

2.2 Rectification

This section is based on standard text books as for example [28] or [29]. Figure 2.2 shows a sketch of a continuous rectification column. The feed F enters the column on a defined height of the column. It can have various thermodynamic states (liquid, partial vapor, superheated vapor, ...). The column internals can be differentiated into trays (plates), structured packing or random packing. The top product is called distillate D. The stream from the bottom is called bottom product B. The section above the feed is called rectifying section. The part below the feed is called stripping section.

2.2.1 Mass balance and McCabe-Thiele-diagram

The following derivations and methods apply only for two component mixtures. The overall mass balance of the column is depicted in the following equation:

$$\dot{F} = \dot{D} + \dot{B} \tag{2.5}$$

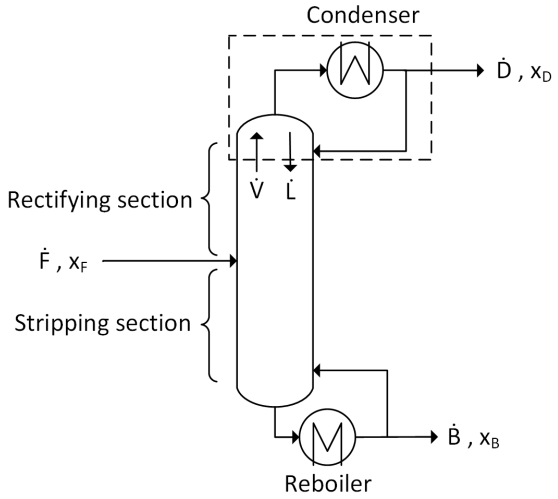

Figure 2.2 Sketch of a continuously working rectification column with mass balance around the head of the column as dashed line

For one component the mass balance can be expressed with the mass fractions of the component in the streams.

$$\dot{F}x_F = \dot{D}x_D + \dot{B}x_B \tag{2.6}$$

The mass balance on the column head is shown in Equation 2.7. The control volume is depicted in Figure 2.2 as dashed line. The mass flow of the rising vapor $\dot{V}$ is equal to the mass flow of distillate $\dot{D}$ and liquid flow $\dot{L}$.

$$\dot{V} = \dot{D} + \dot{L} \tag{2.7}$$

The mass balance can be again expressed for one component by using the mass fraction in the liquid or gas phase:

$$\dot{V}y = \dot{D}x_D + \dot{L}x \tag{2.8}$$

Substituting $\dot{V}$ in Equation 2.8 with Equation 2.7 and defining the reflux ratio (R_L) as shown in Equation 2.10 gives the following equation:

$$y = \frac{x_D}{R_L + 1} + \frac{R_L}{R_L + 1}x \tag{2.9}$$

Equation 2.9 is the operating line of the rectifying section. This equation is a linear function that can be plotted in a x-y diagram. The slope is $\frac{R_L}{R_L+1}$ and the intercept with the y axis is $\frac{x_D}{R_L+1}$. When altering the reflux ratio, the slope and the y axis interception of the operating line is changed. For $x = x_D$, the equation gives y = x. Therefore, the line intercepts with the diagonal in the x-y diagram at $x = x_D$. With a similar approach, you can derive the equation of the stripping section which will be a linear function as well.

Together with the operating line of the stripping section, one can construct the McCabe-Thiele-diagram (Figure 2.3). The q-line is then constructed with the intersection of the operating lines and the point on the diagonal based on the feed composition. The slope of the q line depends on the state of the feed. The slope of the q-line is $\frac{q}{q-1}$ where q is the liquid mole fraction of the feed. For such a design case, the feed state must be changed to fit the constructed feed line which is determined by the operating lines. From the McCabe-Thiele-diagram it is possible to graphically determine the reflux ratio and number of stages which is used for designing a rectification column.

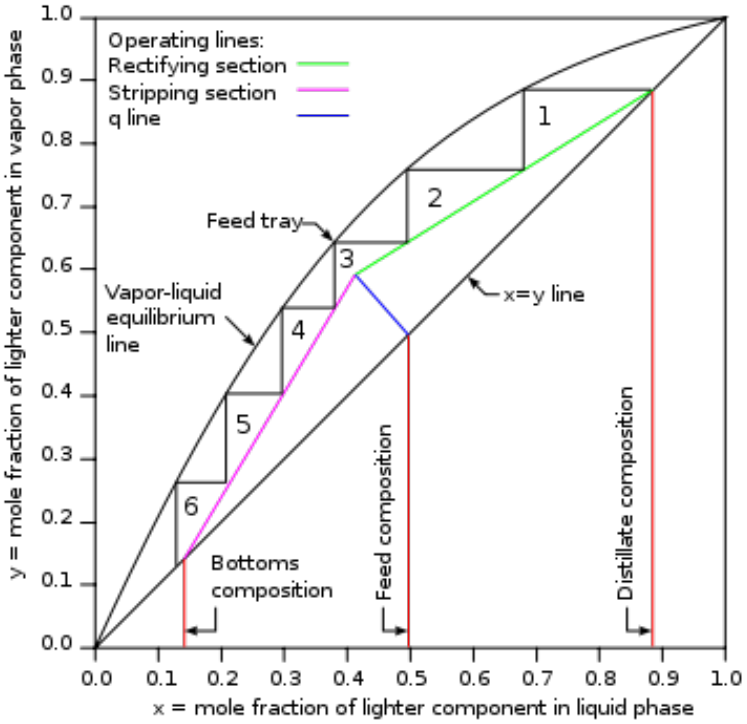

Figure 2.3 McCabe Thiele diagram [30]

2.2.2 Reflux ratio

The reflux ratio (R_L) is defined as the ratio of the stream which is sent back to the column ($\dot{L}$) and which is withdrawn from the system ($\dot{D}$). The R_L can be calculated in terms of mass or molar flow. The following equation describes the R_L:

$$R_L = \frac{\dot{L}}{\dot{D}} \tag{2.10}$$

If almost no distillate is withdrawn, the reflux ratio approaches infinite according to Equation 2.10. The minimum reflux ratio (R_{min}) can be calculated from the McCabe-Thiele-diagram (Figure 2.3). For that, the operating line of the rectifying section is constructed going through two points. The first point is the intersection of the q-line with the x-y-diagram. The second point is the point of distillate concentration on the diagonal. The operating line will show a vapor phase concentration y^*. The real reflux ratio should be 1.1 to 1.3 fold of R_{min} to account for errors in VLE data and to ensure a cost optimal operation (investment cost vs. operating cost).

$$R_{min} = \frac{x_D}{y^*} - 1 \tag{2.11}$$

2.2.3 Distillate to feed ratio

The distillate to feed ratio describes how much distillate is received from the column top in comparison to the feed stream (Equation 2.12). The desired ratio depends on the column settings as well as the concentrations of components in feed and the intended concentration in the top and bottom products.

$$D : F = \frac{\dot{D}}{\dot{F}} \tag{2.12}$$

2.2.4 Number of stages

The number of stages (plates) influences the purity of the product significantly. For larger numbers of stages, the purity of the product increases. Disadvantage of a higher number of plates is the increased column height and investment cost. For columns with plates, the number of stages can obviously be described easily by the number of plates. In packed column the number stages depends on operating parameters like concentration profile and pressure drop in the column.

Since the mixture will not reach equilibrium in a real column on a certain stage, the number of actual (physical) stages is higher than the number of theoretical stages. The number of theoretical stages can be derived from calculation. In order to describe the discrepancy between the actual number of stages n_a and theoretical number of stages n_{th}, the plate efficiency E is introduced.

$$E = \frac{n_{th}}{n_a} \tag{2.13}$$

For packed columns, the height equivalent to a theoretical plate (HETP) is defined. The HETP describes the height of a plate if the packing would be converted into plates. It is calculated as following:

$$HETP = \frac{h}{n_{th}} \tag{2.14}$$

h is the height of the packing and n_{th} is the number of theoretical plates. The number of theoretical plates can be calculated with the knowledge of the type of packing and operating parameters. Low values of HETP indicate an efficient separation since more theoretical stages can be comprised in a smaller height.

2.3 Adsorption

Adsorption describes the selective bond of a compound from a gaseous or liquid phase onto a solid adsorbent. Adsorption can be reversed (Desorption). The adsorption is exothermic and the desorption is endothermic therefore being favored by higher temperatures [31]. There are two types of adsorption: physisorption and chemisorption. In chemisorption, the adsorption is very selective and the desorption is irreversible [31]. The adsorptive (molecules interacting with the adsorbent) is chemically bound to the surface [31]. In physisorption, the weak bond between adsorbent and adsorptive is based on dipole-dipole interactions [31].

Activated carbon (AC) is a widely used adsorbent in technical purification processes. AC is a solid porous material containing more than 90 % carbon [32]. It is derived from carbonaceous material (coal, char, charcoal) either by high temperature oxidation with steam or by low temperature chemical dehydration [33, 32].

The technical realization of a continuous liquid-phase adsorption process is shown in Figure 2.4. In the reaction vessel, the liquid is stirred with the adsorbent. Usually, 1 to 2 hours of mixing are sufficient to reach equilibrium [33]. The mixture is pumped to a filter in which the solid phase containing the impurity is separated from the liquid. The process can be operated as batch or semi-batch process. Activated carbon as adsorbent can be reused after regeneration. Regeneration targets the removal of adsorbed materials on the activated carbon by thermal treatment like in a furnace without oxidizing the carbon [33].

2.3.1 Adsorption of typical species in pulp mill effluents and cleaning of pulp mill effluents

The adsorption of sulphur compounds with AC is an established technology as for example for liquid hydrocarbon fuels [35]. The following section summarizes the work in the field of purifying pulp mill effluents and adjacent topics like the adsorption of species present in pulp mill effluents (H_2S, methyl mercaptan, ...).

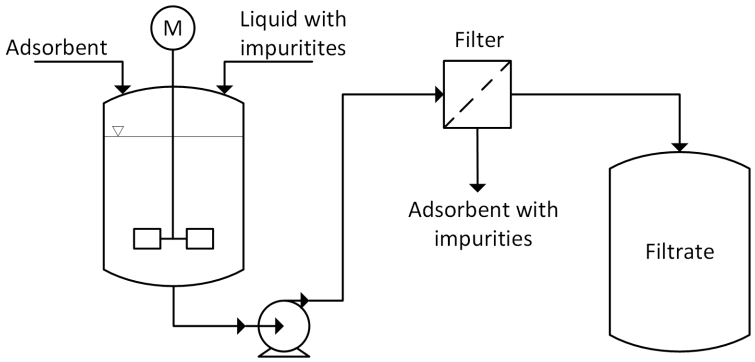

Figure 2.4 Process flow diagram of a process for adsorption from a liquid phase [34]

Studies on the adsorption of compounds contained in the SOG are available. Nguyen and Lee investigated the removal of dimethyl sulfide (DMS) from an aqueous solution of low concentration (max. 0.05 mg/l) by varying reaction time, adsorbent dosage of AC and initial DMS concentration [36]. The adsorption process is better described by the Freundlich isotherm [36]. Bashkova et al. investigated the adsorption of methyl mercaptan and the oxidation product dimethyl disulfide on different AC [37].

Gamelas et al. used AC for the removal of sulfur compounds from stripped condensate of a pulp mill with the goal of reusing the condensate as process water [38]. They found the reduction of most components to proceed very quickly. The process follows a pseudo-second-order kinetics and Langmuir adsorption isotherm. Mollaei et al. investigated the adsorption of S^{2-} ions from black liquor on AC [39]. They found a higher adsorption capacity for S^{2-} ions for lower pH values on AC. Zhang et al. investigates the removal of organic pollutants from acidic bleach plant effluents with AC or polymer resins [40]. Tao et al. experimentally assessed the removal of MeOH from a gas streams with AC [41]. AC is also established for the removal of hydrogensulfide from gas streams in gas cleaning [42].

2.4 Hydrogen production

H_2 can be produced from fossil or renewable resources. 77 % of H_2 is produced from petrochemicals, 18 % from coal and 4 % from electrolysis [43]. Established technologies based on fossil feedstock are gasification, steam methane reforming, partial oxidation, autothermal reforming and pyrolysis [44]. 48 % of H_2 is produced by steam methane reforming of natural gas (2015) [45]. In this process methane and water are passed through tubes filled with catalyst and react to CO and H_2 in an endothermic reaction (see Equation 2.15) [46]. The tubes are heated in a furnace by the combustion of fuel to above 1000 K [46]. H_2 is then purified by pressure swing adsorption [43]. The efficiency of the process is between 70 and 85 % [45]. H_2 prices are estimated to be 2.2 \$/kg in Europe for steam methane reforming [45].

$$CH_4 + H_2O \longrightarrow 3\,H_2 + CO \tag{2.15}$$

Renewable resources for H_2 production are water (electrolysis, thermolysis, photoelectrolysis, biophotolysis) and biomass (biological, thermochemical) [44]. Probably the most mature method for biomass based routes is the gasification of biomass with subsequent separation of H_2 from the syngas. Lowest prices for H_2 from biomass gasification can reach 2.7 €/kg [47]. The predominate method for H_2 production in this thesis is the electrochemical splitting of water also called water electrolysis. Equation 2.16 shows the basic equation for the production of H_2 and O_2 from water.

$$2\,H_2O \longrightarrow 2\,H_2 + O_2 \tag{2.16}$$

The four types of water electrolysers are polymer electrolyte membrane (PEMEL), alkaline (AEL), anion exchange membrane (AEMEL) and solid oxide electrolyzer (SOEL). The first two are commer-

cialized whereas the other two are still in lab scale [48]. Nevertheless, multiple companies are in the process of commercializing the SOEL technology (for example Sunfire GmbH or Topsoe A/S).

Typical characteristics of the electrolyzers are summarized in Table 2.1. Investment cost are expected to drop significantly once the production is standardized and scaled-up [48]. The investment cost for AEL, PEMEL and AEMEL are expected to drop below 200 $/kW in 2050 [48]. The investment cost for SOEL are projected to drop to below 300 $/kW [48]. Additionally, the system efficiency is expected to rise tremendously till 2050. The SOEL show nowadays the highest efficiency. Efficiencies of AEL and PEMEL are comparable. For AEL, PEMEL and AEMEL the efficiency is expected to be above 74 % and for SOEL above 83 % in future [48]. The life time of PEMEL and AEL are comparable. The life time of SOEL is lower and more uncertain due to the limited operational experience and lower TRL. One drawback of SOEL is that currently the pressurized operation is not possible making it necessary to compress the H_2 to the operating pressure of the chemical synthesis.

Table 2.1 Characteristics of electrolyser technologies

	AEL	PEMEL	AEMEL	SOEL	Source
operating temperature (°C)	70 - 90	50 - 80	40 -60	700 - 850	[48]
operating pressure (bar)	1-30	<70	<35	1	[48]
load flexibility (% of nominal load)	20 - 100	0 - 100	-	-100 / +100	[49]
system efficiency based on LHV (%)	43 - 67	40 - 67	48 - 59	61 - 74	[48]
life time (kh)	55 - 120	60 - 100	-	8 - 20	[49]
investment cost (€/kW)	800 - 1500	1400 - 2100	-	>2000	[49]
($/kW)	500 - 1000	700 - 1400	-	-	[48]
maintenance cost (% of invest. cost per year)	2 - 3	3 - 5	-	-	[49]

2.5 CO_2 capture

Carbon capture is a key technology for carbon capture and utilization (CCU) or storage (CCS). The utilization and storage of CO_2 requires a pure CO_2 stream. Currently, there are three main process types available to capture CO_2.

2.5.1 Post combustion capture

In post combustion processes, the CO_2 is separated from flue gases or industrial off gases. The processes can be categorized into adsorption, absorption, cryogenic and membrane based processes [50, 51]. For gas streams with CO_2 concentrations below 10 %, amine absorption processes are more energetically favorable compared to membrane processes [52]. Membrane processes can become competitive at CO_2 concentrations above 20 % [52]. According to Zhang et al., the chemical absorption process is more cost effective for CO_2 concentrations in the feed gas below 30 % compared to hybrid and physical absorption [53].

The focus here will be on the absorption process and in particular on the chemical amine based process. This process is mature and widely applied in industry [54, 55]. In chemical absorption CO_2 is bound via a chemical reaction to an amine in the liquid solution. Figure 2.5 shows a basic setup for an amine based CO_2 absorption process. The concentration of MEA in the liquid solution is in the range of 12 to 32 wt% [56, 57]. Based on the following reversible reaction the CO_2 is bound and released by MEA:

$$C_2H_5ONH_2 + CO_2 \rightleftharpoons C_2H_5ONHCOO^- + H^+ \tag{2.17}$$

The gas stream is washed with water in column C1 to bring the temperature down to 45 to 50 °C, to decrease solvent loss by evaporation in the absorber and to saturate the stream with water for an improved water balance of the process [58]. Next it enters the absorber column (C2) at the bottom. The lean amine solution is fed at the top to ensure a counter-current flow of gas and liquid. The purified gas exits at the top. In the absorber, the CO_2 is chemically bound to the amine via an exothermic and reversible reaction leading to an increase in temperature. The temperature in the absorber is between 40 and 60 °C [59, 58]. The rich amine solution (0.4 - 0.5 mol CO_2/mol MEA [58]) is preheated in a cross heat exchanger and fed to the stripping column (C3). The heat is transferred from the lean amine solution coming from the stripper. However, the lean solution has to be further cooled in a heat exchanger before entering the absorber column. In the stripping column, the CO_2 is set free in an endothermic reaction at elevated pressure (1.5 -2 atm) requiring heat which is supplied by the reboiler [58]. Temperatures in the stripping column are around 100 to 140 °C [59]. The CO_2 leaves the column at the top. The amine solution is recycled to the absorber. More advanced process configurations for energy efficiency improvement are discussed by [60].

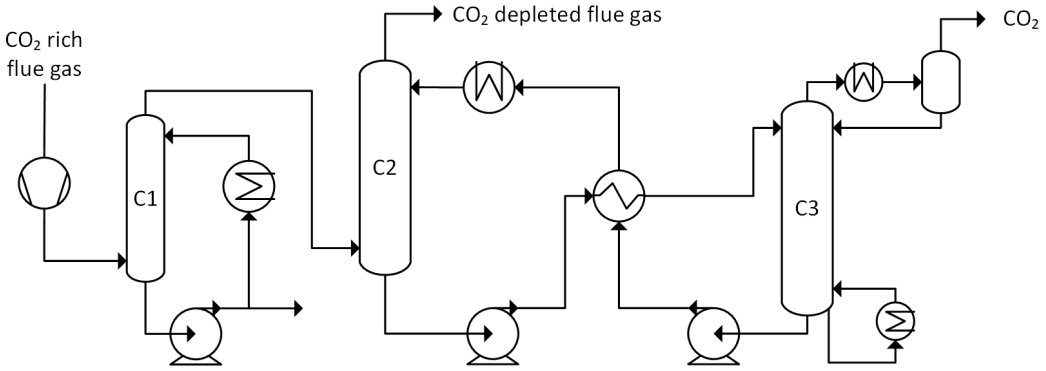

Figure 2.5 Process flow diagram of a CO_2 absorption process based on amines

2.5.2 Pre combustion capture

The pre combustion concept removes the CO_2 before the combustion. Integrated Gasification Combined Cycle (IGCC) power plants can be equipped with a CO_2 capture unit before the H_2 rich gas is combusted in a gas turbine. After the gasification of a carbon containing material, the syngas is treated in a reverse water gas shift unit to shift the equilibrium towards H_2 and CO_2. Afterwards, the CO_2 is removed by a scrubber or membrane. The advantage of the technology is the high flexibility concerning feedstock and product [61]. Additionally, every process step is based on a mature technology [61]. Major disadvantage is the high investment cost and high complexity of such a plant [61].

2.5.3 Oxyfuel

A combustion solely with O_2 instead of air is called oxyfuel combustion. After water condensation, the flue gas will mainly consist of CO_2. The O_2 is usually supplied by an air separation unit [61, 62] but can also be supplied by water electrolysis. In a power plant with oxyfuel combustion the efficiency will drop compared to a conventional power plant by 8 to 11 percentage points [61]. When combusting with O_2, the combustion temperature rises [62]. In order to limit combustion temperatures, typically 60 to 80 % of the flue gas has to be recyled to the combustion chamber [63]. Since no N_2 is present in the flue gas, the resulting flue gas flow is a lot smaller compared to a power plant with air combustion. One difficulty is to avoid false air in the system. The oxyfuel combustion has been tested in multiple pilot and large scale demo plants [64].

In chemical looping, a special technology in the field of oxyfuel combustion, O_2 is introduced via a carrier molecule to the combustion chamber.

2.5.4 CO_2 capture in pulp mills

Several studies have been conducted on the capture of CO_2 from flue gases in pulp mills. Investigations date back to the early 2000s. The special interest in pulp mill arises since pulp mill are large point sources for biogenic CO_2. Capturing and storing the CO_2 would lead to negative emissions which could offset emission from other sectors that are harder or not able to decarbonize. In an European perspective for CCS in the pulp and paper industry, the central European mills have the best potential due to the proximity to storage clusters [65]. The gross of emissions are however released in Sweden and Finland and need to be included for capturing a high amount of CO_2 [65]. Kuparinen et al. assessed the worldwide emissions based on the 15 largest pulp producers to 135 Mt CO_2 per year [66].

All studies consider the post combustion carbon capture with chemical absorption. The main issues for integration in pulp mills is the increased heat demand for the recovery of the absorbing solution. Covering the heat demand can be either done by using medium or low pressure steam extracted from the turbine, using available waste heat, using heat pumps to increase the temperature level of waste heat or by installing additional boilers. Most measure will decrease the power export from the pulp mill. Installing an additional boiler will also result in higher fuel demand and investment cost. Karlsson et al. investigated the transportation and competition with other users for residual biomass on the case of four Swedish pulp mills showing that only 53 to 81 % of the CO_2 emissions can be captured with the supplied biomass [67].

Hektor and Berntsson evaluated the CO_2 capture cost to 20-56 €/t CO_2 considering different ways of heat supply (biomass boiler, natural gas combined cycle (NGCC), heat pump and energy efficiency combined with biofuel boiler) [68]. The NGCC showed the lowest avoidance cost. They also compared the cost for an addition biofuel boiler (25-31 €/t CO_2) or the utilzation of medium pressure steam from the recovery boiler (23-27 €/t CO_2) [69].

Onarheim et al. used a MEA scrubber for carbon capture in a standalone pulp mill and integrated pulp and paper mill [70, 71, 72]. For the market pulp mill increased levelized cost of production of 20 to 154 €/ADt are calculated. The electricity production is decreased by 6 to 80 %. CO_2 avoidance cost are calculated in the range of 62 - 92 €/t CO_2. Capturing CO_2 from the flue gas of the recovery boiler results in a heat demand of 3.76 MJ/kg CO_2 for the MEA process and 2.8 MJ/kg CO_2 for the chilled ammonia process with no waste heat being available for utilization in the process [73]. Skagestad et al. conclude that the partial carbon capture is economically more attractive than full capture due to the higher heat demand for full carbon capture which results in lower electricity production and a need for additional boiler capacity [74]. Partial CO_2 capture cost are in the range of 41 - 57 €/t CO_2 [74]. Nwaoha and Tontiwachwuthiku calculated the capture cost to 138 $/t CO_2 and the additional cost of pulp to 56 $/ADt for MEA scrubbing [75]. Other absorbent and process concepts showed only small financial savings (best being 126 $/t CO_2). Kuparinen et al. calculated the avoidance cost for negative emissions to 75 - 224 $/ t CO_2 [76]. Parkhi et al. used a MEA scrubber for the removal of CO_2 from the lime kiln flue gas resulting in 76 $/t CO_2 or 18 $ /t ADt [77].

For a capture rate of 50 %, CO_2 prices are around 62 - 70 €/t [78]. A credit of 80 €/t CO_2 would decrease the pulp price by 15 €/t pulp [78]. Yang et al. report CO_2 avoidance cost (MEA scrubber) of 31-93 €/t CO_2 [79]. Sagues et al. calculate that the cost of CO_2 capture are close to zero including a 50 $ /t CO_2 tax credit [80].

Other studies not based on absorption are for example electric plasma calcination, oxyfuel combustion or chemical looping. Lefvert and Grönkvist investigated the CO_2 capture on the lime kiln by either oxyfuel combustion or electric plasma arc calcination [81]. Unfortunately, they only report technical parameters and do not provide any economic assessment. The work by Svensson et al. on electric plasma arc calcination was presented earlier showing capture cost of 36 to 60 €/t CO_2 (Section 2.1.2) [27]. Saari et al. investigated the replacement of a circulating fluidized bed boiler by a chemcial

looping system [82]. In terms of electrical efficiency, both systems show similar performance. Santos et al. investigated the replacement of the lime kiln by a calcium looping system [83]. CO_2 abatement cost were at 39 €/t CO_2 and the pulp price increases from 728 €/ADt for the reference pulp mill to 824 €/ADt for the pulp mill with calcium looping.

Another less common source for CO_2 is onsite production of biogas. CO_2 can be separated by many available technologies [84]. Furthermore, ethanol production in sulphite pulp mills via fermentation are also CO_2 sources with high concentrations.

2.6 Synthesis routes based on H_2

2.6.1 Carbon monoxide generation

In this thesis, the production of carbon monoxide (CO) as an educt for FT and acetic acid production can be either provided by the CO_2 electrolysis or the reverse water gas shift reaction.

CO_2 electrolysis

The CO_2 electrolysis is an electrochemical process for the conversion of CO_2 to CO. The overall reaction equation occurring in the electrolysis cell is depicted in Equation 2.18. There are three technologies available: solide oxide electrolysis, molten carbonate electrolysis and low-temperature electrolysis. Currently, the solide oxide electrolysis is about to be commercialized (TRL 8) [85]. A simplified sheme of the already commercialized process called eCOs by Topsoe A/S is depicted in Figure A.1 in the Appendix.

$$2\,CO_2 \longrightarrow 2\,CO + O_2 \tag{2.18}$$

Reverse water gas shift

The reverse water gas shift (RWGS) reaction is an equilibrium reaction depicted in reaction equation 2.19. It is a high temperature process that can be used for the activation of CO_2. Relevant reviews on the RWGS process can be found [86, 87, 88].

$$H_2 + CO_2 \rightleftharpoons CO + H_2O \quad \Delta H = 41\,kJ\,mol^{-1} \tag{2.19}$$

As many side reactions occur, the thermodynamic evaluation of the process is complex. Side reactions are the methanation and solid carbon forming reactions. The formation of methane is an exothermic reaction being therefore favored at lower temperatures. Either CO or CO_2 can act as a feedstock for the methanation reaction as depicted in the following equations [89]:

$$CO + 3\,H_2 \rightleftharpoons CH_4 + H_2O \quad \Delta H = -206\,kJ\,mol^{-1} \tag{2.20}$$

$$CO_2 + 4\,H_2 \rightleftharpoons CH_4 + 2\,H_2O \quad \Delta H = -165\,kJ\,mol^{-1} \tag{2.21}$$

Carbon formation can occur in the RWGS reactor and is an undesired reaction (Equations 2.22-2.24) [89]. Reaction 2.22 (Boudouard reaction) is favored at lower temperature and higher pressure. Methane pyrolysis (Equation 2.23) is thermodynamically favored by low temperatures and low pressure. Reaction 2.24 is favored by lower temperatures and higher pressures. The occurence of the carbon forming reactions take place under different operating conditions meaning that carbon formation is an omnipresent issue in the RWGS reactor.

$$2\,CO \rightleftharpoons CO_2 + C \quad \Delta H = -172\,kJ\,mol^{-1} \tag{2.22}$$

$$CH_4 \rightleftharpoons 2\,H_2 + C \quad \Delta H = -75\,\mathrm{kJ\,mol^{-1}} \tag{2.23}$$

$$H_2 + CO \longleftrightarrow C + H_2O \quad \Delta H = -131\,\mathrm{kJ\,mol^{-1}} \tag{2.24}$$

In order to gain a better picture of the process influenced by many competing reactions Figure 2.6 shows the product composition under equilibrium conditions plotted over the temperature. The model predicts that solid carbon is formed until a temperature of roughly 680 °C. According to Le Chatelier's principle, the extent of the reverse water gas shift reaction increases for higher temperatures due to the endothermicity of the reaction. Besides, the methane formation decreases for higher temperatures since reactions 2.20 and 2.21 are exothermic. The plots show that higher temperatures are beneficial as no carbon formation occurs, the methane fraction is lower and the yield of CO is higher. The drawback of higher temperatures is however the increase in energy demand for heating the process.

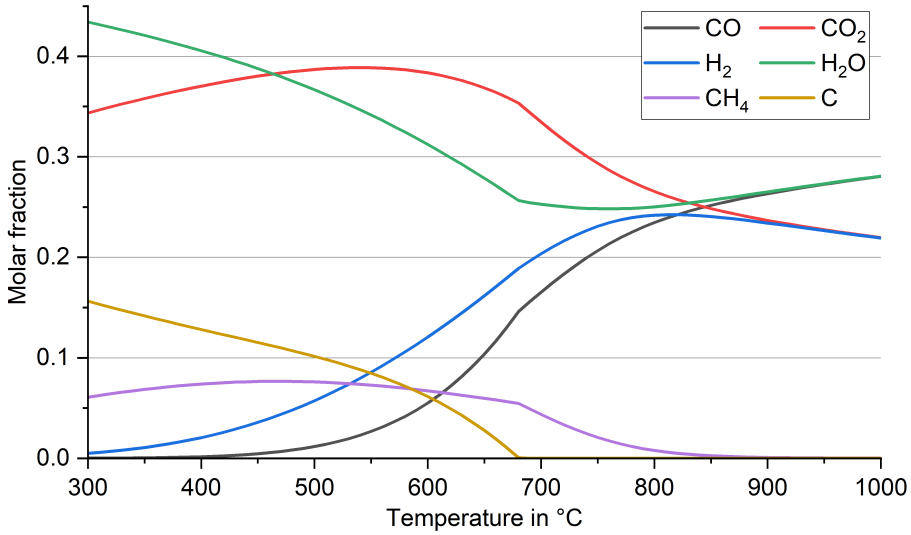

Figure 2.6 Molar fraction of gas and solid at equilibrium (Minimization of Gibbs energy) in the range of 300 to 1000 °C (Thermodynamic model: Peng Robinson with Boston Mathias alpha function, $H_2/CO_2 = 1$)

Other processes

In industrial scale syngas for carbon monoxide production can be generated by partial oxidation of hydrocarbons, steam reforming, coal gasification or recovered from industrial processes (blast furnace off gas, ...) [90]. The carbon monoxide content is between 30 and 85 % [90]. Before gas purification, acidic components like CO_2 or H_2S are removed [90]. The purification is done either by reversible complexation, cryogenic separation, pressure swing adsorption or membrane separation [90]. Medrano-Garcia et al. evaluate different pathways for the production of CO by an optimization to reduce cost and CO_2 emissions [91].

2.6.2 Fischer Tropsch

The Fischer Tropsch (FT) process is an heterogenously catalyzed process for the conversion of syngas to a mixture of hydrocarbons with different chain lengths. The product is called syncrude and consists mostly of alkanes and alkenes. Aromatic and oxygenated products are also formed but in lots smaller amounts. The Fischer Tropsch process has been discovered by Franz Fischer and Hans Tropsch in 1923 at Kaiser Wilhelm Institute for Coal Research in Mühlheim/Ruhr [92]. The first commercial plant was operating in 1936 in Germany [93].

Typical operating pressures are in the range of 10 to 40 bar [94]. The operating temperature is above 200 °C [95, 94]. The FT process can be differentiated in high temperature (300 - 350 °C) and low temperature (200 - 250 °C) FT process [96, 97]. The low temperature Fischer Tropsch process (LTFT) uses iron and cobalt catalysts and produces mainly longer chain alkanes [96]. The high temperature process (HTFT) is iron catalysed and produces mainly shorter chain products with a high selectivity to linear 1-olefins [97]. Iron, cobalt, ruthenium and nickel catalyze the FT reaction whereof only iron and cobalt catalyst were commercialized [97]. An important difference between iron and cobalt as catalyst is the ability of iron-based catalyst to catalyse the water gas shift reaction [98].

Typical reactions for the formation of alkanes, alkenes and alcohols are shown in Equation 2.25, 2.26 and 2.27. The reaction equations are all exothermic.

$$n\,CO + (2\,n + 1)\,H_2 \longrightarrow C_nH_{2n+2} + n\,H_2O \quad \Delta H = n(-146.0)\,kJ\,mol^{-1} \tag{2.25}$$

$$n\,CO + 2\,n\,H_2 \longrightarrow C_nH_{2n} + n\,H_2O \tag{2.26}$$

$$n\,CO + 2\,n\,H_2 \longrightarrow C_nH_{2n+1}OH + (n\text{-}1)\,H_2O \tag{2.27}$$

The reaction mechanism is based on chain propagation which can be described by the chain growth probability α. The product distribution can be modelled with the Anderson-Schulz-Flory (ASF) distribution (Equation 2.28 with w_n: mass fraction of component with chain length n, α: chain growth probability and n: number of carbon atoms). The chain growth probability depends on parameters like H_2/CO ratio, temperature, pressure and catalyst material [95]. Higher temperature and H_2/CO ratio lead to a lower chain growth probability which consequently results in lighter products [98]. The chain growth probability increases for higher pressures [98]. The ASF distribution has weaknesses in comparison to reality. The ASF distribution underestimates the selectivity towards methane and overestimates the selectivity towards ethane [98]. Especially for LTFT processes, the chain growth probability can be expressed as two chain growth probabilities valid for short and long chain products [98].

$$w_n = \frac{1-\alpha}{\alpha} \cdot \alpha^n \cdot n \tag{2.28}$$

In Figure 2.7 the product composition is plotted for typical chain growth probabilities ranging from 0.7 to 0.9. The products are grouped into 5 categories based on their chain length. For HTFT, the chain growth probability ranges from 0.7 to 0.75 [97]. The LTFT chain growth probability is in the range of 0.85 to 0.95 thus producing more longer chain products compared to HTFT [97].

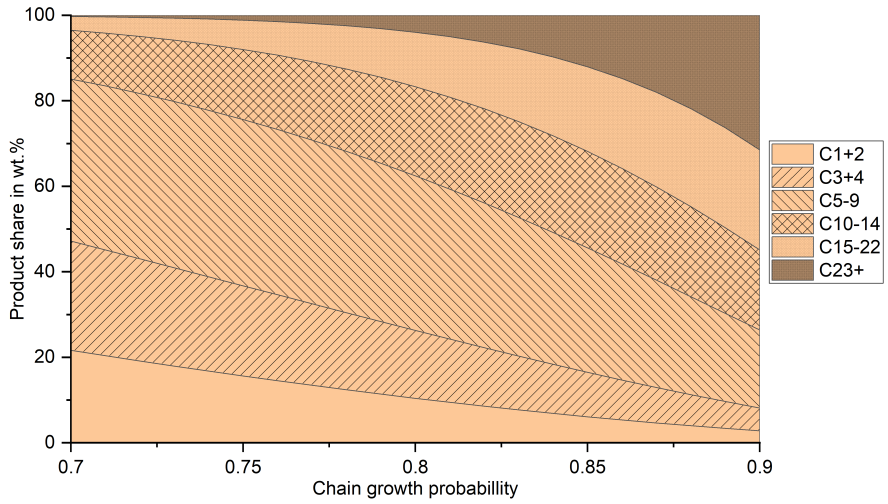

Figure 2.7 Mass fraction of product groups (grouped by carbon number) over the chain growth probability (calculated based on Equation 2.28)

Reactor concepts include fixed bed, slurry phase and fluidized bed reactors [98, 95]. Fluidized bed reactors operate at temperatures above 320 °C with the syngas fluidizing the bed material consisting of catalyst particles [99]. Since longer chain products would condensate and lead to agglomeration of the bed material, only iron-based catalyst exhibiting lower chain growth probabilites are used [96]. The slurry phase and fixed bed reactor operates at around 220 to 250 °C [99]. In a slurry phase reactor, the syngas is bubbled into a suspension of liquid waxes and catalyst particles. The liquid products accumulate in the suspension and gaseous products exit at the top of the reactor. In fixed bed reactors, tubes are usually filled with catalyst. On the shell side, boiling water removes the heat. Newer reactor concepts are microstructured or membrane reactors [100]. For fluidized bed and slurry phase reators, the catalyst can be replaced online and the catalyst has to be separated from unreacted gas and product [98]. In a fixed bed reactor the separation is not an issue but the catalyst can only be replaced during shutdown [98]. The operating conditions in fluidized bed and slurry phase reactors can be regarded as isothermal due to the high heat transfer rates [95]. Additionally, these reactor types show higher per pass conversions [95].

Figure 2.8 shows a process design with a closed loop and open loop gas recycle design. In a first step syngas is produced with multiple raw materials being applicable (for example natural gas, coal, biomass, CO_2). The syngas needs to be conditioned for the correct H_2/CO ratio. The syngas is then converted in the FT reactor to syncrude. After the reactor water, syncrude and tail gas are separated. The tail gas contains unreacted syngas and shorter chain hydrocarbons (in case of N_2 free syngas).

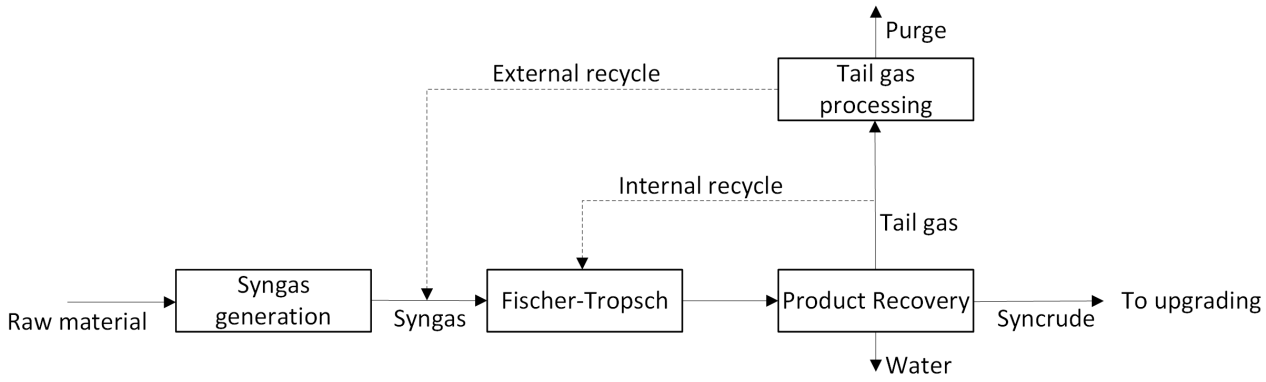

Figure 2.8 Flowsheet of a typical FT process with closed (internal and external recycle with purge stream, dashed line) and open loop design, adapted from [98]

In case of an open loop design, the tail gas is not recycled back to the process. This is feasible if the conversion in the reactor is very high or if an electricity cogeneration is included at the plant [98]. In a closed loop design, part of the tail gas is either directly recycled to the reactor (internal recycle) or it is conditioned and fed back to the reactor [98]. In order to use the FT syncrude as fuel, further upgrading is needed. De Klerk argues that syncrude has better properties for the refining to fuel compared to crude oil [101]. Consequently, a FT refinery should be beneficial in terms of environmental impact, complexity and cost [101]. Typical refinery design are discussed here [102, 103].

2.6.3 Methanol

Methanol (MeOH) is a major base chemical. 85 % of the produced methanol is used in the chemical industry as solvent or for the production of chemicals like formaldehyde, methyl-tert-butyl ether and acetic acid for example [104]. The other applications comprise fuel and energy [104]. In industrial scale, MeOH is only produced from syngas via catalytic conversion [104]. The conventional MeOH production is based on syngas containing H_2, CO and CO_2. The process operates at 200 to 300 °C and 50 - 100 bar [95, 104]. The process for the conversion of H_2 and CO_2 to MeOH is similar to the syngas based process in terms of process design, process conditions and catalyst.

The reactions of syngas to MeOH can be described by the following equilibrium reaction equations (2.29 and 2.30) which are coupled via the water gas shift reaction. Both reaction pathways are exothermic with the CO_2 hydrogenation being less exothermic.

$$CO_2 + 3\,H_2 \rightleftharpoons CH_3OH + H_2O \quad \Delta H = -49.8\,\mathrm{kJ\,mol^{-1}} \tag{2.29}$$

$$CO + 2\,H_2 \rightleftharpoons CH_3OH \quad \Delta H = -91.0\,\mathrm{kJ\,mol^{-1}} \tag{2.30}$$

Since the reactions are exothermic, low temperatures shift the equillibrium to the product side. The reduction of volume also suggest a shift of the equilibrium to the product side for higher pressures. Figure 2.9 shows the MeOH yield at equilibrium conditions for different temperatures and pressures underlining the statements of Le Chatelier's principle that lower temperatures and higher pressures are beneficial for the conversion. For the same operating conditions, the yield is generally higher for the CO hydrogenation. Due to the higher volume reduction for CO hydrogenation, the impact of pressure is stronger revealed by the slope of the curves. Due to the reaction being more exothermic, the impact of temperature is also stronger in comparison to CO_2 hydrogenation. Furthermore, the yield in CO hydrogenation is substantially higher than in CO_2 hydrogenation.

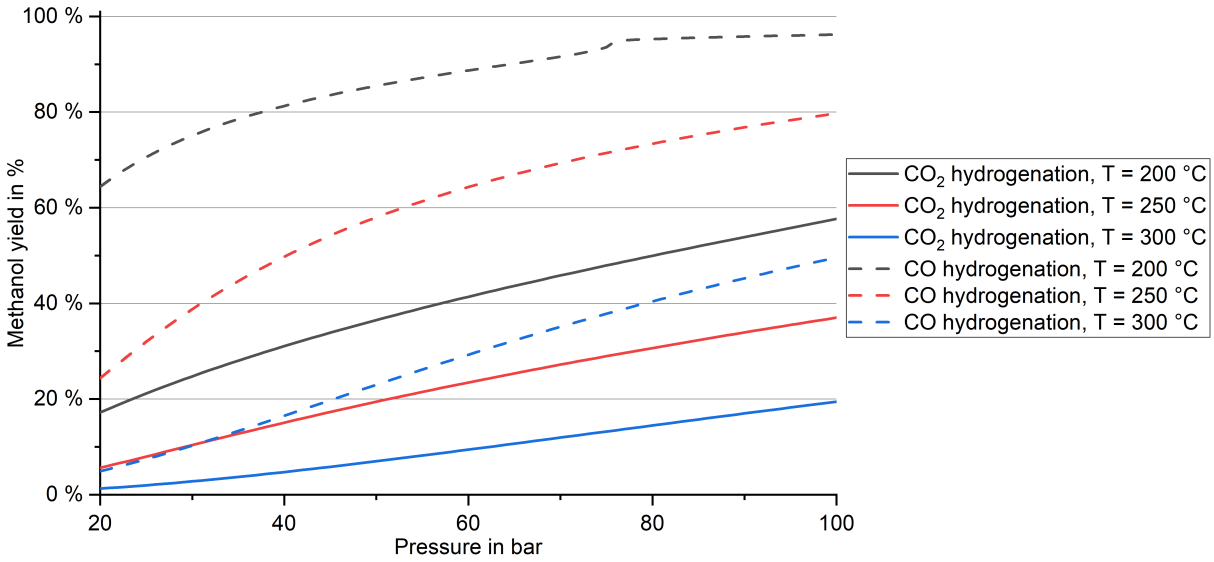

Figure 2.9 Equilibrium compositions for the reaction of CO or CO_2 and H_2 to form MeOH and water based on the minimization of Gibbs energy (Thermodynamic model: RKSMHV2, molar feed ratio according to stoichiometry)

For the low pressure processes employed today, the $Cu/ZnO/Al_2O_3$ catalyst is widely used [104, 105]. The catalyst exhibit a selectivity towards MeOH of above 99 % [104]. Catalysts for the production of MeOH from syngas and H_2/CO_2 are very similar since reaction mechanism, reaction conditions and already present CO_2 in the syngas create similar conditions in both processes [106]. However, experimental tests found a selectivity of above 99.9 % for CO_2 and H_2 as educts [107, 108]. Compared to MeOH synthesis with conventional syngas, the process based on CO_2 and H_2 has a 5 time lower by-product generation [108]. By-products are higher alcohols, DME (dimethyl ether), esters, hydrocarbons and ketones [104].

The typical process design for either feedstock (Figure 2.10) consists of a low temperature liquid gas separation after the reactor. Since the conversion in the reactor is incomplete (50 - 80 % per pass conversion for syngas [104]), the flash drum separates the unreacted gas from the liquid phase consisting of mainly water and MeOH. Unreacted gas is recycled back to the reactor. A small amount of the recycle stream is purged to avoid accumulation of inerts like other gases that are introduced with the reactants. The liquid phase is processed in a purification section to separate the water and MeOH mixture via distillation. Depending on the required purity one or more columns are used [95].

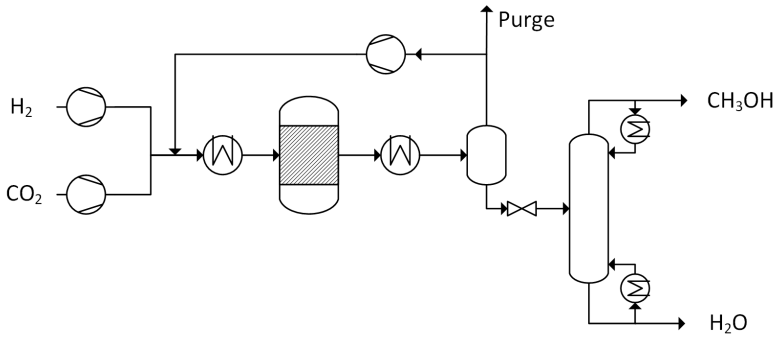

Figure 2.10 Simplified flowsheet of a typical MeOH process [95, 104]

Removing the heat of reaction from the reactor is the major challenge in terms of efficient heat recovery, low by-product formation, low catalyst volume and high conversion [105]. Many commercial fixed bed reactor concepts are available as listed by [95]. The dominating reactor technology are quasi-isothermal steam-raising fixed bed reactors [95]. The multitubular reactor contains the catalyst and syngas on the tube side [104]. The shell side contains boiling water that is leaving the reactor as steam [104]. Other concepts are adiabatic reactors with gas quench or consecutively, indirectly cooled adiabatic reactors [105]. The MegaMethanol process by Lurgi uses a series of 2 reactors (gas cooled and quasi-isothermal) where the outlet from the quasi-isothermal reactor is further reacted on the shell side of the gas cooled reactor cooled by fresh syngas on the tube side [104]. New reactor types under development are fluidized bed, trickle bed, slurry phase, sorption-enhanced and membrane reactors [95, 105].

2.6.4 Synthetic natural gas

Besides the production of synthetic natural gas (SNG) as product, the first application of the process was the removal of carbon monoxide from syngas streams for processes like ammonia production [46]. During the oil crisis in the 1970s, the technology was used to produce SNG with syngas derived from coal gasification [109]. More recently, the feedstock was shifted to CO_2 and biomass [110]. The CO_2 and CO methanation reaction equation is shown in Equation 2.31 and 2.32. The CO_2 methanation is less exothermic than the CO methanation. Both equation are coupled via the water gas shift reaction.

$$CO_2 + 4\,H_2 \rightleftharpoons CH_4 + 2\,H_2O \quad \Delta H = -164\,\mathrm{kJ\,mol^{-1}} \tag{2.31}$$

$$CO + 3\,H_2 \rightleftharpoons CH_4 + H_2O \quad \Delta H = -206\,\mathrm{kJ\,mol^{-1}} \tag{2.32}$$

Since the reactions are equilibrium reactions, the chemical equilibrium is influenced by pressure and temperature. The effects have been studied extensively in literature [111, 112]. In general, the exothermic nature of both reactions suggests a higher conversion to products at lower temperature. The volume reduction of the reaction to the products side indicates that higher pressures are favorable.

Figure 2.11 illustrates the equilibrium composition for different temperatures and pressures. According to Gao et al., carbon formation is not occuring for CO_2 methanation due to the water produced through the reverse water has shift reaction [112]. The carbon formation in CO methanation occurs below 15 atm and for lower H_2/CO ratios [112]. For both process routes the reactions reach high conversions towards the products (below 250 °C for CO_2 methanation and below 300 °C for CO methanation) [112]. Higher pressures above 30 bar usually have no influence on the conversion [112]. Active materials for the methanation reaction are found in group 8 to 10 [110]. Out of these, nickel is mostly used in commercial plants due to being the most selective catalyst with a high activity [110]. Other metals like ruthenium or cobalt are more pricy compared to nickel [110]. The support material of the catalyst influences the catalytic performance. Support materials for nickel catalyst are discussed

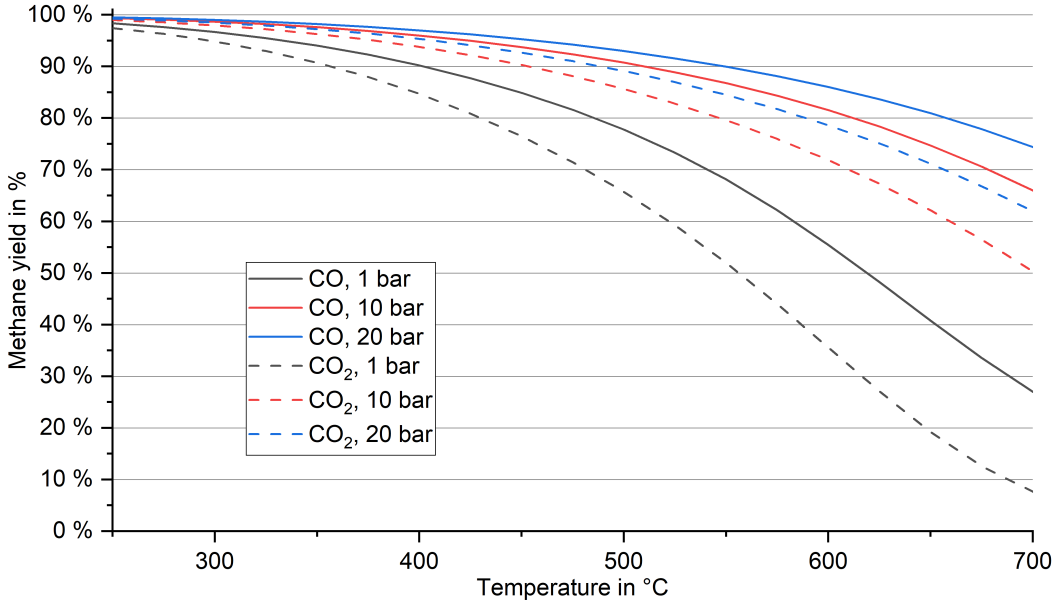

Figure 2.11 Eqilibrium compositions for the reaction of CO or CO_2 with H_2 to form methane and water based on the minimization of Gibbs energy (Thermodynamic model: Soave-Redlich-Kwong, stoichiometric feed composition according to Equations 2.31 and 2.32)

here [113, 110]. Sulphur poisoning is a major issue reducing catalyst life time. Therefore, the sulphur concentration should be kept below several ppb [110].

Reactor concepts can be divided into two phase and three phase concepts [110]. Fixed bed reactors operated under adiabatic or polytropic conditions are the only commercialized reactor concept [110]. In demonstration scale are fluidized bed reactors [110]. Structured reactors and slurry reactors are under investigation [110].

Figure 2.12 shows the TREMP process by Topsoe A/S composed of a series of three adiabatic fixed bed reactors with intercooling. The recycle stream around the first reactor controls the temperature in the first reactor. After the third reactor, water is condensed and separated from the gaseous product. The process allows for heat recovery on a high temperature level.

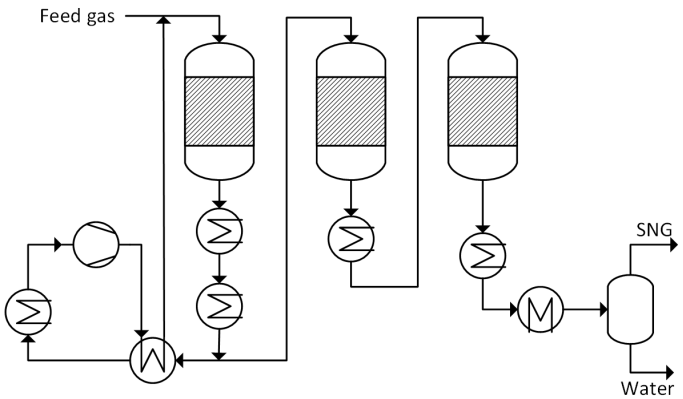

Figure 2.12 Flowsheet of a typical SNG process (TREMP from Topsoe A/S [114])

2.6.5 Hydrogen peroxide

Hydrogen peroxide (H_2O_2) is mainly used for bleaching purposes in many industries [115] like also in the pulp mill for bleaching pulp. It can be produced by either wet chemical, electrochemical or

autoxidation processes [115]. The anthraquinone autoxidation is the most relevant production process for large scale production [115]. Campos-Martin et al. give an overview on all possible production routes [116]. The process can be divided into three major process steps: hydrogenation, oxidation and extraction. Figure 2.13 shows a simplified flowsheet of the process. The overall reaction is equation is fairly simple:

$$H_2 + O_2 \longrightarrow H_2O_2 \tag{2.33}$$

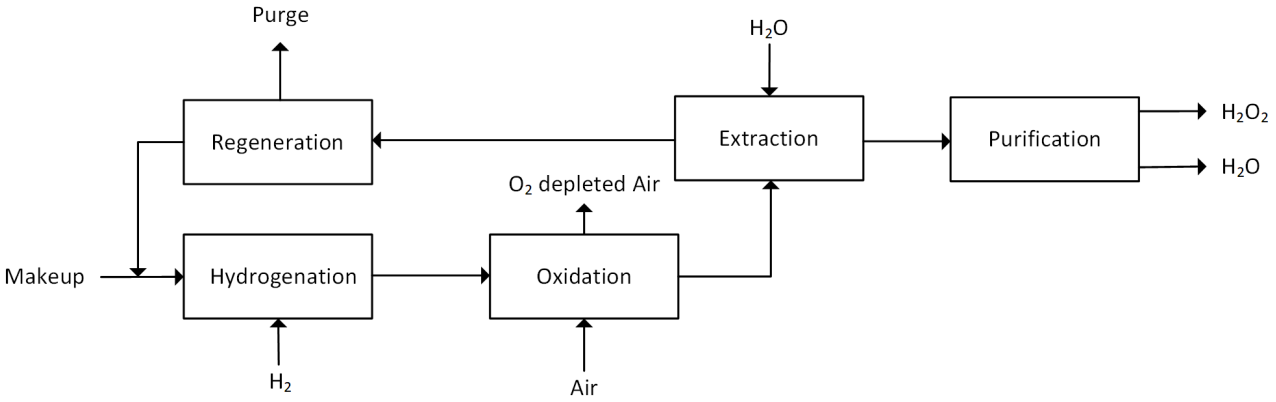

Figure 2.13 Flowsheet of the anthraquinone process for H_2O_2 production

Anthraquinone, most commonly 2-ethylantraquinine, acts as a carrier molecule for H_2. The anthraquinone (AQ) which is dissolved in a working solution, is hydrogenated catalytically yielding anthrahydroquinone (AHQ) according to Equation 2.34. The process operates at 40-50 °C with a hydrogen partial pressure of up to 4 bar [116]. The working solution comprised of solvents and alkylanthraquinone is recycled in the process. A mixture of unpolar and polar solvents are used. AQ dissolves well in nonpolar, aromatic solvents where the AHQ dissolves in polar solvents (especially alcohol and ether) [115]. The hydrogenation reaction is performed with either a slurry or fixed bed catalyst. For the slurry catalyst, a filtration is needed after the reactor to recycle the catalyst to the reactor [115]. The catalyst material is palladium. The conversion towards AHQ is kept below 60 % [116]. Since the reaction is exothermic, the released heat has to be removed. This can be done before the reactor (cooling of feed streams), in the reactor or after the reactor [115].

$$AQ + H_2 \longrightarrow AHQ \tag{2.34}$$

In the oxidation reactor, any presence of hydrogenation catalyst must be avoided since the decomposition of H_2O_2 is catalysed by the hydrogenation catalyst [115]. At temperatures of 30 - 60 °C and atmospheric pressure, air is bubbled into the reactor [116]. The reaction equation of oxidation is shown in the following reaction equation:

$$AHQ + O_2 \longrightarrow AQ + H_2O_2 \tag{2.35}$$

H_2O_2 is extracted with water from the working solution in an extraction column. The concentration of H_2O_2 in the working solution is around 0.8 - 1.9 wt. % [116]. The crude H_2O_2 solution after extraction reaches purities of around 25 - 50 wt. % [116, 115]. Up to 95 % of the H_2O_2 is recovered from the working solution in the extraction step [116]. In a subsequent step the H_2O_2 is distilled under vacuum (5 - 15 kPa) and further purified [115].

The electrochemical production of H_2O_2 should not be neglected as concepts are already commercialized (for example HPNow [117]). The processes play a minor role in industry however in terms of electrification and for comparison with the AQ process supplied by H_2 from water electrolysis it is a suitable process for comparison. Several different process configurations and materials are

discussed [118, 119]. Electrical energy demands are in the range of 12.8 to 17.6 kWh/kg H_2O_2 [115] which is definitely more than for the AQ with water electrolysis. Oloman and Watkinson claim an electrical energy demand of 2 - 7 kWh/kg H_2O_2 which is more competitive in comparison to the numbers reported before [120]. The Huron-Dow process can produce H_2O_2 at low concentrations in an alkaline solution which can be directly used in pulp mills [121].

2.6.6 Acetic acid

Acetic acid (AA) is an important base chemical. More than 65 % of the AA is used in the production of vinyl acetate and cellulose acetate [122]. The worldwide production capacity exceeds 12 Mio. t/a mostly located in Asia and North America [122]. Besides the fermentative production of AA by different bacteria strains, the oxidation of butane, naphta, or acetaldehyde and the carbonylation of MeOH are the most prominent synthetic routes. Where the latter will remain the best choice for large scale production with a current share of about 75 % [122, 123].

In 1913 the carbonylation of MeOH was described by BASF [122]. BASF developed a cobalt-catalyzed process in 1960 [122]. In the 1960s Monsanto established a process based on a promoted rhodium catalyst operating at low pressures of 30 to 60 atm and 150 to 200 °C [122, 124]. The Cativa process based on a iridium catalyst was established 1996 by BP showing substantial improvements in comparison to the Monsanto process [122, 124]. Advantages are operation at lower water concentrations, higher catalyst stability, high reaction rates, reduced formation of liquid by-products and improved CO yields [125].

The production of AA based on the carbonylation of MeOH (see reaction 2.36) proceeds in a liquid phase reactor at pressures of 20 to 50 bar and 150 - 200 °C [126, 123].

$$CO + CH_3OH \rightleftharpoons CH_3COOH \quad \Delta H = -135.6\,\mathrm{kJ\,mol^{-1}} \tag{2.36}$$

Besides the carbonylation of MeOH side reactions as shown in the following can occur.

$$CH_3OH + CO \longrightarrow CO_2 + CH_4 \tag{2.37}$$

$$CH_3COOH + CH_3OH \longrightarrow CH_3CH_2COOH + H_2O \tag{2.38}$$

The process flow diagram is depicted in Figure 2.14. CO and MeOH are fed to the reactor where the carbonylation reaction occurs. Additionally, water, MeOH, methyl acetate, methyl iodide and AA are recycled from the downstream separation steps to the reactor. The heterogeneous catalyst is separated from the liquid mixture and fed back to the reactor. Unreacted gases and light side products are separated in the gas separator and partially returned to the reactor.

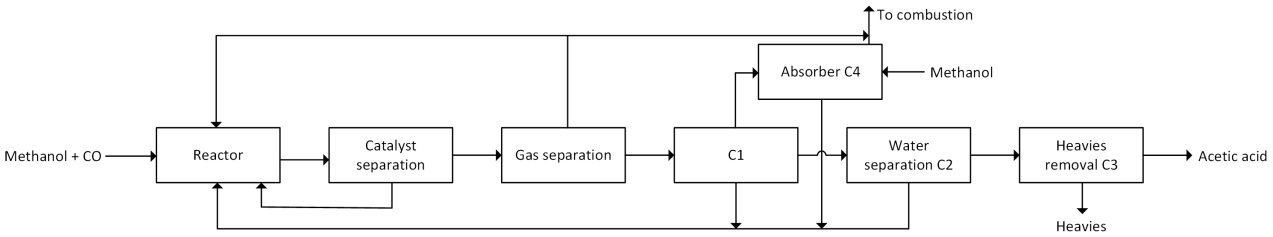

Figure 2.14 Flowsheet of the AA production process (Cativa process) based on [122, 123, 126]

The product stream is fed to the first distillation column C1 as vapor. Light components are separated from the mixture. In column C1 a stream rich in AA is withdrawn as side pull and sent to distillation column C2. The bottom stream of C1 contains mostly water and AA. The top stream contains gases and light components like methyl iodide. C2 removes water. The top product is water with some rest of light components and AA. The bottom product consists of AA and some traces of

propionic acid. In column C3, the propionic acid is removed to reach the required purity of AA. The gaseous stream of column C1 is sent to absorber C4. With MeOH, the methyl iodide is removed from the gas stream. The purge gas stream from C4 and the gas separated from the reactor is combusted.

2.7 Carbon capture and utilization in pulp mills

The concept of integrating PtX concepts in pulp mills is fairly new. For other industries like cement for example, the concepts have already been established. Besides academic research, the possibility to integrate PtX concepts in pulp mills gained attention by industry like Afry [127] or Siemens Energy [128, 129]. Pio et al. discuss the MeOH production in pulp mills based on CO_2 and H_2, from stripper off gases, or with the gasification of biomass in their review [6]. SAF production via FT was also discussed by the same authors in another review [5]. They elaborate on the beneficial integration with pulp mills.

One study from Sweden investigates the production of methane and MeOH in a stand alone and integrated pulp mill with a capacity of 2254 ADt/d [4]. For the stand alone mill a capture rate of 10 %, 20 % and 50 % of the CO_2 in the flue gas of the lime kiln was studied. Results are shown in Table 2.2. The integration of heat influences the loss of electricity generation and is therefore not a linear function of the plant capacity. The MeOH prices range from 467 - 869 €/t for different price assumptions. The prices for methane vary between 74 and 128 €/t.

Table 2.2 Integration of PtX plant for the production of MeOH and methane in a pulp mill [4]

Product		CO_2 captured in kt/y or %		
		27/10	53/20	135/50
MeOH	Produced methanol in t/y	19,400	38,800	97,100
	Electrical demand electrolyzer in MW_{el}	21	41	103
	Loss of electricity production in MW_{el}	1	3	7
Methane	Produced Methane in t/y	9,700	19,300	48,300
	Electrical demand electrolyzer in MW_{el}	26	52	131
	Loss of electricity production in MW_{el}	1	1	0

With the available CO_2 emissions from the Swedish pulp industry, a production amount of 8 Mt methane and 16 Mt MeOH per year can be realized. This would require an electrolysis capacity of 17 GW_{el} and 22 GW_{el}. On a normal winter day the power consumption in Sweden is around 22 GW_{el}. Consequently, the potential of PtX products in Sweden is not limited by the availability of biogenic CO_2 from the pulp industry but by other factors like the electricity grid or the market for the products. The study is based on a process simulation not including a detailed integration with the pulp mill.

Kuparinen et al. calculated MeOH selling prices for 5 mills under different economic scenarios of 552 to 1662 $/t [76]. The mills reach yearly production amounts between 8 and 1029 kt MeOH. Other calculations by the research group showed that MeOH prices of 600 to 800 €/t result for low electricity prices (20 to 40 €/MWh) [130]. Both publications are based on simplified mass and energy balance calculations.

2.8 Other production routes for chemicals and fuels in sulphate pulp mills

This section discusses production routes for fuels and chemicals in pulp mills which are not based on H_2 and CO_2 as main raw material. Mäki et al., Oliveira et al. and Hamaguchi et al. give an overarching picture of possible routes [24, 131, 132]. Some technologies like lignin extraction from black liquor (see below), MeOH purification (see below) or the production of renewable fuel and chemicals from crude tall oil (BioVerno by UPM or SunPine) are already commercialized.

2.8.1 Recovery of MeOH from stripper off gases

The stripper off gases (SOG) contains 35 % MeOH and 65 % water [133]. Additionally, sulfur and nitrogen containing compounds have to be separated from the MeOH to reach commercial grade MeOH. 85 - 95 % of nitrogen impurities consist of ammonia [134]. Sulphur compounds are for example hydrogen sulfide, methyl mercaptan, dimethyl sulfide or dimethyl disulfide [134].

Several suppliers have developed systems for the purification of MeOH from the SOG. Stora Enso developed a process that oxidizes low boiling components of the condensate under the presence of a catalyst and H_2O_2. The MeOH can be recovered by distillation [135]. Andritz Oy aquired a patent for the purification system with 7 separation steps and acidification for the removal of light components. The central step is the removal of sulfur compounds by extraction with a non-polar organic solvent [136]. FPInnovations developed a process with a reverse osmosis for the separation of contaminants from the MeOH stream optionally followed by an adsorption with activated carbon [137]. Andritz Oy developed a new process where salts are precipitated through the addition of acid in a first step. Heavy oil can be added to avoid precipitation in the following distillation [138]. Valmet AB also offers a system for the purification of SOG [139, 133].

Figure 2.15 shows the process for MeOH purification as proposed by A.H. Lundberg Systems. This system is installed in the project partner's pulp mill and was therefore chosen as reference. The incoming SOG is condensed and treated in a decanter separating turpentines. The rest is sent to the top of the topping column. In the column, lighter components like hydrogen sulfide and ammonia are removed as gases and sent to incineration. Since hydrogen sulfide and methyl mercaptane are dissociated at higher pH values, acid (sulphuric acid) needs to be added to lower the pH value for ensuring no dissociation. Since ammonia can react with sulphuric acid, sulphuric acid is added in the middle of the column to ensure the stripping of ammonia in the top section of the column. The bottom product contains less volatile components. In the second column, MeOH is purified and is taken as a side stream close to the top of the column. The head product of the column leaves as vapor and contains the leftover light components. The bottom product contains mainly water and heavy boilers. In a side pull from the column, intermediate boilers are removed to ensure the purity of the MeOH product. 2 - 3 % of the MeOH needs to be sacrificed for this. [140]

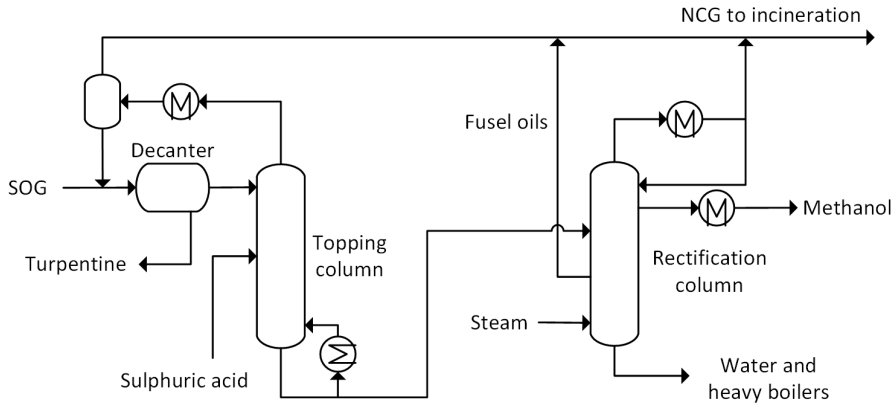

Figure 2.15 Flowsheet of the Lundberg concept for MeOH recovery from SOG, inspired by [140, 141] and the technical documentation of the project partner

2.8.2 Lignin extraction

Lignin contained in the black liquor can be selective separated. It can be used as fuel, material or chemical [142]. Lignin separation from black liquor by precipitation is the most developed and commonly used method [143]. At lower pH values, the solubility of lignin decreases and the lignin

precipitates. Other methods for separation are selective solvent extraction, electrochemical processes or membrane filtration [143, 144].

Four different technologies at pilot and industrial scale for the separation of lignin via precipitation from Kraft black liquor are known: LignoBoost (Valmet), LignoForce (FPInnovations), WestVaco and SLRP (Liquid Lignin Company) [145]. All processes use black liquor with a dry substance content between 20 and 40 % [145]. The processes lower the pH value in a first acidification step by adding CO_2 to precipitate the lignin. By removing lignin from a part of the total black liquor stream, the thermal power input to the recovery boiler is reduced. On the one hand this can enable a higher pulp production since the recovery boiler's thermal power input can be the bottle neck in pulp mills [24]. On the other hand the heat and electricity generation in the mill is reduced at the same time as the energy demand is increased which can lead to a lack of available energy for the mill. Olsson et al. calculated a 3 - 11 % higher steam demand in the evaporator plant with lower electricity production for all cases (up to 30 %) in their assessment of integration of lignin separation in a pulp mill [144].

2.8.3 Hydrothermal processes

Hydrothermal carbonisation produces mainly a biochar which can be used as material or fuel. Multiple feedstock from pulp mills have already been tested in hydrothermal carbonisation: sludge from waste water treatment [146, 147], lignin [148], pulp [148], galactoglucomannan [148], black liquor [149] and TEMPO oxidized cellulose nanofibrils [148]. A first commercial hydrothermal carbonisation plant on the basis of sludge from waste water treatment is running at Stora Enso's pulp mill in Heinola (Finland) [150].

Hydrothermal liquefaction at moderate temperatures (200 - 400 °C) mostly yields a bio oil which can be used in power generation or internal combustion engines [151]. Compared to pyrolysis oil, the carbon content is higher and the O_2 content is lower leading to a less expensive upgrading process for transport fuel production [151]. Ong et al. investigates the integration of co liquefaction of black liquor and pine in a pulp mill [152, 153]. Funkenbusch at al. simulated a hydrothermal liquefaction process based on lignin as raw material [154].

2.8.4 Black liquor gasification

Black liquor gasification (BLG) is a thermochemical process that converts black liquor to syngas which can be used in a chemical synthesis. The technology can in consequence replace the recovery boiler of a pulp mill as it also enables the recovery of the pulping chemicals. Additionally, BLG can be used for debottlenecking the recovery boiler [155]. Chemrec AB and ThermoChem Recovery International commercialized systems for black liquor gasification [156]. The O_2-blown entrained gasifier by Chemrec AB operates at 32 bar and 950 - 1000 °C [157]. One key problem is the material choice for the gasifier [157]. Besides BLG, biomass gasification is discussed for integration in pulp mills. This review gives a good literature overview [158].

Most recent studies on process simulations for BLG with synthesis of fuels or chemicals are reported here. The production of multiple products like for example MeOH, DME, SNG, Fischer-Tropsch fuels, ammonia and H_2 were studied [155, 159, 160, 161, 162, 163, 164, 165, 166, 167, 168, 169, 170]. Additionally, BLG gasification can be combined with a combined cycle for electricity production [171].

Jafri et al. investigated five biofuel production paths based on using partial black liquor streams from pulp mills [155]. Three of these were based on BLG including the MeOH production and methanol-to-gasoline process. Besides the pure gasification of black liquor, they considered the addition of H_2 and the co-gasification with pyrolysis oil. The addition of energy carriers to the gasification route showed no economic benefit. The lowest price achieved was 77 €/MWh. In case of H_2 addition, the mills were required to import electricity.

3 Methodology

This chapter presents the methods used in the thesis comprising of theoretical work based on process simulations with economic and environmental evaluation, and experimental work in the lab and pilot lab.

3.1 Process modeling

Modeling was done with the steady-state flowsheet simulation software Aspen Plus® Version 12. The operation of all process steps is at steady-state conditions (including electrolysis). The software performs mass and energy balance calculations. Thermodynamic models are used to predict properties of components. Models have to be correctly chosen depending on the involved components and process characteristics. A detailed description of the used models can be found in the documentation of Aspen Plus.

3.2 Reference pulp mill and pulp mill integration

The investigation is performed for a non-integrated sulphate pulp mill in Germany. Table 3.1 shows the data of the reference pulp mill as used for the integration with the PtX process and calculations. The data is based on industry information. As the production performance is fluctuating, the presented numbers are based on mean values of data and on operational experience of the employees.

The PtX plants are integrated in terms of energy and material flows into the pulp mill. Figure 3.1 shows the exchanged energy and material streams for the integration of H_2-based routes towards chemicals and fuels (Chapter 4). Not all streams are valid for every PtX product. For example, FC is only transferred to the PtX process for MeOH production.

Externally supplied energy to the PtX process is natural gas and electricity. Natural gas is used in the pulp mill for heating the lime kiln. Additional natural gas is needed for heating of the RWGS reactor by combustion (only for AA and FT syncrude). Electricity from the grid is imported for the supply to the PtX process if the onsite available electricity is exceeded. Any type of purge stream is assumed to be sent to the lime kiln for combustion. The thermal power of replaced natural gas is equal to the thermal power of the purge stream. If the purge stream exceeds the 50 MW_{th} power demand of the lime kiln, additional high pressure steam can be produced in the bark or recovery boiler (Efficiency of 90 % based on LHV of fuel).

The CO_2 released by the pulp mill through combustion processes can be captured and converted to fuels and chemicals. It is assumed that only biogenic CO_2 is captured. This assumption is valid since the plant's demand will not exceed the available amount of biogenic CO_2. The flue gas and capture process is not further specified as the capture process is modeled with a simplified mass and energy balance. The demand for deionized water and waste water treatment can be covered by the available infrastructure onsite. Based on industry information, it is confirmed that the deionized water plant can supply the water electrolysis with the required water purity. For waste water treatment and deionized water production, the electricity demand is considered for an increased demand as shown in Table 3.1. The waste water treatment plant is capable of dealing with the waste water generated in the processes. Dissolved gases (H_2, CO_2, CH_4, C_2H_6, CO), MeOH, alkanes, AA and H_2O_2 can be present in the waste water. The only critical components are AA and H_2O_2. H_2O_2 is already processed to a maximum inlet concentration of a partial waste water stream (25 % of total waste water) of 1.5

Table 3.1 Data of reference pulp mill

Parameter	Value
Annual pulp production	612,067 ADt
Steam generation recovery boiler	512 t/h
Steam generation bark boiler	86 t/h
Total electricity generation	140 MW_{el}
Electricity surplus fed to grid	60 MW_{el}
Thermal power lime kiln	50 MW_{th}
Lime mud flow	25 t_{wet}/h
Water content lime mud	75 wt. %
Foul condensate stream	4.9 kt/a
Bark to bark boiler	162.5 kt_{wet}/a
Other wood residues to bark boiler	76.4 kt_{wet}/a
Annual biogenic CO_2 emissions	1,580 kt/a
Annual fossil CO_2 emissions	75 kt/a
Annual operating hours	7,500 h/a
Annual H_2O_2 demand (pure)	14.7 kt/a
Annual O_2 demand (pure)	27.6 kt/a
Electricity requirement for O_2 production	0.39 MWh_{el}/t O_2
Annual waste water amount	15.8 Mt/a
Electricity requirement for waste water purification	1 kWh_{el}/t
Annual deionized water amount	17.1 Mt/a
Electricity requirement for deionized water production	2.0 kWh_{el}/t water
Annual process cooling demand	2,191,172 MWh_{th}
Electricity requirement for process cooling	15 kWh_{el}/MWh_{th}

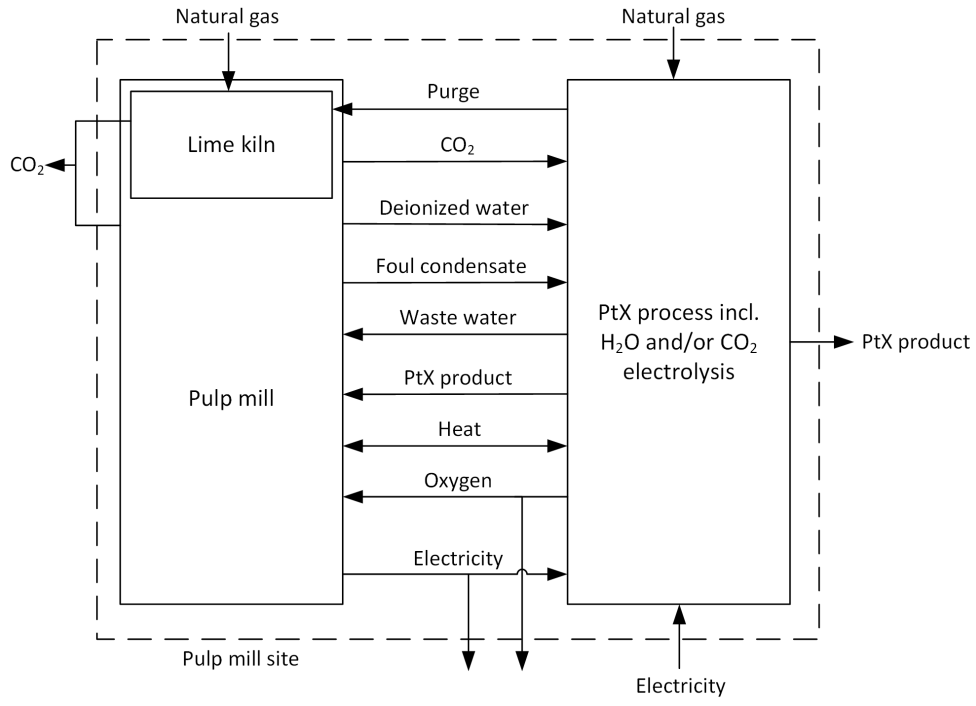

Figure 3.1 Sketch of the exchanged material and energy flows for the integration as used in Chapter 4 for the production of chemicals and fuels based on H_2

g/l. The pH value of AA containing waste water can be regulated by in the neutralization unit if necessary. The other components are not critical.

The pulp mill uses O_2 in the pulp bleaching process which is supplied by a pressure swing adsorption (PSA) plant at a purity of 94 wt. %. The O_2 generated in the electrolysis as by-product can replace the O_2 from the PSA plant. Any surplus O_2 is assumed to be sold for a low price as it is not liquefied or under high pressure. The utilization for the improvement of other processes like O_2-enriched combustion or for the waste water treatment plant is not considered. The available stream from the evaporation plant containing MeOH (FC) is integrated with the Power-to-Methanol plant.

Heat integration was performed by pinch analysis. After the aggregation of heating and cooling duties with inlet and outlet temperature of the streams, the hot and cold composite curves are plotted. The minimum temperature difference was set to 20 °C. A temperature difference of 10 – 20 °C is advised for the chemical and petrochemical industry [172]. The higher bound is chosen for a more conservative result. The available utilities in the pulp mill for heating and cooling are shown in Table B.5 in Appendix B.4. The utilities are used for supply or recovery of heat from the process. The change in steam availability will have an impact on the electricity generation. You will find the calculation approach for the steam cycle in Appendix B.4. The demand for process cooling is the minimum cooling demand determined in pinch analysis. For process cooling the available cooling towers can be used. The electrical energy demands for cooling is shown in Table 3.1. The cooling demand to condense the steam after the turbine which is caused by a change in electricity generation is also considered in the change of cooling demand. It is further assumed that generated or supplied hot water does not affect the steam balance and that a surplus can be used by the pulp mill. If this is not the case, the process cooling demand would increase accordingly.

The integration with the pulp mill for the lime kiln decarbonization is depicted in Figure 3.2. Compared to Figure 3.1, the required CO_2 is solely captured from the lime kiln's flue gas. The integration of heat, deionized water, O_2, electricity, purge streams and waste water treatment is performed as described before. The fuels produced in the fuel preparation process are combusted in the lime kiln together with purge streams if available. Some cases produce PtX products which can be sold to the market.

The required biomass (bark or wood residues like rejects or coarse material) can be rerouted from the bark boiler to the fuel preparation process. If the onsite availability of biomass is not sufficient, additional biomass must be imported from the market. The lack of biomass in the bark boiler reduces the steam production resulting in a lower electricity generation. The reduction of high pressure steam from the bark boiler is calculated based on the energy input of the biomass (LHV based calculation) and the bark boiler efficiency of 87 % (industry data). The decrease of high pressure steam from the bark boiler leads to a lower electricity generation which is calculated as described in Appendix B.4. Additionally, heat integration is performed if applicable to the process.

3.3 Economic evaluation

The economic evaluation of the processes is based on the cost assessment for capital expenditures (*CAPEX*) and operating expenditures (*OPEX*).

3.3.1 Calculation of capital expenditures

In order to calculate the *CAPEX* the purchased equipment cost C of each process components must be evaluated. The fixed capital investment (*FCI*) is calculated according to Equation 3.1. An installation factor of 6 accounts for the additional cost of installing the equipment and for auxiliary equipment [173]. For the electrolyzers no installation factor applies.

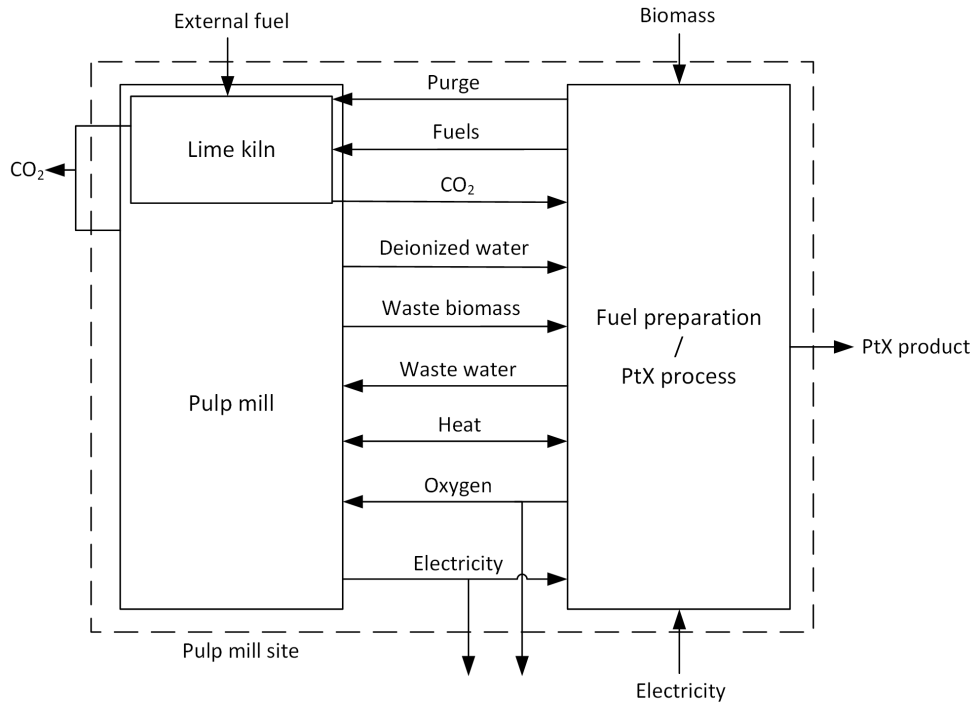

Figure 3.2 Sketch of the exchanged material and energy flows for the integration as used in Chapter 5 for the supply of fuels to the lime kiln

$$FCI = \sum_{i=1}^{n} 6 \cdot C_i + C_{electrolysis} \tag{3.1}$$

The Aspen Economic Analyzer was used for the calculation of equipment sizing and cost in most cases. For equipment that cannot be sized by Aspen the sizing and subsequent cost estimation was performed based on literature data using typial cost scaling equations [173, 174, 175]. The base year for the equipment cost is 2021. The equipment cost is adjusted as described in Appendix C.2.1.

3.3.2 Calculation of operating cost

The operating cost (Operating expenditures: $OPEX$) are calculated as depicted in Equation 3.2. The calculation includes administration cost C_A, plant overhead cost C_{PO}, insurance and taxes C_{I+T}, operating supervision and clerical assistance C_{S+C}, laboratory charges C_{LC}, Labor cost C_L, maintenance cost C_M, cost for natural gas C_{NG}, CO_2 cost C_{CO2}, cost for electricity from the grid $C_{E,Grid}$, cost for electricity from the pulp mill $C_{E,Pulp}$, cost for deionized water C_{DW}, cost for CaO makeup C_{CaO}, cost for biomass $C_{Biomass}$, revenues from O_2 sale $C_{O2,sale}$, savings of O_2 substitution $C_{O2,sub}$, savings from substituted H_2O_2 $C_{H2O2,sub}$ and anthraquinone C_{AQ}. The cost for biomass and CaO are only relevant in Chapter 5. The cost for replaced H_2O_2 and cost for anthraquinone are only needed in the H_2O_2 production process (Section 4.6).

$$\begin{aligned} OPEX = C_A + C_{PO} + C_{I\&T} + C_{S\&C} + C_{LC} + C_L + C_M \pm C_{NG} + C_{CO2} + C_{E,Grid} \cdots \\ \cdots + C_{E,Pulp} + C_{DW} + C_{CaO} + C_{Biomass} - C_{O2,sale} - C_{O2,sub} - C_{H2O2,sub} + C_{AQ} \end{aligned} \tag{3.2}$$

The detailed description of the calculation and assumptions is shown in Appendix C.1.

3.3.3 Levelized cost of product

The total annualized cost (*TAC*) are comprised of the annualized capital cost (*ACC*) and the operating cost (*OPEX*) as shown in Equation 3.3.

$$TAC = ACC + OPEX \tag{3.3}$$

The *ACC* are calculated as shown in Equation 3.4 using the annuity factor *AF*.

$$ACC = FCI \cdot AF \tag{3.4}$$

The *AF* is calculated as shown below including the interest rate (*IR* = 8 %) and plant life time (*PL* = 20 years).

$$AF = \frac{IR \cdot (1 + IR)^{PL}}{(1 + IR)^{PL} - 1} \tag{3.5}$$

The levelized cost of product (*LCOP*) is calculated based on Equation 3.6. The *TAC* are divided by the annual product output. Besides the mass based calculation, the *LCOP* can also be based on the energy content of the product.

$$LCOP = \frac{ACC + OPEX}{m_{product}} = \frac{TAC}{m_{product}} \tag{3.6}$$

3.3.4 Sensitivity analysis

With the sensitivity analysis, the impact of cost components and assumptions can be assessed. Table 3.2 shows the values altered in the sensitivity analysis. Besides economic assumption, technical parameters are changed.

Table 3.2 Upper and lower values used in the sensitivity analysis

	Lower	Base	Upper	Unit
Electricity from grid	20	60	100	€/MWh
Electricity from pulp mill	60	83	100	€/MWh
Natural gas	15	25	50	€/MWh
Fuel oil	50	80	150	€/MWh
Biomass	10	20	30	€/MWh
MeOH market price	400	800	1200	€/t
Interest rate	6%	8%	10%	-
Water electrolysis cost	400,000	600,000	800,000	€/MW
Efficiency water electrolysis	60%	70%	80%	-
CO_2 capture cost	0	50	80	€/t
CO_2 electrolysis cost	600,000	800,000	1,000,000	€/MW
Efficiency CO_2 electrolysis	6.4	5.6	4.8	kWh_{el}/kg_{CO}
Maintenance	5%	7%	9%	of FCI
FCI anthraquinone process	-50%	-	+50%	of FCI

3.4 CO_2 balance

In order to assess the environmental impact of the implemented processes and exported PtX products in terms of climate impact, a simplified CO_2 balance calculation was performed. The used emission factors (EF) are depicted in Table B.4 in the Appendix. The system boundary influences the results

immensely. Here, the system boundary is chosen from the perspective of the pulp mill and not from a national level with a consequential approach.

Figure 3.3 shows the system boundary of the CO_2 balance for Chapter 4. For the integrated PtX plant, the system boundary comprises the pulp mill and the PtX plant. In the greenfield case, the plant is supplied by steam generated with natural gas and electricity only from the grid. In the greenfield case, emissions for waste water and other utilities are not considered. For the integrated PtX plants, all electricity consuming utilities are considered in the electricity balance and therefore included in the CO_2 balance.

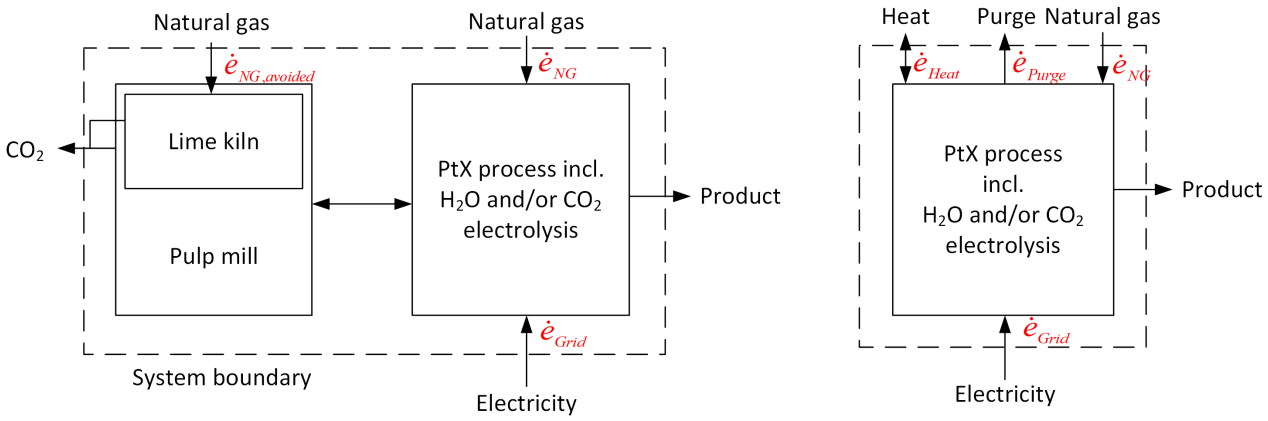

Figure 3.3 Definition of system boundaries for CO_2 balance for integrated (left) and greenfield (right) plant as used in Chapter 4 for the PtX processes

The CO_2 balance for the integrated plant considers emissions from grid electricity (only applicable for the 150 MW_{el} plants) and additional natural gas needed for the PtX plant (Equation 3.7). Additionally, for the combustion of purge streams in the lime kiln, the replaced natural gas is included with a credit in the CO_2 balance.

$$\begin{aligned} \dot{m}_{CO2} &= \dot{e}_{Grid} + \dot{e}_{NG} - \dot{e}_{NG,avoided} \\ &= P_{el,grid} \cdot EF_{grid,electricity} + \dot{m}_{NG} \cdot LHV_{NG} \cdot EF_{NG} - P_{th,purge} \cdot EF_{NG} \end{aligned} \tag{3.7}$$

All product emission factors are either calculated based on the product mass (t CO_2/t product) or the product's energy content (g CO_2/MJ product) as shown in the following equations:

$$EF_{product,mass} = \frac{\dot{m}_{CO2}}{\dot{m}_{product}} \tag{3.8}$$

$$EF_{product,energy} = \frac{\dot{m}_{CO2}}{\dot{m}_{product} \cdot LHV_{product}} \tag{3.9}$$

For the greenfield plant, the product emission factor is calculated according to the following equation. Heat needed or released from the process is assumed with the emission factor of natural gas and a conversion efficiency of 90 % (based on LHV).

$$\begin{aligned} \dot{m}_{CO2} &= \dot{e}_{Grid} - \dot{e}_{Purge} \pm \dot{e}_{Heat} + \dot{e}_{NG} \\ &= P_{el,grid} \cdot EF_{grid,electricity} - P_{th,purge} \cdot EF_{NG} \pm P_{th,heat} \cdot \frac{EF_{NG}}{0.9} + \dot{m}_{NG} \cdot LHV_{NG} \cdot EF_{NG} \end{aligned} \tag{3.10}$$

The system boundary in Figure 3.4 shows the CO_2 balance for the lime kiln decarbonization (Chapter 5). For the lime kiln the annual change in fossil CO_2 emissions is calculated.

The CO_2 balance comprises the fossil emissions from onsite combustion of fossil fuels namely natural gas or fuel oil in the lime kiln ($\dot{e}_{FossilFuel}$). Not all cases show fossil emissions from the

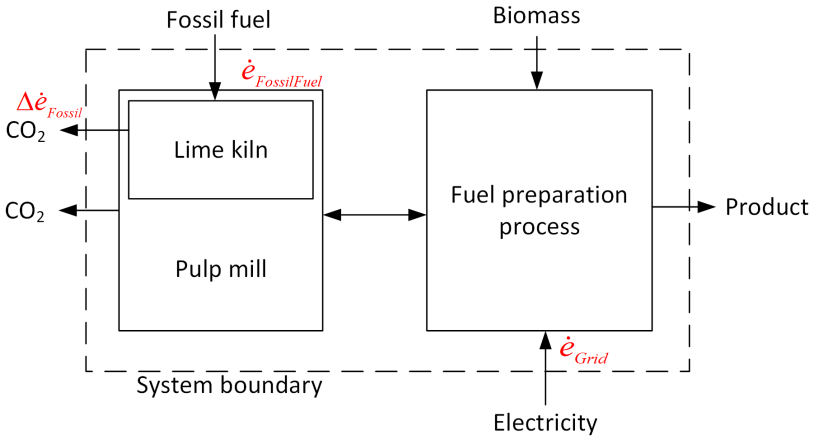

Figure 3.4 Definition of system boundary for the CO_2 balance used in Chapter 5 for lime kiln decarbonization

combustion of fossil fuels. For some cases, additional electricity is needed from the grid. The emissions of the grid electricity ($\dot{e}_{Grid}$) are included in the calculation. The change in annual fossil CO_2 emissions is summarized by the following equation:

$$\Delta\dot{e}_{Fossil} = \dot{e}_{Grid} + \dot{e}_{FossilFuel} \tag{3.11}$$

3.5 Key performance indicators

In order to evaluate and compare the processes, the following key performance indicators (KPIs) are calculated. The Power-to-Fuel efficiency (η_{PtF}) describes the efficiency from electricity to fuel. The electrical power includes the electricity required for water or CO_2 electrolysis ($P_{electrolysis}$) and the auxiliary processes like for example compression and pumping ($P_{Auxiliary}$). For the integrated plants $P_{Integration}$ includes the increase or decrease of electricity availability in the pulp mill caused by the integration. For the greenfield plants, $P_{Integration}$ is excluded. The energy content of the fuel is calculated using the LHV.

$$\eta_{PtF} = \frac{\dot{m}_{Product} \cdot LHV_{Product}}{P_{Electrolysis} + P_{Auxiliary} + P_{Integration}} \tag{3.12}$$

The carbon efficiency (η_{CE}) describes the amount of carbon contained in the product to the amount of carbon feed to the process as CO_2.

$$\eta_{CE} = \frac{\dot{n}_{C,product}}{\dot{n}_{C,CO2}} \tag{3.13}$$

The hydrogen efficiency (η_{HE}) is defined as the hydrogen contained in the final product to the hydrogen entering the process as H_2.

$$\eta_{HE} = \frac{\dot{n}_{H,product}}{\dot{n}_{H2,in}} \tag{3.14}$$

The CO_2 abatement cost (AC) is calculated as shown in the following equation:

$$AC = \frac{C_{process} - C_{reference}}{e_{reference} - e_{process}} \tag{3.15}$$

The investigated process is compared to a reference case. The annual cost (C) and annual CO_2 emissions (e) of both are needed for the calculation. The base case for the calculations in Chapter 5

are based on a natural gas fired lime kiln as reference. The reference for the PtX products in Chapter 4 considers the fossil equivalent with market price and emission factor as the reference. The limitations and issues of AC are discussed in literature [176].

Another indicator for the economic comparison between the products is the increase in pulp price (IPP) for products sold at current market prices. The calculation is depicted in Equation 3.16. The difference between TAC of the production process and annual revenue from product sale at market price of the fossil product has to be covered by the pulp sale. Therefore, the cost difference is divided by the annual pulp production yielding the increase in pulp price in €/ADt (Air Dried ton).

$$IPP = \frac{TAC - m_{product} C_{product,marketprice}}{m_{pulp}} \tag{3.16}$$

3.6 Adiabatic flame temperature

The adiabatic flame temperature (AFT) is the temperature for the combustion of fuel under adiabatic conditions with the stoichiometric amount of air for complete combustion. The AFT is used in Chapter 5 for the calculation of the fuel demand in the lime kiln. The calculation model is implemented in Python using the CoolProp library for calculating the temperature dependent heat capacities.

Input parameters to the model are the elemental composition, the LHV on dry basis and the temperature of the fuels. Combustion air is supplied at 20 °C with a composition of 79 % N_2 and 21 % O_2. The model calculates the air demand for the combustion considering the elements C, H, O and S. With the air demand and the fuel, the flue gas composition is calculated based on an elemental mass balance. The energy balance of the process is iteratively calculated converging towards the adiabatic combustion temperature fulfilling Equation 3.17. The equation shows the energy balance with the energy inputs by air (calculated with the heat capacity and temperature difference) and by the fuel (based on the mass flow and the LHV). The reference temperature T_{ref} is equal to the fuel supply temperature. By doing so, air and flue gas have to be calculated based on this reference temperature. The integral on the right side of the equation depicts the energy of the flue gas based on the heat capacity, temperature difference and mass flow of each component (H_2O, CO_2, SO_2, N_2). The integral is evaluated from the reference temperature T_{ref} to T_{AFT}.

$$\dot{m}_{fuel} LHV_{fuel} + \dot{m}_{air} c_{p,air} (T_{air} - T_{ref}) = \sum_{n=1}^{4} \int_{T_{ref}}^{T_{AFT}} \dot{m}_{fluegas,n} c_{p,n} \, dT \tag{3.17}$$

3.7 Experimental work

The experimental work can be divided into the purification of MeOH via rectification, or selective removal of impurities via activated carbon adsorption and precipitation with Fe(II) ions. For all types of experiments, the same analytic methods are utilized.

3.7.1 Analytic methods

Karl Fischer titration

The Karl Fischer titration is a quantitative method for the determination of water content in a solution. The underlying reaction equation for the method is the Bunsen reaction (Eq. 3.18) [177]. For a surplus of SO_2, the addition of iodide will cause the reaction to occur according to the equation until all the water is consumed. Once the water is consumed, excess iodide will accumulate and can be detected by its brown color. The used device is TitroLine 7500 KF by SI Analytics which is a fully automated volumetric Karl Fischer titration.

$$2\,H_2O + SO_2 + I_2 \longrightarrow 2\,HI + H_2SO_4 \tag{3.18}$$

Nitrogen and sulphur analysis

The total nitrogen and sulphur content contained in the samples are measured with the elemental analyzer multi EA 5000 by Analytik Jena. The sample is combusted and flue gases are sent to the analyzers.

Density measurement

The density measurement with Anton Parr DMA 4500 was used to determine the water and MeOH content. The procedure included the measurement of water before and after a set of measurements in order to confirm that no drift has occurred. Doubles or triplets were measured at 20 °C. Based on available literature data, the MeOH and water content can be calculated [178]. The assumption for this calculation is that the sample only contains water and MeOH. The other present components were neglected as the concentrations are very low.

3.7.2 Methanol samples

The experimental work uses real samples of crude MeOH produced in the pulping process. The samples were not specifically analyzed for the contained compounds. Known parameters are water content and the concentration of total sulphur (S) and nitrogen (N) content. Figure 3.5 shows as diamonds the points from which samples are taken. The technical operation and function of the plant was discussed in Section 2.8.1. Point "1" is the MeOH stream before the decanter and topping column. This sample will have higher concentrations of S, N and turpentines than sample point "2". The topping column removes the light components and the decanter removes the turpentines meaning that sample "2" will generally have lower S, N and turpentine concentrations. The total mass flow of incoming SOG from the pulp mill is 650 kg/h. Based on operational experience, the mass flow can differ depending on for example the season or water content of the processed wood.

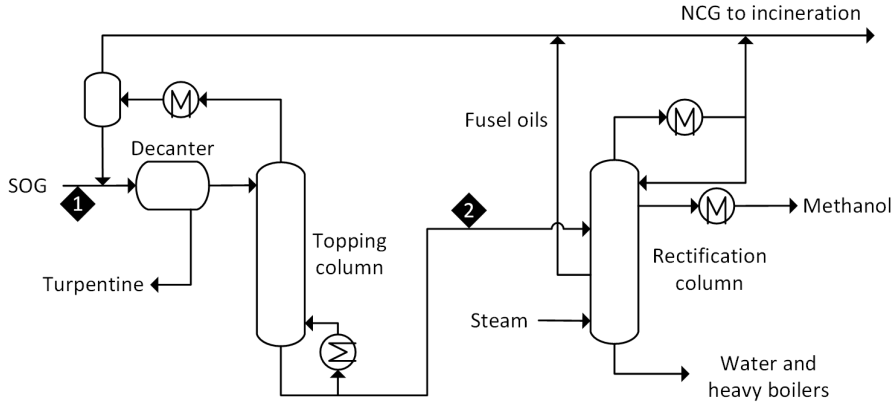

Figure 3.5 Process flowsheet diagram of the MeOH purification plant in operation at the pulp mill. The points of the samples are indicated by two diamond shapes.

Figure 3.6 shows the concentration of S and N in the raw MeOH (sample point "1") for random sampling days. More than one data point is available for 02.09.2021. The points are connected with lines for optical reasons. The 17 data points collected between 02.09.2021 and 29.12.2021 show the wide range of concentrations occurring. The mean value of S and N are 2.71 and 1.13 g/kg. The high variance of the data points shows that the composition of the samples for the experiments vary massively. Consequently, the result are difficult to reproduce with another sample taken on a different day. Furthermore, the samples showed optical differences in color and the amount of turpentines which accumulated as a second phase.

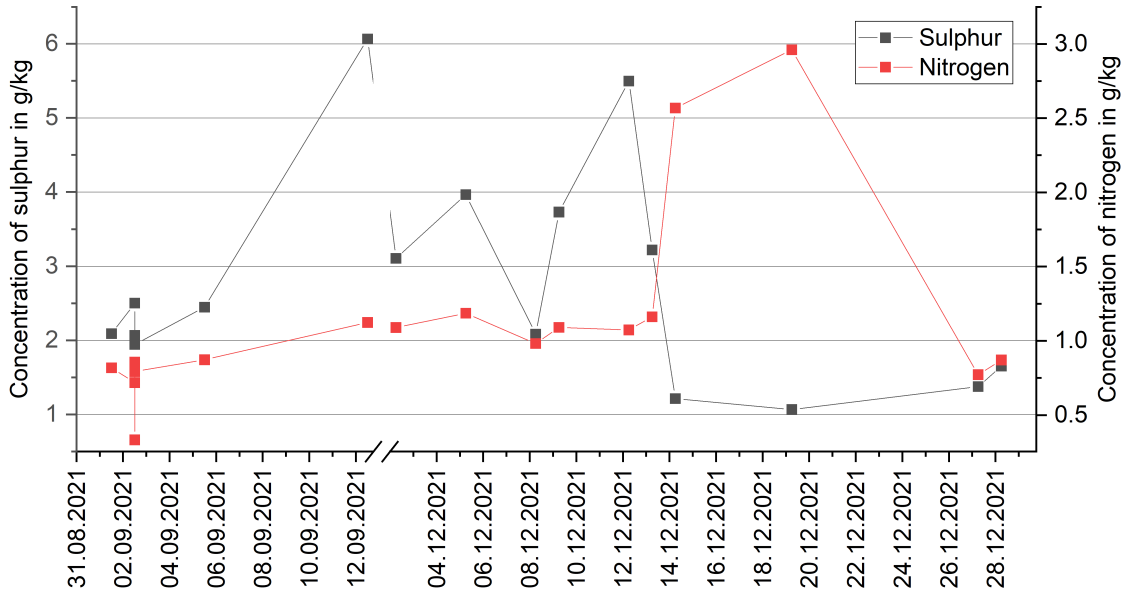

Figure 3.6 Concentration of S and N in the raw MeOH shown for samples taken at point "1" for different days and times

3.7.3 Rectification pilot plant

The experimental purification of MeOH from CO_2 hydrogenation and the FC from the pulp mill is investigated with a pilot plant. The P&ID of the continuously working rectification column is shown in Figure 3.7. The column itself and most of the auxiliary equipment is manufactured of borosilicate glass. Smaller parts are made of premium steel and PTFE. The plant operates under atmospheric pressure.

The feed is pumped from the storage vessel B301 to the column. The pump P301 is a gear pump. The pump power (0 - 100 %) describes the rotations per minute of the electric drive. As it is a gear pump, the volume flow correlates linearly with the pump power. With the density of the feed, the mass flow can be calculated based on the calibration curve of the pump (see Appendix F.1). The pump can deliver a mass flow in the range of one digit kg/h. The feed can be preheated with heat exchanger E303 supplied with heat by thermostat TH303. The feed temperature is measured with T311. The feed position can be changed to every bottom point of a column section as indicated by the small lines in the P&ID. The column body consists of 4 sections (C301 to C304). The inner diameter is 43 mm. The column is packed with Sulzer CY with a total length of 4710 mm. The gauze packing is a high performance packing with a low HETP.

The top of the column is equipped with a cooler and reflux splitter. The splitter is built with a piston that is lifted by a magnet. The piston is moved according to set times for withdrawal of the top products and reflux to the column. The withdrawn product is cooled in E304 and collected in vessel B302. The three way valve between the heat exchanger and storage vessel allows for taking samples during operation.

The reboiler is heated by thermostat TH301. In order to support the circulation of the liquid for improved heat transfer, a small N_2 stream is introduced to agitate the liquid. The reboiler holds around 3 l of volume. The withdrawal of the bottom product is regulated with a siphon. Heat exchanger E305 cools the bottom product. The cooled product flows over the tip of the siphon into the storage vessel B303. The valve in between allows the sampling during operation.

In total, 13 temperature measurements are installed. Including reboiler and condenser, 10 Pt-100 are recording the temperature profile along the column. Further measurements are the feed temperature (T311) and the temperatures of the heating oil leaving the thermostats (T312 and T313). The pressure difference between the column head and the reboiler vapor phase are measured. This measurement

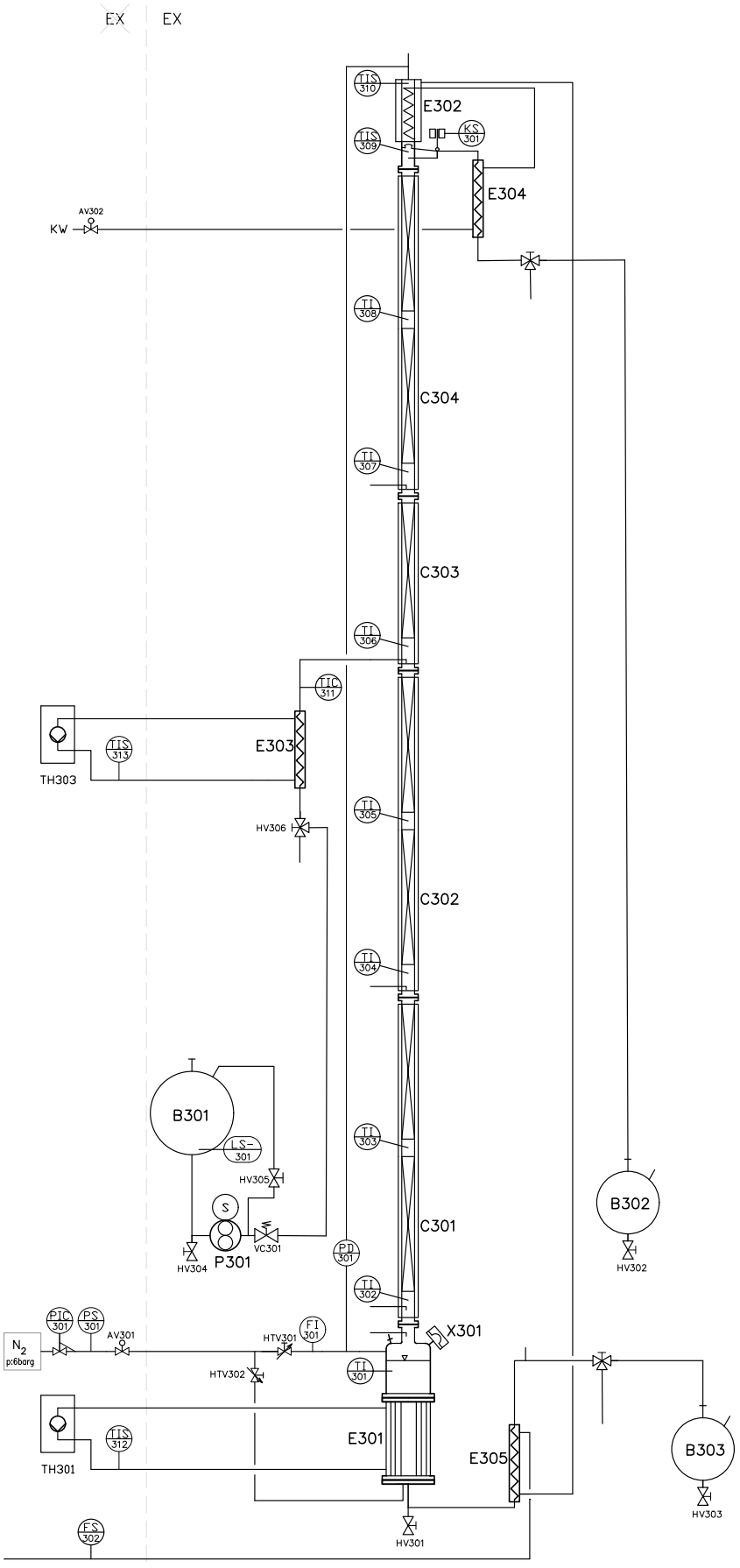

Figure 3.7 P&ID of the rectification pilot plant

hose is constantly flushed with N_2 to avoid the accumulation of liquids. The total flow of N_2 to the column is set to 35 cm^3/min. The N_2 exits at the top of the condenser. All vessels are connected via a hose system to avoid the buildup of pressure. Most of the components of the plant are placed in a vented housing for explosion protection.

The feed is weighted and stored in 5 l canister for the experiments. The scale for preparing the MeOH water mixture has a resolution of 5 g and the scale for the FC samples of 1g. If the integrated purification is investigated, the water MeOH mixture and FC sample is mixed in the canister before being poured into the storage vessel B301. As the reboiler is expected to contain mostly water, the reboiler is filled with deionized water for the start up. The start up phase aims at finding steady-state conditions as quickly as possible.

During the operation, the parameters are set according to the experimental schedule (see Table 6.2 in Chapter 6). The feed enter at T306 with a temperature of 65 °C. Steady-state conditions were found for a stable temperature profile across the column length. The start-up phase takes roughly 2 hours and between experiments, the steady state is reached roughly after one hour. The duration of experiments carry between 1 and 3 hours. Depending on the length of the experiment samples of the bottom and top product are taken several times. The mass flows of the top and bottom stream are collected in the storage vessels. After each experiment samples are taken from the storage vessels as the final value of the product.

The mass balance of the plant is calculated. The input is derived from the density of the feed and the volume flow of the feed. The output comprises the weight of product in the storage vessels B302 and B303. Additionally, the weight of the samples taken during operation are added. The mass based distillate to feed ratio is calculated with the feed stream and the top product. The feed stream, top product and bottom product are sampled. For each sample, the density is measured to calculate the water and MeOH content. Additionally, the total S and N content of the top and bottom samples is analyzed in order to close the elemental mass balance. Additionally, the water content was analyzed by Karl Fischer titration for the feed and top product.

3.7.4 Selective removal of impurities

Activated carbon (AC) or Fe(II) ions are used in experiments for the selective removal of impurities. The experiments can be divided in a more qualitative set of experiments for the determination of general process parameters and a quantitative set with triplets for each setting. The S and N concentration (Section 3.7.1) are determined before and after the experiments. A complete mass balance was not calculated for the process.

The MeOH samples from the pulp mill are filled together with either AC or Fe(II) ions, and a magnetic bar in a glass screw top bottle. The bottle is placed on a magnetic stirrer. AC is from Carl Roth (activated and pulverized). For the supply of Fe(II) ions, iron(II) chloride tetrahydrate (>98 %) was used. Experiments are run usually at 600 rpm. Time of reaction is varied between 1 and 24 hours. The temperature of the experiments is generally at room temperature (air-conditioned lab) except for one experiment at 0°C which was performed in an ice bath. For the qualitative experiments, 80 ml of crude MeOH are used. In the quantitative experiments the volume is reduced to 50 ml. For increasing the pH value, 2 ml of 5 M NaOH solution are added to the bottles to adjust the pH value to roughly 12. After the experimental run, the solid is filtered out with a paper filter. In case of the recycling of the AC, the AC is dried at 105 °C.

4 Process simulation of PtX routes

This chapter presents the mass and energy balance, economic evaluation, CO_2 balance and the process simulations of the integrated PtX production routes. The following processes were modeled:

- Methanol (4.4)
- Synthetic Natural Gas (4.5)
- Hydrogen peroxide (4.6)
- Acetic acid (4.8)
- Fischer Tropsch syncrude (4.7)

The theoretical background of the processes can be found in Section 2.6. The plants are scaled to two plant sizes with an electricity demand of the electrolysis of 50 MW_{el} or 150 MW_{el}. The processes were integrated into the pulp mill. For comparison of key performance indicators and CO_2 emissions, the greenfield plant are used as benchmark for comparison.

4.1 Carbon capture

MEA absorption, a well-established technology for carbon capture from flue gases emitted by power plants, is chosen for post-combustion capture to separate CO_2 [179, 55]. To determine the simplified mass and energy balances, reference data was utilized. A CO_2 capture rate of 90 % was assumed, although higher rates are possible. Higher capture rates would increase energy requirements and costs [179]. The reboiler duty for a 30 wt.% MEA solution ranges from 3.6 to 4.0 GJ/t CO_2 [180]. However, more advanced process configurations can reduce the reboiler duty to a range of 3.52 to 2.22 GJ/t CO_2 [181]. For this study, we assume a reboiler energy demand of 3.5 GJ/t CO_2 operating at 120°C [61, 182]. Cooling requirements were not considered. The electricity demand was estimated at 0.5 MJ/kg CO_2 [183]. CO_2 leaves the process at 25 °C and 1 bar.

4.2 Water electrolysis

The alkaline water electrolyser was chosen as technology for the calculations. Advantages in contrast to PEMEL are predominantly the lower cost [48, 49]. The flexibility of a PEMEL is also not required in case of operation in a pulp mill. The water electrolysis is modeled as a black box model satisfying the mass and energy balance of the process. The mass balance is based on reaction equation 2.16. The purity of H_2 and O_2 was set to 100 %. H_2 leaves the water electrolysis at a pressure of 30 bar and temperature of 80 °C. The investment cost of the electrolyser is 600,000 €/MW. The lifetime was assumed to 10 years. As base case, the efficiency of the electrolysis is chosen to be 70 % based on the LHV of H_2. This number is in line with literature data [48, 49]. The efficiency is supposed to increase to 74 % till 2050 according to Irena [48].

The operation of the water electrolysis releases heat. For a 1 GW electrolyser, the heat removal was assessed to 171 MW for a PEM electrolyser [184]. In this work the waste heat generation is assumed to be 20 % of the electrical power input. The rest (10 % electrical power input) is dissipated to the environment or is used for heating the incoming water to the required operating temperature.

4.3 CO_2 electrolysis

The CO_2 electrolysis model is based on the commercial process by Halder Topsoe called eCOs. It consists of a high temperature solid oxide electrolyser cell and membrane separation (see Appendix A). The reaction proceeds according to Equation 2.18 where CO_2 is reduced to CO on the cathode and O_2 evolves on the anode side. The model is based on a black box model that satisfies the mass balance as described by the reaction equation. Consequently, the carbon efficiency of the process is 100 %. Additionally the energy consumption was estimated to be 7 kWh/m^3 [85, 185]. The CO stream has a purity of 99.5 mol% [2]. Impurity arises only from CO_2 [2]. The CO stream is assumed to leave at 40 °C. The oxygen stream from the anode has a purity of 100 %. The economics for high temperature CO_2 electrolysis in literature are mostly based on a comparison of the process with established electrolysis technologies [186, 187, 188]. In this assessment 800,000 €/MW are used for the investment cost with a life time of 10 years. The cost are comparable to SOEL systems for H_2 production [48, 49, 189].

4.4 Production of methanol

The methanol (MeOH) models and results are presented in this section. Table 4.1 shows the four investigated cases. Since the pulp mill produces a MeOH rich stream at the evaporation plant, this stream is integrated with the Power-to-Methanol process in two cases indicated with "-FC". The condensed SOG is the methanol stream referred to here as "FC".

Table 4.1 Definition of cases for the MeOH models

Case	Plant size in MW_{el}	Foul condensate
50	50	-
150	50	-
50-FC	150	x
150-FC	150	x

4.4.1 Process design and modeling

The flowsheet of the MeOH model also including the pretreatment step for FC is depicted in Figure 4.1. As property method for the parts with high pressure RKSMHV2 was used. In the low pressure separation section the NRTL-RK model was applied. Henry components are defined for CO_2, CO, H_2S, NH_3 and H_2. The foul condensate treatment uses NRTL as property method. According to the IMPCA specification, the purity of MeOH must be higher than 99.85 wt. % and the water content should be below 0.1 wt. % [190]. Therefore in this simulation the purity for MeOH is set to 99.9 wt. %. The sulphur content, relevant for the cases with FC from the pulp mill, is limited to 0.5 mg/kg [190].

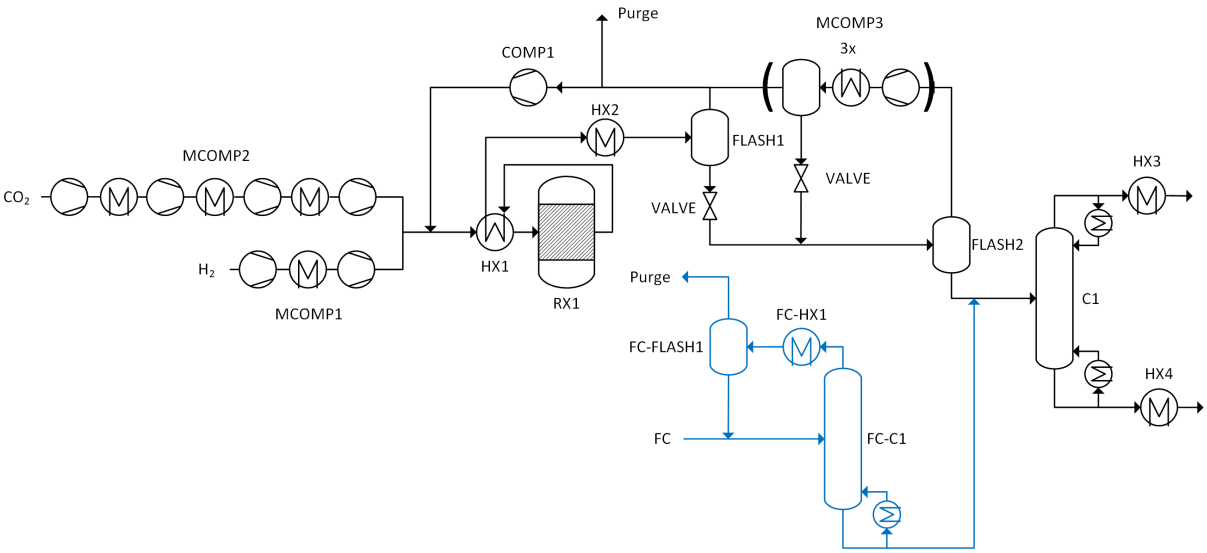

Figure 4.1 Flowsheet of the MeOH model in Aspen Plus. The pretreatment step for the foul condensate (FC) is shown in blue.

CO_2 is compressed in a four stage compressor with intercooling to the process pressure of 50 bar. H_2 is compressed in a two stage compressor with intercooling. The molar ratio of H_2 to CO_2 was set to 3:1 according to the stoichiometry of the reaction equation. The reactor feed is then mixed with the recyled gas stream and preheated before entering the reactor. The outlet temperature of the feed to the reactor was set to 215 °C with a temperature approach of 30 °C. The isothermal reactor at 250 °C is modeled with the kinetcis based on Vanden Bussche and Froment with adjustments by Mignard and Pritchard [191, 192]. Since the rection is exothermal, high temperature heat can be gained from

the reactor. A pressure drop of 2 bar in the reactor was assumed representing the pressure drop in the whole reaction section.

After preheating the feed stream to the reactor, the outlet stream from the reator is cooled to 55°C in order to separate the unreacted gas from the liquid products in FLASH1. The gaseous stream is compressed and recycled back to the reactor feed. A purge of 0.5 wt. % of the recycle stream ensures no accumulation of inert gases. The liquid product stream is degased in another flash drum FLASH2 after pressure reduction to 1 bar. The gaseous stream is compressed in a three stage compressor with cooling and liquid removal between the compressor steps. Liquids are returned to FLASH2. In the distillation column, water and MeOH are separated. The specifications are set to ensure a MeOH content of 0.2 wt.% in the waste water and a MeOH content at the top of 99.9 wt. %. The parameters of the distillation column C1 is shown in Table D.1 in the Appendix. Both waste water and MeOH are cooled to 30 °C.

For the integrated foul condensate treatment, one stripping column separates the light components like H_2S, DMS and NH_3. This pretreatment process is necessary to meet the required purities of sulphur in the final product. The composition of the foul condensate is given in Appendix D.1. Heat exchanger FC-HX1 cools the top product to 60 °C. In the flash separator, MeOH can be recovered as liquid phase. The settings of column F-C1 are also found in Table D.1 in the Appendix.

4.4.2 Technical and energetic analysis

The KPIs of the MeOH production process is summarized in Table 4.2. The carbon efficiency of the MeOH process is 95.8 %. When adding the FC, the carbon efficiency increases further which is based on the mathematical definition of the carbon efficiency. A carbon efficiency above 100 % is reached for 50 MW_{el}-FC as the MeOH output is increased along with no increased CO_2 input following the calculation as described in Equation 3.13. The same observation can be made for the hydrogen efficiency. The calculations incorporates the MeOH output but only the H_2 fed to the process as input. The Power-to-Fuel efficiency of the greenfield process without FC is 56.7 %. Due to the integration with the pulp mill it decreases for the 50 and 150 MW_{el} plant as the process reduces the availability of electricity.

Table 4.2 KPIs for MeOH processes (η_{PtF} in brackets is for greenfield plant)

Case	50 MW_{el}	150 MW_{el}	50 MW_{el}-FC	150 MW_{el}-FC
η_{CE}	95.8%	95.8%	102.2%	97.9%
η_{HE}	63.8%	63.8%	68.1%	65.3%
η_{PtF}	56.5% (56.7%)	55.5% (56.7%)	60.2% (60.5%)	56.7% (58.0%)

The mass balance of the process is shown in Appendix D.1. Furthermore, the mass balance of the contaminants (sulphur and nitrogen containing compounds, and terpenes) introduced with the foul condensate is shown in Table D.4 in the Appendix.

Table 4.3 presents the energy balance of the process. Besides electricity for water electrolysis, the MeOH process also requires electrical energy for compression and pumping which adds 7.4 MW_{el} for the 150 MW_{el} plants to the electricity demand. The integration also causes a higher electricity demand which is further explained in the next section. The energy input via FC is 2.2 MW_{th}. The MeOH production process is a net heat exporter for all cases. However, as shown via pinch analysis, the process requires steam from the pulp mill as not enough high temperature heat is available. The purge streams of the MeOH process and FC pretreatment process are used in the lime kiln and can replace up to 9 % of the thermal energy demand.

4.4.3 Integration

The impact of the MeOH plants on the pulp mill's utilities are depicted in Table 4.4. The O_2 demand of the pulp mill is met for all cases. Indeed, a huge surplus is generated. The increase in waste water

Table 4.3 Energy balance of MeOH process in MW_{el} or MW_{th} ([a] only MeOH considered)

Case	50 MW_{el}	150 MW_{el}	50 MW_{el}-FC	150 MW_{el}-FC
		Input		
Electricity total	52.7	160.9	52.7	161.0
- Water electrolysis	50.0	150.0	50.0	150.0
- Compression	2.5	7.4	2.5	7.4
- Integration	0.2	3.5	0.3	3.6
FC[a]	-	-	2.2	2.2
Heat	11.3	33.9	11.7	34.7
		Output		
MeOH	29.8	89.3	31.7	91.2
Heat	21.5	64.4	21.8	65.2
Purge	1.4	4.3	1.7	4.6

is marginal compared to the treated waste water in the pulp mill. The increase for deionized water is similarly marginal. With the process 3 and 10 % of the available CO_2 of the pulp mill must be captured for the 50 and 150 MW_{el} process. The purge streams can be combusted in the lime kiln and substitute up to 9 % of the heat demand for 150 MW_{el}-FC. The purge streams consist of purge from the head product of FC-C1 and of the recycle stream around the MeOH reactor.

Table 4.4 Impact of integrating the MeOH plants (Positive values for electricity generation due to heat integration means a drop in electricity generation)

	50 MW_{el}	150 MW_{el}	50 MW_{el}-FC	150 MW_{el}-FC	
		CO_2			
CO_2 separated	57,321	171,962	57,321	171,962	t/a
Share of total CO_2	3%	10%	3%	10%	
		O_2			
O_2 production	62,517	187,551	62,517	187,551	t/a
Coverage of O_2 demand	227%	680%	227%	680%	
		Waste water treatment			
Additional amount	22,747	68,241	24,450	69,966	t/a
Increase in waste water	0.1%	0.4%	0.2%	0.4%	
		Deionized water			
Additional amount	70,394	211,182	70,394	211,182	t/a
Increase in deionized water	0.4%	1.2%	0.4%	1.2%	
		Heat integration			
Electricity generation	1.55	4.66	1.60	4.78	MW_{el}
Process cooling demand	4.2	12.5	4.5	13.3	MW_{th}
		Lime kiln			
NG replaced	1.4	4.3	1.7	4.6	MW_{th}

The electricity availability in the pulp mill decreases by 1.55 to 4.78 MW_{el}. The detailed analysis on the electricity balance is presented in Table 4.5. Based on the pinch analysis, the electricity generation in the pulp mill will decrease due to a demand of the MeOH process for low and medium pressure steam. The detailed results of the pinch analysis are presented in Appendix D.1. The increase in electricity demand for waste water treatment, deionized water generation and process cooling is marginal. As the O_2 demand is covered by O_2 from water electrolysis, the O_2 plant can be shut down leading to an electricity availability of 1.43 MW_{el}.

Table 4.5 Effect of integration on the electricity balance of the pulp mill (positive values mean a decrease in electricity availability)

	50 MW_{el}	150 MW_{el}	50 MW_{el}-FC	150 MW_{el}-FC
Waste water treatment	0.00	0.01	0.00	0.01
Deionized water	0.02	0.06	0.02	0.06
O_2	-1.43	-1.43	-1.43	-1.43
Heat integration	1.55	4.66	1.60	4.78
Process cooling	0.06	0.18	0.07	0.19
total	0.20	3.48	0.26	3.60

4.4.4 CO_2 balance

The emission factor of MeOH is shown in Figure 4.2 for the variation of the used grid electricity emission factor. For the 50 MW_{el} plants, represented by horizontal lines in the figure, no electricity is imported from the grid. Since the purge streams can replace natural gas in the lime kiln, the resulting emission factor is -3 g CO_2/MJ for the 50 MW_{el} plant.

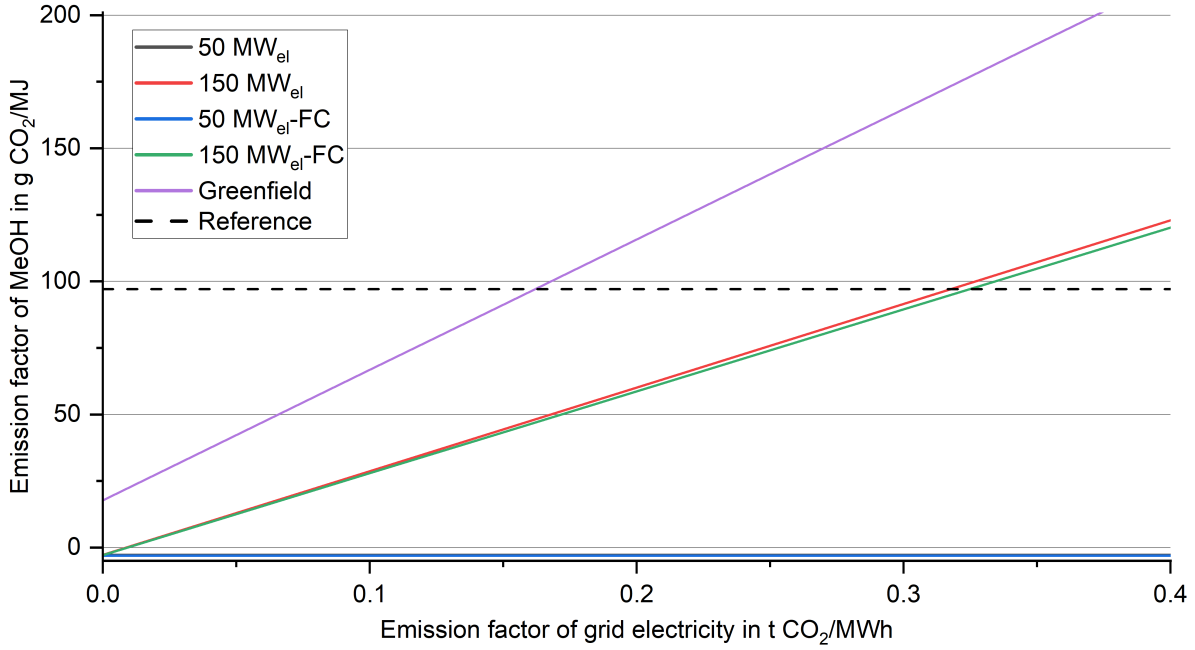

Figure 4.2 Impact of electricity emission factor on the emission factor of MeOH (Reference: 97.1 g CO_2/MJ for MeOH produced from natural gas [193])

The 150 MW_{el} plants show a linear increase with the emission factor of electricity. The intersection with the y-axis is at the same point as the corresponding plant with 50 MW_{el} input to the electrolysis. The slope of both curves is very similar. 150 MW_{el}-FC shows a slightly smaller slope since the product output is increased by the addition of the FC at an equal electricity demand compared to the 150 MW_{el} plants. The greenfield plant shows a higher y axis intersection point as the heat demand of the process is covered by steam generated from natural gas combustion (see Table D.6 in the Appendix). Furthermore, the curve is steeper since all electricity is taken from the grid. Consequently, the impact of the grid electricity is more severe on the product's emission factor. The comparison with the reference value for fossil MeOH gives a marginal emission factor of 0.16 t CO_2/MWh. For the integrated 150 MW_{el} plants the marginal emission factor is roughly at 0.32 t CO_2/MWh.

4.4.5 Economic analysis

The levelized cost of MeOH (LCOM) ranges from 1207 to 1500 €/t as shown in Figure 4.3. The detailed cost breakdown is shown in Table D.5 in the Appendix. The cases including FC have lower cost compared to their equivalent plant size without FC as the added FC increases the product amount with minor additional investment and operating cost. No cost is assigned to the FC. The LCOM drops by 6 and 2 % for the 50 and 150 MW_{el} plant size compared to the plants without FC.

The LCOM is dominated by the operating cost (84 % of TAC) and especially by electricity cost. For the 50 MW_{el} plant, the impact of electricity cost is the highest and accounts for 820 €/t MeOH. The revenue of O_2 sale is in the range of 67 to 72 €/t MeOH. The LCOM is also depicted in Figure 4.3 excluding the electricity cost. The resulting prices are able to be below current market prices (800 €/t). The LCOM without ACC is reduced by 195 to 244 €/t MeOH. Resulting cost are not competitive with current market prices.

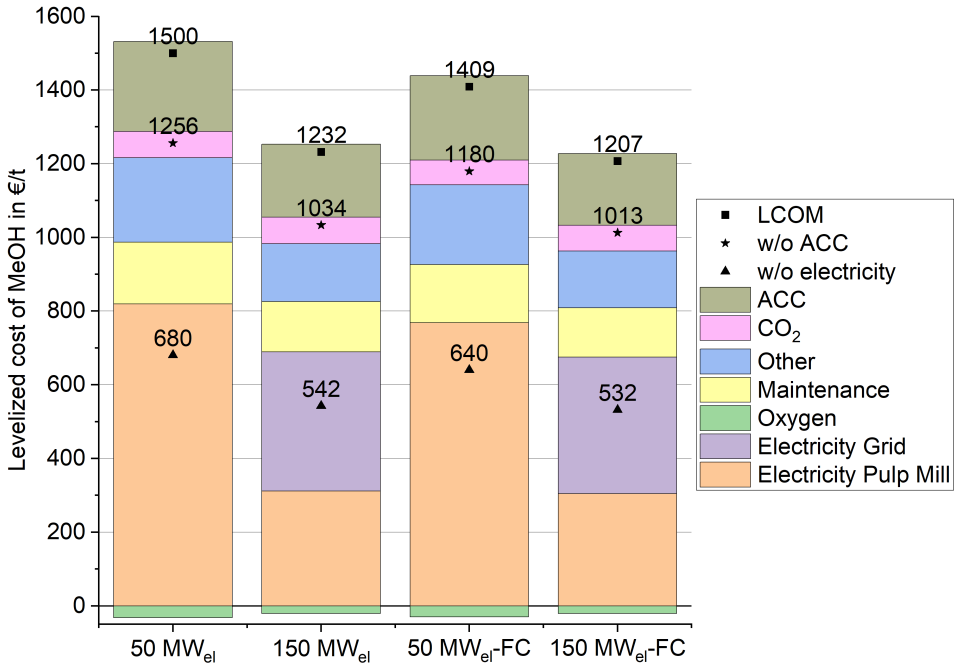

Figure 4.3 Levelized cost of MeOH

The increase in pulp selling price is calculated to a maximum of 85 €/ADt for the 150 MW_{el} plant (Table 4.6). Generally, the 50 MW_{el} plants have lower impact on the pulp price as the product amounts are roughly only one third of the larger plants but associated with higher LCOM. Furthermore, cases with FC show slightly lower prices than without FC. The CO_2 abatement cost are 303 and 349 €/t CO_2 for the 50 MW_{el} plants with FC and without FC. The abatement cost are not calculated for the 150 MW_{el} plants as the cases lead to an increase in CO_2 emissions.

Table 4.6 Increase in pulp selling price in €/ADt for market enumeration (800 €/t) of MeOH and CO_2 abatement cost in €/t CO_2

Case	50 MW_{el}	150 MW_{el}	50 MW_{el}-FC	150 MW_{el}-FC
Increase in pulp price	46	85	42	82
CO_2 abatement cost	349	-	303	-

The sensitivity analysis (see Figure D.1 in the Appendix) confirms the high impact of electricity related changes. The electricity cost shows changes in LCOM of up to 22 %. The cost and efficiency of water electrolysis also influence the LCOM substantially for all cases of up to 13 %.

4.4.6 Discussion

Table 4.7 summarizes studies on the production of MeOH from CO_2 and H_2 since 2019. The table might not be comprehensive. Further reading on process comparisons can be found here [194]. The operating pressure varies between 50 and 92 bar. The most used reactor type is the isothermal reactor operating at 210 to 290 °C. The other reactor modes show a bit wider range of temperatures. Temperatures below 200 °C can be considered unreasonable [104] and is only found in one case. The reactor temperature is a tradeoff between per pass conversion due to the exothermicity of the reaction and the recoverable heat desirably at higher temperatures.

Carbon efficiencies range from 56.6 to 100 %. Due to purge streams, by-product formation and dissolved CO_2 or CO in the liquid streams leaving the process, high carbon efficiencies of 100 % are unreasonable. The lower range of carbon efficiency also seems unreasonable since the process should be optimized to convert as much carbon as possible to MeOH. Most studies report efficiencies above 90 % which is a reasonable value. The Power-to-Fuel efficiency depends on the efficiency of the electrolyser. As SOEL usually reaches higher efficiencies, the resulting PtF efficiency also shows higher values of up to 79 %. For the low temperature electrolysers (usually between 60 and 70 % efficiency), the PtF efficiency ranges between 40 and 60 %.

The plant sizes cover a wide range from 5.9 to 1904 (with electrolysis efficiency of 70 % for [195]) MW_{el}. The LCOM range from 325 to 2646 €/t. Almost all studies report cost below 1000 €/t. The comparison of cost between the lowest reported LCOM is difficult as all studies have different assumptions and boundary conditions. The comparison of electricity cost would be the most valuable parameter to explain the low cost. Zhang et al. report levelized cost below 500 €/t with an electricity price of 62 €/MWh, a high O_2 selling price of 150 €/t O_2 and a high efficiency electrolysis [196]. Schemme et al. and Cordero-Lanzac et al. use a H_2 price of 4.6 €/kg and 3.0 €/kg [197, 198]. The H_2 price in this thesis just based on investment for the electrolysis and electricity cost equals 3.6 or 4.7 €/kg for grid electricity or electricity from the pulp mill. The cost breakdown does not show how the low cost are derived for these publications with extraordinary low LCOM.

Concerning the CO_2 balance, the pulp mill integrated plants show great potential to produce low emission MeOH. The green heat available at the pulp mill is one advantage compared to greenfield plants. Furthermore, the integrated 150 MW_{el} plant can almost produce MeOH that is competitive with MeOH derived from fossil resources based on the German grid mix. For lower emission factors of grid electricity, the plant can easily reach the emission reductions of 70 % as defined by the European Union [210]. For the integrated plants, the emission factor for grid electricity is at roughly 0.1 t CO_2/MWh to reach the 70 % emission reduction. For the greenfield plant the emission factor is 0.02 t CO_2/MWh which can hardly be reached by any means of renewable electricity generation.

4.4.7 Intermediate summary

The production of MeOH via CO_2 hydrogenation was presented in this section. The main findings are:

- The MeOH produced by CO_2 hydrogenation combined with the MeOH from the pulp mill reaches for all plant sizes the required purities of the final product. The FC stream (2.2 MW_{th}) increases the product output and can be valorized.
- The Power-to-MeOH process shows high carbon efficiencies. With FC, the carbon efficiencies can mathematically be increased. The Power-to-Fuel efficiency reaches 56.5 % for the 50 MW_{el} plant. Compared to the greenfield plant, the efficiency is decreased due to the integration with the pulp mill.
- The integration with the pulp mill shows an increased heat demand of the process for low and medium pressure steam which leads to a reduced electricity production. Waste water amount, deionized water demand and cooling demand increase only marginally compared to

Table 4.7 Comparison of studies on the utilization of H_2 and CO_2 for MeOH production since 2019 (numbers are calculated for the LHV if not otherwise stated, [a] based on HHV, [b] Internal rate of return calculation, [c] based on net present value calculation, [d] including heat, electricity and hydrogen, [e] 1 RMB = 0.13 €

Author and year	Electrolyser technology and efficiency	Plant size	Reactor type	Operating pressure (in bar)	Operating temperature (in °C)	η_{CE}	η_{PtL}	Product price	Reference
This work	AEL, 70 %	50 MW_{el} + 150 MW_{el}	isothermal	50	250	95.8 - 102.2 %	55.5 - 60.2 %	1207 - 1500 €/t	-
Adnan and Kibria 2020	PEM, 60 %	475 MW_{el}	-	67	147 - 238	96.5 %	44 %	723 €/t (optimistic: 357 €/t)	[199]
Battaglia et al. 2021	AEL, 56%	10 MW_{el}	isothermal	65	250	86.6 %	42.3 %	846 - 2646 €/t	[200]
Chen et al. 2019	-, 60 %	545 MW_{el}	isothermal	71	255	83.6 %	47.6 % [a]	NPV [c] and IRR [b]	[201]
Cordero-Lanzac et al. 2022	-, 68 %	721 MW_{el}	isothermal	50	300	56.6 %	49.1 %	483 €/t	[198]
Gu et al. 2022	PEM, 80%	8.6 / 86 MW_{el}	isothermal	50	250	86.0 %	61.0 %	325 - 1281 €/t [e]	[202]
Khojasteh-Salkuyeh et al. 2021	PEM, 64 %	465 MW_{el}	2x polytropic	92	215 - 268	90.9 %	47.8 %	-	[203]
Meunier et al. 2020	AEL, 62 %	687 MW_{el}	adiabatic	80	250 - 314	95.4 %	50.3 %	716 €/t	[204]
Nieminen et al. 2019	AEL, 70 %	30 MW_{el}	adiabatic	51	215 - 274	80.5 %	41.9 %	963 €/t	[205]
Nyári et al. 2020	-	1333 MW_{H2}	isothermal	50	230	98.4 %	84.4 % [d]	852 €/t	[195]
Parigi et al. 2019	SOEL, 98 %	10 MW_{el}	isothermal	75	270	57.9 %	58.8 %	≈ 611 €/t	[206]
Schemme et al. 2020	PEM, 70 %	300 MW_{MeOH}	isothermal	80	250	100 %	57.6 %	431 €/t	[197]
Sollai et al. 2023	PEM, 60 %	5.9 MW_{el}	adiabatic	65	210 - 290	95.1 %	46.9 %	960 €/t	[207]
Wang et al. 2019	SOEL, 79 %	multiple	isothermal	70	260	-	66 %	1000 - 1100 €/t	[208]
Yousaf et al. 2022	SOEL, 97 %	416 MW_{el}	isothermal	78	210 - 284	92 %	79 %	990 €/t	[209]
Zhang et al. 2019	SOEL, 90 %	107-108 MW_{el}	isothermal	78	290	90.6 %	68 - 69.4 %	473 - 495 €/t	[196]

the amounts processed in the pulp mill. The pulp mill's O_2 demand can be fully satisfied. The purge streams are energetically used to replace natural gas in the lime kiln.

- The 150 MW_{el} plants show marginal emission factors at roughly 0.32 t CO_2/MWh. The 50 MW_{el} plants show a slightly negative emission factor as no electricity is imported from the grid and natural gas can be substituted in the lime kiln.
- The levelized cost are between 1207 and 1500 €/t with the electricity cost as the most important cost factor. The plants with integrated FC purification show lower product cost. The CO_2 abatement cost are 303 and 349 €/t CO_2 for the 50 MW_{el} plants with and without FC purification. The increase in pulp price ranges from 42 to 85 €/ADt.

4.5 Production of synthetic natural gas

In the following section, the process for the production of SNG from H_2 and CO_2 is introduced and results are presented. Plant sizes with 50 and 150 MW_{el} electricity input to the electrolysis were investigated.

4.5.1 Process design and modeling

Figure 4.4 shows the flowsheet of the SNG model implemented in Aspen Plus. The model uses the Soave-Redlich-Kwong property method which is suitable for hydrocarbon processing and gas processes.

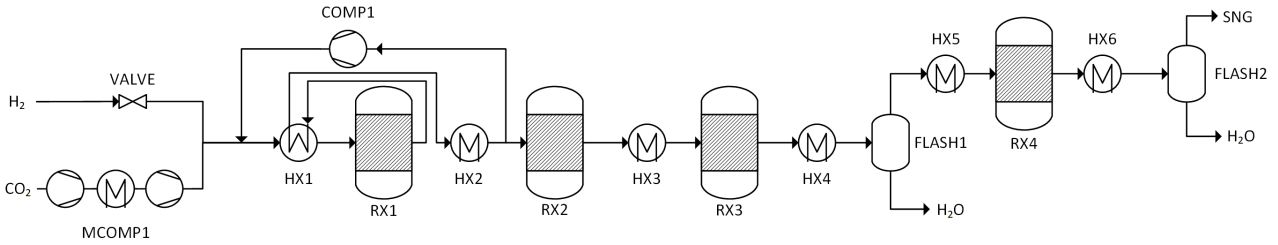

Figure 4.4 Flowsheet of the SNG model in Aspen Plus

CO_2 is compressed in a two stage compressor with inter-cooling to 12 bar. H_2 is throttled from 30 to 12 bar. Together with the recyle stream, the gas is preheated in HX1 by cooling the outlet of reactor RX1. The outlet temperature in this heat exchanger for the cold stream entering the reactor is set to 300 °C with a temperature approach of 30 °C. RX1 and all other reactors are modelled as adiabatic reactors with the kinetic model based on Neubert et al. [211]. The kinetic model is retrieved from Zang et al. including the adjustments of Rönsch et al.[212, 213]. A pressure drop of 0.5 bar was assumed in each reactor to also take into account losses in other parts of the plant like heat exchangers. The gas after RX1 has a temperature of 606 °C. It is cooled to 300 °C after HX2. The stream is split and 65 wt.% is recycled back to RX1 via compressor COMP1. The other gas stream follows a series of adiabatic reactors with inter-cooling and two water knockout drums. The gas in RX2 is heated from 300 °C to 499 °C. It is cooled in HX3 to 250 °C. The temperature after RX3 increases to 377 °C. HX4 reduced the temperature to 25 °C. The condensed water is removed in FLASH1 (adiabatic). After the flash drum the gas stream is preheated to 250 °C before it enters reactor RX4. After cooling the reactor outlet stream to 20 °C, the condensed water is removed in another flash drum. The resulting SNG contains 95.4 mol% CH_4, 3.8 mol% H_2, 0.5 mol% CO_2 and 0.2 mol% H_2O. If the SNG shall be fed to the grid further adjustments to reach the required specification might be necessary like for example drying.

The temperatures occurring in the reactors are in the range of available catalyst from Haldor Topsoe (250 - 700 °C) [114]. Reactors are sized to reach a GHSV of 4000 h^{-1} with a bed porosity of 0.44 [214]. Reactors have a length of roughly 4 to 6 m. The diameter was sized according to the reactor volume.

4.5.2 Technical and energetic analysis

Table 4.8 shows the KPIs for the SNG processes. Carbon and hydrogen efficiency are the same for all processes since the process design is independent of plant size. In terms of carbon efficiency, the SNG production reaches a very high efficiency which is due to the high conversion and the once through process design with no purge streams. The calculation includes only methane as product. Carbon is lost via the waste water and as unreacted CO_2 or CO in the SNG. The hydrogen efficiency is below 50 % with water production through the SNG reaction being the major loss.

Table 4.8 KPIs for SNG processes (η_{PtF} in brackets is for greenfield plants)

Plant size	50 MW_{el}	150 MW_{el}
η_{CE}	98.4%	98.4%
η_{HE}	49.2%	49.2%
η_{PtF}	58.9% (56.5%)	57.7 % (56.5%)

The Power-to-Fuel efficiency depends on the plant size for the integrated plants since integration does not scale linearly with plant size. For this reason, the 50 MW_{el} plant shows a by 1.2 % higher efficiency than the 150 MW_{el} plant. For the greenfield plant, the efficiency is due to no synergistic integration effects lower and independent of plant size.

The energy balance of the SNG plants (Table 4.9) shows a surplus of heat which can be used effectively in heat integration as discussed later. The SNG output is at 28.9 and 86.7 $MW_{th,LHV}$ for the 50 and 150 MW_{el} plant. Besides electricity to the water electrolysis, the process needs electricity for the compressors in the SNG process and for pumping in the MEA process. The amount of additional electricity needed is canceled out by the electricity demand through integration with the pulp mill for the 150 MW_{el} plant. For the 50 MW_{el} plant the electricity demand through integration can excel the demand for compression and pumping. The mass balance of the process is shown in Appendix D.2.

Table 4.9 Energy balance of SNG process in MW_{el} or MW_{th}

Plant size in MW_{el}	50	150
Input		
Electricity total	49.1	150.2
- Water electrolysis	50.0	150.0
- Compression and pumping	1.2	3.7
- Integration	-2.1	-3.4
Heat	6.0	17.9
Output		
SNG	28.9	86.7
Heat	20.3	61.0

4.5.3 Integration

The impact of the SNG process on the pulp mill's utilities is shown in Table 4.10. Generally, the increase in waster water and deionized water demands are marginal in comparison to the mass flows already processed in the pulp mill. The SNG plants are only capable to process 3 or 8 % of the total available CO_2. With O_2 as by-product, the pulp mill is able to cover the O_2 demand. Steam generated with excess heat can be used for the generation of 0.72 or 2.16 MW_{el}.

The overall impact on the electricity balance of the pulp mill is shown in Table 4.11. A marginally increased energy demand is calculated for waste water treatment, deionized water and process cooling. Since the supply of O_2 can be completely satisfied by water electrolysis, 1.43 MW_{el} of the O_2 plant become available. Additional electricity can be generated in the turbines by the utilization of excess heat from the process. Especially high pressure steam can be generated in the SNG processes. In Appendix D.2 you find details on the heat integration. Since the savings of O_2 production do not scale with plant size, the surplus electricity for the 50 MW_{el} plant size will have a higher impact than for the larger plant size.

Table 4.10 Impact of integrating the SNG plants (Positive values for electricity generation due to heat integration means a drop in electricity generation)

Plant size in MW_{el}	50	150	Unit
CO_2			
CO_2 separated	42,991	128,974	t/a
Share of total CO_2	3%	8%	
O_2			
O_2 production	62,516	187,549	t/a
Coverage of O_2 demand	227%	680%	
Waste water treatment			
Additional amount	35,103	105,310	t/a
Increase in waste water	0.2%	0.7%	
Deionized water			
Additional amount	70,393	211,180	t/a
Increase in deionized water	0.4%	1.2%	
Heat integration			
Electricity generation	-0.72	-2.16	MW_{el}
Process cooling demand	2.3	6.8	MW_{th}

Table 4.11 Effect of integration on the electricity balance of the pulp mill (positive values mean additional electricity demand)

Plant size in MW_{el}	50 MW_{el}	150 MW_{el}
Waste water treatment	0.00	0.01
Deionized water	0.02	0.06
O_2	-1.43	-1.43
Heat integration	-0.72	-2.16
Process cooling	0.03	0.10
Total	-2.10	-3.43

4.5.4 CO_2 balance

Since the emission factor of SNG is massively dependent on the carbon intensity of electricity (if imported from the grid), Figure 4.5 shows the emission factor of SNG over the emission factor of the grid electricity. For the integrated 50 MW_{el} plant, the emission factor is calculated to 0 g CO_2/MJ, as it is independent of the grid electricity. For the integrated plant with 150 MW_{el}, part of the electricity is sourced from the grid and therefore the grid electricity influences the emission factor of SNG. Furthermore, the integration with the pulp mill allows for a higher electricity production reducing the need for electricity from the grid (see Table 4.11). For the greenfield plants, all electricity is taken from the grid. A small credit is given for the production of surplus heat which replaces natural gas as energy source. The emission factor for the integrated plant is damped due to the electricity supply from the pulp mill indicated by the decreased slope compared to the greenfield plant's slope.

This fact also becomes obvious when looking at the marginal emission factor for electricity. Natural gas as reference is shown as the dashed horizontal line with a value of 55.8 g CO_2/MJ [215]. The intersection with this line represents the emission factor for electricity to yield SNG with an emission factor equal to the fossil equivalent. The marginal emission factor for the 150 MW_{el} plant are 0.124 for the greenfield or 0.193 t CO_2/MWh for the integrated plant.

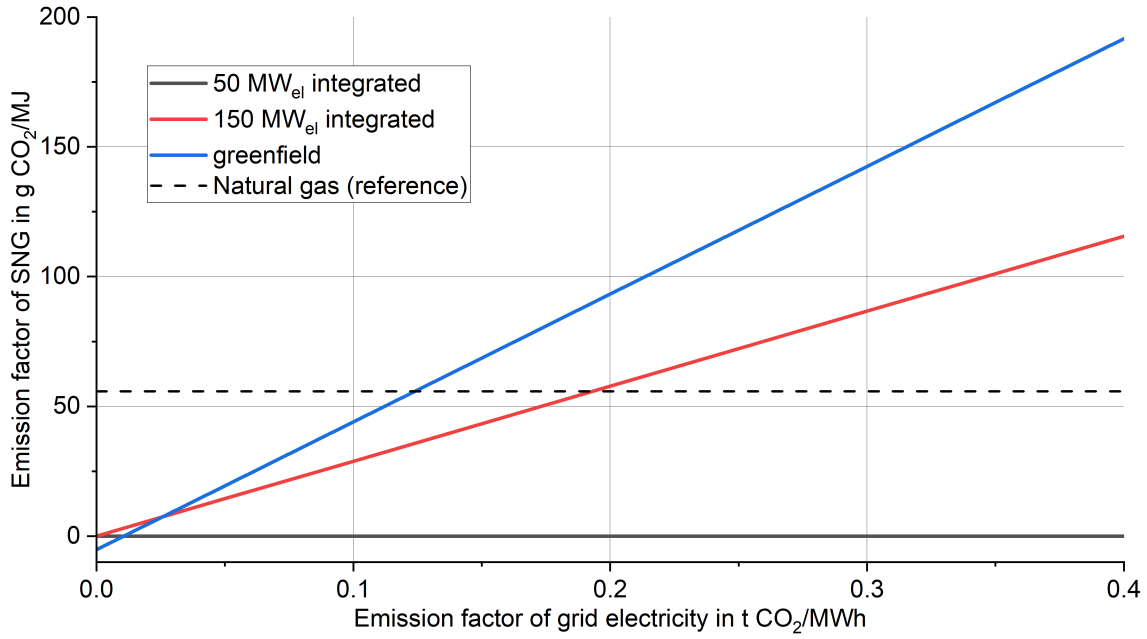

Figure 4.5 Impact of electricity emission factor on the emission factor of SNG (Reference: Natural gas with 55.8 g CO_2/MJ [215])

4.5.5 Economic analysis

The levelized cost of SNG (Figure 4.6) are calculated for 50 and 150 MW_{el} to 240 and 206 €/MWh. The difference in cost between the plant size is derived from the lower cost for the grid electricity and the economy of scale for the capital cost which also translates to other cost categories like for example maintenance. However, only the chemical plant profits from the economy of scale as the electrolysis has a scaling factor of 1. Comparing the levelized cost of SNG to market prices of 25 €/MWh shows the immensely higher cost for SNG. Of course, natural gas is traded on the market with prices variation that can lead to making SNG more competitive. Main cost drivers of the LCOSNG are electricity and the annualized capital cost which account for roughly 58 % and 15 %. The water electrolysis accounts for 80 % or 89 % of the investment cost for the 50 and 150 MW_{el} plant.

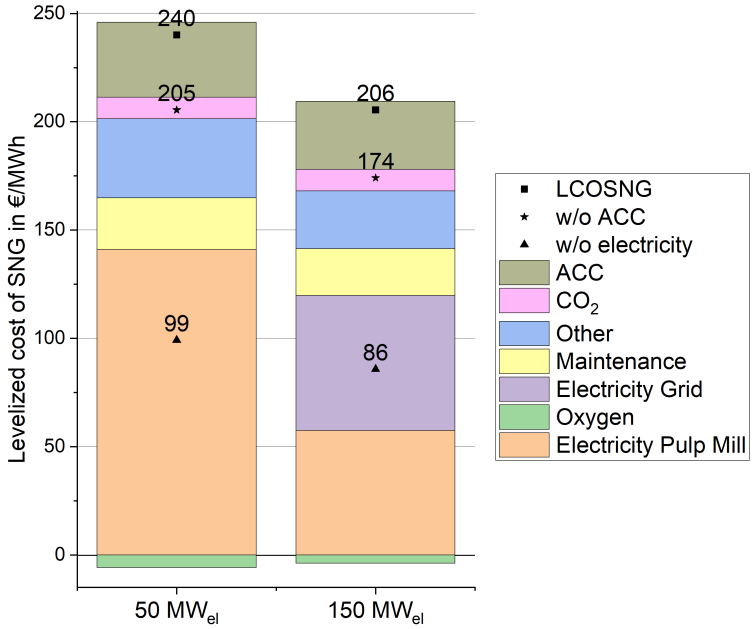

Figure 4.6 Levelized cost of SNG

Since the electricity cost has a very high share, Figure 4.6 shows the levelized cost for an electricity price of 0 €/MWh. For free electricity, the cost drops to 100 or 86 €/MWh which is still a 3 to 4 fold increase compared to the normal market price for natural gas. The stars display the cost without capital cost. Here the levelized cost are reduced by about 35 €/MWh.

The sensitivity analysis in Appendix D.2 shows that electricity related changes have a major impact on the levelized cost of SNG. First of all, the electricity price either for grid electricity or electricity from the pulp mill has a major impact on the cost. It is very obvious that the impact of electricity cost on the total cost predominate. Furthermore, the efficiency of the water electrolysis can change the LCOSNG by roughly + 14 % or by -12 % for both plant sizes. The change in efficiency influences the electricity cost and the investment cost of the electrolysis at the same time. The investment cost of the water electrolysis has a medium strong effect on the LCOSNG. The impact of annuity, CO_2 price and maintenance cost is the smallest for both plant sizes.

The increase in pulp price to cover the SNG sold at market price (25 €/MWh) would be 76 and 192 €/ADt pulp for the smaller and larger plant size. CO_2 abatement cost are calculated to 1076 €/t CO_2 for the 50 MW_{el} plant. Abatement cost are not calculated for the 150 MW_{el} plant since CO_2 emissions are increasing for the German grid mix.

4.5.6 Discussion

Table 4.12 shows recent studies on the production of SNG from CO_2 and H_2. For all studies, the H_2/CO_2 equals 4 which is the stoichiometry of the reaction (see reaction 2.31). Studies on co-electrolysis are not included. However, co-electrolysis shows higher efficiencies and better economics compared to a SOEL for pure H_2 production [216, 217].

Comparing the levelized cost of SNG to market prices for natural gas reveals a big difference. The calculated cost for the integrated cases show 8 to 10 fold higher prices considering a natural gas price of 25 €/MWh. The levelized cost represent production cost not including a revenue for the manufacturer meaning that real market prices must be even higher than the LCOSNG. A green premium can be expected for sustainable SNG. However, this premium is very unlikely to cover the gap between market price and LCOSNG.

SNG prices shown in Table 4.12 generally also show tremendously higher cost in comparison to natural gas. Prices range from 28 to 567 €/MWh. However, a detailed comparison is difficult since economic and technical assumptions differ. The wide scattering indicate the impact of different assumption. Just considering electricity cost and the PtF efficiency of the greenfield process (56.5 %), an electricity price of 14 €/MWh must be applied to reach a LCOSNG of 25 €/MWh. Therefore, very low LCOSNG as calculated by some studies seem very unrealistic.

The PtF efficiency comparison shows also a wide scattering with values mostly above 60 %. Due to the higher efficiency of the SOEL, one would expect even higher PtF efficiency. This relation is however not clearly visible from the data.

4.5.7 Intermediate summary

The production of SNG via CO_2 hydrogenation integrated in a pulp mill was presented. Main findings are:

- The LCOSNG are calculated to 240 and 206 €/MWh for the 50 and 150 MW_{el} plant size. The price clearly exceeds the natural gas price. Main cost driver is the electricity cost.
- Carbon efficiencies of the process are very high (98.4%) due to the almost full conversion and once through process layout without purge streams. Consequently, captured CO_2 can efficiently be converted to SNG.
- Through integration with the pulp mill, waste heat from the SNG process can generate additional electricity in the pulp mill. Together with savings from the O_2 production, the process integration shows a net positive electricity balance. The O_2 demand can be met by the O_2 from the water electrolysis.
- The PtF efficiency of a greenfield plant is 56.5 %. With the pulp mill integration, the efficiency is increased by the electricity surplus of integration to 58.9 and 57.7 % for the 50 and 150 MW_{el} plant.
- The marginal emission factor for grid electricity is 0.124 t CO_2/MWh (150 MW_{el} plant). The integrated plant can more effectively reduce the emission factor of SNG compared to a greenfield plant. One downside of SNG is that it cannot in contrast to other processes substitute natural gas by purge stream combustion in the lime kiln.

A detailed evaluation of using SNG in the lime kiln of the pulp mill is presented in Chapter 5.

Table 4.12 Comparison of studies on the utilization of H_2 and CO_2 for SNG production (F: Flash separation of water, M: membrane separation, MEA: MEA scrubber, MDEA: MDEA scrubber, L: Liquefaction, The numbers are calculated for the LHV if not otherwise stated), [a] H_2 to SNG efficiency, [b] Power to SNG efficiency, [c] including heat, [d] lowest cost in 2021, [e] recycle around the first adiabatic reactor

Author and year	Electrolyser technology	Plant Size	Process Layout	Product upgrading H_2O / H_2 / CO_2	Operating pressure (in bar)	CH_4 content in product (in mol%)	Energy efficiency	Product price	Reference
This work	AEL	50 MW_{el} + 150 MW_{el}	see Figure 4.4	F/-/-	12	95.4 %	58.9 %/57.7 %	240/206 €/MWh	-
Becker et al. 2018	PEM	40 t H_2/d	3 x isothermal reactors in series with water separation after each reactor	F/MDEA/M	20	92.7 %	83.2 % [a]	24 - 237 €/MWh	[218]
Chauvy et al. 2020	PEM	90 MW_{el}	4x adiabatic reactor[e] (T_{in} = 350 °C)	F+M/M/-	10	92.9 %	72.6 %	115 €/MWh	[214]
Chauvy et al. 2021	PEM	10 MW_{el}	4x adiabatic reactor[e] (T_{in} = 350 °C)	F/-/-	10	71.5 %	89.5 % [c]	171 €/MWh	[219]
De Saint Jean et al. 2014	SOEL	876 kW_{el}	4x adiabatic reactor[e] (T_{in} = 300 °C)	F/M/MEA	7.4	96.8 %	74.5 % (HHV) [b]	-	[220]
De Saint Jean et al. 2015	SOEL	879 kW_{el}	4x adiabatic reactor[e] (T_{in} = 300 °C)	F/M/MEA	6.8	97.3 %	75.8 % (HHV) [b]	304 - 567 €/MWh_{HHV}	[221]
Eveloy 2019	SOEL	5.6 MW_{el}	3x adiabatic reactor with intercooling and water separation after 2nd and 3rd reactor	F/-/-	30	95.9 %	74.5 % [c]	-	[222]
Giglio et al. 2015	SOEL	10 MW_{el}	4x adiabatic reactors with intercooling	F/-/-	32.4	94.0 %	76.0 %	48 - 94 €/MWh	[216, 217]
Giglio et al. 2018	SOEL	10 MW_{el}	3x adiabatic reactors with subsequent CO_2 addition and water flash	F/-/-	15	95.0 %	77.4 % [b]	-	[223]
Gutierre-Martin and Rodriguez-Anton 2016	AEL	439 MW_{el}	1) 3x adiabatic[e] (T_{in} = 200 °C) 2) 4x adiabatic (T_{in} = 200 °C) + 1x isothermal (T = 200 °C) 3) 4x adiabatic (T_{in} = 200 °C) + 1x isothermal (T = 200 °C) with CO_2 addition 4) 2x adiabatic reactor with water separation after each reactor[e]	F/-/-	10	94.7 %	83.3 % [a]	29 - 80 €/MWh	[224]
Ipsakis et al. 2021	AEL	2200 MW_{el}	1x isothermal reactor (T = 300 °C)	F/-/-	10	90,5 %	-	ROI calculation	[225]
Momeni et al. 2021	PEM	1697 MW_{el}	1x isothermal reactor (T = 300 °C)	F/?/?	10	100 %	57.3 % [b]	106 - 130 €/MWh	[226]
Morosanu et al. 2018	AEL	200 kW_{el}	1) 5 x adiabatic with intercooling (T_{in} = 250 °C) 2) 1x adiabatic (T_{in} = 250 °C) + 1x isothermal reactor (T = 280 °C) 3) 2x isothermal reactor (T = 280 °C)	F/-/-	10	1) 91.2 % 2) 95.1 % 3) 98,3 %	-	-	[227]
Parigi et al. 2019	SOEL	10 MW_{el}	2x isothermal reactor (T = 300 °C)	F/-/-	15	97.9 %	77.1 %	available	[206]
Perna et al. 2020	PEM	1-6 MW_{el}	4x adiabatic reactor (T_{in} = 250 °C)[e]	F+M/-/-	20	95.9 %	44.3 %	-	[228]
Peters et al. 2019	PEM	8 MW_{el}	1) 1x isothermal 2) 1x isothermal + 1x adiabatic 3) 1x isothermal + 1x adiabatic 4) 1x isothermal + 1x adiabatic 5) 4x adiabatic	F/L/MEA	10/25/30	92.5 %	80.7 - 81.5 %[a]	253 - 279 €/MWh	[229]
Salomone et al. 2023	AEL/PEM	-	3x isothermal reactor with CO_2 addition and water removal	F/-/-	15	97.5 %	-	-	[230]
Qi et al. 2022	SOEL	10 MW_{el}	3x adiabatic reactors (T_{in} = 250 °C)[e]	F/-/-	30	96.0 %	77.2 %	166 €/MWh^{d}	[231]
Wang et al. 2019	SOEL	-	1x isothermal reactor (T = 290 °C)	F/M/M	6	-	98 % 76 %	> 180 €/MWh	[208]

4.6 Production of hydrogen peroxide

This section is concerned with hydrogen peroxide (H_2O_2) production. Table 4.13 shows the three investigated cases. H_2O_2 is used in the pulp mill for pulp bleaching. The pulp mill is supplied with a 50 to 60 wt. % solution of H_2O_2 which is further diluted for application in the pulp mill. In all investigated cases a stream of crude H_2O_2 will be directly used onsite without purification (water removal). The H_2O_2 for the market is purified to 70 wt. %. Three plant sizes are investigated with one being able to exactly cover the H_2O_2 demand of the pulp mill.

Table 4.13 Definition of cases for the H_2O_2 models

Case	Plant size in MW_{el}	Purification
6	5.5	no
50	50	partial
150	150	partial

4.6.1 Process design and modeling

The production process of H_2O_2 is based on the commercial anthraquinone process as described in Section 2.6.5. Figure 4.7 shows the model as implemented in Aspen Plus. The model uses UNIF-LL and NRTL as property methods. Henry components are not used for simplicity. UNIF-LL is suitable for polar, non-electrolyte processes at low pressure with two liquid phases as present in the working solution. The method is limited to a certain temperature range (10 - 40 °C) which is exceeded in parts of the model. Furthermore, the method is only advised for preliminary design calculations. However, it is the best fit for the process type and conditions. NRTL is used for the calculations in the purification section.

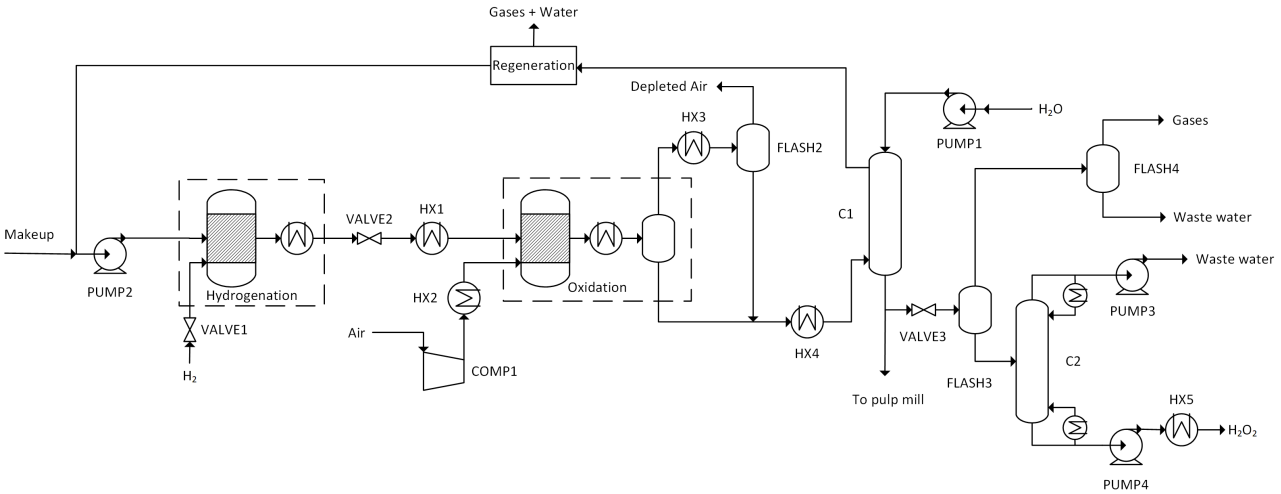

Figure 4.7 Flowsheet of the H_2O_2 model

The working solution consists of the quinone and a solvent mixture. 2-ethyl anthraquinone (AQ, CAS: 84-51-5) is used as quinone which is the most commonly used one [116]. 2-ethyl anthrahydroquinone (AHQ) is not available in the databank and was therefore added by drawing the molecular structure. The quinone concentration in the working solution is 17 wt. % which is the lower bound reported in [232]. In the hydrogenated form it is soluable in polar solvents [115]. Tributyl phosphate (CAS: 126-73-8) is used as the hydroquinone solvent [115] which is supposed to have a concentration of 18 - 35 wt. % in the working solution [232]. The actual concentration in the working solution is set to 25 wt. %. The quinone solvent is supposed to be nonpolar and aromatic. A mixture of

1,3,5-trimethylbenzene (CAS: 108-67-8) and 1,2,3,5-tetramethylbenzene (Isodurene, CAS: 527-53-7) is used as quinone solvents. Isodurene has a concentration of 17 wt. % in the working solution (11 - 42 wt. % [232]). The concentration of 1,3,5-trimethylbenzene is set to 42 % (40 - 60 wt. % [232]).

In the hydrogenation reactor, H_2 and AQ react to AHQ as shown in Equation 4.1. The reaction is catalysed by a palladium catalyst [115]. The hydrogenation reactor can be either designed with a fixed bed catalyst or slurry catalyst system. However, in this model the catalyst presence and reactor design are neglected. The reactor was modeled as RStoic reactor with a heat exchanger for correcting the energy balance of the process step. The conversion of Equation 4.1 is set to 60 % which is in line with literature [116, 233]. The reactor was set to isothermal conditions. A pressure drop of 0.5 bar was assumed. The operating temperature range as reported in literature (40 to 75 °C [116, 232, 233]) is considered. The feed enters the adiabatic reactor with 33 °C. Through the exothermic reaction, the temperature of the stream leaving the reactor rises to 60 °C. The energy balance of the reactor was corrected with the heat exchanger. The released heat during the reaction is calculated with a calculator block. The reaction releases 103.79 kJ/mol [233]. The heat exchanger heats the outlet of the reactor to the correct temperature. Full conversion of H_2 is assumed.

$$H_2 + AQ \longrightarrow AHQ \tag{4.1}$$

The outlet stream of the hydrogenation reactor is throttled to 1.5 bar before the oxidation reaction (Equation 4.2). Before the oxidation reactor the stream is cooled in HX1 to 35 °C. Together with air (inlet conditions: 1 bar and 25°C), which is compressed to 1.5 bar in COMP1, the streams are fed to the reactor. Air enters the process with the composition as indicated in Appendix B.1. The oxidation reactor is modeled as RStoic reactor with heat exchanger and gas-liquid separation. The pressure drop was set to 0.5 bar. The conversion is set to 99 %. The heat of reaction is again adjusted by the heat input of the heat exchanger. The reaction releases 84.92 kJ/mol [233]. The gas phase is separated in the flash operating under adiabatic conditions. The gaseous phase contains mostly the residual air, components of the working solution and H_2O_2. In order to recover the product, the stream is cooled to 20 °C in HX3. In FLASH2 the gas phase is again separate from the liquid phase. The gas phase consists mostly of depleted air, traces of the working solution and H_2O_2. The liquid stream is combined with the liquid stream of the reactor and cooled to 30 °C before the extraction column. The air feed to the oxidation reactor was adjusted to reach a mole fraction of O_2 to 5 % in the gaseous outlet after FLASH2.

$$AHQ + O_2 \longrightarrow H_2O_2 + AQ \tag{4.2}$$

The extraction column is modeled with 5 stages. H_2O_2 is supposed to be withdrawn in the aqueous water phase at the bottom. The water is supplied at 25 °C and pumped to 1.5 bar. The top outlet of the extraction column contains the working solution and traces of water. The water flow is set with a DesignSpec to reach a crude H_2O_2 solution with a mass purity of 40 % as reported in literature [115, 116, 233]. The working solution needs to be treated before recycling. Typical steps are regeneration and drying. Water and gases are removed in an ideal splitter from the working solution in the model. The working solution is pumped back to 4 bar. The lost working solution is replaced and 0.1 wt. % of the AQ in the recycle stream is replaced.

The stream containing H_2O_2 from the extraction column can be further purified. Depending on the case, the stream is either completely or partially sent to the pulp mill. The purification is operated at 0.1 bar to prevent the decomposition of H_2O_2 at higher temperatures [115]. The vacuum pumps at the bottom and top of column C2 provide the required vacuum with the help of VALVE3. In FLASH 3, the leftover gases are removed from the stream at 53 °C. Furthermore, water is removed in this step. The distillation column has 5 stages and purifies the crude solution to 70 wt. %. The losses of H_2O_2 in the top stream are set to 0.01 wt. %. The reflux ratio is set to 0.22 and the distillate to feed ratio to 0.515. The bottom product (H_2O_2) is cooled from 66 to 30 °C.

4.6.2 Technical and energetic analysis

The hydrogen efficiency is calculated to 99.9 %, 97.9 % and 97.8 % for the 6, 50 and 150 MW_{el} plant. The losses of H_2 in form of H_2O_2 occur in the purification step as not all H_2O_2 can be recovered as product. Furthermore, losses occur with the air leaving the oxidation reactor. As no purification is performed, the 6 MW_{el} plant has the highest hydrogen efficiency.

Table 4.14 presents the mass balance of the process. The energy balance can be found in the Appendix D.3. The deionized water is used in the water electrolysis and the extraction column. O_2 contained in the air is used in the oxidation reactor and the air is released with a lower O_2 content. Therefore, the air outlet flow is decreases compared to the inlet flow. The working solution is recirculated in the process. Losses occur with the air leaving the oxidation reactor, waste water or the final product. Therefore a small amount must be compensated by a makeup stream. Additionally, a small portion of the anthraquinone is regularly replaced with each recycle step. The annual demand of the pulp mill for pure H_2O_2 is 14.7 kt. This demand is covered by the crude, non-purified H_2O_2 with a flow rate of roughly 2 t/h (pure). The leftover H_2O_2 is purified and sold on the market. For the 6 MW_{el} plant, the onsite demand of H_2O_2 exactly fits the plant's capacity.

Table 4.14 Mass balance of H_2O_2 process in t/h

Plant size in MW_{el}	6	50	150
Input			
Water	4.0	35.8	107.6
Air	10.5	94.6	283.8
Makeup working solution	0.0	0.3	0.9
Internal			
H_2 (water electrolysis)	0.1	1.1	3.2
Working solution	135.2	1214.1	3642.3
Output			
O_2 (water electrolysis)	0.9	8.3	25.0
Air	8.6	78.2	234.4
H_2O_2 in solution to pulp mill	4.9	4.9	4.9
H_2O_2 pure to pulp mill	2.0	2.0	2.0
H_2O_2 in solution to market	-	22.0	71.5
H_2O_2 pure to market	-	15.4	50.0
Waste water	0.0	17.2	55.8

4.6.3 Integration

H_2O_2 is a molecule that in contrast to the other presented PtX products does not need CO_2 as feedstock for the synthesis. Consequently, no CO_2 is captured and bound. Table 4.15 shows the integration with the utilities of the pulp mill. As stated earlier, the production of H_2O_2 is very water intensive which is reflected in the demand for deionized water and waste water treatement. Besides the deionized water for water electrolysis, water is used for the extraction of H_2O_2 from the working solution. Even though the process itself does not produce water as a side product, the waste water flow is solely from the water for extraction. With the presented production processes, the pulp mill's demand for H_2O_2 can be covered onsite.

The O_2 demand can only be covered by 25 % for the 6 MW_{el} plant. The other plant's O_2 production exceed the required O_2 demand onsite. The heat integration is limited to the exchange of hot water and does not affect the electricity production in the steam turbine. Not all heat can be directly used in the process or recovered as hot water. Therefore, a substantial amount of waste heat must be dissipated to the environment via the process cooling units.

Table 4.15 Impact of integrating the H_2O_2 plants (Positive values for electricity generation due to heat integration means a drop in electricity generation)

Plant size in MW_{el}	6	50	150	
		O_2		
O_2 production	6,905	62,516	187,548	t/a
Coverage O_2 demand	25%	227%	680%	
		Waste water treatement		
Additional amount	184	128,712	418,839	t/a
Increase in waste water	0.0%	0.8%	2.7%	
		Deionized water		
Additional amount	29,851	268,684	806,908	t/a
Increase in deionized water	0.2%	1.6%	4.7%	
		Heat integration		
Process cooling demand	3.9	49.1	151.0	MW_{th}

The electricity balance for integrating the H_2O_2 process is shown in Table 4.16. The electricity generation is not affected as no steam is exchanged between the H_2O_2 process and the pulp mill. The tremendous demand for process cooling leads to a high electricity demand for the operation of the cooling towers. The 50 and 150 MW_{el} plants cover the O_2 demand of the pulp mill and lead to a shut down of the pressure swing adsorption plant. For the 6 MW_{el} plant, the plant is still operational to supply most of the required O_2. In summary, the electricity availability increases for the 6 and 50 MW_{el} plants and decreases for the 150 MW_{el} plant.

Table 4.16 Effect of integration on the electricity balance of the pulp mill (positive values mean additional electricity demand)

Plant size in MW_{el}	6	50	150
Waste water treatment	0.00	0.02	0.06
Deionized water	0.01	0.07	0.22
O_2	-0.36	-1.43	-1.43
Heat integration	-	-	-
Process cooling	0.06	0.71	2.19
Total	-0.29	-0.63	1.03

4.6.4 CO_2 balance

The emission factor for H_2O_2 in dependence of the grid electricity emission factor is shown in Figure 4.8. The reference is based on the conventional process with a concentration of 50 % in solution derived from the Ecoinvent databank [234]. The reference and data presented here is based on pure H_2O_2. The CO_2 emissions are allocated to the total H_2O_2 output.

The emission factor of the 6 and 50 MW_{el} plant is independent of the grid electricity. The process has additionally no impact on the natural gas demand (no purge stream combustion) resulting in horizontal curves are 0 t CO_2/t H_2O_2. The integrated 150 MW_{el} plant shows a linear relationship for the emission factor of the product intercepting in the origin. For the greenfield plants, the production amount of crude H_2O_2 and purified H_2O_2 is kept the same as for the integrated plants. The emissions are allocated on the mass of the purified H_2O_2. The 50 and 150 MW_{el} plants show almost no difference for the final emission factor even though the share of production amounts of crude and purified H_2O_2 differ. The 6 MW_{el} plant is excluded as a greenfield plant. Compared to the integrated 150 MW_{el} plant, the slope is greater since more electricity is sourced from the grid. Furthermore, the curve is offset by 0.1 t CO_2/t H_2O_2 due to the heat required for the process. It can be discussed whether

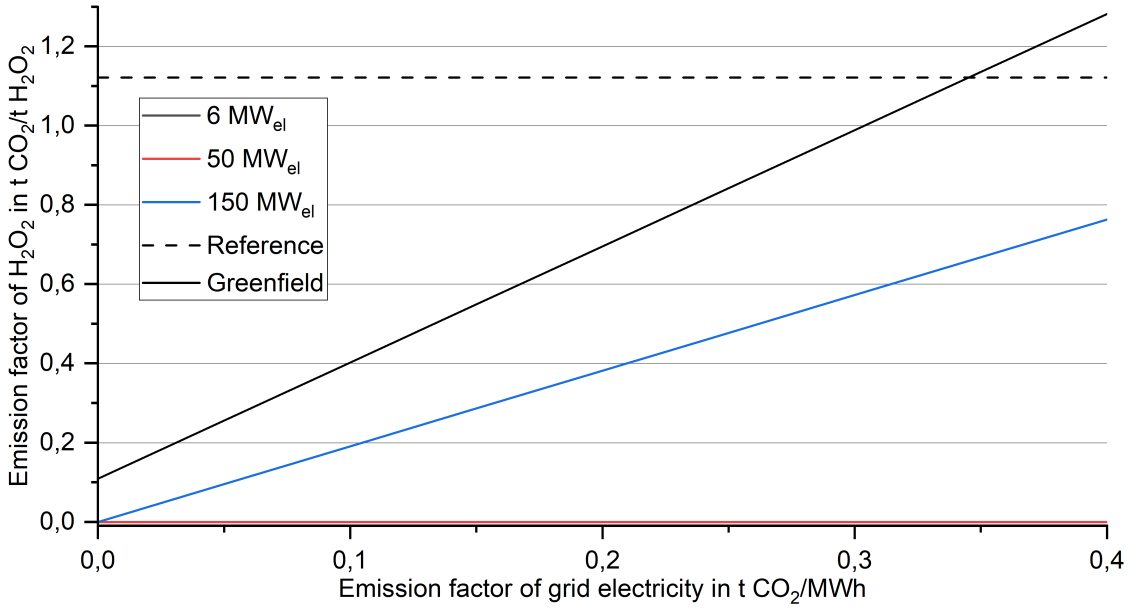

Figure 4.8 Impact of electricity emission factor on the emission factor of H_2O_2 (Reference: 1.12 t CO_2/t H_2O_2 [234])

the low temperature heat can be supplied by waste heat and not by steam derived from natural gas combustion as the required temperature level is below 100 °C. In case of no emissions for heat supply, the curve starts in the origin but still shows a greater slope than for the integrated 150 MW_{el} plant.

The marginal emission factor for the greenfield plants is at 0.33 t CO_2/MWh. For the integrated plant, the marginal emission factor is found to be 0.59 t CO_2/MWh.

4.6.5 Economic analysis

Figure 4.9 shows the levelized cost of H_2O_2 for the three plant sizes. The cost are calculated based on pure H_2O_2 to the market. The crude H_2O_2 to the pulp mill for the 50 and 150 MW_{el} plants is given a credit since it replaces bought H_2O_2. For the 6 MW_{el} plant, the credit for replaced H_2O_2 is removed to yield a positive price. If it is included, the LCOH2O2 would be -45 €/t which is the difference between the market price (750 €/t) and the LCOH2O2 shown in Figure 4.9. For this plant size, all cost are allocated to the H_2O_2 output. The investment cost for the reactors and extraction column could not be sized due to a lack of data availability. Therefore, the equipment cost assumptions are shown in Appendix D.3.

The levelized cost range between 535 and 705 €/t. The share of operating cost ranges from 79 to 86 %. Compared to the other PtX processes, the impact of electricity cost is smaller. The highest impact is found for the 50 MW_{el} plant of 274 €/ t H_2O_2. The replaced H_2O_2, accounts for a credit of 95 and 29 €/t for the 50 and 150 MW_{el} plant. The replacement and makeup of the working solution adds 81 to 92 €/t to the levelized cost. For the 6 MW_{el} plant, the other cost components of the operating cost ("Other" in the figure) take up a higher share. This is due to the fact that some cost components especially based on labor cost do not scale with size and are therefore more influential for smaller plant sizes. Economy of scale and lower electricity cost decrease the product price for the 150 MW_{el} plant compared to the 50 MW_{el} plant. The credit for replaced H_2O_2 is shrinking for the larger plant size as the credit is allocated on a higher volume of sold product in comparison to the 50 MW_{el} plant.

The CO_2 abatement cost show negative values as the levelized cost is below the market price meaning that the reduction of CO_2 will result in a positive revenue from producing H_2O_2. With the same reasoning, the pulp price will decrease if the H_2O_2 is sold at market price. Larger plant sizes

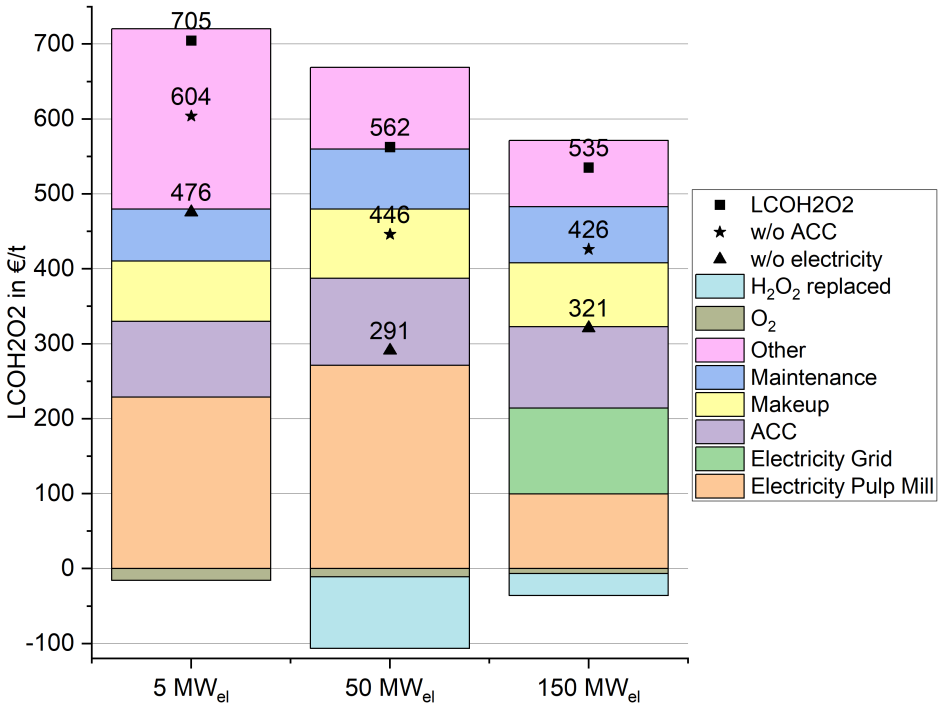

Figure 4.9 Levelized cost of H_2O_2 in €/t

lead to a higher decrease due to the effect of allocating the increased saving on the same amount of pulp.

Table 4.17 Change in pulp selling price in €/ADt for market enumeration (750 €/t) of H_2O_2 and CO_2 abatement cost in €/t CO_2

Plant size in MW_{el}	6	50	150
CO_2 AC	-	-165	-542
Change in pulp price	-1	-35	-132

The figures of the sensitivity analysis are depicted in Appendix D.3. Due to the uncertainty and lack of information involved with modeling this process, the sensitivity analysis is a very important tool. The investment cost of the anthraquinone process has a lower reliability and the cost assessment includes only the major equipment. Many other side processes like for example working solution treatment are not included in the model. Therefore, the variation of the FCI for this process indicates the influence on the levelized cost. Varying the FCI by ± 50 % gives a change of - 13 to 12 % of the final product cost. Even with higher FCI, the levelized cost do only for the 6 MW_{el} plant exceed the market price. The electricity price and water electrolysis related parameters show also a tremendous impact. The annuity factor and H_2O_2 market price show the lowest impact on the levelized cost.

4.6.6 Discussion

The discussion addresses the comparison with the electrochemical process, the impact of partial purification, model validation and economics.

The reported electrical energy demand of the electrochemical production of H_2O_2 ranges from 2 to 17.6 kWh/kg H_2O_2 [115, 120]. For the electrified H_2O_2 process presented here, the electrical demand ranges from 2.8 to 3 kWh/kg H_2O_2 considering the pulp mill integration and crude H_2O_2 after the extraction process. The electrical energy intensity of the anthraquinone process is in the lower range of the electrochemical process. Therefore, the energy consumption which is also one of the main

cost drivers can reach similar consumption figures for both process options. Consequently, the main difference in cost will be mostly based on the investment cost difference of the two systems. The investment cost are also affecting some of the operating cost. Usually, the electrochemical processes produce H_2O_2 at low concentration making the purification very costly and energy intensive. Depending on the purification and peripheral equipment for the electrochemical process, the utilization of the electrochemical process might be especially interesting for the supply of the onsite demand since no purifiaction is necessary. Building the anthraquinone process of the sizes for the 6 MW_{el} plant seems unreasonable. Especially for this small capacity it is questionable as the process is quite complex and the cost scales with size. Here the electrochemical production process might be the better option.

The goal of integrating the H_2O_2 process into the pulp mill is to reduce cost and energy consumption. The crude H_2O_2 can be directly used in the pulp mill. The pulp mill needs a stream of crude H_2O_2 with 2 t H_2O_2/h. This translates to a saved heat demand in the purification column of 1.7 MW_{th} in the condenser and reboiler. The feed flow to the distillation is reduced by 13 or 4 % for the 50 or 150 MW_{el} plant. The reduced feed flow leads to a smaller column size which reduces the investment cost and related operating cost. However, this change is especially marginal for bigger plants. Furthermore, the reduced heat demand reduces the cost for heat. For greenfield plants, the heat might be attributed with cost and has also an impact on CO_2 emissions.

No other process simulation data or pilot plant data are available in the scientific literature on the production process. Therefore, the model validation and comparison has to be done with figures indicated in literature sources. All data reported here is based on the 150 MW_{el} case. Goor et al. report a H_2 demand of 60 to 65 kg H_2 per t H_2O_2 produced [115]. The process gives a H_2 demand of 59.8 kg H_2/t H_2O_2 which is at the lower range indicating an efficient H_2 utilization. The process model considers a full conversion of H_2 in the hydrogenation reactor which is reasonable. However, H_2 dissolved in the working solution as well as side reactions of the anthraquinone are not considered which would increase the figure presented above.

The requirement for anthraquinone is reported to 7 t AQ/t H_2O_2 [115]. The process model shows 11.7 t AQ/t H_2O_2 which results in a higher mass flow of AQ and of the working solution in general. The concentration of H_2O_2 in the working solution after the oxidation reactor is supposed to be between 0.8 and 1.9 wt. % [116]. The process model shows a concentration of 1.4 wt. % which is in line with the literature and contradicts the before mentioned high flow of AQ and working solution. The recovery of H_2O_2 in the extraction step should be at 95 % [116]. The model's recovery is at 100 % exceeding the literature value. Goor et al. report a replacement of 1-3 kg quinone per t of H_2O_2 [115]. In the models a replacement of 5.8 kg/t H_2O_2 is implemented. Therefore, the cost of quinone replacement are considered conservatively.

The levelized cost of H_2O_2 are below the market price and seem very competitive. The investment cost considers only the main equipment. Not included are for example auxiliary process steps which add to the investment cost like the purification and special treatment of the working solution or the special treatment of residual streams leaving the plant like air or waste water. The increase in investment cost as shown in the sensitivity analysis increases the levelized cost of H_2O_2. Nevertheless, the levelized cost are in a reasonable range close to the market price and the assessment can be further improved with more information on the process technology and increased detail of the process model. 300 $ per t H_2O_2 are reported for the capital cost [235]. The capital cost calculated are 1/3 of the reported cost varying between 109 to 116 €/t H_2O_2. Therefore, the capital cost might be underestimated in the calculations.

Furthermore, the assessment of the emission factor for H_2O_2 shows that the process is in comparison to the other PtX processes very promising. Even with a less efficient process than modeled here, the reachable emission factors can guarantee a successful decrease of CO_2 emissions for a wide range of grid emission factors.

4.6.7 Intermediate summary

This section presents the production of H_2O_2 based on H_2 from water electrolysis. The key findings and conclusions are:

- The process shows an efficient utilization of H_2. All plant sizes can supply the pulp mill with the required amount of crude H_2O_2. The working solution is internally recycled and results in a huge mass flow.
- The levelized cost of H_2O_2 is below the market price. Bigger plant sizes show lower cost. The impact of electricity price is not as significant as for other PtX processes.
- The emission factor of H_2O_2 produced in the 6 and 50 MW_{el} plant is zero. The marginal emission factor for grid electricity to reach equal emissions as the fossil comparator is 0.59 t CO_2/MWh for the 150 MW_{el} plant. For the greenfield plant the marginal emission factor is 0.33 t CO_2/MWh. The numbers indicate the high potential to reduce CO_2 emissions even with higher emission factors for electricity.
- The production of H_2O_2 is a very water intensive process with a high demand for deionized water and waste water treatment. Furthermore, no CO_2 can be captured and bound in the product. The low temperature level of heat in the process has no impact on the electricity generation. However, the demand for process cooling leads to a higher electricity demand for the operation of the cooling system.
- CO_2 abatement cost are negative since the cost of H_2O_2 is below the market price. The levelized cost below market price lead also to a reduction in pulp selling price ranging from -1 to -132 €/ADt.
- The presented process represents novel data for the utilization of H_2 to produce green H_2O_2. Due to the lack of data for validation of the process models and costing data, the results need to be considered carefully. However, the results seem extremely promising in terms of cost and CO_2 emissions. H_2O_2 should be investigated further as a promising PtX product.

4.7 Production of Fischer Tropsch syncrude

This section deals with the modeling and results of the FT process. Table 4.18 shows the different cases under investigation. The cases use different types of syngas preparation (RWGS unit with water electrolysis or CO_2 electrolysis with water electrolysis), gas loop designs (open and closed loop) and plant sizes (50 MW_{el} and 150 MW_{el} to electrolysis). The concept to utilize CO_2 electrolysis as syngas preparation for FT processes was first proposed by van Bavel et al. [236]. This section was in most parts already published [237, 238].

Table 4.18 Cases of the FT process (CL: closed loop, OL: open loop)

Cases	Syngas preparation	Gas loop design	Plant size in MW_{el}
RWGS-CL-50	RWGS	CL	50
RWGS-CL-150	RWGS	CL	150
RWGS-OL-50	RWGS	OL	50
RWGS-OL-150	RWGS	OL	150
CO2E-CL-50	CO_2 electrolysis	CL	50
CO2E-CL-150	CO_2 electrolysis	CL	150
CO2E-OL-50	CO_2 electrolysis	OL	50
CO2E-OL-150	CO_2 electrolysis	OL	150

4.7.1 Process design and modeling

The FT process requires a syngas rich in H_2 and CO. In this work, the syngas is either supplied by a RWGS process based on H_2 from water electrolysis and CO_2, or by separate CO_2 and water electrolysis. Figure 4.10 shows the flowsheet as implemented in Aspen Plus.

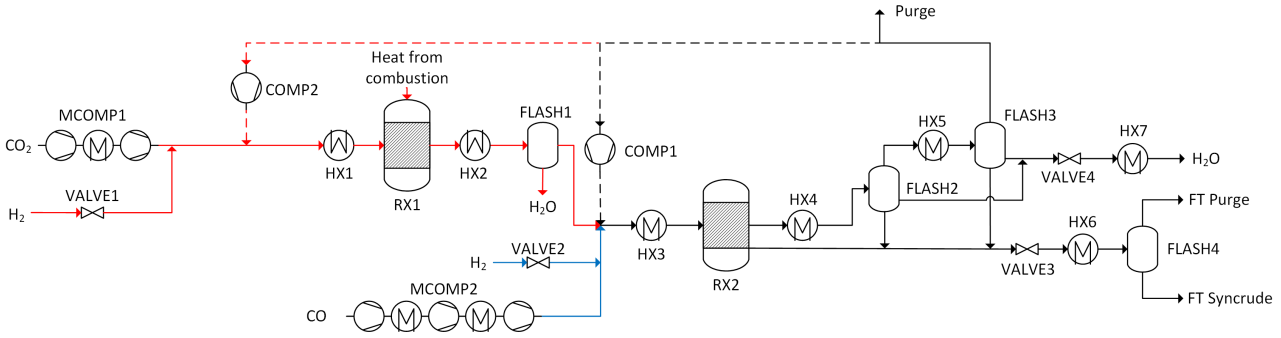

Figure 4.10 Flowsheet of the FT model showing the two types of syngas preparation (red: RWGS, blue: CO_2 electrolysis) and gas loop design (open (without dashed lines) and closed loop design (with dashed lines))

The conversion of CO_2 in the RWGS unit is described by Equation 2.19. The RWGS reaction is endothermic and requires high-temperature thermal energy input to drive the equilibrium reaction. The process flowsheet of the RWGS process, as modeled in this study, is illustrated by the red lines in Figure 4.10. H_2 enters the process from water electrolysis at a pressure of 30 bar and a temperature of 80 °C. CO_2 is supplied at 25 °C and 1 bar. The operating pressure of the RWGS process is 26 bar. Therefore, H_2 is throttled, and CO_2 is compressed in a two-stage compressor with intercooling to 30 °C to reach the operating pressure. Prior to entering the RWGS reactor (RX1), the gases are heated to 300 °C in HX1. Preheating the reactor inlet with the outlet flow is limited to avoid metal dusting, which refers to the disintegration of metals into carbon and metal particles at temperatures of 400 to 800 °C under high CO partial pressures potentially leading to material degradation [239]. To avoid extreme temperatures on both sides of heat exchanger, preheating the inlet and cooling the outlet in the temperature range of metal dusting should be avoided.

The RWGS reactor (RX1) is modeled as an RGibbs reactor that minimizes Gibbs energy. It is assumed to be a fired tubular reformer with catalyst-filled tubes heated by combustion, similar to the concept used in steam methane reforming [240]. Combustion heat is necessary to achieve high temperatures in the reformer tubes for supplying heat to the endothermic reaction (Eq. 2.19). The reactor temperature is set at 900 °C. A pressure drop of 1 bar is assumed. Purge streams from the FT process or natural gas (if purge streams are insufficient) are used as fuel. The efficiency of the fired heater is assumed to be 90% based on the LHV of the fuel. The outlet stream from the reactor is cooled to 30 °C, and water is separated in an adiabatic flash drum (FLASH1). The separated water is sent to the wastewater treatment plant.

The syngas generation concept with CO_2 electrolysis involves a three stage compressor with intercooling to 30 °C for the compression of CO which is supplied at 40 °C and 1 bar. The CO_2 electrolysis itself is modelled with a simplified mass and energy balance as described in Section 4.3. H_2 is throttled to the operation pressure of 25 bar.

This study utilizes the LTFT process, operating within the temperature range of 200 to 250 °C, which predominantly yields wax, diesel, and naphtha [97]. The waxes obtained can be further processed through hydrotreating to produce hydrocarbons with shorter chain lengths. This process is not inlcuded here. The produced syncrude needs further treatment in a refinery before being suitable as fuel. The FT synthesis generates a mixture of various chain lengths and component types, such as alkanes, alkenes, aldehydes, and alcohols. The distribution of chain lengths can be described using the ASF distribution, as shown in Equation 2.28. The reaction mechanism is based on chain propagation and the chain growth probability α represents the likelihood of chain propagation or termination. By employing the ASF distribution, it becomes possible to calculate the mass fraction w_n of a species with a specific chain length n.

To determine the chain growth probability α, Equation 4.3, derived for a cobalt catalyst, was employed [241]. In this equation, c denotes the molar concentration of H_2 and CO, k_α represents the selectivity constant (56.7 x 10^{-3}), β signifies the selectivity exponential parameter (1.76), ΔE_α represents the selectivity activation energy difference between propagation and termination reactions (120.4 x 10^{-3} J mol^{-1}), T denotes the temperature in Kelvin, and R represents the gas constant in J mol^{-1} K^{-1}. Since the chain growth probability underestimates the production of methane [98], the selectivity towards methane was adjusted in the model as also done in other studies [242]. The selectivity was fixed to 2 wt.%.

$$\alpha = \frac{1}{1 + k_\alpha (\frac{c_{H2}}{c_{CO}})^\beta exp(\frac{\Delta E_\alpha}{R}(\frac{1}{493{,}15} - \frac{1}{T}))} \tag{4.3}$$

The FT reactor (RX2) was simulated as a stoichiometric reactor, achieving a per pass conversion rate of 60 % for CO, and operating at a temperature of 220 °C. A slurry bed reactor was chosen with an inlet H_2/CO ratio of 2. A subroutine in Aspen Plus was utilized to calculate the chain growth probability and product distribution based on the ASF equation. In this model, the focus was solely on alkanes as the main products in LTFT, considering alkanes with chain lengths up to 40 carbon atoms. To simplify the calculations, the chain lengths ranging from 31 to 35 and 36 to 40 were combined and represented as alkanes with chain lengths of 33 and 38, respectively. When employing a Co catalyst in LTFT, the assumption of considering only alkanes can be justified due to the minimal formation of olefins and oxygenates [103]. The reactor model utilized a zero-dimensional approach, where the input concentrations of H_2 and CO, as well as the isothermal reactor temperature, were used to calculate the chain length distribution. It is important to note that in a real reactor, the temperature and concentration profiles vary spatially, resulting in a location-dependent chain length distribution.

At the reactor temperature, longer chain alkanes exist in the liquid phase and accumulate within the slurry phase of RX2. The catalyst suspended in the liquid phase is separated from the liquid FT products. The separation process was not included in the model. The gas phase exiting the reactor contains alkanes and unreacted reactants. In the case of a closed loop design, the gas phase also contains light alkanes introduced by the recycle stream. Heat exchanger HX4 reduces the

temperature of the gas to 130 °C. Subsequently, in flash drum FLASH2, the gas phase is separated from the two liquid phases consisting of water and medium-chain-length alkanes. Further cooling to 25 °C, followed by another flash drum (FLASH3), accomplishes the separation in two liquid phases and a gas phase. The total wastewater generated from the FT process is collected and then throttled to 1 bar before being cooled to 30 °C in HX7. This cooling step is necessary for subsequent treatment in the wastewater plant. The liquid syncrude fractions are collected and throttled to 1 bar as well. The cooled syncrude, at a temperature of 30 °C, undergoes separation into liquid and gas phases in FLASH4. Lighter components and gases that were dissolved under higher pressure are removed during this stage. The purge stream is combusted. More information on the syncrude is given in Appendix D.5.

The gaseous stream from FLASH3 can either be completely purged (in open loop design) or mostly recycled (in a closed loop design). All purge streams from the FT plant are incinerated preferably in the RWGS unit or else in the lime kiln. In a closed loop design, the tail gas is predominantly recycled. To avoid the accumulation of inerts and alkanes with lower chain lengths, a purge stream of 5 wt.% is extracted from the recycle stream. In the RWGS configuration, the internal recycle accounts for 65 wt.%, while the external recycle stream is set at 30 wt.%. In CO_2 electrolysis-based processes, there is no external recycle, and 95 mol% of the recycle stream is directed back to the FT reactor. All recycle streams need to be compressed to the operating pressure to compensate for pressure losses in reactors RX1 and RX2.

4.7.2 Technical and energetic analysis

Table 4.19 shows the KPIs of the cases for comparison. The highest carbon efficiency is reached for RWGS-CL at almost 80 %. The carbon efficiency of the CO2E-CL cases are slightly below RWGS-CL. Obviously, the open loop configurations reach lower carbon efficiencies. Interesting to see is that CO2E-OL has higher carbon efficiencies than RWGS-OL. This is due to no loss of CO_2 with the tail gas.

Table 4.19 KPIs for FT processes (η_{PtF} in brackets for greenfield plants)

Case	RWGS-CL		RWGS-OL		CO2E-CL		CO2E-OL	
Plant size in MW_{el}	50	150	50	150	50	150	50	150
η_{CE}	79.8 %	79.8 %	26.6 %	26.6 %	78.4 %	78.4 %	44.2 %	44.2 %
η_{HE}	29.0 %	29.0 %	13.4 %	13.4 %	40.3 %	40.3 %	24.3 %	24.3 %
η_{PtF}	39.5 % (36.8 %)	38.8 % (36.8 %)	17.0 % (16.6 %)	16.7 % (16.6 %)	30.6 % (29.7 %)	30.1 % (29.7 %)	17.4 % (17.0 %)	17.5 % (17.0 %)

Hydrogen efficiencies are higher for the closed loop configuration and for cases with CO_2 electrolysis. Consequently, CO2E-CL reaches the highest efficiency with 40.3 %. For CO_2 electrolysis the loss of H_2 via water which is generated in the RWGS process is reduced and therefore the hydrogen efficiency is increased. The highest Power-to-Fuel efficiency is found for RWGS-CL-50. The efficiencies are in contrast to hydrogen and carbon efficiency dependant on the plant size as the integration with the pulp mill does not scale linearly with plant size. Open loop configurations have for both syngas production concepts a similar efficiency. However, for the the closed loop configuration, the RWGS process is superior. Even when including the natural gas needed for the RWGS reactor, the efficiency would only drop to 34 % which is still above CO2E-CL. The efficiencies for greenfield plants are generally lower than the integrated ones which is due to the fact that no additional electricity available through heat integration or shutdown of O_2 production is available.

The energy balance in Table 4.20 shows that besides energy for water and CO_2 electrolysis of 50 or 150 MW_{el}, electrical energy is also needed for pumping and compression work. The power demand accounts for 3 to 5 % of the total electrical energy demand. For CO2E the demand is lower than for RWGS as the recycle streams are smaller and less CO_2 needs to be captured.

Table 4.20 Energy balance of FT processes in MW

Scenarios	RWGS-CL		RWGS-OL		CO2E-CL		CO2E-OL	
Plant size in MW_{el}	50	150	50	150	50	150	50	150
				Input				
Electricity total	51.7	155.2	52.3	156.9	51.4	154.2	51.4	154.2
- Water electrolysis	50.0	150.0	50.0	150.0	28.4	85.3	27.5	82.5
- CO_2 electrolysis	0.0	0.0	0.0	0.0	21.6	64.7	22.5	67.4
- Compression	1.7	5.2	2.3	6.9	1.4	4.2	1.4	4.2
Natural gas	4.3	12.8	0.0	0.0	0.0	0.0	0.0	0.0
Heat	11.3	33.8	12.5	37.4	6.8	20.5	6.4	19.2
				Internal				
Heat RX1	9.7	29.2	5.7	17.1	0.0	0.0	0.0	0.0
				Output				
Syncrude	19.0	57.1	8.7	26.0	15.3	45.8	8.7	26.2
Purge	5.5	16.4	20.6	61.9	5.7	17.1	21.4	64.3
Heat	32.9	98.8	25.0	75.0	15.0	45.1	11.4	34.1

The RWGS reactor requires between 5.7 and 29.2 MW_{th} for heating. For RWGS-OL the heat demand is lower as no recycle stream increases the mass flow in the reactor. Since the purge streams and tail gas streams are not sufficient to supply the RWGS reactor in the closed loop configuration with enough thermal energy, additional natural gas is needed. Surplus purge streams are finally used in the lime kiln. For the processes with CO_2 electrolysis all purge streams are used in the lime kiln. Generally, all processes are net heat exporters. Syncrude outputs are similar for the open loop configurations. However, for the closed loop configuration RWGS-CL shows higher syncrude outputs compared to CO2E-CL.

Table 4.21 shows the mass balance of the processes. Water and CO_2 demand is greater for the RWGS cases compared to CO2E cases. Water increases due to a higher H_2 production for the conversion of CO_2 to CO in the RWGS unit. The CO_2 demand is higher as CO_2 electrolysis converts CO_2 to CO with a higher selectivity. Tail gas flows are smaller for CO2E cases as no CO_2 is diluting the gas stream. Furthermore, for open loop configurations the flows are lower as no recycle stream is increasing the flow. The higher flow rates for RWGS indicate the need for bigger equipment and consequently higher capital cost. Additionally no external recycle is used in CO2E cases. The compressor COMP2 is therefore not needed. O_2 production by water and CO_2 electrolysis are higher for RWGS than for CO2E cases. Accordingly, waste water generation and purge stream are higher for RWGS cases.

4.7.3 Integration

Table 4.22 shows the impact of the FT processes on the utilities in the pulp mill. Captured CO_2 is in the range of 3 to 15 % of total CO_2 available. All cases are able to cover the O_2 demand of the pulp mill. Actually, a tremendous amount of O_2 surplus can be sold or used otherwise. The increase in waste water flows is well below 1 % compared to the total waste water treated in the pulp mill. Waste water flows are lower for cases with CO_2 electrolysis. So is the demand for deionized water.

By the utilization of waste heat from the FT process, all cases except RWGS-OL and CO2E-OL-50 increase the generation of electricity. Especially for RWGS-CL, the additional heat generation by natural gas combustion in the RWGS reactor allows the production of steam. A more detailed picture of heat integration is shown in Appendix D.5. For all processes, the demand for process cooling increases. Except for RWGS-CL, which needs additional natural gas, all cases can provide a good portion of thermal energy needed in the lime kiln thereby substituting natural gas. For CO2E-OL, the lime kiln's demand is exceeded and the surplus purge stream is used for high pressure steam generation.

Table 4.21 Mass balance of the FT processes in t/h ([a] from FLASH4)

Scenarios	RWGS-CL		RWGS-OL		CO2E-CL		CO2E-OL	
Plant size in MW_{el}	50	150	50	150	50	150	50	150
Input								
Water	9.4	28.2	9.4	28.2	5.3	16.0	5.2	15.5
CO_2	7.6	22.9	10.6	31.9	6.1	18.3	6.3	19.0
Natural gas (RWGS)	0.3	1.0	0.0	0.0	0.0	0.0	0.0	0.0
Internal								
Tail gas	15.8	47.4	5.8	17.3	7.6	22.9	2.2	6.5
Internal recycle	10.3	30.8	0.0	0.0	7.3	21.8	0.0	0.0
External recycle	4.7	14.2	0.0	0.0	0.0	0.0	0.0	0.0
H_2 (water electrolysis)	1.1	3.2	1.1	3.2	0.6	1.8	0.6	1.7
CO (CO_2 electrolysis)	0.0	0.0	0.0	0.0	3.9	11.6	4.0	12.0
Output								
O_2 (water electrolysis)	8.3	25.0	8.3	25.0	4.7	14.2	4.6	13.8
O_2 (CO_2 electrolysis)	0.0	0.0	0.0	0.0	2.2	6.6	2.3	6.9
Syncrude output	2.0	6.0	0.9	2.8	1.6	4.7	0.9	2.7
Waste water	5.8	17.4	4.9	14.8	2.4	7.1	1.5	4.6
FT purge[a]	0.1	0.3	0.0	0.1	0.2	0.5	0.0	0.0
Purge	0.8	2.4	5.8	17.3	0.4	1.1	2.2	6.5

Table 4.22 Impact of integrating the FT processes (Positive values for electricity generation due to heat integration means a drop in electricity generation)

Scenario	RWGS-CL		RWGS-OL		CO2E-CL		CO2E-OL		Unit
Plant size in MW_{el}	50	150	50	150	50	150	50	150	
CO_2									
CO_2 separated	57,244	171,733	79,628	238,881	45,627	136,882	47,540	142,620	t/a
Share of total CO_2	3%	10%	5%	15%	3%	8%	3%	9%	
O_2									
O_2 production	62,516	187,549	62,516	187,549	52,139	156,418	51,679	155,038	t/a
Coverage of O_2 demand	227%	680%	227%	680%	189%	567%	187%	562%	
Waste water treatment									
Additional amount	43,618	130,857	37,115	111,343	17,858	53,574	11,520	34,561	t/a
Increase in waste water	0.3%	0.8%	0.2%	0.7%	0.1%	0.3%	0.1%	0.2%	
Deionized water									
Additional demand	70,393	211,180	70,393	211,180	40,028	120,085	38,727	116,182	t/a
Increase in deionized water	0.4%	1.2%	0.4%	1.2%	0.2%	0.7%	0.2%	0.7%	
Heat integration									
Electricity generation	-2.24	-6.72	0.00	0.00	-0.12	-0.35	0.28	-3.01	MW_{el}
Process cooling demand	7.3	22.0	1.0	3.0	1.5	4.4	0.4	9.5	MW_{th}
Lime kiln									
NG replaced	0.0	0.0	14.9	44.8	5.7	17.1	21.4	50.0	MW_{th}

Table 4.23 allows a more detailed view on the change in electricity balance. The increase in waste water, deionized water and process cooling leads to a minor increase in electricity demand. Heat integration (for more detail see Appendix D.5) as discussed before leads especially for RGWS-CL to a significant increase in electricity generation. Together with the O_2 production which accounts for 1.43 MW_{el}, all cases show an increase in total electricity availability.

Table 4.23 Effect of integration on electricity balance for FT processes

Scenario	RWGS-CL		RWGS-OL		CO2E-CL		CO2E-OL	
Plant size in MW_{el}	50	150	50	150	50	150	50	150
Waste water treatment	0.01	0.02	0.01	0.02	0.00	0.01	0.00	0.00
Deionized water	0.02	0.06	0.02	0.06	0.01	0.03	0.01	0.03
O_2	-1.43	-1.43	-1.43	-1.43	-1.43	-1.43	-1.43	-1.43
Heat integration	-2.24	-6.72	-	-	-0.12	-0.35	0.28	-3.01
Process cooling	0.11	0.32	0.01	0.04	0.02	0.06	0.01	0.14
Total	-3.54	-7.76	-1.39	-1.32	-1.51	-1.68	-1.14	-4.27

4.7.4 CO_2 balance

The emission factors of syncrude are calculated and compared to the fossil comparator of 94 g CO_2/MJ according to the RED II Directive [210]. Electricity based fuels need to reach a 70 % emission reduction in relation to the fossil comparator. The system boundaries and calculation do not adhere to the RED II rules. Therefore, the comparison to the emission reduction goals of RED II need to be treated with caution.

Figure 4.11 shows the emission factors for syncrude. In contrast to the small scale plants which can cover their electricity demand onsite, the large scale plants are highly impacted by grid electricity. Therefore, the emission factor for syncrude of larger plant sizes are above the fossil comparator. The smaller plant size do actually show negative values for the emission factor except for RWGS-CL-50. The cases RWGS-CL need natural gas for the heating of the RWGS reactor and thus emit additional CO_2 which accounts for 12.5 g CO_2/MJ. The impact of avoided natural gas in the lime kiln is obviously higher for the open loop configurations. In the closed loop configuration with CO_2 electrolysis, the natural gas saving reduce the emission factor by 20.8 g CO_2/MJ. The case CO2E-OL-50 shows the lowest emission factor for the smaller plant size. For the larger plant size, RWGS-CL-150 shows the lowest emission factor.

Since the impact of used electricity is tremendously influencing the emission factor of syncrude, Figure 4.12 shows the variation of the carbon intensity of the used grid electricity for integrated and greenfield plants. Since smaller plant sizes are not supplied with electricity from the grid, the emission factor is independent of the grid electricity emission factor. Therefore the cases are shown as horizontal lines in the graph. Theses configurations are well below the fossil comparator. For the greenfield plant using only electricity from the grid, the emission factor of syncrude is independent of the plant size and therefore the graph only shows one line for each case (in total four). For the integrated plants of RWGS-CL, RWGS-OL and CO2E-CL with different plant sizes, the intersection with the y axis is at the same point with the exception of CO2E-OL. For this case, the purge stream of the 150 MW_{el} plant exceeds the thermal power demand by the lime kiln. Consequently, the natural gas reduction potential is exceeded and the surplus heat reduces the electricity demand from the grid.

The marginal emission factor of electricity to reach syncrude emission factors equal to the fossil comparator are generally higher for the integrated plants in comparison to greenfield plants. Marginal emission factors for integrated plants are in the range of 0.18 to 0.21 t CO_2/MWh. For greenfield plants the marginal emission factor range from 0.1 to 0.15 t CO_2/MWh. The curves are steeper for open loop configurations for integrated and greenfield plants compared to the closed loop configurations. This

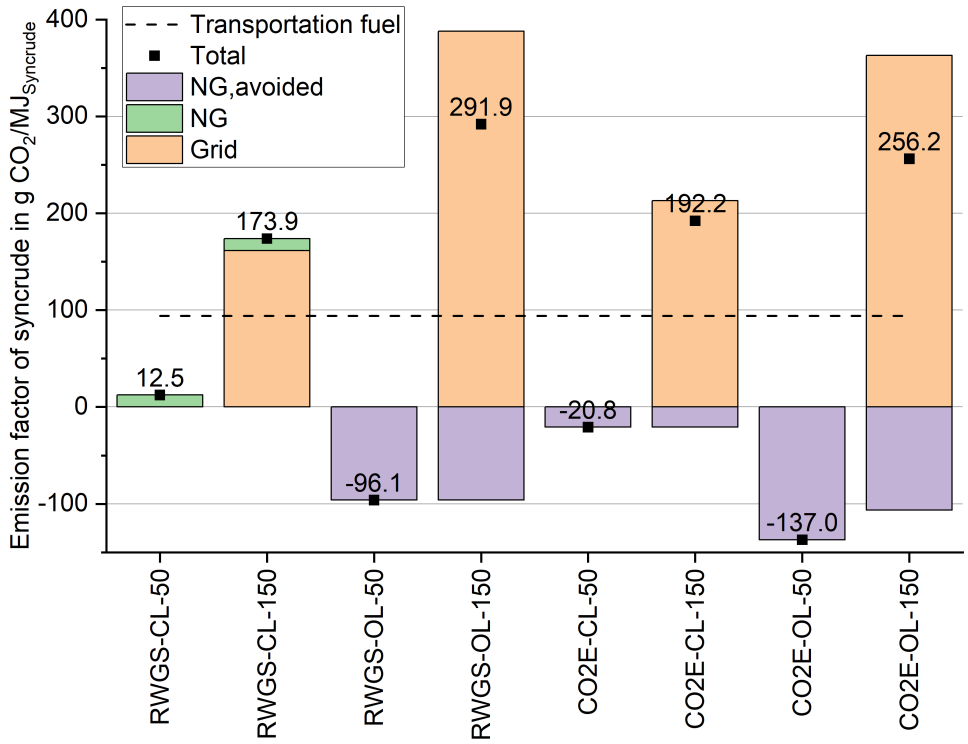

Figure 4.11 Emission factors for FT syncrude of the integrated plants in g CO_2/MJ (Transportation fuel: 94 g CO_2/MJ [210])

means that the emission factor of syncrude increases more significantly with the emission factor of electricity compared to closed loop configurations. On the other hand, open loop configurations show a lower y axis intersection point meaning that for lower grid emission factors these cases can reach lower emission factors for syncrude. Processes with CO_2 electrolysis show marginally lower emission factors with the exception of CO2E-CL-150. This case shows higher emissions than RWGS-CL-150 above 0.25 t CO_2/MWh.

4.7.5 Economic analysis

The economic analysis shows levelized cost of syncrude to be between 3.35 and 7.84 €/kg as shown in Figure 4.13. The levelized cost expressed in other units and the detailed cost breakdown is shown in Appendix D.5.

The majority of the cost (82 - 85 %) comes from operating expenses. In all cases, the electricity cost contributes the largest proportion to LCOS, ranging from 51 to 61 %. The impact on LCOS follows a descending order, with electricity cost, maintenance cost, and the ACC being the three most influential factors. The lowest LCOS value is observed in case RWGS-CL-150 at 3.35 €/kg. Generally, larger plant sizes exhibit lower LCOS due to the benefits of scale in investment cost and reduced grid electricity cost. Additionally, LCOS are considerably higher for the open-loop configuration meaning that the economic benefit from substituting natural gas is limited. The revenue generated from substituting natural gas in the lime kiln has a greater impact compared to the sale of O_2. The highest savings from natural gas amount to -0.59 €/kg for CO2E-OL-50, whereas the highest savings from O_2 sale are -0.18 €/kg for RWGS-OL-50.

The sensitivity analysis (see Appendix D.5) shows that electricity cost, efficiency of water electrolysis and cost of water electrolysis have the highest impact on the LCOS. The impact of the natural gas price, especially interesting for the open loop configurations, is not very significant. Figure 4.13 shows also the levelized cost either without expenses for electricity or without expenses for ACC. Without cost for electricity, the lowest cost can be found at 1.63 €/kg for RWGS-CL-150 showing again that

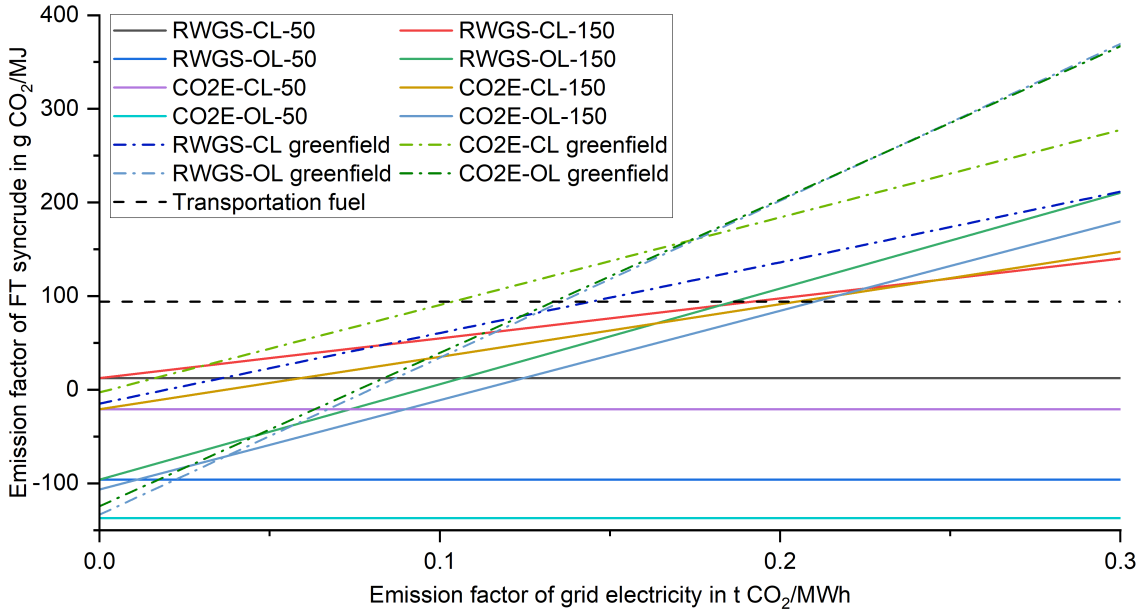

Figure 4.12 Emission factor of syncrude varying carbon intensity of electricity

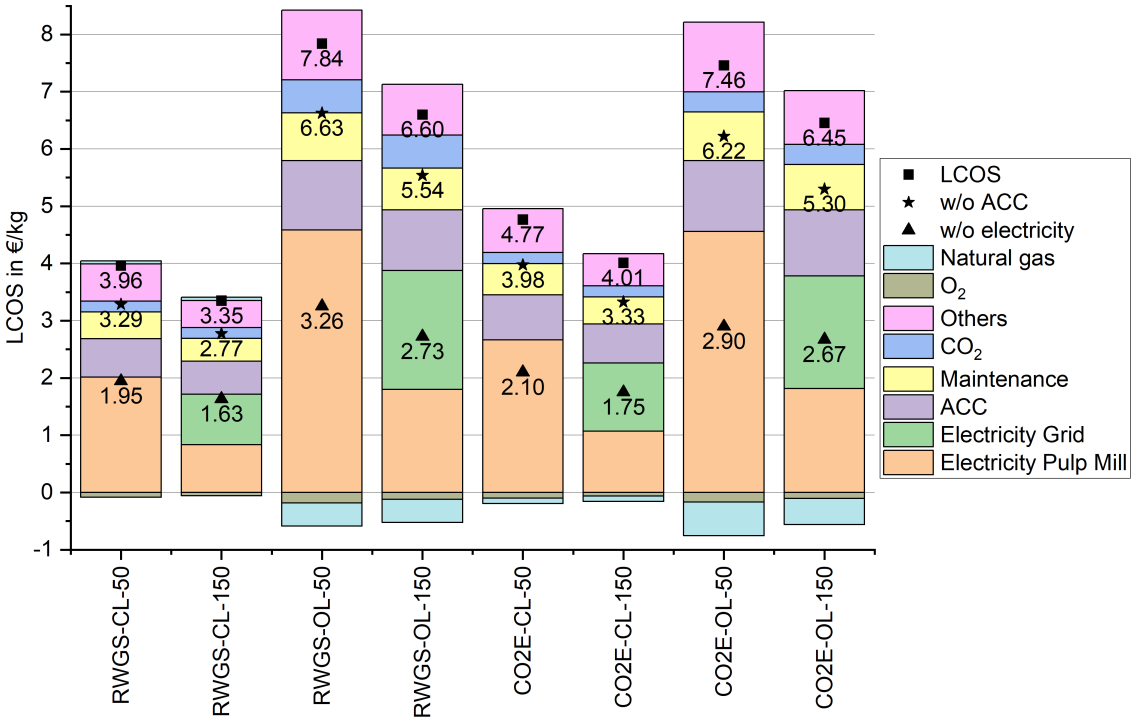

Figure 4.13 Levelized cost of FT syncrude in €/kg

electricity cost is a major cost factor. For the same case, not including ACC the cost are calculated to 2.77 €/kg.

If the syncrude is sold at the market price of crude oil (0.74 €/kg based on 100 $/Bbl and 0.85 kg/l), the extra expense incurred by the FT process needs to be compensated through pulp sales. The increase in pulp price is shown in Table 4.24. For the smaller plant, the cost of pulp sales price rises by 75 to 80 €/ADt. The production cost for the larger plant size experiences an approximate increase of 190 €/ADt.

Table 4.24 Increase in pulp selling price in €/ADt for market enumeration of FT syncrude and AC in €/t CO_2

Scenarios	RWGS-CL		RWGS-OL		CO2E-CL		CO2E-OL	
Plant size in MW_{el}	50	150	50	150	50	150	50	150
Increase in pulp price	78	191	80	199	77	187	75	195
CO_2 AC	1144	-	1103	-	991	-	848	-

If applying a CO_2 tax to the change in fossil emissions onsite which would have to be paid by the pulp mill, the cost for the CO_2 tax will impact the levelized cost of syncrude as shown in Figure 4.14. These scenarios are especially interesting for open loop configurations since the substitution of natural gas reduces fossil CO_2 emissions. For RWGS-CL the levelized cost are increasing as the additional combustion of natural gas in the RWGS reactor increases the fossil CO_2 emission. All other curves are descending. The slope of the open loop cases is steeper than for the closed loop cases as more natural gas is replaced in the lime kiln. Nevertheless, the intersection points with the closed loop cases lay above 600 €/t CO_2. This analysis shows that open loop cases become only under favorable market conditions at high CO_2 prices competitive.

For the CL-150 case, CO_2 electrolysis becomes cheaper than RWGS at 560 €/t CO_2. For the 50 MW_{el} plant size this point is at 680 €/t CO_2. The impact of CO_2 tax on the additional natural gas consumption is therefore rather small.

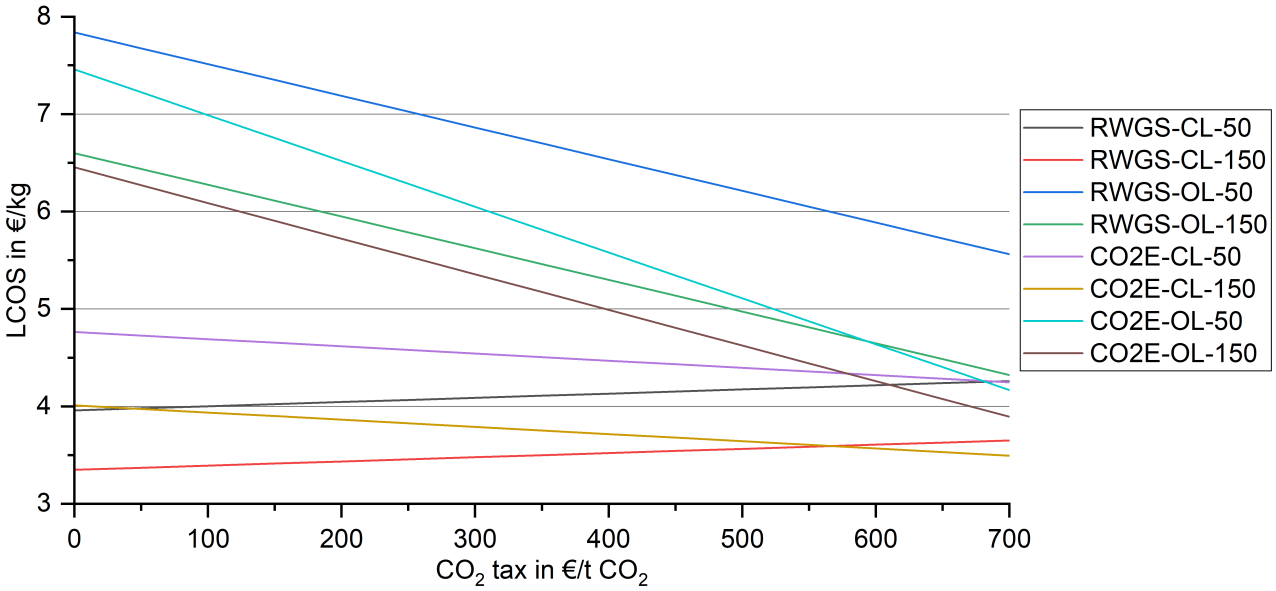

Figure 4.14 Impact of CO_2 tax for fossil CO_2 emissions on the levelized cost of FT syncrude

4.7.6 Discussion

Table 4.25 shows available studies on the production of fuels via the FT process. Raw materials for the process are CO_2 and H_2. Syngas preparation is performed with the RWGS process. The table does not include concepts based on co-electrolysis for the production of the required syngas.

The per pass conversion of the studies varies between 40 and 85 %. The assumption of 60 % is therefore reasonable. Higher per pass conversions are beneficial in terms of investment and operating cost. The product separation was in most studies modelled with flash separators. Some studies, especially focusing on the production of fuels include distillation as a way to separate the mixture into suitable fractions. Furthermore, some publications include hydrocracking as an upgrading step to increase the yield in fuels. The impact of the H_2 demand is neglectable as shown by König et al. The H_2 demand accounted for less than 0.5 % of the total H_2 demand of the PtL process [243].

The carbon efficiency of this work differs substantially between the cases. In the open loop design, the carbon efficiency shows very low values compared to the closed loop design. A carbon efficiency of roughly 80 % in the closed loop design is also confirmed by Hannula et al. and König et al. [244, 243, 242]. High carbon efficiencies as calculated by Albrecht et al. and Dietrich et al. seem unreasonable because of the purge stream to purge shorter chain alkanes [245, 246]. The only feasible option is to reform the tail gas with a reformer or RWGS reactor breaking down the short chain alkanes to syngas. For this the internal recycle has to be further decreased. The high carbon efficiency in Albrecht et al. and Dietrich et al. also lead to high Power-to-Fuel efficiencies and low product cost. The maximum Power-to-Fuel efficiencies in this thesis are reached with the RWGS process. Similarly, many studies confirm the Power-to-Fuel efficiency of roughly 40 % for the RWGS technology in closed loop configuration [244, 243, 242, 247, 248, 249, 240, 89]. One study considering the CO2E path reports a PtF efficiency of 53 % which is tremendously higher than the efficiency calculated here [250].

Product price comparison is difficult due to different economic assumptions (for example: plant size, electricity price, CO_2 price, ...). Albrecht et al. and Dietrich et al. calculate low product prices which seem based on their high carbon and Power-to-Fuel efficiency too promising. Also Schemme calculated very low product prices. The prices calculated by Dimitriou et al. are on the other hand extremely high. One reason is that the calculation is for a small scale plant. However, the comparison to fossil crude oil can be drawn. The calculated levelized cost of syncrude for case RWGS-CL-150 at 3.35 €/kg is 4.5 times higher than the current crude oil price. For case RWGS-OL-50 (highest LCOS), the cost is 10.1 times higher. Generally, the LCOS calculated by other authors are also well above the current crude oil prices.

The comparison of emission factors for syncrude was shown in Figure 4.11. The results show specifically that the smaller plant sizes are beneficial since no grid electricity is necessary. For the 150 MW_{el} plants, the grid electricity is a huge burden. However, bigger plants can also reach a cut in product's emission factor compared to fossil transportation fuel. Additionally, compared to greenfield plants which have to retrieve all the electricity from the grid, the integrated plants show lower emissions. This is due to the savings in natural gas and the damped demand for grid electricity. The assumption of giving a credit for the substituted natural gas for process heat is not in line with current legislation. If this credit is not given, the integrated plants would still have a lower emission factor for syncrude than the greenfield plants. Another process option can be the electrically heated RWGS reactor. This technology is commercialized by many companies already. Since the RWGS-CL cases are very promising in terms of efficiency and cost, the CO_2 balance could be improved with an electrically heated reactor avoiding natural gas combustion in the fired reactor and substituting natural gas in the lime kiln with the purge stream made available.

The produced syncrude needs to undergo treatment in a refinery before utilization as fuel or chemical. Syncrude can be either co-processed in an existing refinery or in dedicated refineries for processing FT syncrude [103]. Additional emissions for processing like hydrocracking and material losses in the processing needs to be considered. Therefore, the emission factor of the final product would increase compared to the emission factors presented here.

Technical parameters like per pass conversion or chain growth probability (including H_2/CO ratio, reactor temperature and pressure) were not changed in this study. For the impact of technical parameters please refer to the literature [89, 240, 258].

Table 4.25 Comparison of studies on the utilization of H_2 and CO_2 for FT fuel production (CL: closed loop, OL: open loop, HC: hydrocracker, [a]converted to €, [b] at 825°C and 5 bar, [c] based on H_2, [d] conversion 1 £= 1.15 €, [e] conversion 1 $ = 0.85 €)

Author and year	Gas Loop Design	Operating conditions of reactor	Per pass conversion	Chain growth probability	Product separation	Product upgrade	η_{CE}	η_{PtL}	Product price	Reference
This work	CL/OL	220 °C, 25 bar, $H_2/CO = 2$	60 %	0.84	2x Flash	-	26.6 - 79.8 %	16.7 - 39.5 %	3.35 - 7.84 €/kg	-
Adelung et al. 2021 Adelung and Dietrich 2022	CL	220 °C, 25 bar, $H_2/CO = 2$	40 %	0.84	1+8 x Flash	HC	88 %	38.7 %[b]	≈ 3.2 €/kg	[240, 89]
Albrecht et al. 2017	CL	230 °C, 25 bar, $H_2/CO = 2.05$	40 %	0.85	5x Flash	HC	98 %	50.6 %	2.74 - 2.85 €/l	[245]
Atsonios et al. 2023	CL	240 °C, 35 bar, $H_2/CO = 2$	85 %	0.92	1x Flash	HC	90.7 %	70.9 % [c]	-	[251]
Dimitriou at al. 2015	OL	220 °C, 30 bar	80 %	0.85	1x Flash	-	-	-	18.2 - 34.0 €/l [a]	[252]
Dietrich et al. 2017	CL	225 °C, 25 bar, $H_2/CO = 2.05$	40 %	0.85	5x Flash	HC	98.9 %	50.6 %	3.76 €/kg	[246]
Gao et al. 2021	CL	300 °C, 30 bar, $H_2/CO = 2$	-	-	1x Flash + Decanter	-	-	53.6 %	1.20 €/l[e]	[253]
Hannula et al. 2020	CL/OL	220 °C, 20 bar, $H_2/CO = 2$	75 %	0.92	1x Flash	-	50 - 55 % OL 65 - 89 % CL	33 - 36 % OL 37 - 42 % CL	-	[244]
Kirsch et al. 2020	OL/CL	240 °C, 30 bar, $H_2/CO = 2$	60 %	-	2x Flash	HC	-	-	-	[254]
König et al. 2015	CL	225 °C, 25 bar, $H_2/CO = 2.05$	40 %	0.85	4x Flash	HC	73.0 - 73.7 %	43.3 - 44.6 %	5.81 €/kg[e]	[243, 242]
Marchese at al. 2020	CL	228 °C, 25 bar, $H_2/CO = 1.9$	75 %	-	Flash + 2x destillation	-	-	34.4 %	-	[255]
Markowitsch at al. 2023	CL	220 °C, 25 bar, $H_2/CO = 2.08$	40 %	0.92	2x Flash	-	85.0 - 85.5 %	41.5 - 53.9 %	8.55 - 10.60 €/kg	[248]
Ordonez et al. 2021	CL	225 °C, 25 bar, $H_2/CO = 2.05$	40 %	0.85	6 x Flash	HC	-	38.1 %	-	[249]
Rojas-Michaga et al. 2023	CL	240 °C, 35 bar, $H_2/CO = 2$	75 %	-	1 x Flash + distillation	HC	88 %	28.1 %	5.93 €/kg[d]	[256]
Schemme 2020	CL	210 °C, 30 bar, $H_2/CO = 1.8$	80 %	0.92	3 x Flash + distillation	HC	-	48.5 %	2.25 €/ l_{DE}	[257]
Zang at al. 2021	CL (H_2 recycle)	220 °C, 24.3 bar, $H_2/CO = 2.2$	52.5 %	-	distillation	HC	45.5 %	39.3 - 41.0 %	-	[247]

4.7.7 Intermediate summary

This section explores the integration of a FT process into a pulp mill, examining various plant sizes, gas loop designs, and syngas preparation methods. The findings suggest that utilizing CO_2 and H_2 for FT syncrude production in a pulp mill holds promise for enhancing environmental viability and the efficiency of the FT process. The combined and integrated processes yield the following results:

- In the open loop configuration, carbon efficiency is lower, and in closed loop design, it doesn't exceed 80 %. The use of RWGS as a syngas preparation process leads to lower hydrogen efficiency due to water production as a by-product.
- CO_2 electrolysis in the syngas production process is less cost-effective with lower carbon and Power-to-Fuel efficiency for closed loop scenarios. However, in open loop cases, it outperforms in terms of carbon, hydrogen and Power-to-Fuel efficiency, and cost.
- Heat integration and the substitution of O_2 produced in the pulp mill result in higher onsite electricity availability, improving Power-to-Fuel efficiency compared to a greenfield plant.
- The levelized cost for syncrude ranges from 3.35 to 7.84 €/kg, decreasing for larger plant sizes and increasing for open loop configurations. In closed loop configurations, RWGS cases exhibit lower costs than CO_2 electrolysis cases. However, for open loop configurations, plants based on CO_2 electrolysis have lower LCOS.
- Integration of 50 MW_{el} plants into the pulp mill generally show low emission factors of the product, while 150 MW_{el} plants increase emissions due to grid electricity. CO_2 electrolysis-based plants show lower emissions than RWGS-based plants. Using an electrically heated RWGS reactor can improve the CO_2 balance of the process.
- If market prices are paid for syncrude, a smaller plant size can be compensated with a pulp sales price increase of 74–79 €/ADt. This cost increases to approximately 190 €/ADt for larger plant sizes.

4.8 Production of acetic acid

The acetic acid (AA) production process is presented and discussed in the following section. Four cases which differ in terms of plant size and CO production process are investigated as shown in Table 4.26.

Table 4.26 Definition of cases for the AA models (CO2E: CO_2 electrolysis)

Case	CO production	Plant size in MW_{el}
RWGS-50	RWGS	50
RWGS-150	RWGS	150
CO2E-50	CO2E	50
CO2E-150	CO2E	150

4.8.1 Process design and modeling

The AA production is based on the commercial Cativa process. Raw materials are CO and MeOH. MeOH is produced as described in Section 4.4. CO is provided via the RWGS reaction or CO_2 electrolysis. The CO_2 electrolysis is modelled as a black box (Section 4.3).

The RWGS model is depicted in Figure 4.15. Compared to the process in the FT synthesis, an additional membrane separation step is included. The Peng Robinson equation of state with Matthias coefficients is used as property method.

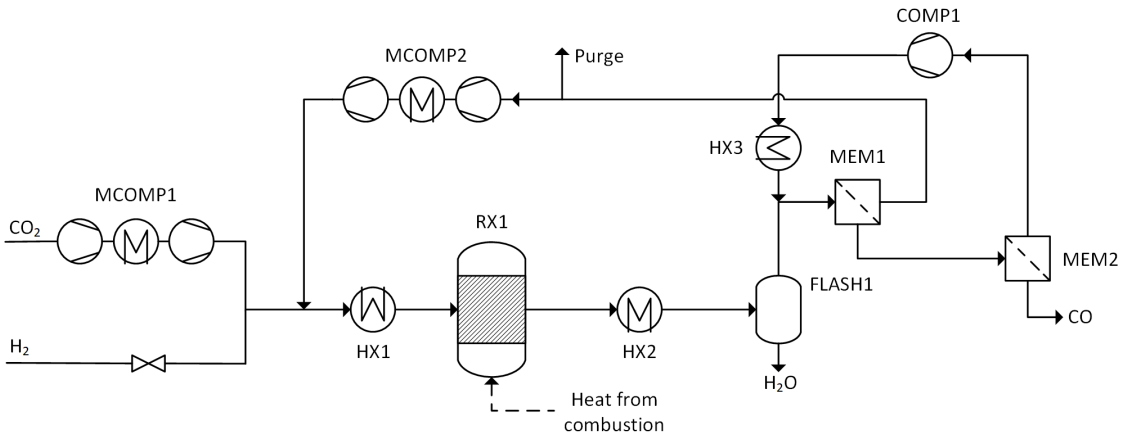

Figure 4.15 Flowsheet of the RWGS process for the production of CO as raw material for the Cativa process

The feed consisting of CO_2 and H_2 is mixed with the recycle stream coming from the first membrane stage. CO_2 is compressed in a two stage compressor with intercooling to 15 bar. The molar H_2/CO_2 ratio before the reactor is adjusted to 1 by changing the flowrate of CO_2. The reactor feed is preheated to 300 °C. A maximum preheating is not possible due to metal dusting (see 4.7.1). The RWGS reactor operates at 900 °C and has a pressure drop of 1 bar to account for losses in the whole process. The reactor minimized the Gibbs energy and finds the thermodynamic equilibrium. Since the reaction in the reactor is endothermic, sufficient heat to maintain an isothermal temperature of 900 °C has to be supplied by combustion. After cooling to 30 °C in HX2, water is flashed under adiabatic conditions in FLASH1 from the gas stream.

The membrane separation model is based on two membrane stages. The process configuration follows an industrial example reported by Teuner et al. [259]. The split ratios in the membrane stages were set based on an educated guess (see Table D.16 in the Appendix). For the retentate and permeate a pressure drop of 0.2 bar and 10 bar was assumed. The permeate of the first stage is recycled back to the RWGS reactor via a two stage compressor with intercooling. A purge stream of 0.5 wt. % is

implemented to avoid accumulation of inerts. The retentate of the first stage is enriched in CO and further enriched in the second membrane stage to a CO concentration of 98.95 mol %. Teuner at al. report a purity of 99.25 or 99.48 Vol. % for a similar process with membrane separation [259]. The CO leaves at a pressure of 13.6 bar. The permeate of the second stage is recycled back to the inlet of the first stage after compression to 14 bar and cooling to 30 °C.

The Cativa model was developed based on information by patents and other literature sources. As property method NRTL with the Hayden-O'Connell equation of state for the vapor phase (dimerization of carboxylic acids) was used. The process can bedivided into the reactor and purification section (Flowsheet see Figure 4.16).

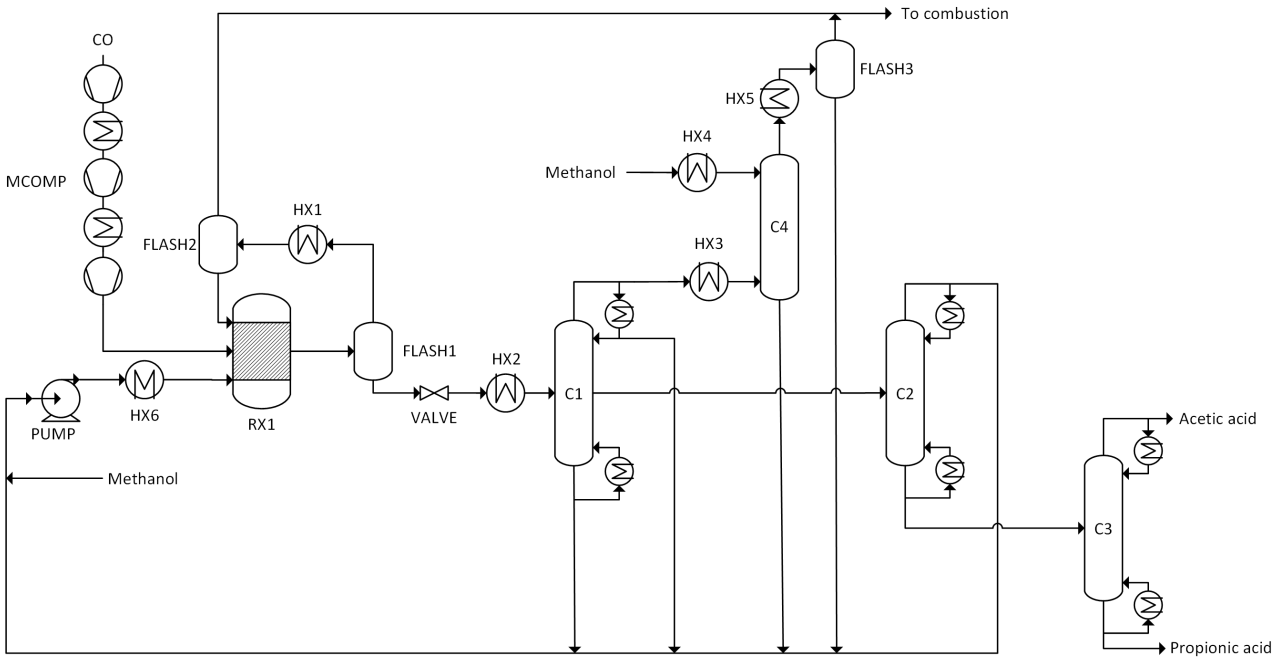

Figure 4.16 Flowsheet of the Cativa model for AA production

The reactor RX1 was modelled as a RStoic reactor at 200 °C [260, 126, 261] with the reactions and corresponding conversion rates shown in Table 4.27. Reaction rates are based on [123, 125]. The production of propionic acid was adjusted to reach 600 to 800 ppm in the bottom product of C2 [125, 124]. The operation temperature of the reaction section is 35 bar which is a typical operation pressure [123, 260, 126, 261] as the carbonylation rate drops significantly for partial pressures of CO below 10 bar [125, 262].

Table 4.27 Conversion in RStoic reactor of Cativa process

Reaction equation	conversion	based on
$CO + CH_3OH \longrightarrow CH_3COOH$	0.98	MeOH
$CH_3OH + CO \longrightarrow CO_2 + CH_4$	0.005	CO
$CH_3COOH + CH_3OH \longrightarrow CH_3CH_2COOH + H_2O$	0.0008	MeOH
$CO + H_2O \longrightarrow H_2 + CO_2$	0.005	CO

The liquid fed to the reactor is pumped to 35 bar and preheated in HX6 to 180 °C. The composition is set to 9.7 wt. % methyl iodide (CH_3I), 4.7 wt.% water and 14.4 wt.% methyl acetate which is in line with literature and patents [125, 126, 260, 263]. The CO is compressed to the operating pressure. CO purity should be above 99 mol % containing less than 0.3 mol % H_2 [261, 263]. The reactor outlet is sent to FLASH1 in order to separate gases from the liquid stream. The gaseous stream is cooled to 5 °C and flashed in another separator to recycle the condensed species. The gaseous product mostly containing gases like H_2, CO, CO_2 and CH_4 are sent to incineration.

The liquid product from FLASH1 is expanded to 1 bar and vaporized before entering column C1 [126]. C1 has 20 stages and the feed enters on stage 13 with 112 °C. The reflux ratio is set to 4 and the distillate to fed ratio is set to 0.185. In C1, low boilers like CH_3I are separated as head product. The bottom product contains the catalyst, AA and water. The catalyst is not explicitly modeled. The bottom product stream is set to 1.5 mol % of the feed stream. The side draw contains mostly water and AA which is further purified in column C2. Here, water is separated as head product. C2 has 50 stages with feed stage 13. The distillate to feed ratio is set to 0.12 and the reflux ration to 40. The bottom stream exits with a purity of 99.77 wt. % and needs further purification to reach the desired purity of 99.85 wt. % (glacial acetic acid). Column C3 separates propionic acid from the final product which is produced as side product. C3 has 20 stages and feed stage is on stage 6. The distillate to feed ratio is set to 0.9975 and the reflux ration to 3.3. AA is cooled to 30 °C in HX7.

The gaseous top stream of column C1 is further cooled to 25 °C and washed in absorber C4 (8 stages). MeOH enters at the top of the column with 25 °C. The goal is to remove methyl iodide from the gas stream. The MeOH flow rate is set to reduce the methyl iodide concentration in the gaseous product stream to below 50 ppm. The gas stream is cooled to 5 °C and flashed to recover MeOH. The rest is purged and sent to combustion. All liquid streams except the bottom stream of C3 which contains propionic acid are collected and recycled to the reactor. The recycle stream was closed by adjusting the makeup flows with an excel tool.

4.8.2 Technical and energetic analysis

The carbon efficiency of both routes for CO generation show very high carbon efficiencies (Table 4.28). Even for such a long process chain from CO generation, MeOH production to finally AA production, the processes show a carbon efficiency above 95 %. The efficiency of the CO_2 electrolysis is higher as the process has no losses via a purge stream and as the purity of CO in the CO stream is higher in comparison to the RWGS unit leading to less carbon losses via gaseous purge streams in the Cativa process. The hydrogen efficiency of the CO_2 electrolysis based processes is higher than for the RWGS based processes. This is due to the fact that H_2 is lost as water in the RWGS process.

Table 4.28 KPIs for the Cativa processes ([a] including natural gas for heating the RWGS reactor)

CO generation	RWGS		CO2E	
Plant size	50	150	50	150
η_{CE}	95.5%	95.5%	96.1%	96.1%
η_{HE}	47.4%	47.4%	63.3%	63.3%
η_{PtF}	53.9%	53.1%	47.9%	47.1%
$\eta_{PtF,NG}$[a]	49.2%	48.5%	-	-
$\eta_{PtF,greenfield}$	54.8%	54.8%	49.1%	49.1%

The PtF efficiency for processes with RWGS unit exceed the one of CO_2 electrolysis based processes. However, the RWGS reactor heating is also a tremendous energy input to the process which should not be neglected. If also the natural gas demand of the RWGS reactor is considered in the calculation the efficiencies of RWGS and CO2E come closer together. However, the efficiency of the RWGS based process is still higher. For the greenfield plant, the efficiencies are higher compared to the integrated plant as no cut in electrical energy generation is considered here (see Section 4.8.3).

Annual AA production amounts are 55.6 (RWGS-50), 166.9 (RWGS-150), 48.6 (CO2E-50) and 145.9 kt/a (CO2E-150). The table with the mass balance can be found in Appendix D.4. The energy balance is shown in Table 4.29. The energy demand for water electrolysis equals the predefined 50 and 150 MW_{el} for RWGS. In CO2E cases the electrolysis demand is split between water and CO_2 electrolysis. CO_2 electrolysis accounts for 35 % of the power input to the electrolysers. 65 % are fed to the water electrolysis. Together with pumping and compression power, the defined electricity input to the

electrolysers is exceeded by 8 to 12 %. As will be reported in the next section, integration with the pulp mill leads to a decreased electricity generation onsite.

Table 4.29 Energy balance of the AA production process in MW ([a] for heating the RWGS reactor, [b] of MeOH, Cativa or RWGS process)

CO generation	RWGS		CO2E	
Plant size in MW_{el}	50	150	50	150
Input				
Electricity total	55.0	167.4	54.1	165.2
- Water electrolysis	50.0	150.0	32.7	98.1
- CO_2 electrolysis	0.0	0.0	17.3	51.9
- Compression and pumping	4.1	12.2	2.8	8.4
- Integration	0.9	5.2	1.3	6.7
Natural gas[a]	3.7	11.0	0.0	0.0
Heat	23.3	70.0	23.2	69.7
Internal				
H_2	35.0	105.0	22.9	68.7
CO	9.9	29.8	8.7	26.0
MeOH	22.1	66.4	19.3	57.9
Output				
AA	29.6	88.9	25.9	77.7
Purge[b]	1.6	4.8	1.1	3.4
Heat	39.0	116.9	25.9	77.8

All cases show a heat surplus. The heat surplus of the RWGS processes is larger due to the fact that additional natural gas is combusted in the RWGS reactor. The heat surplus however as shown by pinch analysis does not turn into steam generation since much heat is available at low temperature levels. The energy efficiencies of CO generation including only electricity as input are 50 % for CO_2 electrolysis and 79 % for the RWGS unit. If also the heat demand of the RWGS reactor is considered, the efficiency drops to 56 %. The numbers show, that for these assumptions, RWGS is the more efficient CO generation technology.

4.8.3 Integration

The integration with the pulp mill's utilities is shown in Table 4.30. The increase in deionized water demand and waste water amount is marginal. The amounts are lower for the cases with CO_2 electrolysis as less deinoized water is needed for water electrolysis and no waste water is generated in the CO production process by CO_2 electrolysis. The O_2 production exceeds the demand in all cases. The 50 MW_{el} plants are able to make use of 5 % of the available CO_2 onsite. For the 150 MW_{el} plant, 14 or 16 % of the available CO_2 need to be captured. The purge streams of MeOH production, CO generation via RWGS and AA production is used in the RWGS reactor for heating. Therefore, in these cases no purge stream is combusted in the lime kiln. For CO generation based on CO_2 electrolysis, the purge streams are used to substitute natural gas in the lime kiln.

The AA production process has a high demand for low and medium pressure steam as shown by heat integration in Appendix D.4. Therefore, the electricity generation in the turbine drops substantially as steam is extracted for the AA process. The drop in electricity generation reaches 7.99 MW_{el} for CO2E-150. Table 4.31 shows the whole impact of integration on the electricity balance. Besides lower electricity generation through heat integration, waste water treatment, deionized water generation and process cooling cause a higher need for electricity. The shutdown of the O_2 plant makes 1.43 MW_{el} available. In total, the integration causes a decreased electricity availability for all cases.

Table 4.30 Impact of integrating the AA processes (Positive values for electricity generation due to heat integration means a drop in electricity generation)

CO generation	RWGS		CO2E		
Plant size in MW_{el}	50	150	50	150	
		CO_2			
CO_2 separated	85,293	255,878	74,080	222,232	t/a
Share of total CO_2	5%	16%	5%	14%	
		O_2			
O_2 production	62,515	187,545	54,124	162,370	t/a
Coverage of O_2 demand	227%	680%	196%	589%	
		Waste water treatment			
Additional amount	34,294	103,063	14,811	44,596	t/a
Increase in waste water	0.2%	0.7%	0.1%	0.3%	
		Deionized water			
Additional demand	70,392	211,175	46,041	138,124	t/a
Increase in deionized water	0.4%	1.2%	0.3%	0.8%	
		Heat integration			
Electricity generation	2.26	6.35	2.66	7.99	MW_{el}
Process cooling demand	4.24	12.66	3.32	9.93	MW_{th}
		Lime kiln			
Natural gas replaced	0.0	0.0	1.1	3.4	MW_{th}

Table 4.31 Effect of integration on electricity balance for the AA production

CO generation	RWGS		CO2E	
Plant size in MW_{el}	50	150	50	150
Waste water treatment	0.00	0.01	0.00	0.01
Deionized water	0.02	0.06	0.01	0.04
O_2	-1.43	-1.43	-1.43	-1.43
Heat integration	2.26	6.35	2.66	7.99
Process cooling	0.06	0.18	0.05	0.14
Total	0.91	5.17	1.29	6.74

4.8.4 CO_2 balance

The emission factor of AA is shown in Figure 4.17 for the utilization of the German grid mix. The reference value is taken from a Life Cycle Assessment database. The 150 MW_{el} plants overshoot the reference value due to the high impact of the grid electricity. Additionally, 0.10 t CO_2/t AA are added to the RWGS cases for reactor heating by the combustion of natural gas. RWGS-150 shows a lower emission factor than CO2E-150. For the CO2E cases, a credit of 0.04 t CO_2/t AA is assigned for the substitution of natural gas by purge stream combustion in the lime kiln. For both cases, the 50 MW_{el} plants show a tremendously lower emission factor compared to the reference and the 150 MW_{el} plants.

Figure 4.18 shows the emission factor of AA over the electricity factor of the imported grid electricity. Due to no grid electricity import for the 50 MW_{el} plant sizes, the emission factor of AA is independent of the grid electricity. The additional natural gas combustion in RWGS-50 leads to a positive emission factor. For CO2E-50, the emission factor is slightly negative as natural gas is substituted by purge streams.

The 150 MW_{el} plants share the same y-axis intersection as their corresponding 50 MW_{el} plant. The slope of CO2E-150 is slightly steeper than for RWGS-150. Starting at a lower y-axis value, the

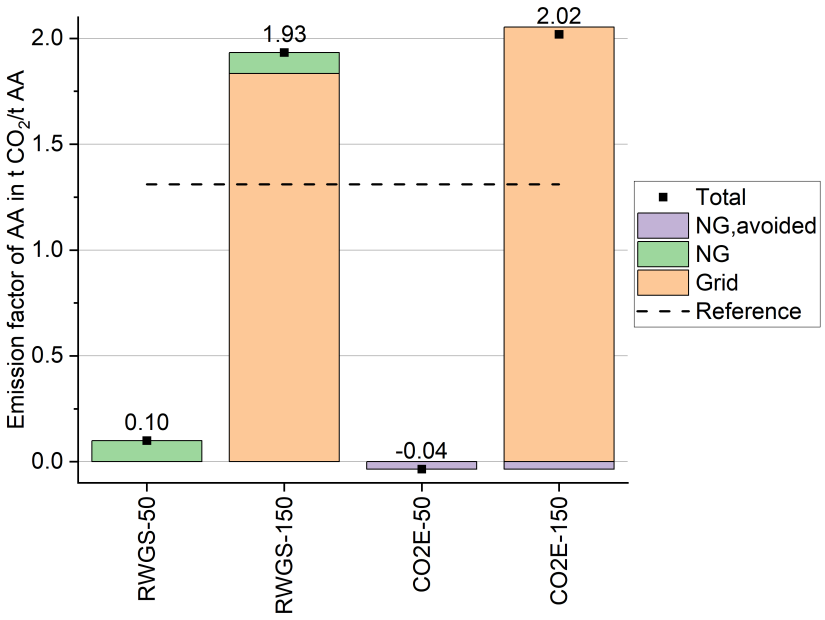

Figure 4.17 Emission factors of AA for the integrated plants (Reference: 1.31 t CO_2/t AA [234])

CO2E-150 curve intersects with RWGS-150 at 0.23 t CO_2/MWh. After this point RWGS-150 would be beneficial in terms of emissions. However, the difference between the two cases is marginal. The marginal emission factor with equal emissions as the fossil reference are at roughly 0.25 t CO_2/MWh for both cases. The curves of the greenfield plants show due to full grid electricity utilization a higher slope. Additionally, the curves have a higher y-axis intersection which is due to heat demand supplied by natural gas combustion for heating the RWGS process and for steam supply to the process. The marginal emission factor for electricity is at 0.08 and 0.10 t CO_2/MWh for the greenfield plants.

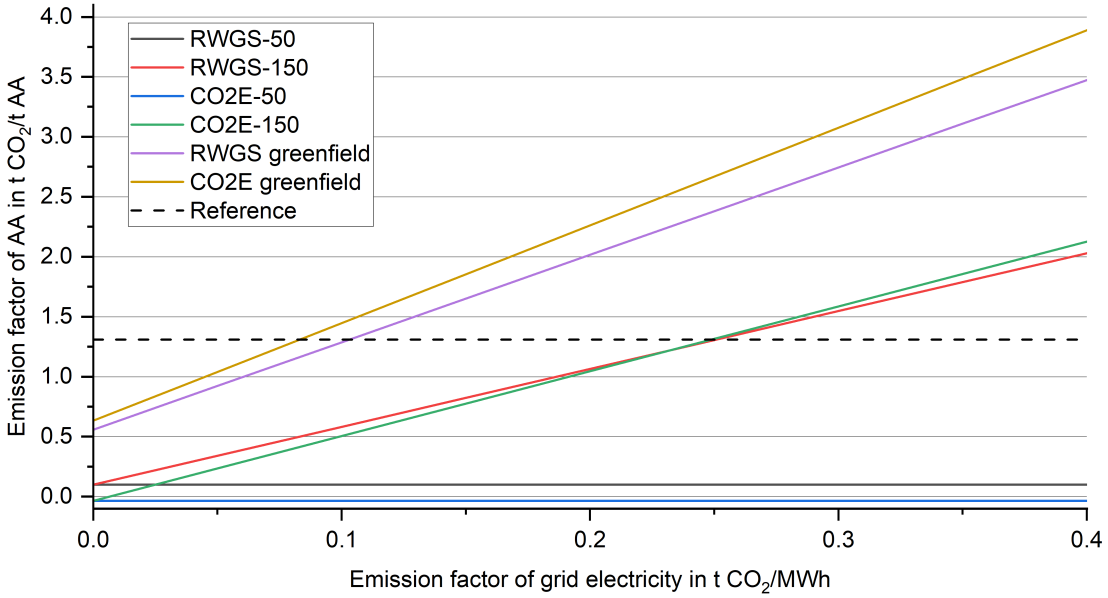

Figure 4.18 Emission factor of AA varying the carbon intensity of importedelectricity (Reference: 1.31 t CO_2/t AA [234]

4.8.5 Economic analysis

The levelized cost of AA is shown in Figure 4.19. A detailed cost break down can be found in Appendix D.4. Levelized cost are in the range of 1065 to 1386 €/t. Larger plants show lower cost due to the economy of scale and lower electricity cost for the grid electricity. The revenue from O_2 sale amounts to 15 - 24 €/t AA. Cost for electricity is in the range of 45 to 52 % of the TAC. The ACC is the second most influential cost factor with a share of 17 to 19 %. The water and CO_2 electrolysis accounts for 43 to 72 % of the FCI. Especially for CO2E-150 the cost impact of the electrolysis is due to no economy of scale more dominant. The rest of the FCI is attributed to the chemical process equipment.

As electricity is the most influential cost driver, Figure 4.19 also shows the levelized cost excluding electricity. The LCOAA drops by 692 to 513 €/t AA with a more significant drop for 50 MW_{el} plants. The LCOAA without cost for electricity would be lower than current market prices. For the exclusion of ACC from the cost calculation, the decrease is only 191 to 258 €/t AA. Again for the smaller plant size the drop is more significant.

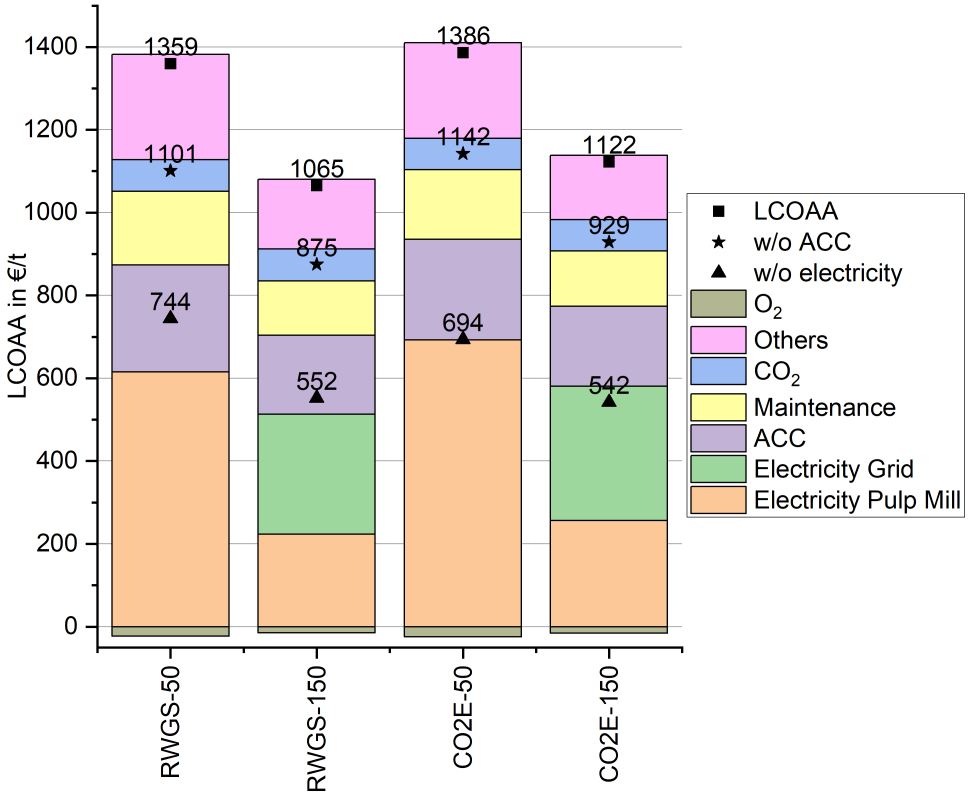

Figure 4.19 Levelized cost of AA

The sensitivity analysis in the Appendix D.4 shows the impact of economic and technical assumptions on the LCOAA. For all cases the impact of electricity cost is the most significant. For the 150 MW_{el} plants a change in grid electricity price causes a change of +/- 18 % or +/- 19 % for RWGS-150 and CO2E-150. For CO2E-150 all other changes result in a maximum change of 7 % of the LCOAA. The efficiency of water electrolysis shows for RWGS-150 the second most significant change of -8 to 10 %. All other assessments are below 7 %. For the 50 MW_{el} plants besides electricity cost, the efficiency of water electrolysis and maintenance cost are also significant. For RWGS-50, the impact of water electrolysis efficiency is due to the higher installed power in comparison to CO2E-50 more significant.

Further economic analysis is shown in Table 4.32. The increase in pulp price calculation considers a market enumeration (900 €/t) for AA. As the calculated LCOAA is close to the market price, the highest pulp price increase is 53 €/ADt (CO2E-150). The smallest increase is calculated for CO2E-150

at 39 €/ADt. The CO_2 abatement cost are 380 and 361 €/t CO_2 for RWGS-50 and CO2E-50. Due to an increase in emissions, the CO_2 abatement cost for 150 MW_{el} plants are not reported here.

Table 4.32 Increase in pulp selling price in €/ADt for market enumeration of AA and CO_2 abatement cost in €/t CO_2

CO generation	RWGS		CO2E	
Plant size in MW_{el}	50	150	50	150
Increase in pulp price	42	45	39	53
CO_2 abatement cost	380	-	361	-

4.8.6 Discussion

The model validation is difficult due to limited availability of data in literature. Jones reports a CO utilization of above 94 % [124]. In the models presented here, the CO utilization reaches 97.6 % (CO input compared to the final product output). The side pull from column C1 is reported to have an AA concentration of 93-94 % [126]. In the model, the side pull shows a concentration of 95.4 wt. % which is close to the range as reported in the patent. A comparison to the only available process model in literature by Dimian and Kiss [123] is useless as they did not validate their model. Furthermore, data for comparison is lacking and the soundness of the modeling approach can be improved.

The economic comparison with the market price shows that AA can be a promising product. For green AA, the market price would be also higher than for fossil AA making it even more interesting in terms of economics. However, the process route is quite long and it is questionable if pulp mills are keen to dive into chemical process engineering. Compared to the other PtX routes, AA production not only needs the Cativa process which is itself already very complex but also the MeOH and CO production. The willingness of a pulp mill to invest in this chemical site is questionable. Therefore, a partnership with a chemical company might be useful to realize the project onsite. Otherwise a split production of AA might be an option. MeOH produced in the pulp mill can be used for AA production with fossil CO at a different site than the pulp mill. This would harness the green heat supply by the pulp mill to the Cativa process which has a tremendous heat demand.

4.8.7 Intermediate summary

This section presented the production of AA in a pulp mill based on two different CO generation technologies. Main findings are:

- Both process routes show despite many process steps carbon efficiencies above 95 %. In terms of energy efficiency, the RWGS process routes are superior compared to CO_2 electrolysis. However in terms of hydrogen efficiency, the CO_2 electrolysis is more efficient.
- Besides electricity for the electrolysis processes, compression and pumping also requires a significant amount of electricity. Purge streams are available for combustion in the RWGS reactor or the lime kiln. The RWGS cases need also additional natural gas to satisfy the heat demand of the RWGS reactor. The electrically heated RWGS reactor could be a way to improve the CO_2 balance.
- All cases require low and medium pressure heat from the pulp mill. The availability of low carbon heat is beneficial in comparison to greenfield plants. However, in all cases the cut in electricity generation by heat integration together with higher demands for other utilities results in a net reduction of electricity availability in the pulp mill.
- The emission factor of AA is dependent on the emission factor of the used grid electricity for the 150 MW_{el} plants. With the German grid mix, the emission factor of AA will exceed the

fossil reference. The marginal emission factor for the 150 MW_{el} plants are at 0.25 t CO_2/MWh (0.08 to 0.1 t CO_2/MWh for the greenfield plants). The supply of green heat to the process is besides the damped impact of electricity the main difference of the integrated compared to the greenfield plants.

- LCOAA are in the range of 1065 to 1386 €/t AA. Main cost driver is the electricity cost and the ACC. Larger plant sizes show lower LCOAA. The LCOAA is very promising in comparison to market prices for fossil AA.
- The CO_2 abatement cost are 361 and 380 €/t CO_2 for CO2E-50 and RWGS-50. The increase in pulp price is moderate at 39 to 53 €/ADt.

4.9 Holistic discussion and comparison of production routes

This section deals with the comparison of the various routes and products that were presented in Sections 4.4 to 4.7. From the comparison, the best process options for integrating PtX routes into pulp mills are evaluated and discussed. General statements of the integrated plants can also be transferred to greenfield plants.

4.9.1 Integration and technical parameters

This section discusses and compares the processes in terms of technical parameters and integration into the pulp mill. All shown figures show values which are normalized by the input of electrical energy to the PtX plant including power demand of electrolysis, compression and pumping, and integration. As the values are normalized with the electricity demand including the pulp mill integration, the values do not transfer directly to greenfield plants. Figure 4.20 shows the CO_2 flows in the pulp mill. CO_2 from imported electricity is excluded in the figure. The bound CO_2 is obviously always smaller than the captured CO_2 flow. The ratio of bound to captured CO_2 is also a representation of the carbon efficiency. However, for MeOH cases, the carbon of FC found in the product is not included in this CO_2 balance. The bars for H_2O_2 are zero as no CO_2 is captured for this production process and no natural gas is substituted or additionally consumed. The highest flow of bound CO_2 per input of electricity is reached for AA production meaning that this process can bound the most CO_2 per input of electricity. The lowest values for bound CO_2 are found for the open loop FT processes as the tail gas is burnt and CO_2 is released with the flue gas of the lime kiln or RWGS reactor.

The substitution of natural gas in the lime kiln by the combustion of purge streams reduces the CO_2 emissions from natural gas combustion. The CO_2 savings equal zero for SNG, AA-RWGS, FT-RWGS-CL and H_2O_2 as no purge streams are available. The highest values are found for the other FT processes. Additional CO_2 emissions arise from the combustion of natural gas which happens only in the RWGS reactor for FT syncrude and AA production.

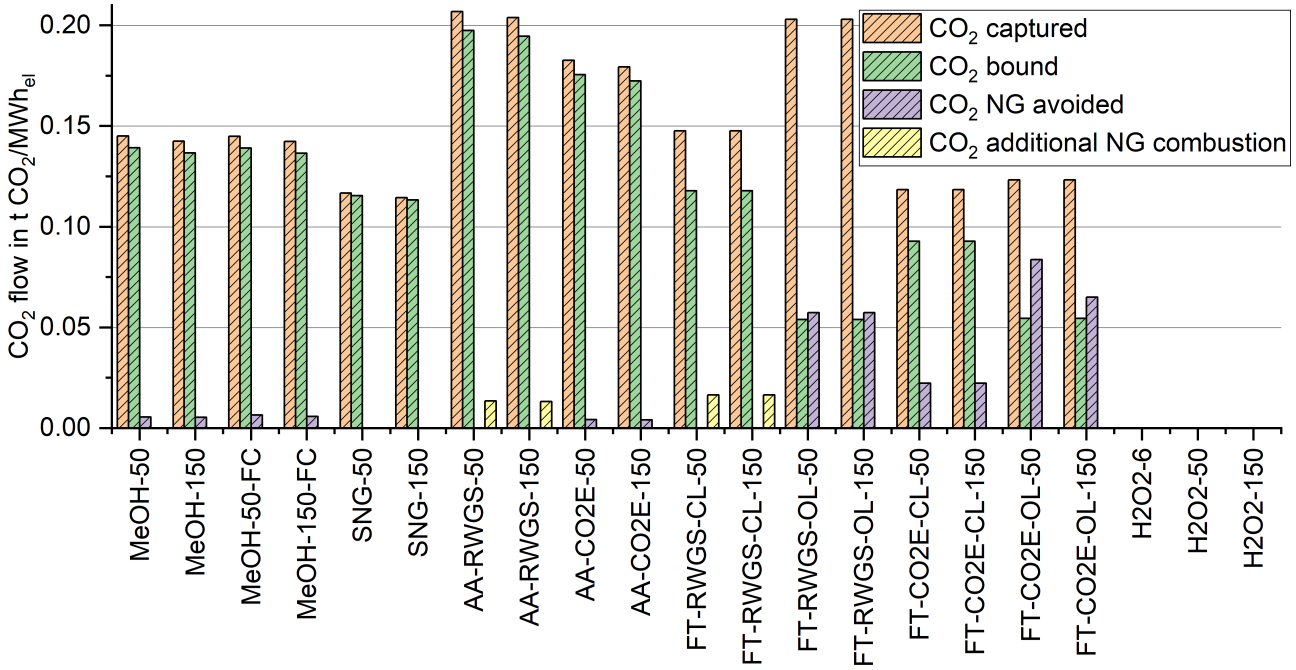

Figure 4.20 Comparison of CO_2 flows in t CO_2/MWh_{el} (CO_2 from grid electricity not shown)

The impact on the steam balance of the pulp mill is depicted in Figure 4.21. The steam energy flow is aggregated not taking into account the temperature levels. H_2O_2 neither exports nor imports steam

resulting in no bars in the diagram. A very high steam demand is found for MeOH and AA. As MeOH already shows a quite high thermal energy demand, the AA process, especially the purification steps including 3 distillation columns, are added to the steam demand of the MeOH process. A high steam demand means a reduction of steam availability in the pulp mill which results in a reduced electricity generation. For increasing plant sizes, the required steam supply by the pulp mill can exceed the onsite availability. Consequently, the PtX process and pulp mill would need another energy source like an additional fuel boiler. Steam export to the pulp mill, as for SNG, FT-RWGS-CL, FT-CO2E-CL and FT-CO2E-OL-150, means an increased generation of electricity which can however be limited by the capacity of the turbine. An energetic improvement of the CO_2 capture process which is one of the main steam consumers can reduce the steam demand of the PtX process tremendously. This would shift all bars upwards. Nevertheless, MeOH and AA processes will most likely remain steam importers.

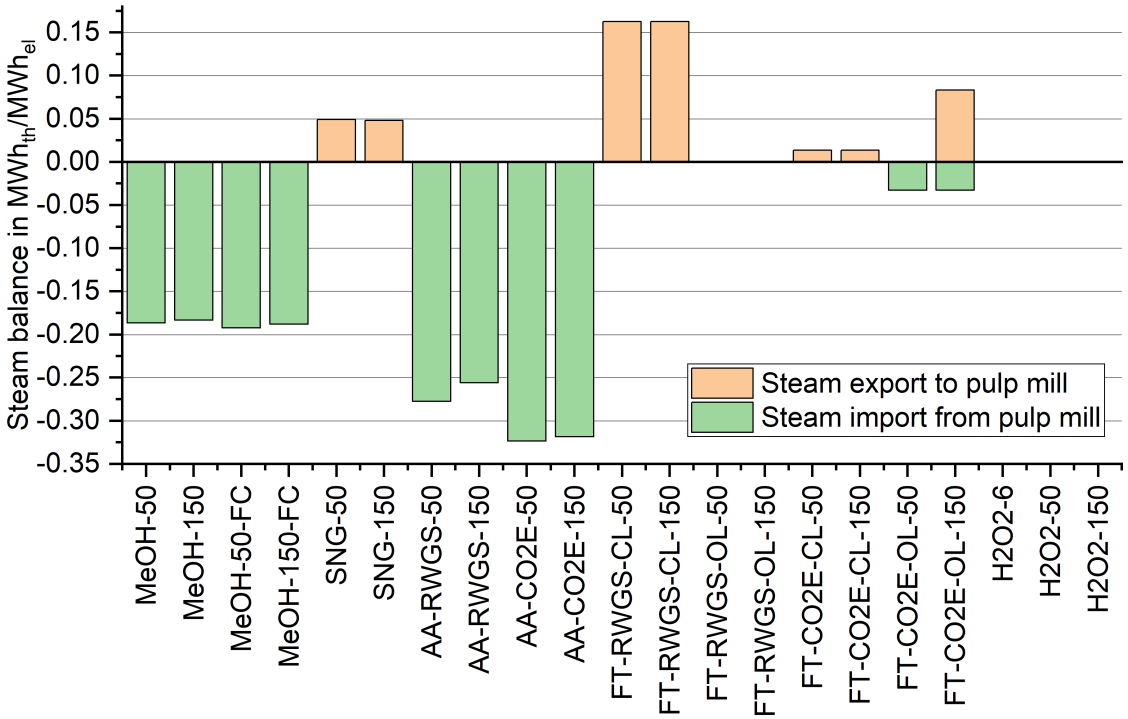

Figure 4.21 Comparison of steam import and export of the PtX processes in MWh_{th}/MWh_{el}

In summary, steam exporting processes are advised for mills with available capacity in the turbine for electricity generation. This might also be the best option for integrated mills or mills planning to invest in a lignin separation (provided available turbine capacity). Mills with an already high energy surplus will be capable of integrating a steam importing PtX processes. For example a mill with a limited capacity in the turbine, planned energy efficiency increasing measures or an expansion of the production capacity requires an investment in the steam cycle to increase the electricity generation capacity. In this case, a steam importing PtX plant erases the need for the steam cycle modification. Since the numbers are derived from pinch analysis, the real life heat integration might be different. The ΔT of 20 K was used to get a more conservative result. However, the setup of the heat exchanger network needs to be designed specifically for each pulp mill. Generally a non-ideal heat integration means less interchanged energy and a higher demand for heating and cooling utilities. Consequently, the numbers in Figure 4.21 are subject to changes.

Figure 4.22 shows the normalized flows of waste water, O_2, deionized water and process cooling. The demand for deionized water and production of waste water correlate. Higher deionized water demand means that more H_2 is produced which will produce waste water as side product in the reactions with CO_2/CO (except for H_2O_2 as product). The O_2 production is very similar for processes

using only water electrolysis as the power input is equal per definition. For cases using water and CO_2 electrolysis, the O_2 production is lower. Pulp mills with a bottleneck in deionized water production or waste water treatment are advised to choose process with lower figures for these utilities like for example MeOH, AA-CO2E or FT-CO2E. As explained earlier, processes with CO_2 electrolysis show a lower waste water amount. The MeOH process produces very little waste water but exhibits a high demand for deionized water. Especially, H_2O_2 is very water intensive. Deionized water is used for water electrolysis and additionally for the extraction of H_2O_2. Furthermore, the process has a high demand for process cooling. The demand for the 6 MW_{el} plant is lower due to no purification of the crude H_2O_2. For the other processes, the cooling demand is in similar ranges except for some FT cases with very low cooling demand. For pulp mills with a limited cooling capacity, H_2O_2 is not advised. The cooling demand was derived from pinch analysis. The real heat exchanger network as stated earlier might not reach the ideal heat integration as calculated. Therefore, an even higher process cooling demand might arise. Furthermore, it is unclear if the heat transferred to hot water can be efficiently used onsite or sold to a third party.

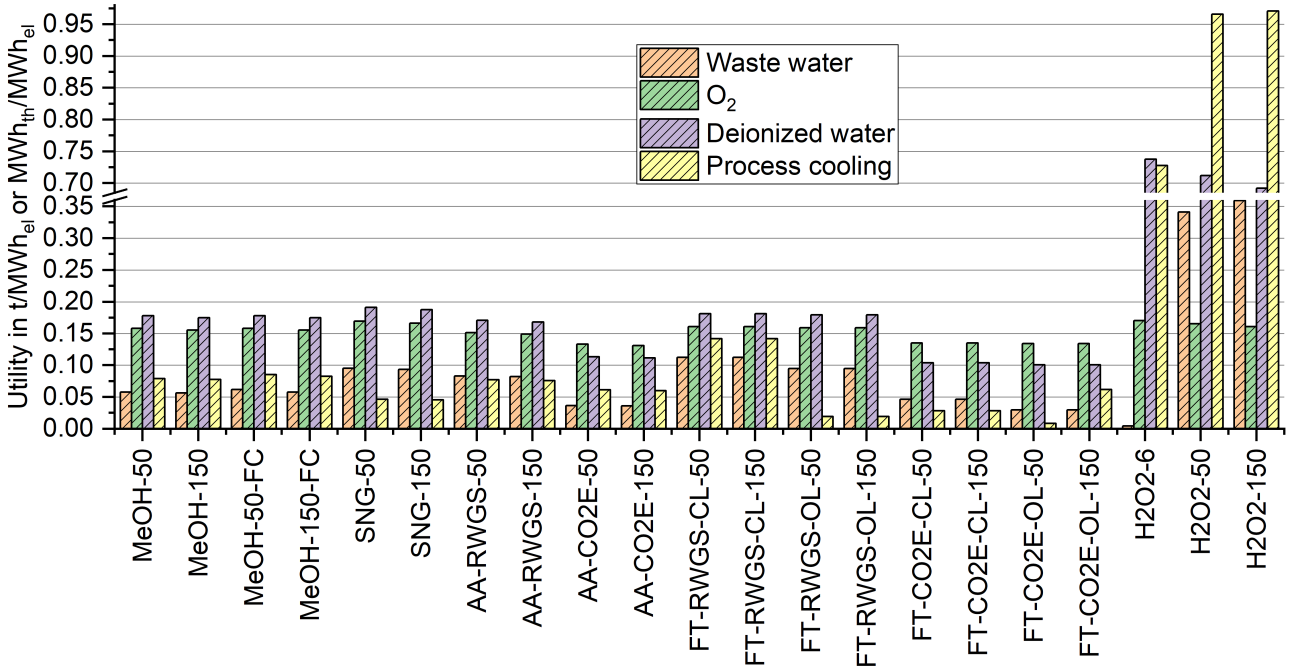

Figure 4.22 Comparison of normalised waste water, deionized water, O_2 and process cooling demand/flow in t/MWh_{el} or MWh_{th}/MWh_{el}

The by-product O_2 is valorized onsite for the substitution of O_2 derived from onsite production (or truck delivery to the pulp mills if no on-site generation is available). The production of O_2 usually exceeds the onsite demand. Therefore, the O_2 production is not a critical factor for choosing the PtX production process. If the utilization of O_2 beyond the required demand can be realized (for example in the waste water treatment plant or for O_2-enriched combustion), the O_2 production amount might become important.

Figure 4.23 reports the purge stream for combustion in the lime kiln. The figures shows only the purge stream combusted in the lime kiln not including purge streams combusted in the RWGS reactor. The cases with RWGS unit consume the purge stream themselves and additional natural gas for reactor heating is needed. No purge streams for combustion in the lime kiln are found for SNG, AA-RWGS, FT-RWGS and H_2O_2. SNG and H_2O_2 have no purge streams at all. MeOH and AA have purge streams with a low thermal power compared to the open loop configurations of the FT process which are designed to supply the lime kiln with fuel besides the syncrude production. For FT-CO2E-OL the difference between the 50 and 150 MW_{el} plant derives from the fact that the total tail

gas of the 150 MW_{el} plant exceeds the lime kiln's capacity and is therefore combusted in the recovery or bark boiler.

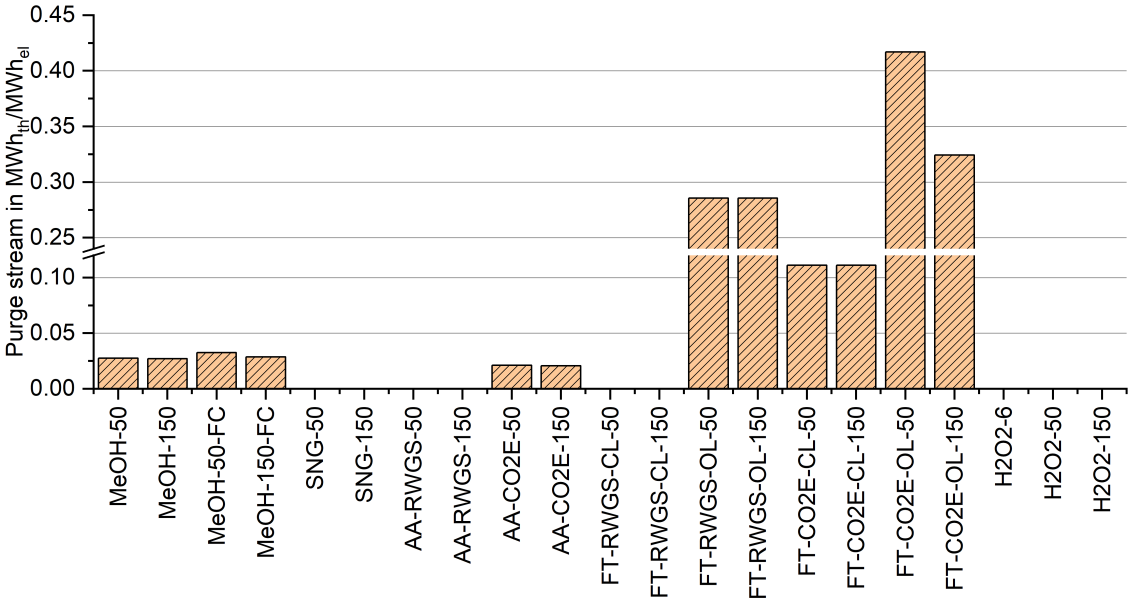

Figure 4.23 Comparison of purge streams sent to the lime kiln for combustion in MWh_{th}/MWh_{el}

Consequently, pulp mills aiming for a simultaneous decarbonization of the lime kiln should go for a process with high purge stream to the lime kiln. For pulp mills with an already decarbonized lime kiln the high purge stream flow might not be beneficial.

4.9.2 Economics

In this section, the economics are compared in terms of pulp price increase and in terms of difference between LCOP and market price. With this assessment the economically most favorable routes can be identified.

Figure 4.24 compares the levelized cost of product to the fossil comparator. 0 % indicates equivalent cost. It is important to keep in mind that the levelized cost exclude a revenue for the producer. Therefore, market prices of the products must be higher than the LCOP to generate a revenue for the producer. The graph shows that MeOH and AA (derivate of MeOH) are the closest to the market price. The increase is between 18 and 87 %. For free electricity, the cost decrease to a maximum of 40 % reduction compared to the fossil product. Excluding the ACC from the cost calculation leads to a less significant product price change of -3 to 57 %. H_2O_2 shows a cost reduction for all cases ranging from -6 to -29 %. For free electricity, the cost are further reduced by up to -61 %. The cost of the H_2O_2 process must be treated with caution as explained earlier (Section 4.6). SNG and FT syncrude prices are a lot higher than market prices of fossil products. SNG overshoots market prices by 724 and 864 %. The increase for FT syncrude is in the range of 353 to 959 %. Even without electricity cost or ACC, the products still show a tremendous increase compared to the fossil comparators.

The comparison also shows that LCOP are dependent on production capacity of the plant. In order to further lower the product cost, larger plant sizes can be considered. However, the maximum plant size is not limited by the available CO_2 but by the available heat onsite if no additional heat generation capacity should be installed. Schemme shows for MeOH production that the resulting price changes from 1.985 €/l_{DE} (50 MW_{MeOH} output) to 1.867 €/l_{DE} (441 MW_{MeOH} output) [257]. König shows a dependence of plant capacity on the product cost for annual production amounts below 1 Mt/a [258]. The levelized cost of syncrude changes between 3.64 to 3.36 €/kg. Based on these assessments, the LCOP can be slightly reduced with larger plant capacity but the effect is not extremely significant.

More significant in this thesis is the assumption for electricity cost of grid electricity which is lower than for the electricity supplied by the pulp mill.

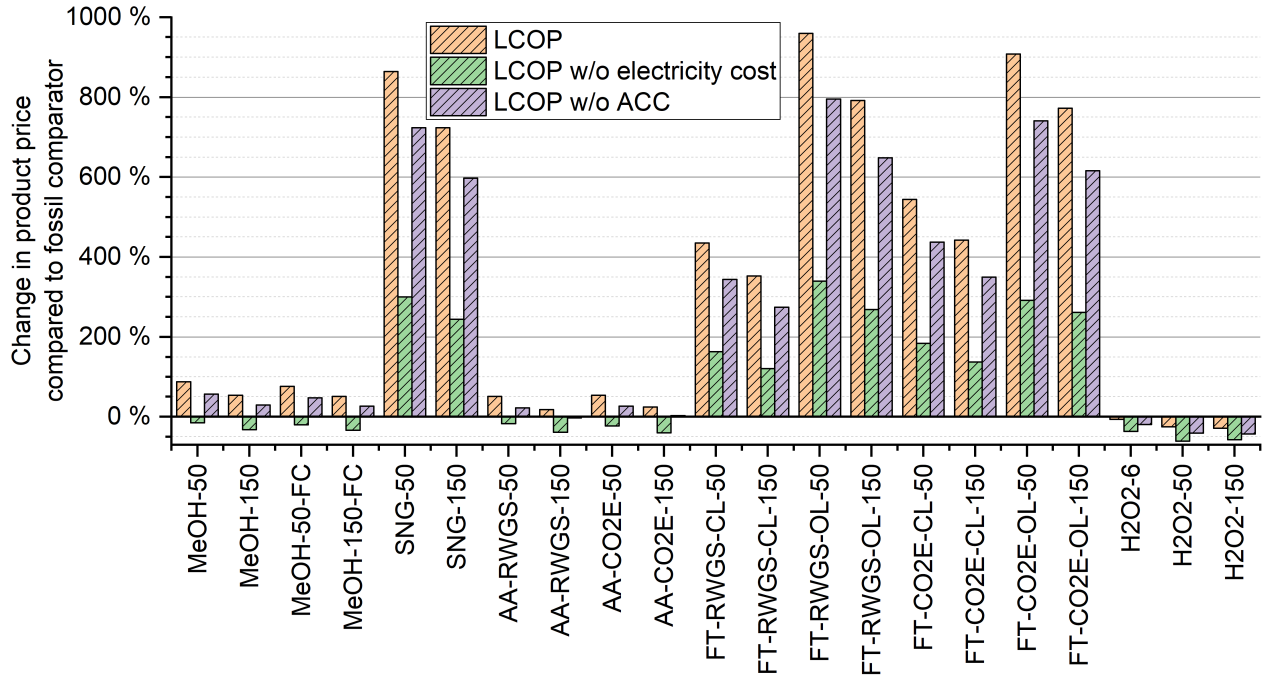

Figure 4.24 Comparison of LCOP to the market prices of the fossil equivalents (MeOH: 800 €/t, Natural gas: 25 €/MWh, AA: 900 €/t, H_2O_2: 750 €/t, Crude oil: 0.74 €/kg)

Figure 4.25 gives a more detailed insight in the composition of the TAC. The ACC's share is below 20 % for all cases. For SNG the share is the smallest with the exception of H2O2-6. The impact of ACC is the highest for the H_2O_2 production routes except H2O2-6. As discussed before, electricity cost for electricity imported from the grid or received from the pulp mill are the biggest share of TAC. Electricity cost account for up to 61 % of TAC. The amount of electricity imported from the grid is bigger compared to the electricity provided by the pulp mill for the 150 MW_{el} plants. The share of imported grid electricity is however not significantly greater than the pulp mill's electricity as the price is lower. Especially for the AA production processes and FT-RWGS-CL, the impact of electricity cost on the TAC is lower compared to the other processes. Especially low is the impact indeed for H_2O_2. Higher operating cost come from makeup of anthraquinone. Furthermore, H2O2-50 and -150 also contain a credit for replaced H_2O_2 which distorts the assessment.

Figure 4.26 shows the impact on the pulp selling price assuming that market prices are paid for the products. The change in pulp selling price ranges from -132 to 199 €/ADt. Market prices for pulp are in the range of 300 to 800 €/ADt. Negative prices are found for H_2O_2 as the calculated LCOH2O2 is below the market price. The lowest price increase is found for MeOH and AA meaning that these products are also promising in terms of economics. Since AA is a derivate of MeOH, the prospects for this product are similarly good. Further derivates from MeOH could be investigated as promising routes.

However, the calculated increase in pulp price depends massively on the assumed market price of the product and the pulp mill's capacity. A change of these two variables will impact the increase of pulp price. Pulp mills with a higher pulp production capacity will show a lower increase in pulp price since the deficit would be allocated on a higher pulp production. Higher market prices will also reduce the increase in pulp price or even lead to a decrease in pulp price for LCOP below market prices. Furthermore, the market price of fossil product will not be equal to the market price of sustainable products. It can be expected that the PtX products from the pulp mill can attain much higher market prices than the fossil product. This leads to an even smaller or negative pulp price increase.

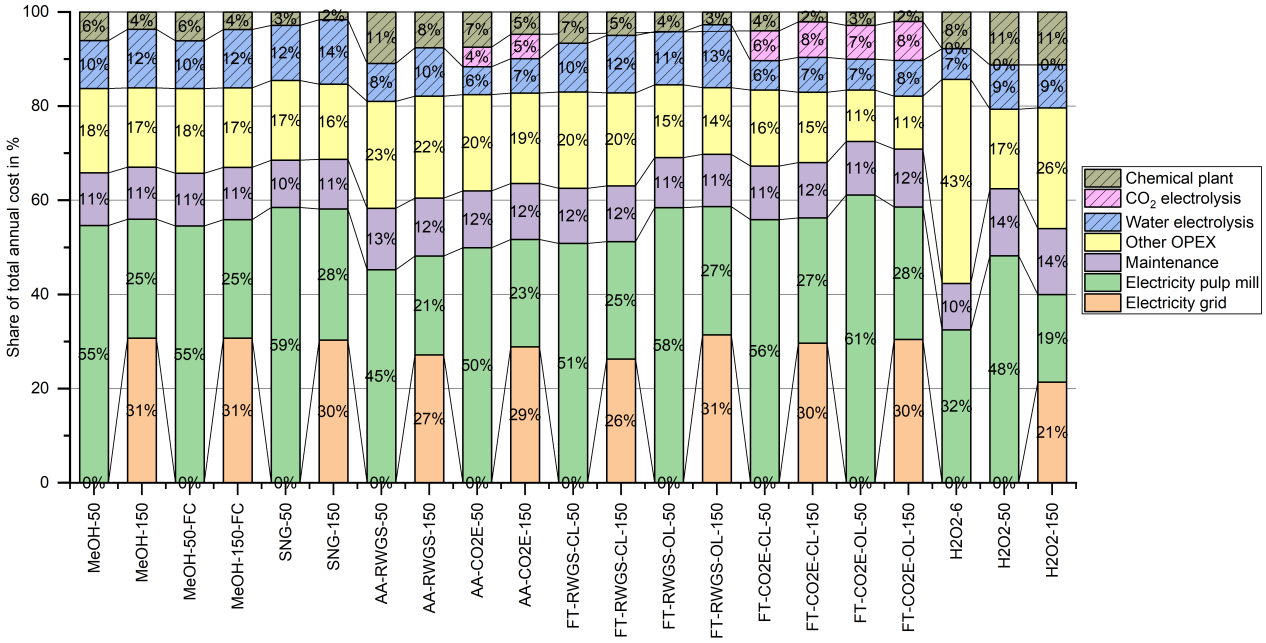

Figure 4.25 Comparison of TAC broken down for the most relevant cost categories (ACC contribution is hatched)

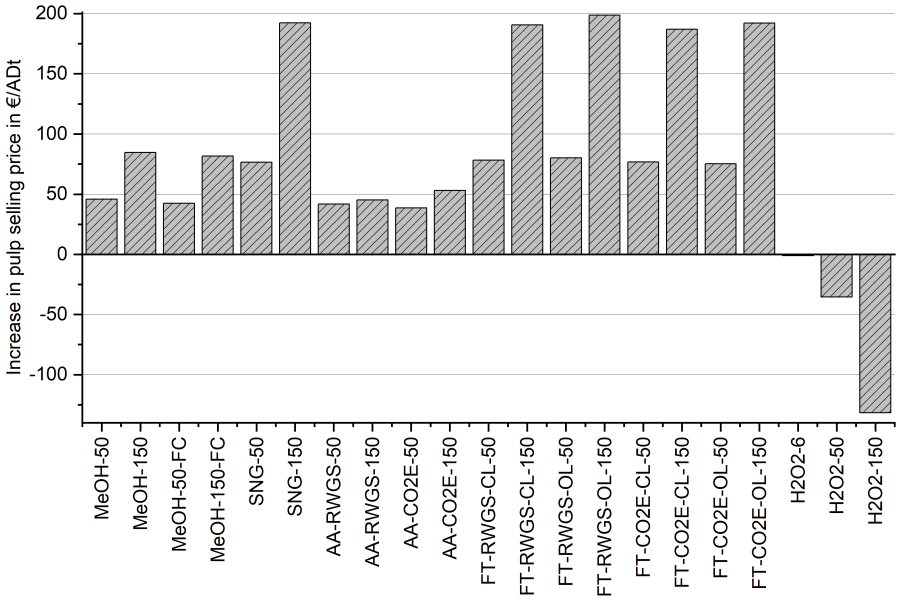

Figure 4.26 Increase in pulp price if market prices are enumerated

Table 4.33 shows the CO_2 AC for cases with a reduction in CO_2 emissions. The AC are organized in ascending order. Following the merit order principles, lower AC are more cost effective in reducing CO_2 emissions than higher AC. The by far lowest cost, as also already discussed in this section before, is found for H_2O_2 followed by MeOH and AA. The cost for H_2O_2 are negative meaning a CO_2 reduction equals a reduction of cost. For the other cases, the reduction of CO_2 emissions will cause higher cost.

Table 4.33 Comparison of CO_2 abatement cost in €/t CO_2

Process	CO_2 abatement cost
H2O2-150	-542
H2O2-50	-165
MeOH-50-FC	303
MeOH-50	349
AA-CO2E-50	361
AA-RWGS-50	380
FT-CO2E-OL-50	848
FT-CO2E-CL-50	991
SNG-50	1076
FT-RWGS-OL-50	1103
FT-RWGS-CL-50	1144

The calculation of AC is very sensitive to different assumptions like for example market prices for the fossil comparator. The comparison with literature based on different assumptions than in this thesis needs to be treated with caution. Ueckerdt et al. calculated AC for e-gasoline to 800 €/t CO_2 or to 1200 €/t CO_2 for e-methane which is in the same range than the values calculated here [264]. The product's AC must also be assessed in terms of the sector they can be used for. MeOH can be used for fuel blending. Therefore, it would be a more cost effective way to reduce CO_2 in the transport sector than FT fuels. The blending of MeOH is limited and therefore other fuels are still needed for a deeper decarbonization. On the other hand, MeOH can be used as feedstock in the chemical industry. Here ACs for biomass based MeOH are assessed to -150 to 450 €/t CO_2 [265]. In the chemical industry, MeOH has to compete with other sustainably produced raw materials but also with other technological options like CCS or energy efficiency measures for example.

4.9.3 Efficiency

Figure 4.27 shows carbon, hydrogen and Power-to-Fuel efficiency for all investigated cases and products. Power-to-Fuel and carbon efficiency do not apply to the production of H_2O_2.

Carbon efficiencies range from 26.6 % for FT-RWGS-OL to 102.2 % for MeOH-50-FC. The highest carbon efficiencies are reached for MeOH, SNG and AA. The open loop FT routes harness carbon efficiency for the supply of fuel to the lime kiln. High carbon efficiencies should be preferred as CO_2 separation is an energy intensive process. The heat demand of the CO_2 scrubber influences the heat integration with the pulp mill immensely. If the captured CO_2 can be efficiently stored in a product, the CO_2 reduction of the pulp mill is increased. The hydrogen efficiency is the highest for H_2O_2 production as the selectivity of the process is very high and almost no side products and no water are produced. For process routes with either RWGS or CO_2 electrolysis, the hydrogen efficiency will be higher for the routes with CO_2 electrolysis.

The Power-to-Fuel efficiency ranges from 16.7 % for FT-RWGS-OL-150 to 60.2 % for MeOH-50-FC. Generally high efficiences are reached for MeOH, SNG and AA-RWGS. The open loop FT processes again sacrifice the efficiency for the supply of fuel gases to the lime kiln. However, also the closed loop cases are limited in efficiency compared to other products like MeOH or SNG. Despite the low

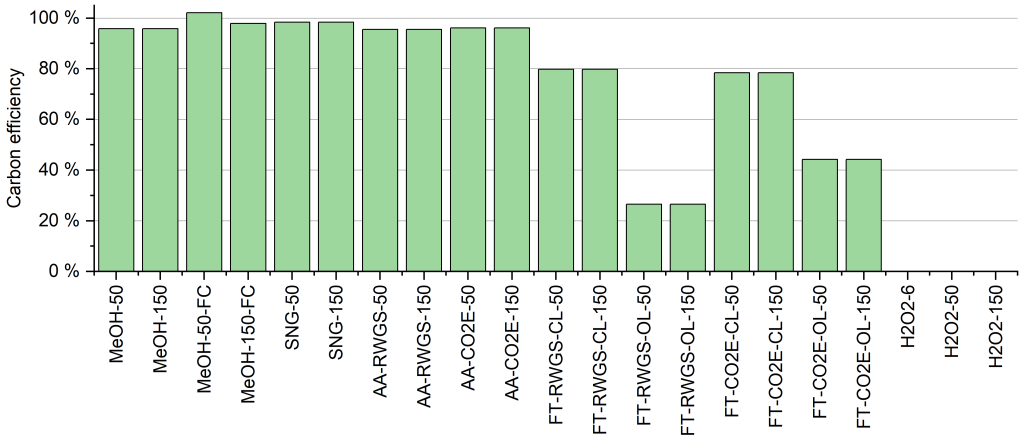

(a) Carbon efficiency

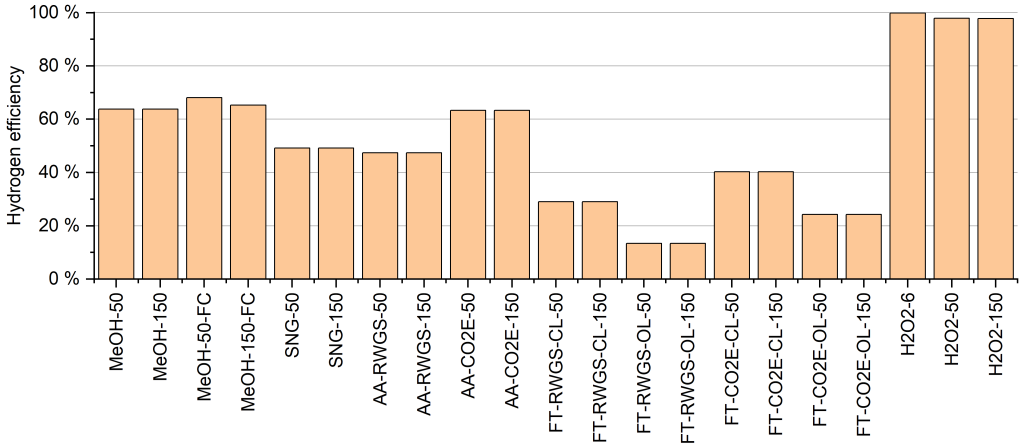

(b) Hydrogen efficiency

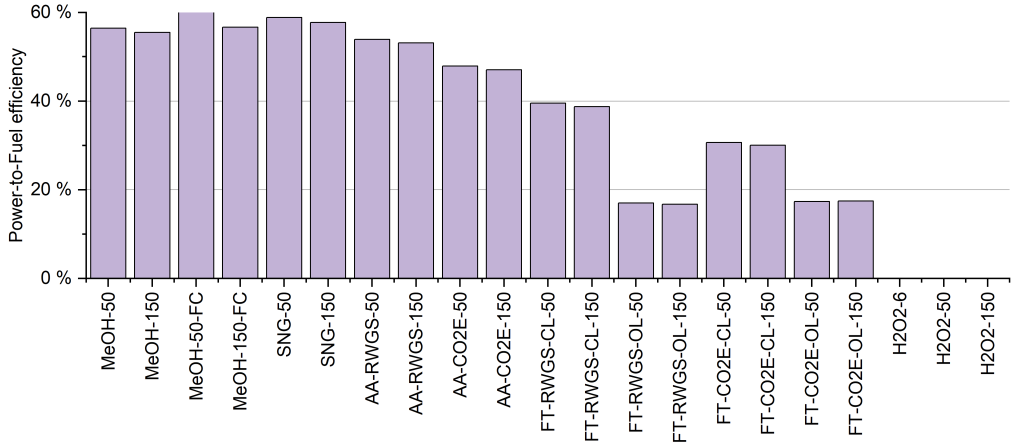

(c) Power-to-Fuel efficiency

Figure 4.27 Carbon, hydrogen and Power-to-Fuel efficiency for comparison

efficiency, FT syncrude might have a market for decarbonization of niches that cannot be decarbonized by other renewable or PtX product.

4.9.4 CO_2 emissions

In order to determine the most promising product in terms of CO_2 emission reduction, Figure 4.28 shows the product specific emissions normalized by the fossil comparator (MeOH: 97.1 g CO_2/MJ, SNG: 55.8 g CO_2/MJ, H_2O_2: 1.12 t CO_2/t H_2O_2, FT syncrude (transportation fuel): 94 g CO_2/MJ, AA: 1.31 t CO_2/t AA). Through normalization, the products can be compared to each other. The zero line equals the same CO_2 emissions as the fossil product. Consequently, negative values mean a reduction of CO_2 emissions.

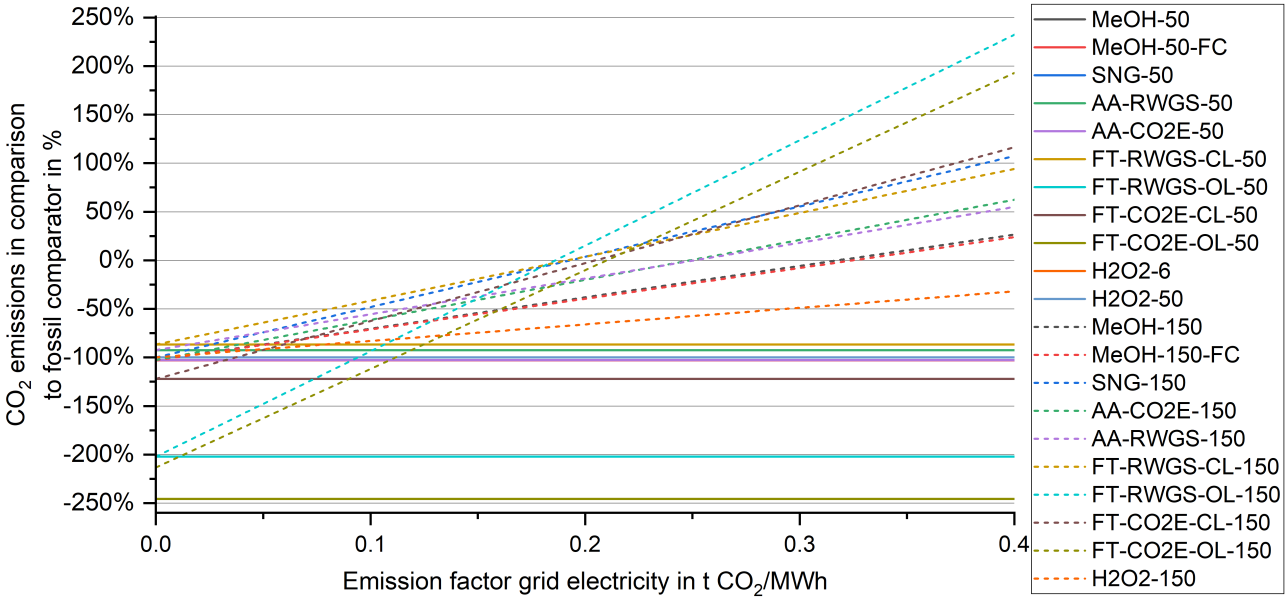

Figure 4.28 Comparison of CO_2 emissions (normalized by fossil comparator, 150 MW_{el} plants represented as dashed lines)

Despite the many lines, the figure is supposed to show some general trends. The 50 MW_{el} (and 6 MW_{el}) plants show horizontal lines as they are independent of the grid electricity. Consequently these plants have the best potential to produce low or even negative emission products. The most significant decrease can be observed for the FT plants: - 246 % for CO2E-OL-50, - 202 % for RWGS-OL-50 and -122 % for CO2E-CL-50 which is mostly associated with the substitution of natural gas in the lime kiln. Inversely FT-RWGS-50 shows the highest emission factor due to additional natural gas combustion.

The 150 MW_{el} plants are represented by linear curves. The marginal emission factor for the products is roughly in the range of 0.2 bis 0.3 t CO_2/MWh (excluding H_2O_2). At this emission factor for grid electricity, the emission factor of the PtX product equals the fossil comparator. In order to reach an emission reduction, the emission factors for grid electricity must be below the marginal emission factor. Figure D.38 in Appendix D.6 zooms in on the area of the marginal emission factor for a more precise assessment of the routes. Lower grid emission factors are required to reach the legislative goals defined by the EU for electricity based fuels (roughly 0 to 0.15 t CO_2/MWh). H_2O_2 however, does not cross the zero line for the considered range of grid electricity emission factor and shows the lowest emissions for a wide range. Besides different zeros, the curves of the 150 MW_{el} plants exhibit different slopes. For a higher grid emission factor, MeOH shows comparatively the lowest product emission factor. In this region, FT syncrude produced by RWGS-OL-150 and CO2E-OL-150 show the highest increase. Contrary, for lower grid emission factors, these cases exhibit the highest decrease in emissions due to the impact of substituted natural gas. For the region of low emission

grid electricity, in all other cases than RWGS-OL-150 and CO2E-OL-150 the emission factors of the products are moving closer together.

For greenfield plants (not shown in the graph), the marginal emission factor would be a lot lower than for the pulp mill integrated plants. Marginal emission factors are well below 0.2 t CO_2/MWh. Consequently, very low emission factors for electricity are required to reach the same product emission factor as for the pulp mill integrated plants.

The plant size will of course also influence the resulting emission factor as it affects the amount of imported grid electricity. The calculations here were only performed for two exemplary plant sizes (except for H_2O_2). For smaller plant sizes, the demand for grid electricity is usually lower or equals zero. Therefore, the resulting emission factor of the product will be the lowest. For larger plant sizes, the demand for grid electricity increases. The ratio of electricity delivered by the pulp mill would approach zero for huge plant sizes. Consequently, the product almost exhibits the emission factor of a greenfield plant excluding the impact of heat supply. Therefore, very large plant sizes harness the advantage of utilizing a high share of low carbon electricity from the pulp mill but keeping the advantage of green heat to some extent. Furthermore, the plant size is limited by the availability of heat in the pulp mill. If the heat availability is exceeded, the needed heat must be delivered by other resource possibly leading to additional CO_2 emissions.

Some products are replacing the fossil production routes that can be easily introduced to the market. These products can therefore lead to a faster CO_2 emission reduction instead of products for which a new infrastructure needs to be established (for example FT syncrude upgrading). Furthermore, the graph does not show which product is more promising as it reduces emissions in a hard to abate sector.

4.9.5 CO_2 electrolysis vs. RWGS

CO_2 electrolysis and RWGS process are investigated as competing technologies for the supply of CO to the AA and FT process. All graphs for comparison are found in the Appendix D.7. In general, the comparison of the FT-OL process shows a very different behavior than the conventional FT-CL or the AA process.

Figure D.39 in Appendix D.7 shows the graphs for the efficiencies. In terms of hydrogen efficiency, the CO_2 electrolysis based paths are superior as no H_2 is used for the conversion of CO_2 to CO in the RWGS process. The water resulting from the RWGS reaction decreases the hydrogen efficiency substantially. For the carbon efficiency, all the routes are very similar except for FT with open loop configuration. In this case, CO_2 electrolysis outperforms the RWGS process as the tail gas of the RWGS process removes much carbon from the process containing much unconverted CO_2. The Power-to-Fuel efficiency of RWGS cases is higher for all cases except FT-OL. Here, the CO_2 electrolysis based processes are slightly more efficient. If the natural gas is also taken into account for the other cases in the calculation, the efficiency of the RWGS process would drop but still be higher than CO_2 electrolysis.

The comparison of the levelized cost of product between CO_2 electrolysis and RWGS process (Figure D.40) shows higher cost with CO_2 electrolysis based cases for AA and FT-CL. Only for FT-OL, the processes with CO_2 electrolysis show slightly lower LCOS. Nevertheless, the only remarkable cost difference is found for FT-CL processes. For the other cases the difference is below 5 %.

The assessment of CO_2 emissions (Figure D.41) shows that the CO_2 electrolysis based processes exhibit lower emissions for the 50 MW_{el} plant size compared to the RWGS cases. This is mainly due to no additional natural gas needed and increased amount of natural gas substituted in the lime kiln. For the 150 MW_{el} plants the slope of the curves are similar. Lower emission factors are preferable for FT-CO2E-150-CL and AA-CO2E-150 as the curves intersect with the corresponding RWGS cases at roughly 0.2 t CO_2/MWh. For FT-OL-150, RWGS is generally preferable.

5 Decarbonization and defossilization of the lime kiln

This chapter deals with the decarbonization and defossilization of the lime kiln as the lime kiln can be one of the last point sources for fossil CO_2 in pulp mills. In order to further reduce fossil emissions, three feedstock options namely biomass, CO_2 or electricity for the production of H_2, and combinations of those are viable. Other possible solutions like for example plasma calcination or electrical heating are not considered here. Furthermore, all investigated systems can probably be technically retrofitted without immense changes to the system. The theoretical background for lime kilns in pulp mills can be found in Section 2.1.2. As the process is very similar to cement production, the presented concepts can also be used in the cement industry. In Figure 5.1, the mass balance (and electricity to electrolysis) of all process options are shown. In Section 5.1, the considered cases are defined. The modeling and evaluation is presented in Section 5.2. Based on the model, the generated results for mass and energy balances, CO_2 balance and economics are presented in Section 5.3. The results are discussed in Section 5.4 and subsequently summarized in the conclusion.

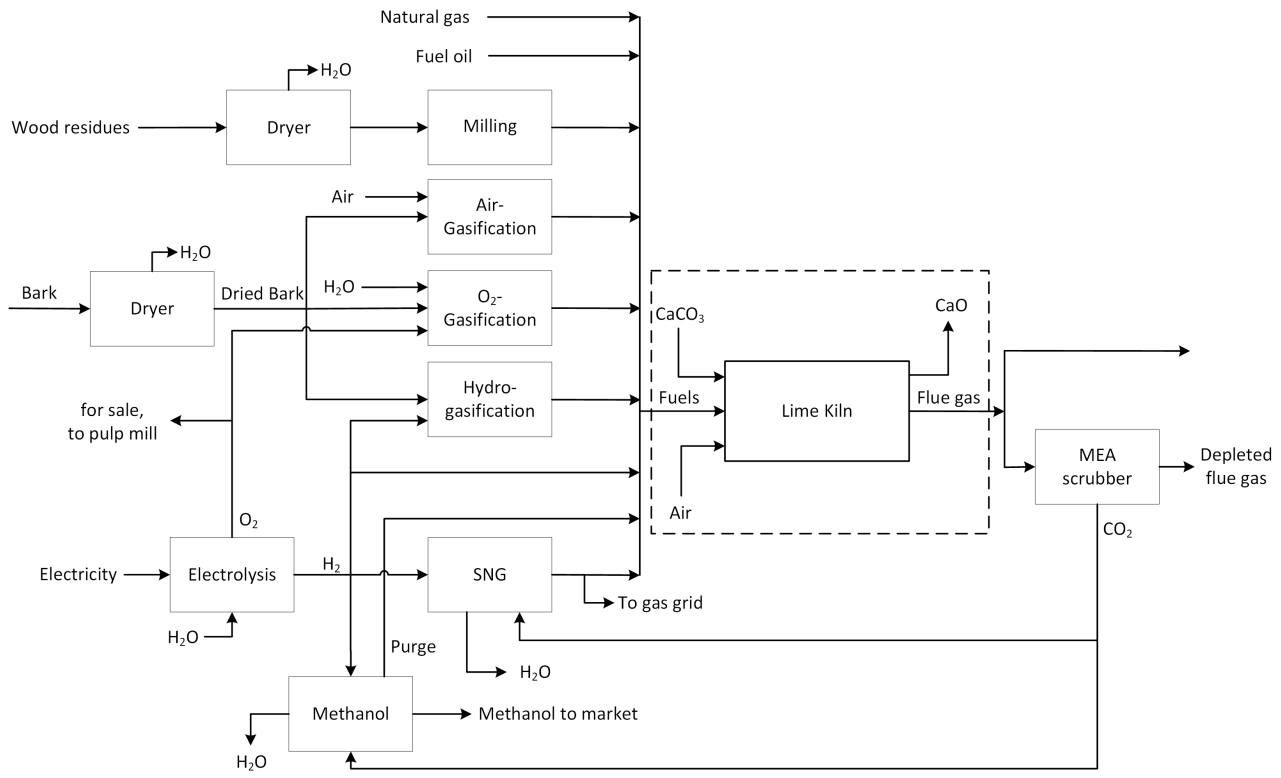

Figure 5.1 Overview on process options (not all flows apply for every case, dashed box shows the available lime kiln)

5.1 Investigated cases

The decarbonization and defossilization of the lime kiln is investigated for 10 different cases as shown in Table 5.1. The table indicates which fuel is used and if CO_2 is captured and further processed to

SNG or MeOH. The combustion of natural gas in the lime kiln is defined as the base case. The only other cases relying on fossil fuels are FO and H2-NG. Fuel oil can be used as alternative fuel in the lime kiln by the pulp mill without any technical challenges.

Table 5.1 Presentation of cases investigated for the decarbonization and defossilization of the lime kiln (NG: natural gas, PC: producer gas, SG: syngas, SNG: synthetic natural gas, FO: fuel oil, W: wood residues, MeOH: Methanol)

Cases	Share of thermal power						Carbon capture	SNG/MeOH production
	NG	PG/SG	H_2	SNG	FO	W		
Base Case (BC)	100 %	-	-	-	-	-	-	-
FO	-	-	-	-	100 %	-	-	-
Wood	-	-	-	-	-	100 %	-	-
H2-NG	50 %	-	50 %	-	-	-	-	-
H2-SNG-partial	-	-	50 %	50 %	-	-	partial	SNG
H2-SNG-full	-	-	50 %	50 %	-	-	full	SNG
G-Air	-	100 %	-	-	-	-	-	-
G-Air + H2	-	50 %	50 %	-	-	-	-	-
G-H2	-	100 %	-	-	-	-	-	-
G-O2-MeOH	-	100 %	-	-	-	-	full	MeOH

The utilization of H_2 in the lime kiln must be limited. Based on a withdrawn patent by Heidelberg Cement AG, an addition of up to 50 % of the thermal power as H_2 is viable in lime kilns [21]. This limit is used in the assessments here. In H2-NG, natural gas is partially substituted by H_2 from water electrolysis based on this assumption. In order to further decrease CO_2 emissions, in H2-SNG-partial CO_2 from the lime kiln's flue gas is captured and converted to SNG which is burnt in the lime kiln. The amount of captured CO_2 equals the required amount needed for the synthesis. With this system, carbon is recycled and no fossil CO_2 is emitted onsite. Full carbon capture leads to a surplus SNG production which is fed to the gas grid. The H2-SNG process with carbon recycling is inspired by [266, 267].

The biomass based process options are based on the combustion of milled wood residues or the gasification of bark with different gasification agents. Wood can be milled and the powder is combusted in the lime kiln. Bark can be either gasified with air, H_2 or O_2/H_2O. Air gasification is an already established process in pulp mills and yields a producer gas with very low heating value (G-Air). If the availability of bark is limited, G-Air + H2 can reduce the bark demand by substituting 50 % of the producer gas with H_2. In hydrogasification, the combination with H_2 as gasification agent reduces also the bark demand in comparison to G-Air. The resulting syngas contains a high amount of methane. The idea for G-O2-MeOH is to make use of the O_2 from water electrolysis in the gasifier. O_2/H_2O gasification is a more efficient process to produce a syngas with high heating value compared to air gasification. MeOH is chosen as the best PtX option available in terms of cost and efficiency for the utilization of the CO_2. MeOH is sold on the market.

5.2 Modeling

Modeling was done with Aspen Plus V12. The water electrolysis was modeled as black box which is explained in Section 4.2. The SNG and MeOH model are already presented in Section 4.5 and 4.4. The same parameters and settings are used in this chapter.

5.2.1 Lime kiln

The lime kiln is modeled with a simplified mass balance as shown in Figure 5.2. The energy balance is simplified by calculating the theoretical energy demand of the lime kiln.

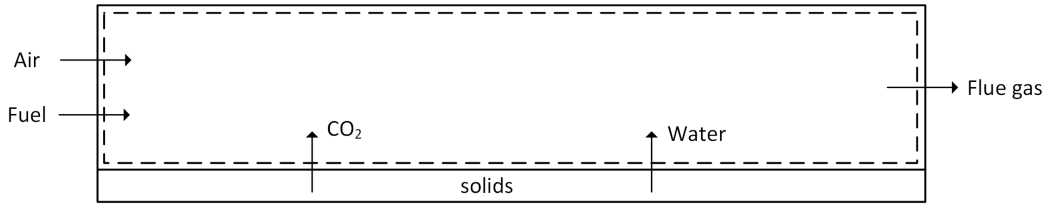

Figure 5.2 Mass balance of the lime kiln (dashed lines)

The mass balance of the lime kiln model comprises only the gas phase including the combustion reaction, water evaporation from the lime and CO_2 from the lime. The goal of the model is to calculate mass flow and composition of the flue gas as well as input flows of combustion air and fuel. Detailed modeling of the whole process is out of the scope of this work. For example, the heat transfer inside the rotary kiln must be simulated for every fuel with CFD. This would in return influence the auxiliary equipment like air preheating and flash dryer which must be included in the modeling as well. Additionally, the impact of CO_2 partial pressure in the flue gas has an impact on the required temperature in the lime kiln. However, this effect was found to neglectable as shown in E.4 in the Appendix.

The combustion air flow was adjusted so that 3 mol % of O_2 are found in the wet flue gas after the lime kiln. The air composition is shown in Table B.2. The wet lime mud enters with a dry solid content of 75 wt. % and a total mass flow of 25 t/h. It is assumed, that the product stream leaving the lime kiln is completely dry. Therefore, the complete water of the lime mud enters the gas phase. It is also assumed that the incoming lime consists of 100 % $CaCO_3$ and that the $CaCO_3$ to CaO conversion is 98 % on mass basis. The resulting CO_2 from this reaction enters the gas phase.

The thermal energy demand in the lime kiln depends on the used fuel as stated by different authors [25, 268, 20]. Svedin et al. developed an empirical formula based on CFD simulations for the required heat input (heat rate: HR, in GJ/t CaO) in a lime kiln [268]. The heat input depends on the adiabatic flame temperature (T_{AFT}) in °C and the flame length (FL) in m as shown in Equation 5.1 [268]. The impact of the AFT is dominant since it is a four-digit figure compared to the FL which is a two-digit figure. The results of the adiabatic flame temperature calculation and composition of fuels are shown in the Appendix E.1.4 including values for comparison from literature. A flame length of 7 m was used based on industry information. Only for Wood, the flame is expected to be more bushy and was therefore reduced to 5 m. The flame length must be determined specifically for each case either with experiments [269] or numerical simulations [270, 271, 272].

$$HR = 14.1 - 0.00365T_{AFT} + 0.0481FL \tag{5.1}$$

The calculated heat rates are not matching with the heat input reported by the model pulp mill. Therefore, the heat inputs of the different fuels were normalized based on the base case. The base case is the combustion of natural gas. The thermal input is 50 MW_{th}. The thermal power of the other fuels is scaled accordingly leading to the heat demands shown in Table E.1 in the Appendix.

5.2.2 Carbon capture

The MEA scrubber is based on a simplified mass and energy balance as described in Section 4.1. The varying CO_2 concentrations in the flue gas, will cause a change in reboiler heat demand. However, Gardarsdottir et al. showed that this impact is marginal in the range of 10 to 30 mol % under adiabatic conditions in the adsorption column and is therefore neglected in the calculations here [273].

5.2.3 Dryer

Before gasification or milling, biomass must undergo drying. This biomass drying process employs a belt dryer operating with a heat supply at 90 °C. The temperature of the heat stream leaving the dryer is at 60 °C. The assumed thermal energy consumption for every ton of evaporated water is at 1.3 MWh_{th}, while the electrical energy consumption amounts to 32 kWh per ton of dry biomass [274]. To model the biomass dryer, a simplified mass and energy balance calculation is employed, utilizing these energy consumption figures and the removed water content as key parameters. Water leaves in gaseous form and is released to the atmosphere.

5.2.4 Wood powder production

The combustion of wood powder comprises the wood drying and milling. Typically hammer mills are used to grind wood to a particle size of 1-3 mm [15, 20]. The mill consumes 50 kWh/t of oven dry wood [20]. The mill is modeled with a simple energy balance to calculate the electricity demand.

5.2.5 Gasification

Three gasification models with either Air, H_2 or O_2/H_2O as gasification agent model the conversion of solid bark into producer gas or syngas. A flowsheet of the gasification models is shown in Figure 5.3. The equipment in the dotted boxes are only used for the indicated cases. As type of gasifier, a circulating fluidized bed gasifier was chosen. The elemental composition of bark and wood residues can be found in Appendix B.2.

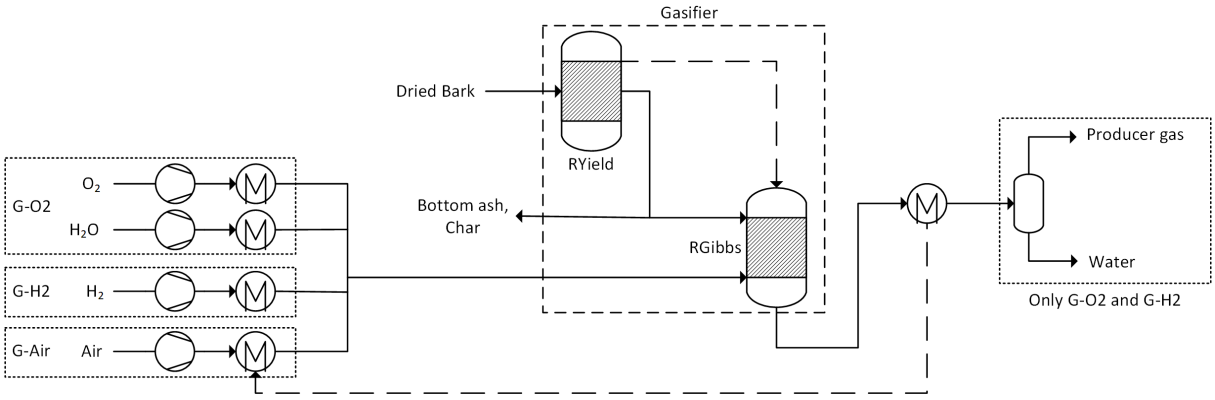

Figure 5.3 Flowsheet of the gasification process as modeled in Aspen Plus for cases G-Air, G-H2 and G-O2 (dotted boxes differentiate between the cases)

After drying the moisture content of the biomass is reduced from 38.2 to 15 wt.% which is a typical water content of biomass for gasification [275]. The gasification is modeled using a RYield and RGibbs reactor performing the decomposition and the chemical equilibrium calculations. In the first reactor, the bark is decomposed into its elemental composition. In the RGibbs reactor, the chemical equilibrium composition of the available components comprised of biomass and gasification agent is calculated. Since the equilibrium models underpredict the methane formation, the methane content at the outlet of the RGibbs reactor was fixed. For air gasification it was fixed to 5 mol % [276, 277] and for O_2/H_2O gasification the value was set to 10 mol % [278, 277] which is in line with experimental values. A pressure drop of 0.2 bar is set in the gasifier to account for the pressure drop in the whole process chain. The temperature of the gasifier was set to 800 °C for G-Air, 850 °C for G-H2 [279] and 900 °C for G-O2. The temperature was regulated by adjusting the flow rate of the gasification agents for G-Air and G-O2. The temperature of the gasifier in G-H2 was adjusted by the preheating of the H_2 stream in the heat exchanger. In the gasifier for G-H2 a temperature approach of -161.8 °C as proposed by Mozaffarian and Zwart was implemented in the RGibbs reactor [279]. In all gasifiers,

1 wt. % of carbon and 50 wt. % of ash are removed as char and bottom ash from the process. The removed carbon accounts for unconverted char in the gasifier. For G-H2, the carbon conversion is 80 % and therefore the carbon removal was set to 20 wt. % [279].

The gasification agents fluidize the bed material and bark. Due to the implemented pressure loss and set operating pressures, the gasification agent undergo compression or pumping. Air is preheated to 291 °C with heat from producer gas cooling. O_2 and water are preheated to 400 °C starting from 80 °C as received from the water electrolysis and 20 °C as from the water grid. Water is also evaporated in this step. H_2 is preheated to 409 °C. The producer gas or syngas from the gasifier is cooled in the heat exchanger after the gasifier. In G-Air, the stream is cooled to 700 °C and the heat is supplied to increase the temperature of the air for gasification. The producer gas was not further cooled. The latent heat of the gas stream is important in the lime kiln since the lower heating value of the producer gas is very low. In G-H2 and G-O2, the gas was cooled to 30 °C to recover valuable high temperature heat and to enable the water separation in the following flash drum. The water removal was implemented since the gases carry a high fraction of water. It is a possibility of reducing the mass flow of the fuel to the lime kiln in order to decrease the mass flow of the resulting flue gas. The syngas and producer gas are not further purified since it is not used for a chemical synthesis. Impurities introduced to the lime kiln will be removed via a larger lime purge stream and the flue gas is cleaned according to legislative requirements.

5.3 Results

The results section presents the mass and energy balances of the processes divided by fuel preparation (5.3.1), lime kiln (5.3.2) and PtX process (5.3.3). Based on the simulation results, the processes are integrated into the pulp mill with focus on utilities, biomass availability and change in electricity balance. The cases are assessed in terms of CO_2 emissions (5.3.5) and economics (5.3.6).

5.3.1 Fuel preparation

The tables for mass and energy balance are shown in the Appendix E.1.1 and are not further elaborated on here. The focus here is on the energy efficiency of the fuel preparation. The energy efficiency of the fuel preparation as an indicator for comparison is shown in Table 5.2. The energy efficiency is calculated including the energy flows and values shown in the table. Wood has the highest efficiency with 100 % as wood is directly used in the process without any process that decreases the energy content of the fuel. The second highest efficiency is found for H2-NG. As a part of the natural gas is replaced by H_2 which is produced with an efficiency of 70 % the process shows a high fuel preparation efficiency. For the other processes, the efficiency is in between 62.5 and 68.9 %. The efficiency of the gasification based routes is higher than for H2-SNG. G-Air+H2 is more efficient than G-Air since the production of H_2 is more efficient than the production of producer gas. These numbers do not account for the integration with the pulp mill and therefore neglect the full impact on the fuel preparation efficiency.

The increased energy input quantifies the increase in energy input compared to BC. This also takes into account the change in fuel demand in the lime kiln. Therefore this figures gives a clearer picture of the energy demand. Due to the higher fuel demand and rather low energy efficiency, G-Air shows the highest increase of 32.2 MW. The electrified version of this case (G-Air+H2) has a lower fuel demand and higher energy efficiency yielding an increase in energy demand of only 25.6 MW. As expected, the lowest values are found for Wood and H2-NG. Table E.4 in the Appendix shows the composition of the liquid and gaseous fuels as fed to the lime kiln. The fuel composition for wood is given by the laboratory analysis in Table B.3.

Table 5.2 Energy efficiency of fuel preparation (BC and FO excluded. H2-SNG means H2-SNG-partial. Values in MW except for efficiency figures.)

	Wood	H2-NG	H2-SNG	G-Air	G-Air + H2	G-H2	G-O2
Input							
Wood residues/Bark	50.2	0.0	0.0	81.6	38.1	26.5	72.8
Natural gas	0.0	23.7	0.0	0.0	0.0	0.0	0.0
Electricity	0.0	33.8	75.8	0.6	37.5	50.9	0.4
Output							
Wood	50.2	0.0	0.0	0.0	0.0	0.0	0.0
PG/SG	0.0	0.0	0.0	55.8	26.0	0.0	49.0
NG/SNG (also G-H2)	0.0	23.7	23.7	0.0	0.0	49.0	0.0
H_2	0.0	23.7	23.7	0.0	26.0	0.0	0.0
Energy efficiency	100.0%	82.4%	62.5%	67.9%	68.9%	63.3%	66.9%
Increased energy input	0.2	7.5	25.8	32.3	25.6	27.4	23.2

5.3.2 Lime kiln

This section presents the results for the lime kiln including the mass balance with focus on flue gas mass flow and composition. The mass balance of the lime kiln is presented in Table 5.3. Lime mud (wet) means the whole solid and liquid input to the lime kiln and burnt lime (dry) means the produced solid product. The converted limestone and resulting burnt lime is constant in all cases as it is given by the pulp mill data. However, the fuel mass flows differ substantially. The fuel flow depends on the LHV of the fuel and on the heat demand of the lime kiln for this fuel (see Table E.1).

Especially, for gasification with air and O_2 (G-Air, G-Air+H2 and G-O2), the fuel flow is extraordinary high. In case G-Air+H2 the mass flow can be decreased by the addition of H_2 in comparison to G-Air. The gasification with H_2 (G-H2), results in a low fuel flow due to a high LHV of the fuel in comparison to the other gasification processes. Especially for G-Air and G-O2 with a high fuel mass flow, the flue gas mass flow is accordingly high. However, the flue gas mass flow also depends on the amount of combustion air required by the fuel.

Table 5.3 Mass balance of the lime kiln in t/h

	BC	FO	Wood	H2-NG	H2-SNG-partial	H2-SNG-full	G-Air	G-Air + H2	G-H2	G-O2
Input										
Fuel	3.8	4.1	9.5	2.5	2.4	2.4	42.7	20.7	3.5	19.8
Air	80.0	79.4	63.2	70.1	70.2	70.2	80.7	58.9	75.1	76.3
Limestone (wet)	25.0	25.0	25.0	25.0	25.0	25.0	25.0	25.0	25.0	25.0
Output										
Flue gas	97.7	97.4	86.6	86.6	86.6	86.6	137.3	93.5	92.5	110.1
Burnt lime (dry)	11.1	11.1	11.1	11.1	11.1	11.1	11.1	11.1	11.1	11.1

The resulting flue gas comprises the combustion products, and water and CO_2 from the lime burning process. The mass flow and volume flow of flue gas is shown in Figure 5.4. As already mentioned, an increase in flue gas flow can cause problems due to increased particle removal from the lime kiln and overloading of the flue gas cleaning system. The change in flue gas flow arises, besides different fuel mass flows, from different air requirements for combustion of the fuels and different fuel demands based on Equation 5.1. For example the release of 1 MJ of heat during stoichiometric combustion requires 0.33 kg air for H_2 and 0.40 kg air for methane. The normal volume flows behave similarly to the mass flows.

In the following we will only refer to the mass flows. The combustion of natural gas (BC) represents the benchmark for comparison (indicated by the dashed line in the figure). Higher flue gas flows are found for G-Air and G-O2 due to a high fuel and combustion air mass flow. The mass flow for G-Air increases by 41 % compared to BC. With 13 % mass flow increase, G-O2 shows the lowest mass

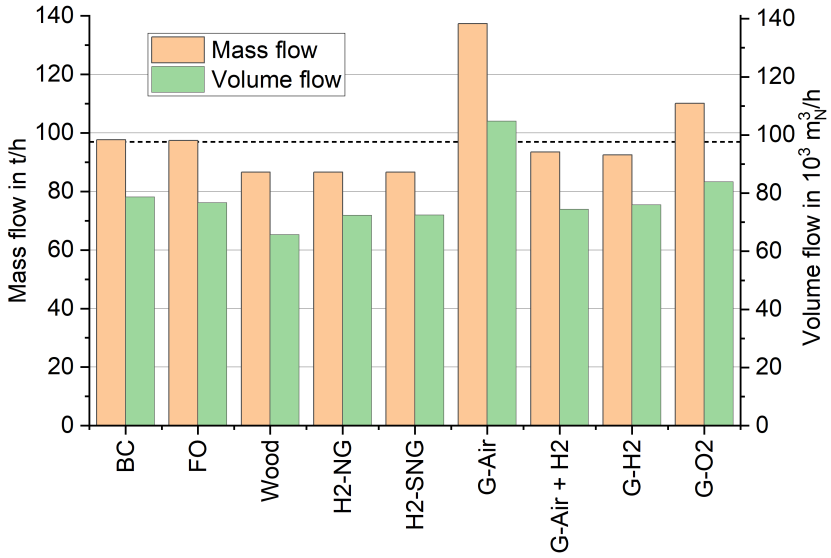

Figure 5.4 Mass and volume flow of flue gas from the lime kiln for different fuels

flow increase. G-Air is one of the most prominent option with the issue of an increase in flue gas flow possibly exceeding the technical limits of the plant. In this case, the other processes might be prefered.

The flue gas composition is shown in Figure 5.5. This is especially interesting for the CO_2 capture process. The CO_2 concentration determines the applicable technology and consequently energy demand and cost. The figure shows the molar composition of dry flue gas. In the wet flue gas, the O_2 concentration is set to 3 mol% which translates to roughly 4-5 % in the dry flue gas. Argon introduced with the combustion air is roughly at 1 mol %. The cases H2-NG and H2-SNG have roughly a 50 % reduction of CO_2 from fuel combustion. However, the additional CO_2 from the $CaCO_3$ conversion also contributes to the CO_2 in the flue gas leading to a final CO_2 concentration of 12 %. G-O2 has the highest CO_2 concentration due to the amount of CO_2 already present in the syngas.

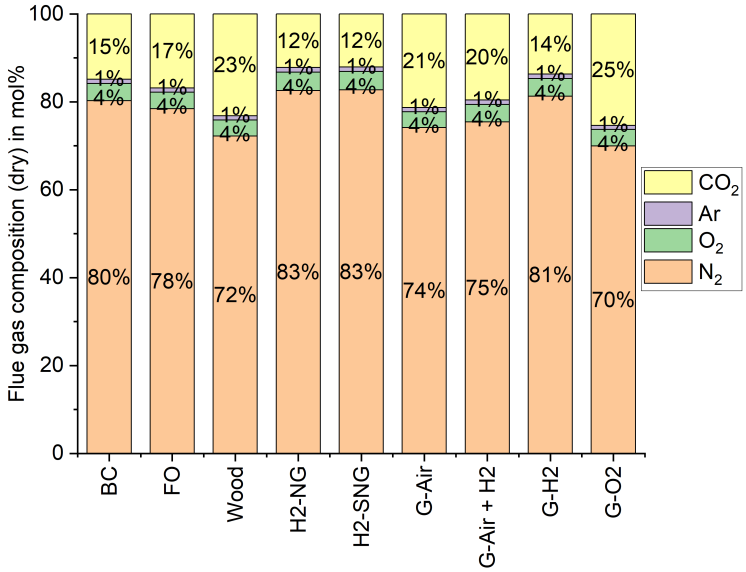

Figure 5.5 Composition (dry, mol%) of flue gas from lime kiln

5.3.3 PtX processes

Table 5.4 shows the energy balance of the PtX processes for the production of SNG and MeOH including water electrolysis and CO_2 capture. The mass balance is shown in Table E.3 in the Appendix.

Table 5.4 Energy balance of PtX processes in MW

	H2-SNG-partial	H2-SNG-full	G-O2
Input			
Electricity total	42.0	99.1	205.9
- Electrolysis	41.0	96.7	196.2
- Compression	0.3	0.8	5.6
- MEA	0.7	1.5	4.2
Heat SNG/MeOH	0.3	0.7	12.4
Heat MEA	4.6	10.8	29.2
Output			
SNG/MeOH	23.7	55.9	115.2
Heat SNG/MeOH	8.5	20.0	44.9
Heat Electrolysis	8.2	19.3	39.2

The demand of H_2 is increasing from H2-SNG-partial to G-O2. G-O2 has a huge plant size compared to the other investigated plants in this thesis. It reaches an electrical energy demand of 196.2 MW_{el} for the electrolysis. Accordingly all other heat streams for heating and cooling are bigger than in comparison to the SNG cases. The output of SNG in case H2-SNG-partial equals the demand for operation of the lime kiln. H2-SNG-full can export 32.2 MW_{th} SNG.

5.3.4 Integration

In comparison to the PtX routes in Chapter 4, the decarbonization of the lime kiln has for most cases a lower impact on the pulp mill's utilities (Table 5.5). Waste water originates from SNG or MeOH production, and as condensate from gasification with H_2 or O_2/H_2O. The amount of waste water is the largest for G-O2. Deionized water is needed for the cases involving water electrolysis. Higher demands due to larger electrolysis sizes, are observed for H2-SNG-full and G-O2. Similarly, O_2 from water electrolysis can replace O_2 normally generated on-site. For all cases enough O_2 is produced to satisfy the pulp mill's demand. Even a tremendous surplus is generated for most cases.

Table 5.5 Impact on utilities of pulp mill in t/a ([a] available for pulp mill and sale)

	BC	FO	Wood	H2-NG	H2-SNG-partial	H2-SNG-full	G-Air	G-Air + H2	G-H2	G-O2
Waste water treatment										
Additional waste water amount	0	0	0	0	28,767	67,919	0	0	20,589	106,266
Increase in waste water	0.0%	0.0%	0.0%	0.0%	0.2%	0.4%	0.0%	0.0%	0.1%	0.7%
Deionized water										
Additional demand	0	0	0	47,520	105,158	183,531	0	52,287	71,248	275,675
Increase in deionized water	0.0%	0.0%	0.0%	0.3%	0.6%	1.1%	0.0%	0.3%	0.4%	1.6%
O_2										
O_2 production[a]	0	0	0	42,193	93,370	162,958	0	46,426	63,261	212,102
Coverage of O_2 demand	0%	0%	0%	153%	339%	591%	0%	168%	229%	769%

Biomass is a major feedstock for some cases. The biomass availability and demand are shown in Table 5.6. As the biomass is normally combusted in the bark boiler of the pulp mill, rerouting the biomass towards the lime kiln changes the steam production of the bark boiler as the biomass is normally thermally recycled in the boiler. In cases Wood and G-Air, the available biomass onsite is not sufficient for the supply. The lacking biomass needs to be either imported or internal resources must be used more efficiently to free the required biomass. For the other cases the onsite biomass supply is sufficient. For G-Air+H2 and G-H2 part of the required energy is not only derived from biomass

but also complemented by electricity/H_2. Therefore, the biomass input is reduced compared to the non-electrified processes. The thermal energy demand of the lime kiln is similar for G-Air and G-O2. However, for G-O2 the thermal energy supply consists of syngas and the purge stream of the MeOH process. Therefore, the energy demand of the syngas is lower leading to a lower biomass demand.

Table 5.6 Biomass availability and demand for lime kiln fuel supply in t_{dry}/a, ([a] wood residues,[b] bark)

	Wood	G-Air	G-Air + H2	G-H2	G-O2
Biomass needed	67,432	116,014	54,093	37,709	98,839
Biomass availability	48,823[a]	100,404[b]	100,404[b]	100,404[b]	100,404[b]
Share of available biomass	-38%	-16%	46%	62%	2%

The reduction of biomass availability for steam generation in the bark boiler leads to a massive reduction in high pressure superheated steam production and consequently electricity generation (Table 5.7). The cut in electricity reaches around 18 MW_{el} for G-O2 and G-Air as these processes have the highest demand for biomass (bark). The electrified gasification routes G-Air+H2 and G-H2 have a lower biomass demand and therefore lower impact on the electricity generation from the bark boiler. However, these processes will increase the total electricity demand due to water electrolysis.

The impact of waste water treatment and deionized water production is marginal for all cases. The saving in O_2 production accounts to 1.43 MW_{el} for cases involving water electrolysis as the O_2 demand can be completely covered. The composite curves for heat integration are presented in the Appendix E.3. H2-SNG and G-H2 generates surplus heat which can be exported to the pulp mill as HP steam which is converted to 0.59 to 1.40 MW_{el}. Wood, G-Air, G-Air+H2 and G-O2 are supplied with LP and MP2 steam. The change in electricity demand of process cooling is influenced by heat integration and by the reduced bark boiler load. The pinch analysis gives a cooling demand which cannot be covered by heat integration. The contribution is marginal. The reduced biomass combustion however leads to a lower steam production and consequently lower cooling demand for complete condensation of the low pressure steam after the turbine. The gasification based cases show through the high biomass demand a more distinct reduction in electricity demand ranging from 0.21 to 0.57 MW_{el}.

Table 5.7 Change in electricity balance caused by integration of lime kiln decarbonization (negative values mean higher electricity availability)

	BC	FO	Wood	H2-NG	H2-SNG -partial	H2-SNG -full	G-Air	G-Air + H2	G-H2	G-O2
Waste water treatment	0.00	0.00	0.00	0.00	0.00	0.01	0.00	0.00	0.00	0.01
Deionized water	0.00	0.00	0.00	0.01	0.03	0.05	0.00	0.01	0.02	0.07
O_2	0.00	0.00	0.00	-1.43	-1.43	-1.43	0.00	-1.43	-1.43	-1.43
Heat integration	0.00	0.00	0.62	0.00	-0.59	-1.40	0.88	0.41	-0.66	5.98
Process cooling	0.00	0.00	-0.29	0.00	0.03	0.06	-0.57	-0.31	-0.19	-0.32
Bark boiler	0.00	0.00	9.43	0.00	0.00	0.00	18.32	9.87	6.88	18.04
Total	0.00	0.00	9.76	-1.42	-1.96	-2.71	18.63	8.55	4.63	22.35

5.3.5 CO_2 emissions

Figure 5.6 shows the origin of the CO_2 in the flue gas. Only in cases BC, FO and H2-NG fossil CO_2 is present in the flue gas. This CO_2 is derived from the combustion of fossil fuels like natural gas or fuel oil. The share of fossil emissions in FO is higher due to the higher emission factor of this fuel in comparison to natural gas. Important to note is that the mass flow of biogenic CO_2 from $CaCO_3$ conversion (Equation 2.1) is constant but the share varies depending on CO_2 from fuel combustion which varies due to different emission factors and mass flows of the fuel. For example G-Air has the highest share of biogenic CO_2 from fuel as the fuel mass flow is very high and as the fuel already caries 23.9 wt.% of CO_2.

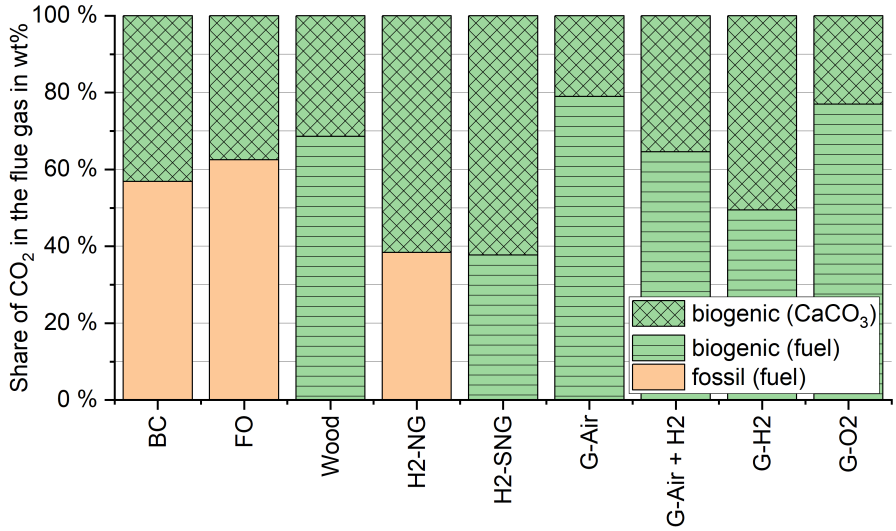

Figure 5.6 Origin of CO_2 in the flue gas

The CO_2 balance was calculated as described in Section 3.4 including only the change in fossil CO_2 emissions. Figure 5.7 shows the difference in annual fossil CO_2 emissions in comparison to natural gas (BC). Reaching negative emissions of 76 kt CO_2/a means a full reduction of fossil energy related CO_2 emissions in the lime kiln process. Generally, the CO_2 balance is a function of the grid electricity emission factor for cases G-O2, H2-SNG-full and H2-SNG-partial since in these cases electricity is imported from the grid. The amount of imported electricity and consequently the slope of the curve is decreasing in the order as named before. In these cases, 150.6 MW_{el}, 70.2 MW_{el} and 13.9 MW_{el} are imported from the grid together with the corresponding CO_2 emissions. The marginal emission factor, defined as the emission factor of electricity to reach equal emissions than BC, is calculated at 0.144 and 0.067 t CO_2/MWh for H2-SNG-full and G-O2. The marginal emission factor of 0.730 t CO_2/MWh for H2-SNG-partial shows that emission reduction can be even achieved for very high grid emission factors.

Contrary, all other cases show no change in CO_2 emissions over the grid emission factor since no electricity from the grid is imported. Even with a lower thermal power demand, the annual emissions for FO are higher due to the higher emission factor of fuel oil. The CO_2 emissions increase by 20 kt/a. A decrease of emissions by 76 kt/a is calculated for Wood, G-Air, G-H2 and G-Air+H2. Case H2-NG shows emission reduction by 40 kt/a. In this case, fossil CO_2 emissions are still generated by natural gas combustion. The annual amount of biogenic CO_2 which is stored in the product amounts to 47.4 kt for SNG to the grid in H2-SNG-full and to 214.9 kt for MeOH in G-O2.

5.3.6 Economic assessment

The basis of economic assessment are described in Section 3.3. The assumptions here are that the lime kiln process must not be technically modified for different fuels. For example, investment cost for burner, flue gas cleaning or other infrastructure (sludge drying or other disposal in case of no disposal in the bark boiler) is excluded as reliable cost estimates are difficult. The calculations presented are at a CO_2 certificate price of 0 €/t CO_2.

Special features of the operating cost are the additional purge in the calcium cycle and the biomass utilization. For the biomass based fuels (Wood, G-Air, G-Air+H2, G-H2 and G-O2) non-process elements are introduced to the lime kiln and a higher purge is required to regulate the accumulation of these elements. For wood powder combustion, the effect might be more severe as all biomass together with the impurities introduced to the lime kiln. In the gasification based cases, part of the ash which contains the critical substances, is already removed as bottom ash and therefore reduces the input of critical elements. However in all cases a purge of 1 wt.% of the resulting CaO is assumed

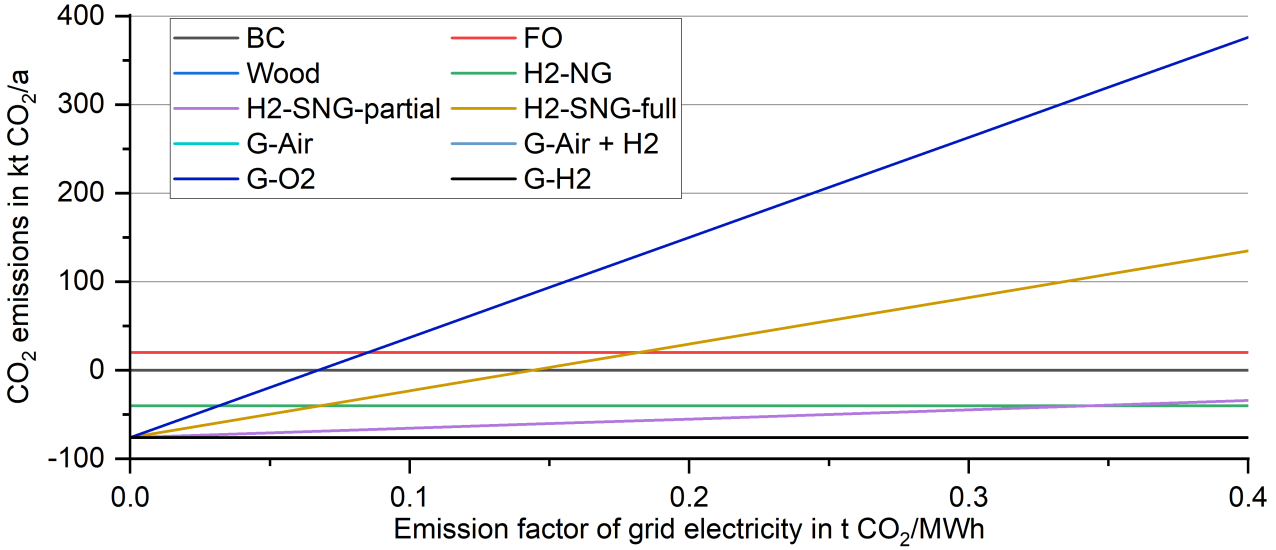

Figure 5.7 Change in annual fossil CO_2 emissions of the pulp mill with different fuel supply for the lime kiln calculated with varying grid electricity emission factor

amounting to 734 t CaO annually. A CaO price of 280 €/t is confirmed by industry. Biomass as raw material for the before named cases is indirectly included in the cost calculation. The waste biomass is usually combusted in the bark boiler and the generated steam is used for electricity generation. Therefore, a decreased biomass availability to the boiler leads to lower electricity production. The loss in electricity production is accounted for as it cannot be sold to the grid. In some cases biomass needs to be supplied externally and is therefore bought for market price.

In this section, the comparison is based on the TAC and not the levelized cost of product like in Chapter 4. The breakdown of the TAC is shown in Table 5.8. Natural gas combustion, as the reference case, causes annual cost of 9.4 M€ which are only derived from natural gas cost. For FO, the annual cost derive from the cost for fuel oil consumption. In all other cases, investment cost are associated with the new process options further leading to investment related operating cost like maintenance, labor, etc. Additionally, energy cost for biomass or electricity apply. Highest cost are found for the cases involving H_2. Compared to the base case, the TAC for H2-SNG-full shows the highest increase (1075 %). The most promising option in terms of cost is Wood with an increase of only 37 % in TAC compared to BC.

For all cases except BC and FO, the investment cost contribute to the TAC. For Wood, the ACC contributes only to 6 % to the TAC. The highest contribution of 42 % is calculated for G-O2 which is due to the high cost for water electrolysis. Generally, the investment cost of water electrolysis dominate in all cases involving H_2 and range from 72 % (G-Air+H2) to 100 % (H2-NG) of ACC. The operating cost account for 84 to 94 % of TAC (excluding BC, FO and G-O2). For BC and FO, the TAC consist solely of the fuel cost. For G-O2, the share of operating cost is only 58 % which is due the reduction of operating cost generated by the revenue for MeOH. The revenue does confound the calculations as the revenue decreases the operating cost and thus increases the share of ACC. The impact of SNG sale is not as significant due to the lower production amount and the lower price of SNG in comparison to MeOH. The impact of purging CaO is marginal for all cases. Electricity cost will be for most cases except BC and FO one of the major cost components. The reduction in electricity generation for biomass based processes causes a substantial electricity deficit. This influence can be observed in Wood and G-Air which have no high electrical energy demand themselves but reduce the onsite electricity generation as biomass cannot be used in the bark boiler for steam generation. However, water electrolysis as the major consumer of electricity exhibits a higher impact compared to the lack of electricity production.

Furthermore, Table E.6 shows the TAC cost if either the cost categories electricity cost or ACC are excluded. For an electricity price of 0 €/MWh, Wood and G-O2 reach lower TAC than BC. The marginal electricity price is at 45 and 39 €/MWh respectively. Compared to FO, the marginal electricity price ranges from 27 to 76 €/MWh for G-O2, H2-NG, G-Air+H2, G-H2 and H2-SNG-partial in increasing order. Therefore, the plant location and regional electricity price for electricity import as well as electricity sale is an extremely important factor for the economic assessment. The exclusion of the ACC (paid off plant), lowers the TAC. However, it does not change the order of economic competitiveness with Wood and G-Air being still the most competitive cases.

Based on the difference in TAC between BC, and the respective case including CO_2 prices, the increase in pulp selling price can be calculated. Figure 5.8 shows the impact on the pulp selling price with varying CO_2 certificate prices for fossil emissions. The figure exemplifies the economic trade off between CO_2 emissions which affects the cost of CO_2 tax and the TAC of the case.

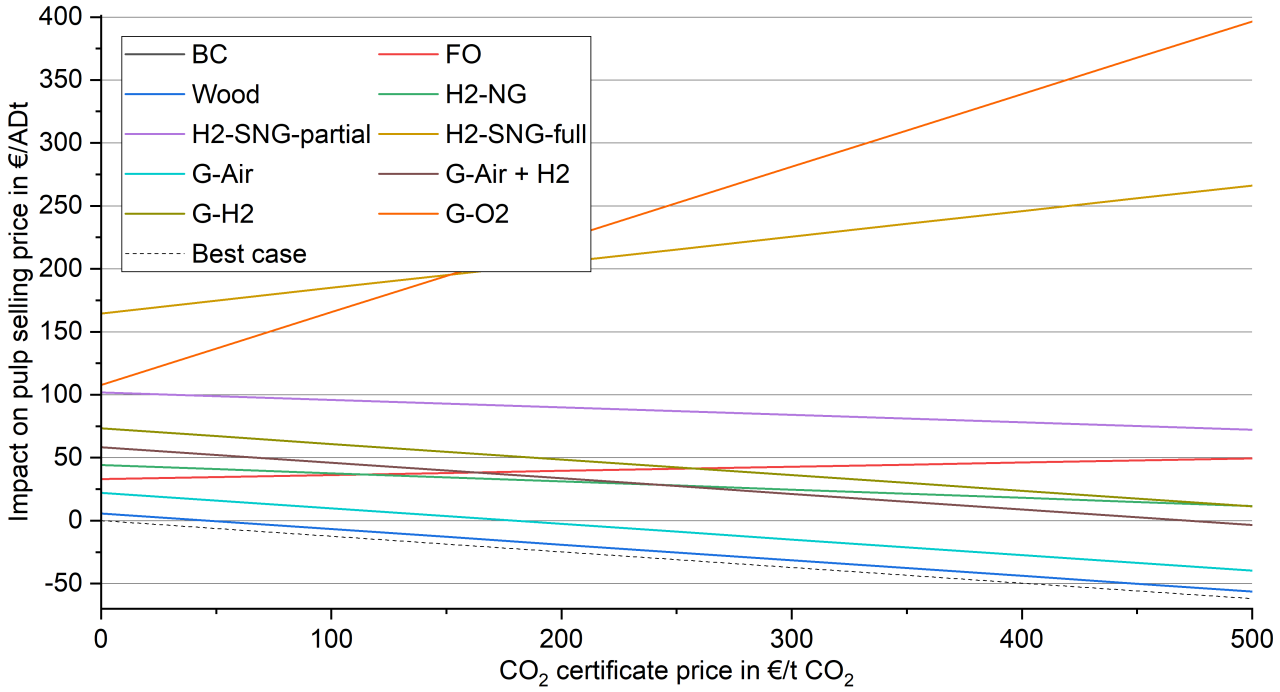

Figure 5.8 Impact of cases and CO_2 certificate price on pulp selling price (calculations based on fossil CO_2 emissions)

The increase in pulp selling prices varies between 9 and 165 €/ADt for a CO_2 tax of 0 €/t CO_2. The slope of the curves in Figure 5.8 refers to the cost caused by fossil CO_2 emissions. The pulp selling price increases with CO_2 price for cases H2-SNG-full, G-O2 and FO. These cases have higher CO_2 emissions compared to the base case leading to higher cost for CO_2 emissions with increasing CO_2 price. The slope of pulp selling price increase is the largest for G-O2 and the smallest for FO. All other cases show a negative slope. The same slope is observed for Wood, G-Air, G-H2 and G-Air+H2. "Best case" in the graph has the same slope as these cases resulting in no fossil CO_2 emissions. It refers to a best possible generic case with the same TAC than BC and no fossil CO_2 emissions. The proximity of the curves for Wood and G-Air show that not much further improvements are possible in terms of economics and CO_2 emissions. Of course, lower TAC than for BC would be possible to further decrease the pulp selling price but this would be implemented as the state of the art and seems therefore very unrealistic. The CO_2 emission reduction is roughly similar for H2-SNG-partial and H2-NG resulting in a similar slope which is less steep than for the cases discussed before.

Interesting are the break even points. The area of negative pulp selling prices means that the measure will save cost in comparison to BC. In the investigated range, only Wood, G-Air and G-Air+H2 are able to reach negative prices. The break even points are roughly at 50, 180 and 470 €/t

Table 5.8 Breakdown of cost for lime kiln decarbonization in M€ (OS and CA: Operating supervision and clerical asisstance)

	BC	FO	Wood	H2-NG	H2-SNG-partial	H2-SNG-full	G-Air	G-Air + H2	G-H2	G-O2
Total annual cost	9.4	29.5	12.9	36.4	71.7	110.1	23.0	45.1	54.3	75.4
Change compared to BC		215%	37%	289%	665%	1075%	145%	381%	479%	704%
OPEX	9.4	29.5	12.0	32.3	61.1	92.4	20.1	38.8	46.5	43.7
Labor	0.0	0.0	0.9	0.9	1.1	1.1	1.0	1.0	1.0	1.2
Laboratory charges	0.0	0.0	0.1	0.1	0.2	0.2	0.1	0.2	0.1	0.2
OS and CA	0.0	0.0	0.1	0.1	0.2	0.2	0.1	0.2	0.1	0.2
Natural gas	9.4	0.0	0.0	4.4	0.0	0.0	0.0	0.0	0.0	0.0
Fuel oil	0.0	29.5	0.0	0.0	0.0	0.0	0.0	0.0	0.0	0.0
Deionized water	0.0	0.0	0.0	0.1	0.2	0.4	0.0	0.1	0.1	0.6
Electricity pulp mill	0.0	0.0	6.5	21.0	37.4	37.4	12.0	28.7	34.5	37.4
Electricity grid	0.0	0.0	0.0	0.0	6.2	31.6	0.0	0.0	0.0	75.9
Product revenue	0.0	0.0	0.0	0.0	0.0	-6.0	0.0	0.0	0.0	-125.1
CO_2	0.0	0.0	0.0	0.0	1.8	4.2	0.0	0.0	0.0	11.2
Biomass	0.0	0.0	2.1	0.0	0.0	0.0	1.6	0.0	0.0	0.0
O_2	0.0	0.0	0.0	-1.1	-1.6	-2.3	0.0	-1.1	-1.3	-3.1
Maintenance	0.0	0.0	0.6	2.8	7.2	12.2	2.0	4.3	5.3	21.7
CaO	0.0	0.0	0.2	0.0	0.0	0.0	0.2	0.2	0.2	0.2
Insurance and Taxes	0.0	0.0	0.2	1.2	3.1	5.2	0.9	1.9	2.3	9.3
Plant overhead	0.0	0.0	1.0	2.3	5.1	8.1	1.9	3.3	3.9	13.9
Aministration	0.0	0.0	0.2	0.2	0.2	0.2	0.2	0.2	0.2	0.2
ACC	0.0	0.0	0.8	4.1	10.5	17.7	2.9	6.3	7.7	31.6
Electrolysis	0.0	0.0	0.0	4.1	9.1	16.0	0.0	4.5	6.2	24.0
Gasification	0.0	0.0	0.0	0.0	0.0	0.0	2.9	1.7	1.5	2.0
SNG/MeOH	0.0	0.0	0.0	0.0	1.4	1.8	0.0	0.0	0.0	5.6
Wood handling	0.0	0.0	0.8	0.0	0.0	0.0	0.0	0.0	0.0	0.0

CO_2 respectively (see Table 5.9 for CO_2 abatement cost). The positive pulp selling prices mean an increase in pulp production cost if these technologies are used. If an increase in pulp production cost cannot be avoided, the lowest increase is more attractive meaning that G-O2, H2-SNG-partial and H2-SNG-full will never be able to compete under these market conditions.

The CO_2 abatement cost are shown in Table 5.9. Only technologies with lower CO_2 emissions than BC are shown in the table. Based on this evaluation, the most cost effective process option would be the technology with the lowest abatement cost (Wood). H2-SNG-partial shows the highest abatement cost. Additionally, the abatement cost excluding the electricity cost are given in the second row. Especially for the electricity intensive processes, the AC decrease tremendously. However, also the cases with lower dependency on electricity show a change in AC.

Table 5.9 CO_2 abatement cost in €/t CO_2

	Wood	H2-NG	H2-SNG-partial	G-Air	G-Air + H2	G-H2
AC	46	678	1715	179	472	592
AC w/o electricity	84	385	773	145	217	260

5.4 Discussion

5.4.1 Comparison with literature and model validation

The available literature on concepts for decarbonization using renewable fuels or carbon capture were reviewed in Section 2.1.2 and 2.5.4. In comparison to the CO_2 abatement cost of the options presented here, the plasma based process with capture and storage cost of 36 to 60 €/t CO_2 seems more cost competitive [27]. For the market pulp mill, electricity prices below 60 €/MWh make the process cost competitive compared to a fuel oil fired lime kiln. The investigated options with high degree of electrification (H2-SNG-partial, G-Air + H2 and G-H2) are not even capable to be cost competitive at free electricity. However, compared to fuel oil, the break even electricity price is 28 €/MWh for H2-NG, 76 €/MWh for H2-SNG-partial, 49 €/MWh for G-Air + H2 and 63 €/MWh for G-H2 which are closer to the plasma calcination concept.

Kuparinen and Vakkilainen investigated renewable fuels with focus on biomass as fuel for the lime kiln [25]. The investigation showed a resulting price for biomass based fuels of 10 to 17 €/MWh for varying electricity prices. The price for lignin ranges from 20 to 21 €/MWh. The price for H_2 starts at roughly 17 €/MWh and increases linearly. The integration with the pulp mills shows a decrease in sellable power of 5.2 to 75.8 MW_{el} with H_2 as the only option not to cover the whole thermal power demand of the lime kiln. The same is observed here. The surplus power would not be sufficient to supply all the thermal power needed for pure H_2 combustion.

The capture of CO_2 from lime kiln flue gas was explicitly modelled by Parkhi et al. showing capture cost of 65 €/t CO_2 and an increase in pulp price of 15 €/ADt [77]. Comparing the calculated abatement cost with carbon capture shows that only Wood is competitive. All other options show tremendously higher cost. However, the safe storage and cost of storage also needs to be addressed for carbon capture and storage. Furthermore, the complete capture of CO_2 is usually not achieved meaning that the emission reduction is limited to a certain extent. However, also biogenic carbon is captured and can therefore lead to net negative emissions. Rey et al. modelled a gasifier for supplying producer gas to the lime kiln [280]. They found a payback time of 21.2 years. For the simultaneous production of produced gas for the lime kiln and for an IGCC, the payback time drops to 19.2 years.

The thermal power demand in the lime kiln is changing with fuel. The operational experience shows that the thermal power demand is reduced for fuel oil in comparison with BC. This is also confirmed by the model lime kiln that the fuel oil fired lime kiln has a lower energy demand than natural gas fired.

5.4.2 Further process options and improvements

An SOEL can improve the overall process performance due to a more efficient production of H_2. This would lead to a lower electricity consumption and possibly lower electricity import from the grid. The lower electricity import further leads to lower CO_2 emissions. Additionally, high temperature heat transfer between the lime kiln and the SOEL can improve economics and lowers the demand for electrical heating. The production of MeOH instead of SNG for the combustion in cases H2-SNG is also an option to improve economics as MeOH is a more cost competitive product than SNG. However, MeOH production lowers the availability of electricity compares to SNG as shown in Section 4.4. Furthermore, the SNG production could be operated flexibly to satisfy the demand of the lime kiln at any time. A surplus production can be fed to the grid. This concept would have a guaranteed load for the production of SNG. Under oxyfuel combustion, the flue gas would contain only H_2O and CO_2 which can be fed to a co-electrolysis to produce syngas. The syngas can either be combusted directly or converted to a PtX product like SNG or MeOH which can be combusted or sold to the market.

Additionally, the carbon capture units can be further tailored to the CO_2 concentration of the flue gas as for some cases the concentration of CO_2 exceeds classical concentrations found in flue gases. Besides using rigorous process models, different capture technologies can be used. For example scrubbers with more energy efficient absorption media establishing in the market or other technology concepts like scrubbers other than amines (Selexol, Rectisol, ...) or pressure swing adsorption can be investigated. CCS is an economically feasible process route besides the investigated cases here. Capture cost were discussed in 2.5.4. Compared to the calculated AC, the capture of CO_2 is an economic feasible option. However, the transportation infrastructure and save storage have to be addressed.

5.4.3 Retrofitting

The proposed options are all viable with a high technical maturity. However, retrofitting the technology to the existing infrastructure might be challenging. Retrofitting such processes must be tailored to the specific pulp mill as site specific features of pulp mills must be considered. Especially, the integration is very site specific. The results generated here are therefore specific for the model pulp mill and allow only for general conclusions for other mills. For a greenfield plant, the planing of the lime kiln can of course be easily adapted to any other available process like LimeArc (plasma-based calcination [26]) or Leilac (electrically heated calcination [281]).

For retrofitting the investigated options, the increased flue gas mass stream is a major concern. The flue gas mass flow can, as already mentioned, exceed the capacity of the flue gas cleaning system or increase the removal of particles from the lime kiln through increased flow velocities. As shown in Figure 5.4, the mass flow increases especially for G-Air and G-O2 by 40.6 % and 12.7 % respectively. For all other cases, the mass flow decreases meaning that it is not a concern. The decreased mass flow actually means that the production capacity of the lime kiln can be increased and with that the total pulp production of the mill. The higher mass flows will however overload the pulp mill's flue gas treatment capacity calling for investment in the flue gas cleaning system especially the electrostatic precipitator and fan. Process related changes like lower O_2 content in the flue gas or higher dry matter content of the lime mud could decrease the flue gas flow to some extent. Based on Hellgren, a lower gasification temperature could actually further decrease the volume flow of the producer gas as more longer chain gas components and tars are formed [282]. The gasification temperature optimum is likely below 750 °C but depends also on the type of feedstock. With the adjustment of the gasifier temperature, the mass fuel mass flow can be decreased leading to a decreased flue gas flow.

Even though most of the biomass flows needed in the investigated options are available onsite the rerouting of the energy flow will impact the pulp mill's energy system as stated in Section 5.3.4. This change is very mill specific and depends on many factors. Besides the lack of electricity generation, the operation of the bark boiler is questionable for some cases. The minimum load of the bark boiler

($P_{th,max}$ = 87 MW_{th}) is in the one digit MW_{th} for dry fuels with a normal heating value. However, the boiler is also used for the disposal of sludge. If biomass is combusted with wet sludge, the minimum load is at around 50 % of the maximum load. With this constraint on the bark boiler operation, the sludge has to be either dried before combustion or disposed externally both leading to additional cost. The evaluation shows that for G-Air and G-O2 the reduction in boiler load is above 50 %. For these cases the operation of the bark boiler is not feasible anymore with wet sludge leading to higher cost for the sludge disposal.

Table 5.10 Retrofittability in terms of reduced bark boiler load

	Wood	G-Air	G-Air + H2	G-H2	G-O2
Reduction in boiler load	-29 %	-69 %	-37 %	-26 %	-69 %

Options to tackle the biomass shortage for cases Wood and G-Air (Table 5.6) besides market purchase are to change process parameters in the screening of wood chips that make more fine materials available or to process more log wood instead of buying wood chips which would increase the amount of bark being available. Another concern might be emission limits of the flue gas that have to be met. The biomass based routes contain an additional nitrogen load that besides thermal and prompt NO_x formation will cause additional emissions in the lime kiln's flue gas.

5.4.4 CO_2 emission reduction

The goal of this chapter is the evaluation of reducing CO_2 emissions from the lime kiln operation. First of all, only the energy related emissions can be reduced. The process related emissions from calcination can only be reduced with CCS.

The process related CO_2 in the lime kiln is of biogenic origin. The energy related emissions of the investigated process routes are either of biogenic or fossil origin. In order to reach a complete reduction of fossil emissions, biomass is a key raw material. As shown, only electricity based routes are not capable to supply enough energy to the lime kiln based on the availability of surplus electricity in the pulp mill or technical constraints of H_2 addition to the fuel. Biomass-based routes or electricity boosted biomass-based routes are capable to totally erase fossil emissions. For H2-SNG-partial, the break even emission factor is at 0.73 t CO_2/MWh (comparison with natural gas fired lime kiln). Therefore, the technology is viable for reducing CO_2 emissions. As this value is compared to natural gas as the base case, break even emission factors are even higher for the comparison with fuel oil. The comparison with H2-SNG-full or G-O2 is due to the production of side products difficult. As already discussed in 5.4.1, the CO_2 capture is economically also a very interesting option. Especially in comparison to some of the investigated cases which heavily rely on electricity resulting in higher cost (H2-NG, H2-SNG, G-Air + H2 and G-H2).

CO_2 AC are a common tool to compare technologies in terms of the most economic options for CO_2 reduction. The comparison between the investigated cases is valid as they are based on the same assumptions. However, the assumptions do influence the results extremely as shown in Table 5.9 for the AC with and without electricity cost. Therefore, the values have to be treated carefully and the comparison must be assessed critically. Especially the comparison to values of other studies might not be valid. Furthermore, the calculated AC are valid for the assumed market conditions. For other market conditions, especially lower electricity prices, the result can change dramatically. Technologies with a CO_2 AC below 100 €/t CO_2 are competing concepts with direct electrification like Lime Arc, CCS, Wood and G-Air.

5.5 Conclusion

The decarbonization and defossilisation of the lime kiln was assessed and discussed in this chapter. Different cases based on biomass, CO_2 or electricity are investigated. The modeling and integration with the pulp mill was performed. Central conclusions are:

- The concentration of CO_2 in the flue gas depends on the used fuel. Higher concentrations of up to 25 mol % can be reached for biomass based cases. Higher concentrations can make the CO_2 capture process more efficient.
- CO_2 from the calcination reaction is of biogenic origin and accounts for 43 wt. % in the flue gas for BC. BC, FO and H2-SNG are the only cases which show fossil emissions in the flue gas. In all other cases, the CO_2 is of biogenic origin. The share of CO_2 from calcination differs for these cases due to different fuel and combustion air mass flows, and CO_2 content in the unburnt fuels.
- The reduction of fossil CO_2 emissions compared to BC is independent of the used electricity for Wood, G-Air, G-H2, G-Air+H2 and H2-NG as no electricity is imported from the grid. Case FO shows higher emissions than BC. The CO_2 balance of H2-SNG-partial, H2-SNG-full and G-O2 is influenced by the imported electricity from grid. Wood, G-Air, G-H2 and G-Air+H2 are solutions for a fossil free pulp mill.
- Waste biomass is available and can be rerouted from the bark boiler to the lime kiln leading to a tremendously lower onsite electricity generation. Other than that, biomass based cases have usually very little impact on other utilities. Especially electricity based cases have a huge impact on the pulp mill concerning O_2, deionized water and waste water treatment.
- Main cost drivers are connected to electricity cost and investment cost of water electrolysis. The operating cost usually make up for the highest share in TAC.
- A price on CO_2 makes some cases cost competitive with the BC. Wood has the lowest CO_2 price at 50 €/t CO_2. The second lowest AC of 180 €/t CO_2 is found for G-Air. Some cases will never be cost competitive for the investigated range of possible CO_2 prices. Cases with H_2, have a lot higher abatement cost in comparison to solely biomass based cases.
- The retrofittability is critical in terms of flue gas mass flow for the lime kiln and loss in thermal power supply to the bark boiler.

CO_2 reduction at reasonable cost is more easily reached by biomass based cases. Especially Wood and G-Air, as already employed in industry, are very promising. Cases relying on electricity as main feedstock show high cost and only limited CO_2 reduction due to electricity import from the grid. However combining biomass and electricity as raw materials like for G-Air+H2 or G-H2 can be promising to reduce CO_2 emissions. If biomass availability is a bottleneck in the pulp mill, these options reduce the biomass demand compared to only biomass based cases.

6 Methanol purification

This chapter is concerned with the experimental results of the combined MeOH purification with MeOH from the PtMeOH process and FC. Since the MeOH stream from pulping contains many impurities, a validation experiment was used to compare the simulation to experimental data. In order to simplify the simulation, only key components were modelled. Not only does that reduce computing time, but it also lowers the amount of binary parameters needed for the property method. Table D.2 in the Appendix shows the composition for FC.

6.1 MeOH purification concepts and simulations

The process configurations with focus on the purification of the PtMeOH and FC stream are shown in Figure 6.1. The pFC concept includes the pretreatment of FC like in the process by A.H. Lundberg Systems [140]. The light components are removed in column FC-C1. Together with the MeOH from the PtMeOH plant, the streams are dewatered in column C1. The other concept on the right includes the joint dewatering of both MeOH streams relying on the dilution of impurities. A first calculation of thumb showed that for small PtMeOH plants, the required purities cannot be reached.

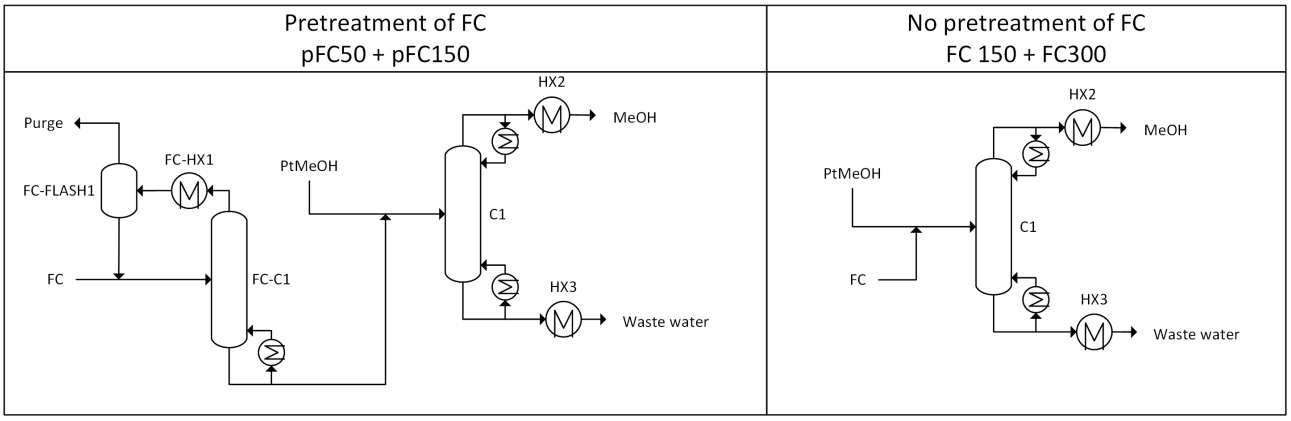

Figure 6.1 MeOH purification concepts including pretreatment or no pretreatment of FC

6.1.1 Process modeling

The process models were implemented in Aspen Plus as shown in the Figure 6.1. The models are very similar to the MeOH models in Section 4.4. As property method, NRTL was used. Henry components are defined for H_2, H_2S and NH_3 in the whole flowsheet. The process operates at 1 bar. The FC is entering at 50 °C with a flow rate of 650 kg/h and the composition as shown in Table D.2 in the Appendix. The PtMeOH is at 65 °C with an equimolar composition of MeOH and water.

In the pFC cases, FC and the recycled stream from the flash separator are entering the stripper column above stage 1. The column has 10 stages and the D:F ratio is set to 0.1. The heat exchanger FC-HX1 cools the top product to 60 °C. In the adiabatic flash drum, the gaseous product containing low boilers are sent to incineration. The liquid product is recycled to the process to decrease the MeOH loss. The bottom product of FC-C1 enters together with the PtMeOH stream column C1 on stage 24. The total number of stages is set to 30. The reflux ratio and D:F ratio is adjusted to reach a top product purity of 99.9 wt. % and a loss of MeOH via the bottom product of 0.2 wt. %. The

resulting reflux ratio is 1.060 and 0.973 for the pFC-50 and pFC-150 case. The D:F ratio is 0.498 and 0.500. For the FC cases, the column C1 has the same settings as described for the pFC simulations. The resulting reflux ratio is 1.175 and 1.305 for FC-150 and FC-300. The D:F ratio is found to be 0.500 for both simulations.

6.1.2 Results

The process modeling yields the results as shown in Table 6.1 for the MeOH stream. The results from the simulation are compared to the corresponding experiments in Figure 6.12 for the S content of the top product. The results here are found for the presented settings. An optimization in terms of energy and economics of the model settings was not performed.

Table 6.1 Results for the purified MeOH stream

	FC-150	FC-300	pFC-50	pFC-150	
MeOH output	16.4	32.5	5.5	15.7	t/h
MeOH recovery	97.68%	98.81%	99.30%	99.68%	
MeOH purity	99.800%	99.900%	99.900%	99.900%	
S content	20.37	10.32	2.81	0.98	mg S/kg

The heat demand of column C1 is shown in Figure 6.2. The energy demand is normalized by the product output. The energy demand of the reboiler is always higher than the cooling demand of the condenser. For pFC, larger plant sizes show a smaller heat demand in contrast to FC cases which show a larger heat demand for bigger plant sizes.

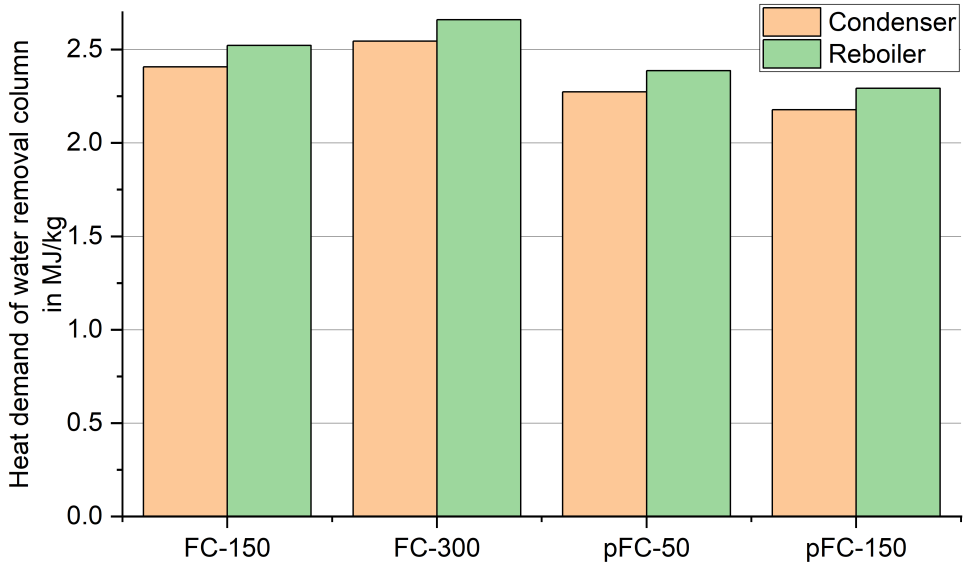

Figure 6.2 Heat demand of water removal column C1

The cost of MeOH purification is shown in Figure 6.3. For the 150 MW_{el} plant size of the PtMeOH plant, the normalized FCI of the pFC scenario shows a slightly lower cost in comparison to the FC scenario. For the FC scenarios, the FCI for the purification decreases with plant size due to the economy of scale for the process equipment. For the pFC scenario, the process equipment of the pretreatment will remain the same for different plant sizes. Nevertheless, the impact of the purification unit is marginal in comparison to the LCOM. For the 150 MW_{el} plants, the pFC shows slightly lower cost due to an decreased product output but a lower ACC. Furthermore, one must take the operating cost into consideration which are neglected here. The cost assessment only considers the ACC derived from cost data from Aspen Plus including currency and year adjustment.

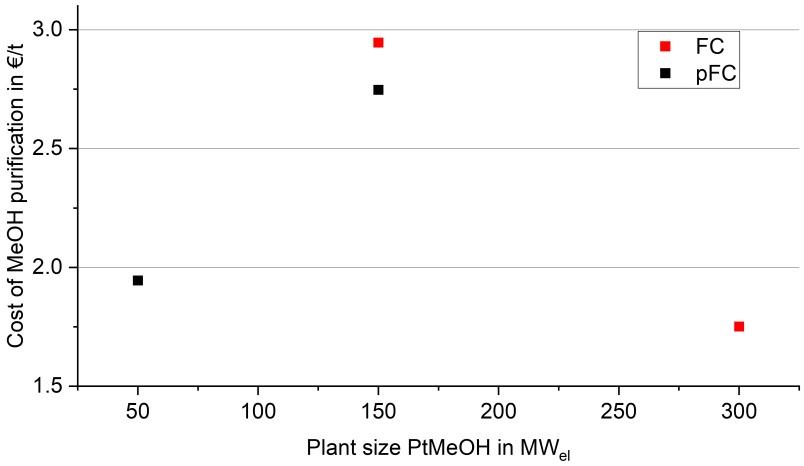

Figure 6.3 Cost for purification of MeOH

6.2 Selective removal of sulphur and nitrogen compounds

The MeOH stream from the pulp mill is heavily contaminated with S and N compounds. The idea is to use a prepurification step for the removal of most of the contaminants before the removal of water in a distillation column. The goal is a high removal of contaminants in order to reach the S concentration in the final MeOH product after water removal according to specifications. The concept is similar to pFC as presented in Figure 6.1 with the difference of replacing the stripper column system with an adsorption system.

One idea is the utilization of activated carbon (AC) for the adsorption of S and N species on the surface using a process layout as shown in Figure 2.4. The other option is the precipitation of the S components with Fe(II) ions. The process layout would be similar to the one for AC. Furthermore, a combination of both methods is investigated. The precipitation of S on the example on H_2S is depicted in the following equations. The reactions can be transferred to other S compounds, too. The reaction indicates the beneficial influence of a high pH value. The produced iron sulfide (FeS) is insoluable in water and can therefore be easily separated from the liquid phase via filtration.

$$H_2S_{(aq)} + OH^- \rightleftharpoons H_2O + HS_{(aq)}^- \tag{6.1}$$

$$HS_{(aq)}^- + OH^- \rightleftharpoons H_2O + S_{(aq)}^{2-} \tag{6.2}$$

$$Fe_{(aq)}^{2+} + S_{(aq)}^{2-} \rightleftharpoons FeS_{(s)} \tag{6.3}$$

6.2.1 Results

Based on a parameter screening, the following statements could be deduced by single experiments. The results are qualitative as the result were obtained by single experiments.

- An increased adsorbent dosage improves the removal of sulphur species. The influence on improved nitrogen removal is not that significant. The same observation can be made for an increased reaction time. This means that not all N components can be adsorbed on AC or that the dosage of AC has to be even further increased.
- Lower temperatures are beneficial for the adsorption process as expected. An experiment at 0 °C showed an improved adsorption for S species.
- Higher pH values are found beneficial for the adsorption as compounds are deprotonated improving the adsorption.
- The precipitation with Fe(II) ions shows that the amount of added ions does not influence the removal amount. Higher pH values are not beneficial for the removal contrary to expectations. Leftover ions which cannot be removed as precipitated FeS are found in the MeOH. According to the IMPCA specification 0.1 mg Fe ions are allowed per kg [190]. Therefore, the method interferes with the specifications. Also a combination of AC adsorption with Fe ion precipitation did not lead to an especially improved outcome.
- In one set of experiments, the AC was reused. For that the AC was dried in the oven. For the reused AC, the data shows no significant impact for a one time reuse.

The precipitation with Fe(II) ions is excluded from the possible process options as AC is more promising in terms of removal of contaminants and residual adsorbant left in the MeOH. Therefore, the adsorption with AC is investigated in more detail for the removal of impurities from the crude MeOH. Quantitative results are presented in the following. Figure 6.4 shows the concentration of S and N after the experiment. Generally a higher dosage of AC yields a higher removal of contaminants. The higher surface area allows more species to adsorb on the surface resulting in a higher removal of the adsorpt species. For S, the removal follows approximately a linear relationship between final

concentration and AC dosage. With 8 g of AC almost all S species could be removed. For N, the removal is not as efficient. The curve shows no clear trend. The removal of these species appears to be increasing with increased AC dosage. If the removal follows a linear relationship as for S cannot be confirmed. The data indicates a decrease of contaminant concentration until a plateau is reached. A less effective removal can also point at the fact that not all N species adsorb on the AC and are therefore not removable with adsorption resulting in the mentioned plateau.

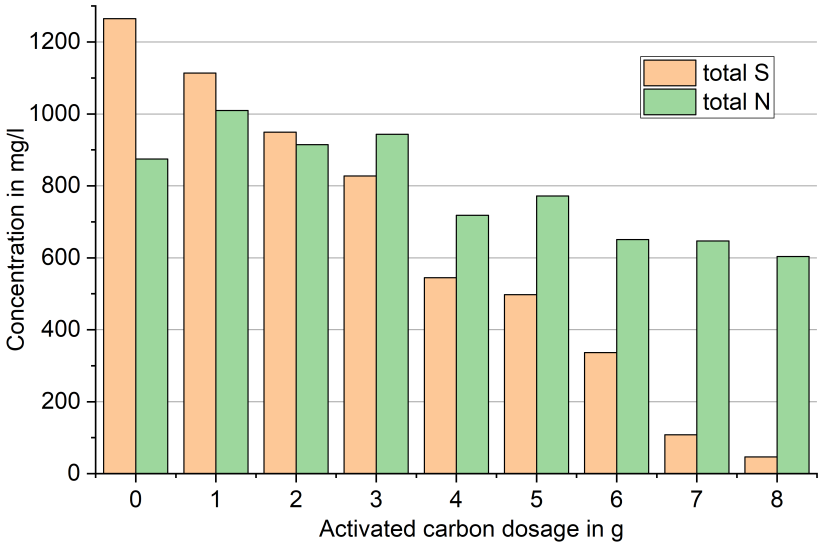

Figure 6.4 Contaminant concentration of the final product in dependence of the adsorbent mass (measured in triplets, at room temperature, t = 2h, pH ≈ 12, stirrer speed: 600 rpm, V_{liquid} = 50 ml)

The effect of adsorption time was found to be not majorly influential as shown in Figure 6.5. The results show a very unclear picture.

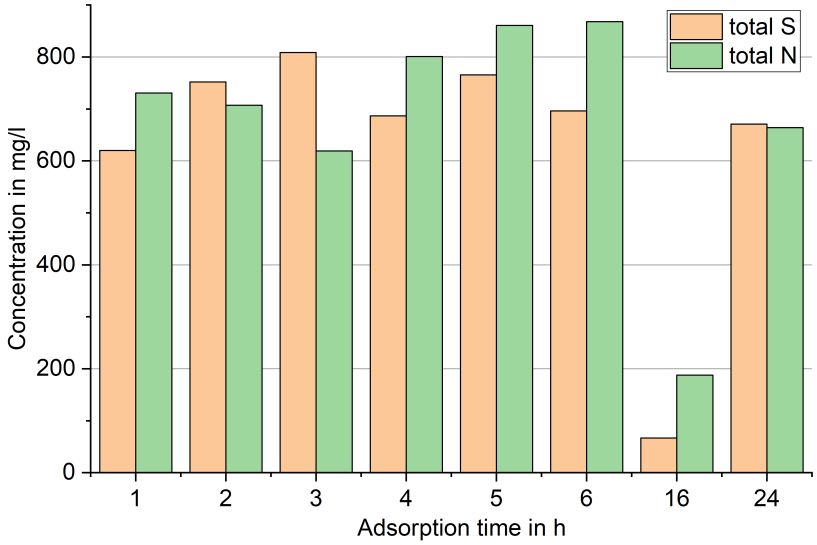

Figure 6.5 Contaminant concentration of the final product in dependence of the stirring time (measured in triplets, m_{AC} = 3 g, at room temperature, pH ≈ 12, stirrer speed: 600 rpm, V_{liquid} = 50 ml)

6.3 Distillative purification

The results of the operation of the pilot plant described in Section 3.7.3 are presented here. Table 6.2 gives an overview of the experiments. The pump power translates to a volume flow as shown by the pump calibration curve in Appendix F.1. The experiments are categorized in runs involving only MeOH from CO_2 hydrogenation (PtMeOH) or runs with MeOH from PtMeOH and pulp mill. Here the pretreated and non-pretreated cases are differentiated. The categories depicted in Table 6.2 are used in the following graphs to improve the understandability of the graphs.

Table 6.2 Parameters of experiments (Δp in mbar)

Experiment	FC	PtMeOH	Parameters for operation			Category
			Δp	R_L	Pump power	
V5_1	-	x	2.2	2	45%	PtMeOH
V5_2	-	x	2.2	1.4	45%	PtMeOH
V5_3	-	x	2.2	1.4	50%	PtMeOH
V6_1	-	x	2.0	1.4	48%	PtMeOH
V6_2	-	x	2.2	1.4	48%	PtMeOH
V6_3	-	x	2.4	1.4	48%	PtMeOH
V7_1	-	x	2.2	1.4	48%	PtMeOH
V7_2	-	x	2.2	1.4	46%	PtMeOH
V8_1	x	150	2.2	1.4	48%	FC-150
V8_2	x	150	2.2	1.4	50%	FC-150
V9_1	x	150	2.2	1	52%	FC-150
V9_2	x	150	2.2	1.8	48%	FC-150
V11_1	x, pretreated	150	2.2	1.4	49%	pFC-150
V11_2	x, pretreated	150	2.2	1.4	47%	pFC-150
V12_1	x, pretreated	50	2.2	1.4	47%	pFC-50
V12_2	x, pretreated	50	2.2	1.4	49%	pFC-50
V13_1	x, pretreated	150	2.2	1.4	49%	pFC-150
V13_2	x, pretreated	150	2.2	1.4	51%	pFC-150
V14_1	x, pretreated	50	2.2	1.4	49%	pFC-50
V14_2	x, pretreated	50	2.2	1.4	51%	pFC-50
V15_1	x	300	2.2	1.4	48%	FC-300
V15_2	x	300	2.2	1.4	50%	FC-300
V16_1	x	200	2.2	1.4	48%	FC-200
V16_2	x	200	2.2	1.4	50%	FC-200

Most experiments were performed for a pressure drop of 2.2 mbar along the column. In V6, the pressure drop was changed to investigate the impact of this parameter. The reflux ratio (R_L) is changed between 1 and 2 which is sufficient for the separation as confirmed by Aspen Plus simulation. The pump power is changed between 45 and 52 %. V5 to V7 investigate the separation of a MeOH water mixture as received by CO_2 hydrogenation with a molar composition of 1:1.

The other experiments investigate the combined purification of MeOH from PtMeOH and FC. V8, V9, V15 and V16 use MeOH sampled from point "1" in Figure 3.5. The plant sizes of the PtMeOH process are 150, 200 or 300 MW_{el} electricity input to water electrolysis. Preliminary assessments showed that the dilution effect for a 50 MW_{el} PtMeOH plant is not efficient to reach the required limits for S. Therefore, the experiments start with the 150 MW_{el} plant. The larger plant sizes of 200 and 300 MW_{el} can further dilute the impurities and are more likely to reach the required specifications. For V9_2 the end of the experiment was missed. V11 to V14 use MeOH from sample port "2" in Figure 3.5. This pretreated stream has a lower load of contaminants. Therefore the combined purification is more likely to reach the required specification.

6.3.1 Mass balance error

One issue is the closure of the total mass balance and the S/N mass balance. Figure 6.6 shows the error in total mass balance over the temperature at the top of the condenser (T310). Based on operational experience, the cooling water temperature and outside temperature influence the mass balance error. The cooling water is drinking water from the grid. This became obvious during test runs with water and MeOH during the summer times with an obvious lack of output mass flow. The condenser has a small hose for discharging the N_2. Via this hose, the MeOH can leave the system. The hose was filled with liquid after the experiments. The higher outside temperatures impact the temperature in the compartment as the air is constantly supplied and removed from it.

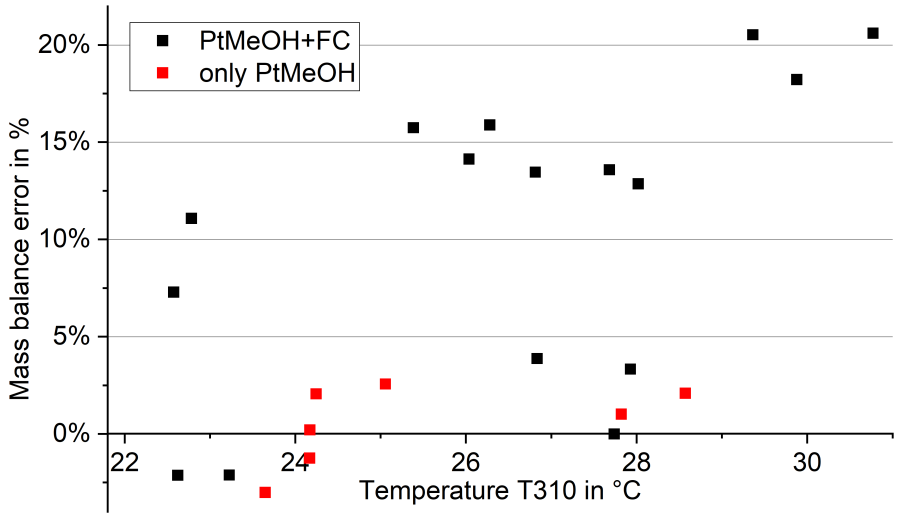

Figure 6.6 Total mass balance error in dependence of the temperature above the condenser (T310, mean value)

The cooling water temperature and mass flow will influence the temperature in the condenser. The cooling water flow was kept constant for the experiments as higher flow rates would exceed the plant's pressure rating. The cooling water passes through the top product cooler. In this step, the temperature of the cooling water is increased. The increase is greater if more product is withdrawn as top product. T310 indicates the temperature at the top of the condenser. Higher temperatures would mean an insufficient cooling in the condenser. To correlate the temperature of T310 with the mass balance error, Figure 6.6 shows the temperature T310 and the mass balance error. Positive deviation means that the input is greater than the output of the plant which would be the case for lost material via the N_2 purge as suspected.

T310 ranges roughly from 22 to 31 °C. The data points are discriminated into experiments with MeOH from PtMeOH, and with MeOH from PtMeOH and the pulp mill. The experiments with only PtMeOH show mass balance errors below 3 %. This shows that the plant's operation is possible with small mass balance errors. The closure of the mass balance seems also more reliable for the PtMeOH runs. For the combined purification, the mass balance error is in the positive range as high as 21 %. The data indicates that a positive correlation between the error in mass balance and the temperature can be established. However, also for similar temperatures of T310, the experiments with FC show higher mass balance errors compared to only PtMeOH.

The error in the S and N balance is shown in Figure 6.7. The maximum range of the error lies between -59 and 346 %. Negative values mean that the feed contains more S or N than the output. Generally, the flows for S and N during an experiment are very small (below 1 g) showing the amounts that are traced in the experiments. Positive errors mean that the output of the components S and N is greater than the input which contradicts the conservation of mass. Especially, the larger bars point at measurement errors.

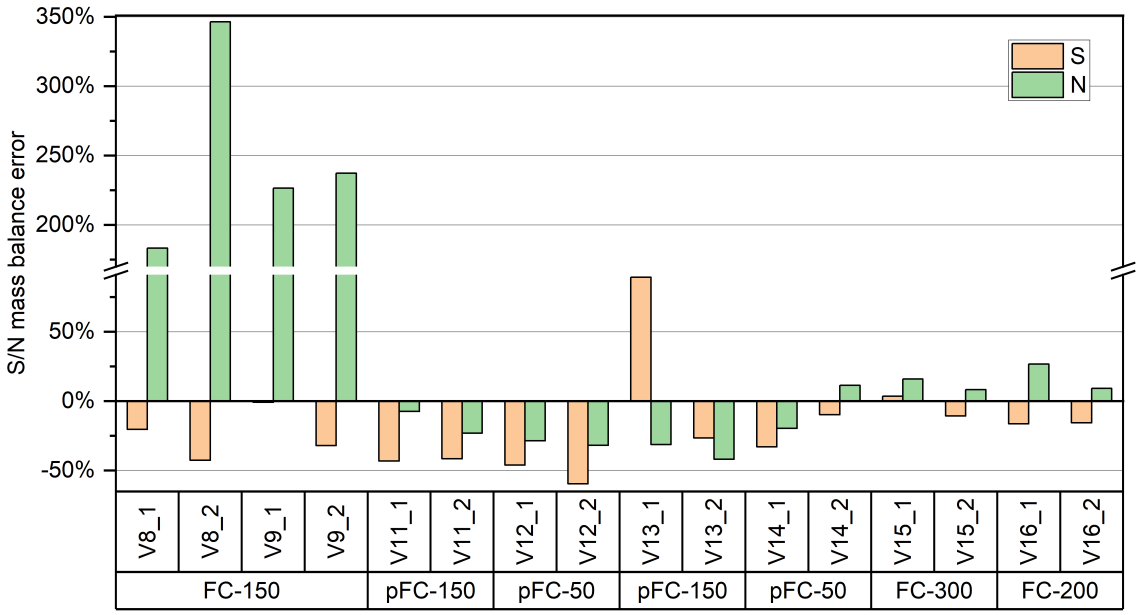

Figure 6.7 S and N mass balance error of the experiments involving FC

Negative values mean a lack of S and N in the products. Possible explanation is that the light S and N containing components leave with the N_2 stream at the top of the column since they cannot be condensed. The positive values arising mostly for N contradict this explanation as all N components are expected to be very light and should therefore be difficult to condensate in the top of the column. Thus, the error for S and N must have the same sign. Obviously, this is not true in the experiments. Inaccuracies can occur for contamination of the experimental setup as the column was not cleaned after the experiments. Whether the laboratory analysis is accurate must be further investigated.

6.3.2 Temperature data

This section presents the temperature profile along the column, and the temperature of condenser and reboiler. The temperature of the feed stream is shown in Appendix F.2.

Figure 6.8 depicts the temperature profile from reboiler to condenser along the column for all experiments. The profile is arranged periodically and not according to the position of the temperature measurement position along the length of the packing. The presented data points are mean values. For most experiments the reboiler temperature is at 100 °C which equals the boiling point of water. The condenser temperature ranges from 64 to 74 °C. The boiling point of MeOH is 64.7 °C. A higher temperature in the condenser relates with a higher temperature above the condenser (T310).

The majority of the experiments (except for three experiments) show a similar temperature profile. The temperature profile for V5_3, V9_2 and V13_1 are off. Below the feed point, the temperature is constant for T302 to T306. Sections with the same temperature will have the same concentration in the liquid and gas phase resulting in no separation. Consequently, these stages do not contribute to the performance of the column meaning that the installed number of stages exceeds the requirement. The packing height can actually be reduced.

Figure 6.9 gives the temperatures of the reboiler and condenser. The reboiler temperature is constant at roughly 100 °C for all experimental runs. Outliners are V5_3 and V9_2. V9_2 is no reliable experiment as the end of the experiment was missed. V5_3 also showed an unusual temperature profile along the column. The standard deviation of the reboiler temperature is very small. Higher standard deviations are observed for the condenser temperatures. Furthermore, the difference in mean temperature across the experiments is much larger than for the reboiler temperature.

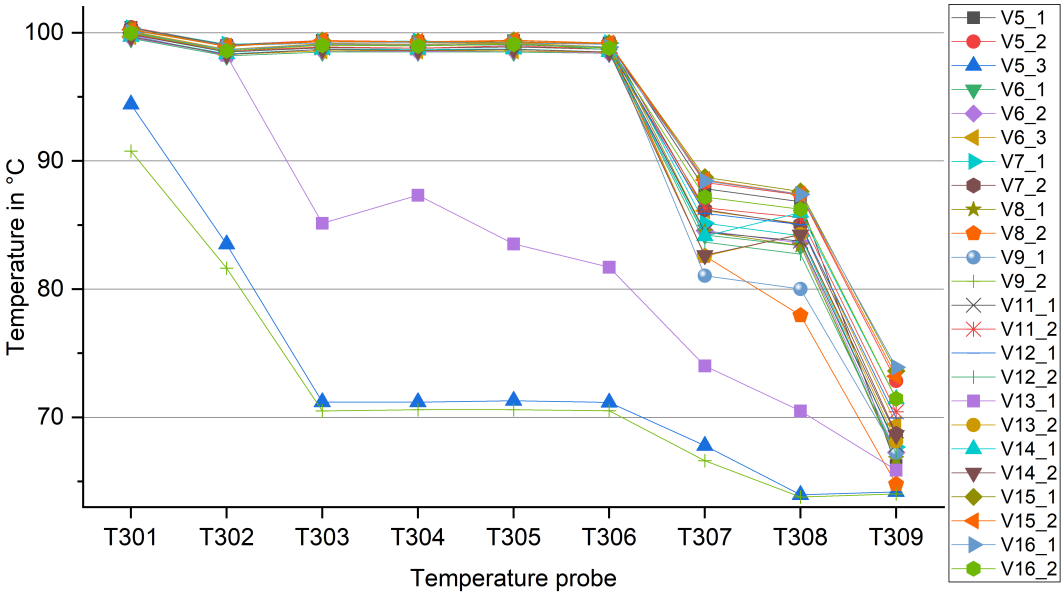

Figure 6.8 Mean values of temperatures from reboiler to condenser

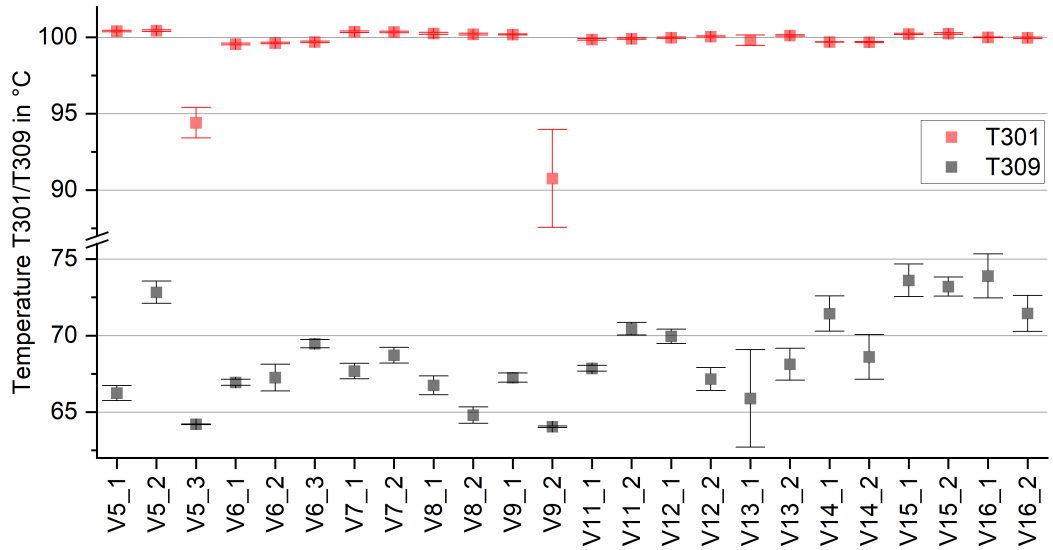

Figure 6.9 Temperature (mean value with standard deviation) of reboiler (T301) and condenser (T309)

6.3.3 Distillate to feed ratio

Figure 6.10 shows the D:F ratio of all experiments. The D:F ratio is calculated with the feed stream derived from the pump power and the measured weight of the top product. The horizontal lines show the theoretical D:F ratio for reaching either 90 or 100 wt. % concentration of MeOH in the top product with no MeOH in the bottom product. The feed is a mixture of water and MeOH with a molar ratio of 1:1. The D:F ratio increases for lower purity as more water ends up in the top product.

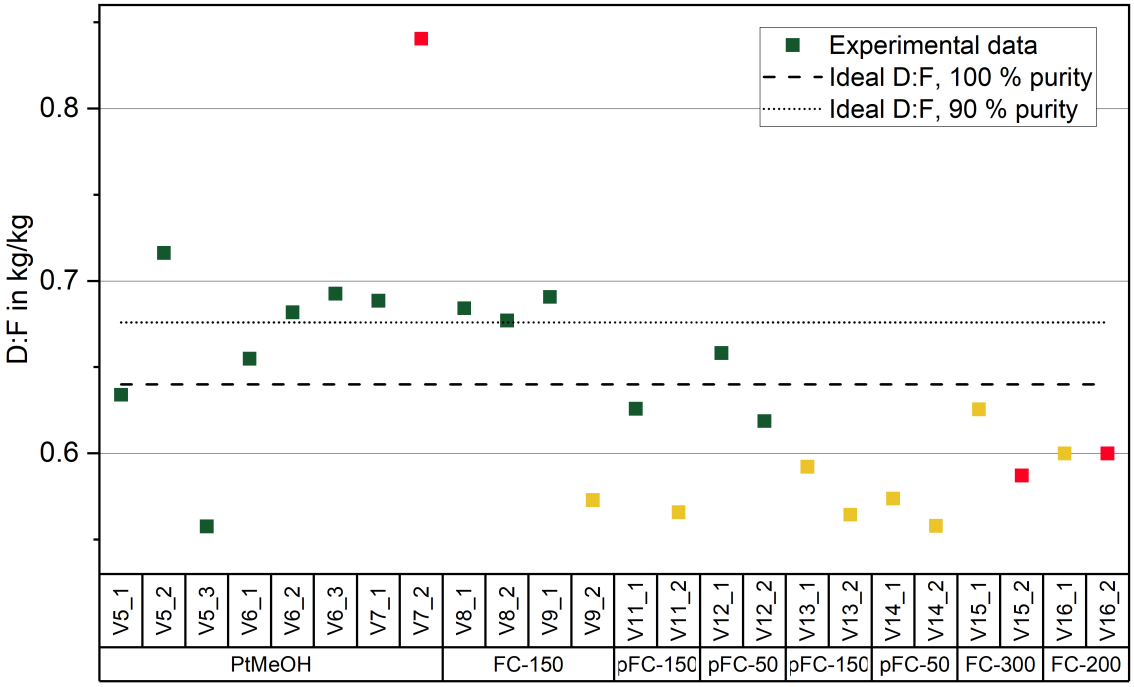

Figure 6.10 Distillate to feed ratio (Color of the data points show the mass balance error: below 10 % (green), between 10 and 20 % (yellow) and above 20 % (red))

Due to the error in mass balance (Section 6.3.1), the D:F ratio is correct for experiments with low error in mass balance. For most experiments, the output stream is lower than the input stream meaning that the D:F ratio calculation is incorrect leading to low calculated D:F ratios. The mass balance error is indicated in the figure by the color of the data points. The mass balance error is categorized into below 10 % (green), between 10 and 20 % (yellow) and above 20 % (red).

6.3.4 Purity

Figure 6.11 shows the MeOH content of the top and bottom product. The values are determined by density measurement. Samples are taken after the experiment from the storage vessels to get a mean concentration.

For all experiment except V5_3 and V9_2, the concentration of MeOH in the bottom product is zero. For the exceptions, the MeOH in the bottom product goes along with a very high concentration in the top product. The MeOH appears in the bottom as the D:F ratio is very low (see Figure 6.10). The limited withdrawal of top product results in the removal of MeOH via the bottom product adhering to the conservation of mass. Especially for V5_3 the explanation with the D:F ratio is very reliable due to a low mass balance error. For V9_2 this eplanation with the D:F ratio is imprecise. The highest MeOH concentration in the top product (99.05 wt. %) with no MeOH in the bottom product is found for V8_2. The results show that high purity MeOH can be produced with the pilot plant.

In order to constantly and reliably reach the desired purities a tedious trimming of the process parameters (mostly feed mass flow and R_L) is required. However, even for the same settings a steady and reproducible operation of the plant is challenging. Three sets of experiments have the same

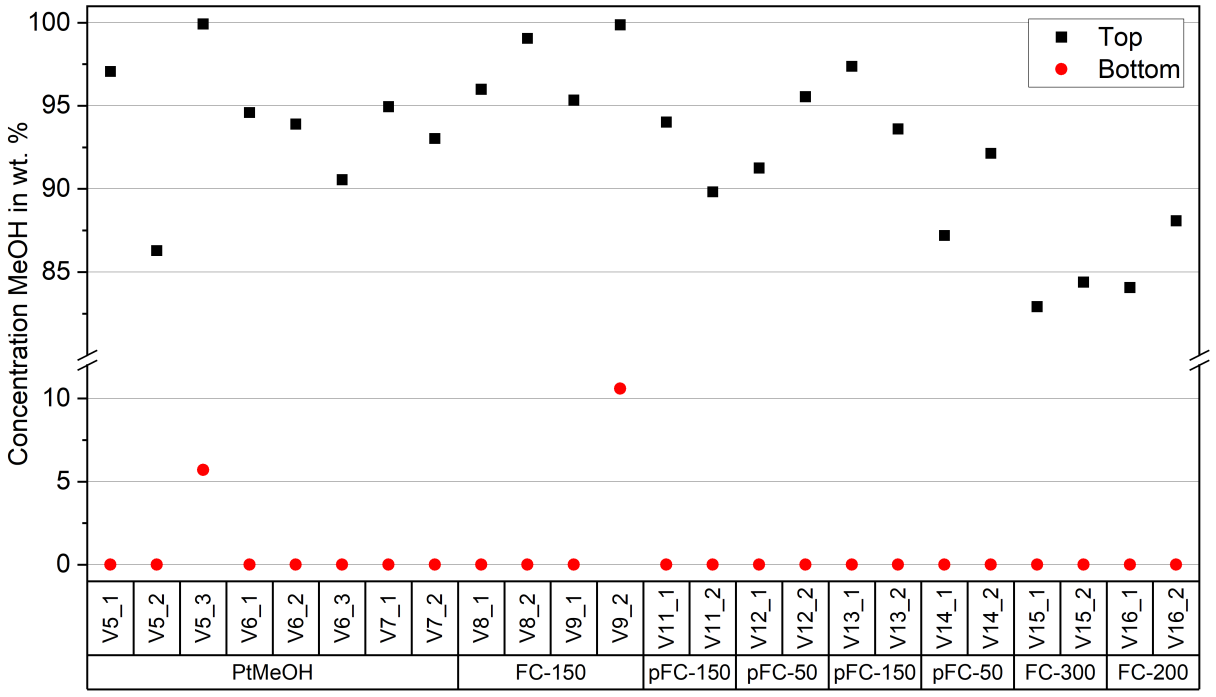

Figure 6.11 MeOH content in the bottom and top product

experimental parameters but show different concentrations. For V7_1 and V6_2 (both PtMeOM), the resulting MeOH concentration are 94.95 and 93.90 wt. %. The MeOH concentration for V11_1 and V13_1 (both pFC-150) are 94.02 and 97.37 wt. % which can also be slightly influenced by different pretreated FC samples. For pFC-50, experiments V12_2 and V14_1 result in 95.55 and 87.30 wt. %.

Figure 6.12 shows the concentration of total S and N in the top product for experiments with the combined purification. The concentration of contaminants could be reduced from a mean value of 2710 and 1130 mg/kg including water to below 250 mg/kg for the final product with little water content. According to IMPCA specifications the maximum concentration for S is 0.5 mg/kg which is exceeded for every experiment [190]. The experiments with non-pretreated FC shows especially for FC-150 very high contaminant concentrations. The results for N have to be treated cautiously due to the large error in mass balance (see Figure 6.7). Generally, experiments with pretreated FC show lower concentrations for N than for S. Experiments with non-pretreated FC show the opposite trend. FC-300 shows lower concentrations than FC-200 as the impurities are diluted. For reaching the specifications an even higher degree of dilution is needed. For pFC-50, the contaminant concentrations are higher in comparison to pFC-150 due to the dilution of the impurities. The experiments with pretreated FC can usually reach very low concentrations for N. The S concentration is also well below 50 mg/kg.

The horizontal lines in Figure 6.12 show the S concentration as calculated by the process simulation in Section 6.1 for the indicated cases. The cases without FC pretreatment (FC-150 and FC-300) show lower concentrations than the experiments. The trend of lower S concentration is obviously confirmed by the models. The trend is also observed for pFC-50 and pFC-150. Through the pretreatment, the S concentration of the MeOH product is reduced significantly compared to the FC cases. Nevertheless, the experimental results show generally a lot higher concentration in comparison to the model results. For pFC-150, the set off is however the smallest.

Reasons for the difference can be the total S or N content of the samples which differ from the generic stream implemented in Aspen Plus. As shown earlier, the samples can differ in contaminant concentration (see Figure 3.6). Furthermore, the generic composition based on literature values and assumptions might differ from the actual composition used in the experiments. The presence of other components and other concentrations of all components influences the separation processes in the model which leads to a different contaminant concentration in the final product.

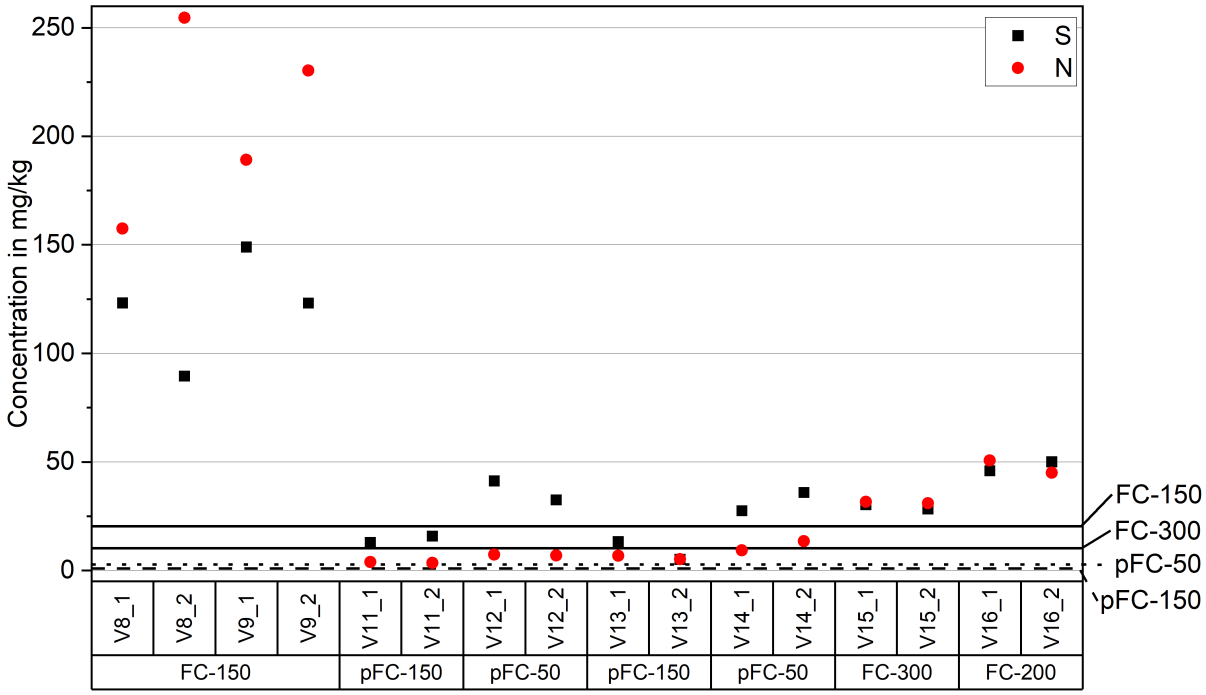

Figure 6.12 Total S and N concentration in the top product (IMPCA specification for S: 0.5 mg/kg. The horizontal lines for FC-150, FC-300, pFC-50 and pFC-150 are derived from Aspen simulation in Section 6.1)

6.3.5 Validation of simulation

Aspen Plus is used to compare and validate the experimental results with the simulation for the PtMeOH experiments. The experimental results of V7_1 are used as reference. Two simulations are performed. One uses the values derived from the experiment and the other one is modified to meet the MeOH purity of the top product as given by the experiment. The simulation of the rectification column uses the RadFrac model in Aspen Plus. The feed stream is set to 2.42 kg/h at 65 °C with a concentration of 64.0 wt. % as used in the experiment. The column internals are modeled as Sulzer CY with a height of 4.71 m as in the pilot plant. The column is filled with the packing from stage 2 to 49. Stage 1 is the condenser and stage 50 is the reboiler. The stages do represent real stages as the column internals are defined as packing. The feed to the column enters at a relative height of 0.57 which equals stage 21 in the model. The RR is set to 1.4 and the D:F ratio is set to either 0.689 as calculated from the experiment or altered to reach the purity as in the experiment.

The column settings and specifications of input and output streams are shown in Table 6.3. The reflux ratio and feed (mass flow and concentration) is equal for simulations or experiment. There is a small deviation in the concentration which is due to the sample preparation for the experiment. The errors are calculated in relation to the experimental values. The D:F ratio for the simulation is set to the one calculated from the experimental data. Due to the mass balance error of - 3 %, the actual D:F ratio is different from the calculated one. In order to reach higher MeOH purities at the top, the D:F ratio of the modified simulation is decreasing. Without the modification the simulation predicts a lower MeOH concentration in the top product. The bottom product contains for all cases no MeOH.The feed flows are equal for the experiment and the simulations. With the corrected D:F ratio, the mass flows of the top and bottom product are closer to the values of the experimental results. The temperatures in the reboiler are for all cases very similar around 100 °C. The condenser temperature have a higher variance between the cases.

To further investigate the temperatures in the process, Figure 6.13 shows the temperature profile along the height of the column. The x axis shows the relative packing height. The reboiler is found at a relativ packing height of 1. The condenser is at a relative packing height of 0. As the pilot plant has a

Table 6.3 Comparison of simulation and experiment for V7_1

	Experiment	Model		Model modified	
	V7_1	Value	Error	Value	Error
D:F (wt. based)	0.689	0.689	-	0.6745	2.1%
RR (wt. based)	1.4	1.4	-	1.4	-
MeOH content Top (wt. %)	0.949	0.929	2.2%	0.949	0.0%
MeOH content Bottom (wt. %)	0.000	0.000	-	0.000	-
MeOH content Feed (wt. %)	64.03%	64.01%	0.0%	64.01%	0.0%
Mass flow top product (kg/h)	1.639	1.667	-1.7%	1.632	0.4%
Mass flow bottom product (kg/h)	0.826	0.753	9.8%	0.788	4.9%
Mass flow feed (kg/h)	2.420	2.420	-	2.420	-
Temperature condenser (°C)	67.7	66.1	2.5%	65.5	3.3%
Temperature reboiler (°C)	100.4	99.6	0.7%	99.6	0.7%

temperature measurement in the liquid (T301) and vapor phase (T302) of the reboiler, two data points are shown at a value of 0. The other temperature measurements of the pilot plants are distributed along the column. The points of measurement are normalized based on the length of packing that lies between the reboiler and the temperature measurement point to calculate the relative packing height. Nine temperature measurements are available from the experiment. For the simulations, 50 data points for 50 virtual stages (including reboiler and condenser) are available. The modified simulation model shows slightly lower temperatures in the rectifying section.

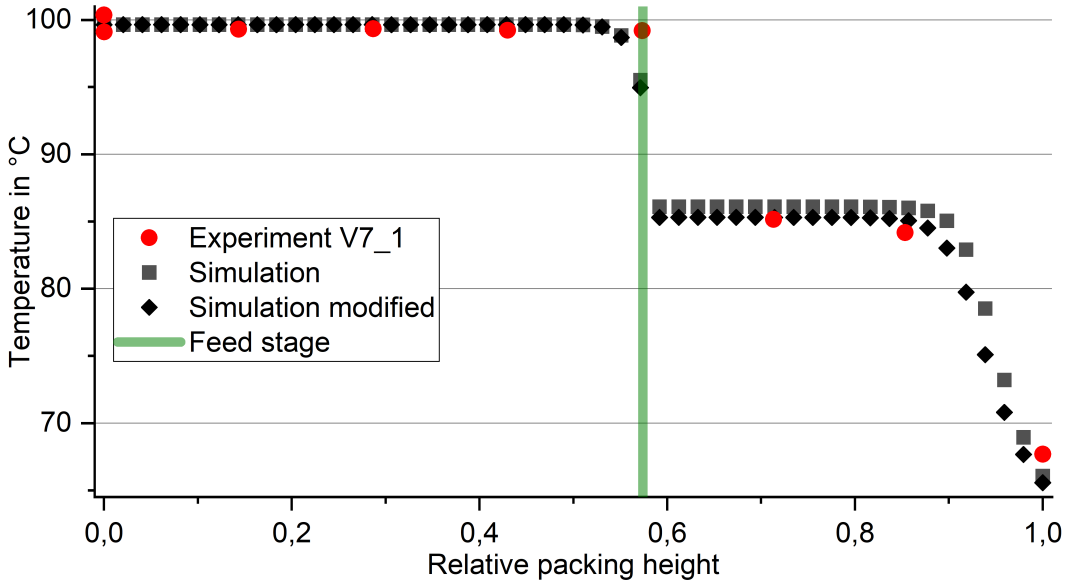

Figure 6.13 Comparison of temperature profile for simulation and experiment

6.4 Conclusion

Purification concept

The process simulations show that MeOH purities can be reached. The S content of the MeOH is however not satisfied by any case. The pFC cases are suitable for smaller plant sizes of the PtMeOH plant and the FC cases are suitable for larger plant sizes to reach the required purities. In order to confirm the results more rigorous modeling and comparison with experiments are necessary. Since the flow rate of FC is generally quite small, the impact on capital and operating cost of this stream is neglectable. However, the processes need to be designed robustly to ensure a fulfillment of the purities as the composition of the FC differs immensely.

Experiments on selective removal of contaminants

Based on the experimental results presented above the adsorption with AC or precipitation with Fe(II) ions are regarded as not viable for the removal of contaminants. The general proof of concept is established. The utilization of Fe(II) ions can remove S species but the ions must also be removed from the final product to meet the MeOH specifications. Furthermore, the removal is not effective. The utilization of AC showed an effective removal of S species but less effective for N species. However, high amount of AC are required to reach high removal efficiencies.

Considering the upscaling, the economics of these batch processes will not be competitive to for example a stripper column. The amount of AC needed to remove the contaminants result in high operating cost. In the experiments, 50 ml of crude MeOH are mixed with up to 8 g of AC. Under these process conditions, a cost effective operation cannot be established even with a recycle and regeneration of the AC. Using a different AC with other properties might decrease the required mass of AC but the effect will not be a game changer. However, the process might be an option for the final cleaning of the product if the purified MeOH after rectification cannot reach the required purities. However, still for this application the economics might not be favorable for the adsorption process.

Rectification experiments

The replication of the rectification experiments is difficult. Even for the same experimental settings, the results in terms of purities are not matching. Besides experimental and measurement errors, the FC stream can have very different compositions. The total mass balance error for the PtMeOH experiments is smaller than for the combined purification experiments. The error for the component S and N can be huge. High MeOH purities can be reached with the pilot plant. However, the limit for S in the MeOH product cannot be reached. Furthermore, the comparison with the simulations results show a difference between experiment and simulation. The model validation of the PtMeOH purification with process simulation shows a good alignment of the process parameters. Suggestions for further work can be the better understanding of contaminants in the FC stream in order to tailor the processes. Already established processes like Merox by UOP for the removal of mercaptanes could be tailored to the application in the pulp mill.

7 Transferability and European potential

This chapter discusses how the concepts and processes presented in the chapters before can be used in sulphite pulp mills, integrated pulp mills (pulp production combined with paper production) or other industries. Furthermore, the production amounts of PtX products are assessed in an European context. The availability of biogenic CO_2 is a chance for sustainable production of PtX products which are required in future in case of a phase out of fossil resources. Furthermore, PtX is an option for pulp mills to quickly reduce their CO_2 emissions. A pulp mill concept with lower CO_2 emissions based on non-thermal utilization (no combustion) of by products will require research efforts and high investments. Therefore, PtX is a readily available technology to tackle the problem.

The total chemical pulp production in Europe was 27.5 Mt (2022) of which only 1.6 Mt were sulphite pulp [283]. Even though the sulphate pulp dominates the market, the potential of the sulphite pulp mills shall not be neglected. Sulphite pulp production plays especially in Germany an important role. Other locations of sulphite pulp mills are mostly in Austria and South Africa. There are 4 sulphite and 2 sulphate pulp mills in Germany as shown in Table 7.1. The production capacity for sulphate pulp exceeds the production of sulphite pulp. The sulphite pulp mills are all integrated and the sulphate pulp mills are all non-integrated pulp mills.

Table 7.1 Pulp mills in Germany ([a] operation ends in 2024)

Name	Type	Integration	annual pulp production in t
Sappi Ehingen	Sulphite	Integrated	150,000
Sappi Stockstadt[a]	Sulphite	Integrated	145,000
Sappi Alfeld	Sulphite	Integrated	120,000
Essity Mannheim	Sulphite	Integrated	220,000 + 35,000 from straw
Mercer Stendal	Sulphate	Non-integrated	740,000
Mercer Rosenthal	Sulphate	Non-integrated	360,000

7.1 Transferability to sulphite pulp mills

In the following the integration of PtX processes into sulphite pulp mills are discussed in general and with respect to the German situation. The main difference or similarities for transferring the concepts and results from sulphate to sulphite pulp mills are the following:

- Onsite H_2 generation: Non-integrated sulphite pulp mills will have an electricity surplus, similar to non-integrated sulphate mills. Integrated sulphite and sulphate pulp mills have either only a small or no electricity surplus at all. As all sulphite pulp mills in Germany are integrated mills, the exploitation in terms of green electricity utilization is limited.
- Lime kiln: Sulphite pulp mills do not have a lime kiln since it is not needed for their chemical recycling loop. Consequently, using the advantage of separating CO_2 from a flue gas with higher CO_2 content is not present. Consequently, the concepts for decarbonizing and defossilizing the lime kiln developed in Chapter 5 cannot be transferred to sulphite pulp mills. Nevertheless, the concepts can be transferred to the other industries as discussed in Section 7.3.
- Availability of biogenic CO_2: The combustion of spent sulphite liquor and bark, similar to sulphate pulp mills, generates biogenic CO_2 emissions which can be captured from the flue

gases. Sulphite pulp mills are due to the high thermal power of the combustion facilities also huge point source for biogenic CO_2. Nevertheless, no flue gas with higher CO_2 partial pressure like from the lime kiln is available.

- Ethanol production: The spent sulphite liquor can be used for fermentation to produce ethanol. Usually, the spent sulphite liquor is burnt in a recovery boiler to supply energy to the mill. Therefore, in most cases additional combustion facilities are needed to supply the mill with sufficient energy if the spent sulphite liquor is used for ethanol production [284]. This urge increases with an integrated ethanol fermentation process since the heating value of the SSL is decreased and the ethanol fermentation process itself needs energy [284]. Ethanol generated in a sulphite pulp mill is a platform chemical that can be transformed into different chemicals. The question arises here if CO_2 or CO_2 derived chemicals can be used for further upgrading of the ethanol to make use of the available biogenic CO_2. An examples would be ethyl acetate with acetic acid produced from CO_2 and H_2 [285].

$$CH_3COOH + CH_3CH_2{-}OH \longrightarrow CH_3{-}COO{-}CH_2CH_3 + H_2O \tag{7.1}$$

  Further conversion to other products like ethylene, diethyl ether, acetone, 1-butanol, butadiene and so forth is possible [286]. In these processes CO_2 or CO can be used as feedstock [287]. However, processes for the further conversion of ethanol are very long process chains and therefore the interest of pulp mills might be limited to build such complex chemical plants. Furthermore, the pulp mill lacks the close proximity to industry with the demand for the products which are for example gaseous feedstock for polymer production generally produced onsite and not transported.

- H_2 utilization: Besides chemical conversion routes, the need for H_2 in the transport sector is also existing in sulphite pulp mills.

- Heat integration: Heat integration is possible as in the sulphate pulp mill. The steam cycles of the recovery boiler and conversion of steam to electricity in a turbine is similar to sulphate pulp mills.

- Waste water treatment and deionized water plant: The waste water treatment plants could be used for the treatment of waste water from the PtX process. A deionized water plant is available at sulphite pulp mills, too.

- Purge and tail gas combustion: Purge gases can be co-combusted in the combustion facilities. A regulatory approval needs to be obtained for adding these gases to the bark or recovery boiler.

- H_2O_2: H_2O_2 is an universal bleaching agent for pulp. Therefore, an onsite production process would also be attractive for sulphite pulp mills.

- O_2 demand: If required for bleaching, the O_2 demand can be covered by O_2 produced as by-product of water electrolysis.

- MeOH purification: There is no MeOH generated as by-product in sulphite pulp mills. Thus, the combined purification as investigated in the thesis is not applicable.

7.2 Transferability to integrated pulp mills

For pulp mills with an integrated paper production, the main issue for integration is the availability of excess electrical and thermal energy onsite. Integrated pulp mills can require an external energy input whereas non-integrated pulp mills are exporters of energy (mostly electricity) [288]. Data of an example pulp mill shows that for a modern non-integrated pulp mill the electricity sale to the grid is

reduced by one third compared to a non-integrated pulp mill [288]. However, some integrated pulp mills actually need external fuel for operation. Onarheim et al. showed that for an integrated pulp mill, heat from an auxiliary boiler would be needed for large scale CO_2 capture (without chemical conversion process) [72]. In contrast, the non-integrated mill needs no imported thermal energy [72].

The assessment of excess energy onsite is very site specific and depends on many factors like for example type of produced paper or energy efficiency of the mill. Generally, the availability of green electricity and heat is reduced in integrated pulp mills compared to non-integrated pulp mills. An additional electricity demand can easily be covered by import from the grid. For lacking heat, the electricity generation in the turbine can be reduced or externally supplied fuel can be combusted. The other integration options like purge combustion, waste water treatment, deionized water production etc. is not touched by integrated pulp mills comparing integrated and non-integrated pulp mills.

The consequences for integrating PtX plants into an integrated pulp mill are very site specific and have to be investigated in detail for every case. Generally, smaller plant sizes will be preferable in order to satisfy the heat demand by the available heat avoiding the import of additional fuel. Electricity can be sourced from the grid if needed. Furthermore, PtX processes like SNG will be preferred due to a steam surplus (increased production of steam) instead of processes with a steam demand like for many other PtX routes (see Section 4.9.1).

7.3 Transferability to other industries

In this section, the further utilization of process concepts and results for other industries is discussed. The decarbonization concepts as described in Chapter 5 aims at providing a gaseous fuel which can be used for combustion in high temperature processes to provide the required heat. One option would be the primary production of metals like iron, copper or zinc which are high temperature processes [289]. For example, the integration of the SNG process was investigated for the blast furnace [290]. Whether the other concepts for the generation of combustible gases presented in this thesis are technically applicable to the iron and steel, and non-ferrous metal industry must be examined in detail.

In the sector of non-metallic minerals which uses furnaces for their high temperature processes an utilization of the processes is also feasible. These processes require mostly high temperatures above 500 °C [289]. Examples are glass melting, tiles and ceramics burning, clinker production, and lime burning. In glass melting high temperatures are required in a furnace to melt the glass. Different fuel options including SNG, H_2 and syngas from biomass gasification are discussed in literature [291]. In the lime kiln processes for the production of CaO from $CaCO_3$ like in the pulp mill, the presented processes can be adapted. However, the integration with available waste biomass and other utilities like O_2 utilization or waste water treatment plant are in most cases not possible.

One major issue of transferring the production of fuels and chemicals as presented in Chapter 4 to other industries is the availability of biogenic CO_2. Since most processes are based on fossil resources as feedstock and for energy supply, the availability of biogenic CO_2 is limited to for example pulp mills, wood based production processes like saw mills, waste combustion, biogas plants and power plants fueled by biomass. However, the other areas of integration like green electricity availability, waste water treatment plant, purge stream combustion facility, deionized water plant or heat integration are not available for most other sites with available biogenic CO_2. To summarizes, pulp mills appear to be the most suitable and all-encompassing option for the PtX processes due to the possibility of full integration. All other options are lacking the full integration.

7.4 European potential

This section addresses the potential of CO_2 utilization in the European pulp industry. The calculation is based on the annual pulp production in Europe of 27,548 kt (sulphite and sulphate pulp) [283]. The annual CO_2 emissions are estimated to 55,098 kt CO_2/a based on an emission factor of 2 t

CO_2/ADt [66]. It is assumed that 90 % of the CO_2 are captured for utilization. With the mass and energy balances obtained in Chapter 4, the PtX product amounts, H_2 demand and electrolysis power demand is calculated (Table 7.2). The power demand of the electrolysis uses 8,000 full load hours for the calculation.

Table 7.2 Production amounts of PtX products from CO_2 of the European pulp mills (Numbers in brackets show the share of the total annual demand worldwide with 106 Mt for MeOH [292], 145.35 EJ for NG [293], 184.21 EJ for crude oil [293] and 14 Mt for AA [294]. [a] based on RWGS)

	Product output in Mt/a	Product output in TWh/a	H_2 demand in Mt/a	Electrolysis power in GW
MeOH	34.6 (32.6 %)	193	6.8	40.6
SNG	18.2	250 (0.6 %)	9.1	54.1
FT[a]	12.9	124 (0.2 %)	6.8	40.6
AA[a]	32.4 (231.1 %)	129	4.6	27.3

The substitution of fossil primary energy carriers like natural gas and crude oil is below 1 % for the worldwide consumption figures. The MeOH production can cover 32.6 % of the annual demand. By partially converting the MeOH demand, the natural gas demand will also drop as natural gas is the primary feedstock for MeOH production. For AA which is a derivate of MeOH, the annual production amount is exceeded. These numbers show that for bulk energy carriers like natural gas or crude oil huge production capacities are required to satisfy the worldwide demand. Furthermore, the electricity demand can most likely be only partially covered by the electricity available onsite. Detailed data on electricity generation in the pulp mills is not available. Assuming that a huge share of the electricity has to be provided by grid electricity, the required low emission electricity has to be available.

8 Conclusion

The thesis is concerned with the integration of PtX routes for the production of fuels and chemicals, and with the decarboniztaion and defossilization of the lime kiln. The processes presented in the thesis are technologies which are mostly readily available and which can be retrofitted to the pulp mill. Pulp mills are very attractive sites for the integration of these technologies. No other sector can compete with the low carbon and extensive infrastructure available at pulp mills. The conclusion summarizes the main results of the thesis shortly as the Chapters 4 to 6 already contain conclusions. The later part aims at providing a more holistic view on the topic.

The assessment of different PtX processes showed that H_2O_2, MeOH and AA are the most promising routes in terms of economics. Furthermore, the emission reduction for H_2O_2 production is possible also with a higher emission factor of the electricity mix in comparison to the other routes. The integration with the pulp mill reveals that the increase in deionized water and waste water treatment demand is marginal compared to the pulp mill's production amounts. The O_2 demand of the pulp mill is generally overshot by O_2 from the electrolysis. The effect of heat integration depends on the PtX process. Generally, the electricity availability can increase or decrease depending on the plant sizes, process configuration and PtX product. The assessment of RWGS and CO_2 electrolysis as competing technologies for FT syncrude and AA generally shows benefits for the RWGS routes.

The reduction of fossil fuel use in the lime kiln can be accomplished by fuels based on biomass or electricity. The utilization of wood powder and producer gas from biomass gasification with air showed the lowest cost while erasing all fossil CO_2 emissions. One major issue with biomass utilization is the rerouting of biomass from the bark boiler to the lime kiln causing reduced steam production in the bark boiler. For pulp mills with a limited biomass availability, the H_2 boosted processes are an option to reduce the biomass demand. Biomass is an extremely valuable energy source for the supply of low carbon energy. Therefore, the utilization of biomass for generation of electricity should be avoided and it should be used instead for the substitution of fossil fuels in the lime kiln to avoid fossil CO_2 emissions.

The utilization of FC in the combined purification with PtMeOH can valorize this side stream in the pulp mill. Concepts with prepurification are advised for smaller PtMeOH plants. For bigger plant sizes, the effect of dilution requires at some point no prepurification. However, the simulation results have to be validated by the experimental test runs performed on the pilot plant. The operation showed difficulties in terms of mass balance and reaching the purities for S/N in the product in comparison to the simulations.

Generally, the location of the pulp mill influences the economics and choice of process variant. As shown in the economic evaluation of the processes, the most influential factor of the total annual cost is the electricity price. Furthermore, the investment cost and efficiency of the electrolysis is also important. The efficiency will also influence the cost for electricity. Therefore the electricity price of the surplus electricity which is fed to the grid as well as the electricity price of the grid electricity influence the economics of the processes significantly. Furthermore, the emission factor of grid electricity is relevant for the CO_2 balance of the process. A low carbon grid electricity enables a low carbon emission production at high full load hours of the electrolysis.

The overall goal of reducing CO_2 emissions should follow the merit order principle for CO_2 abatement cost. The best options to reduce CO_2 emissions are the ones with the lowest CO_2 abatement cost. Therefore, the results for PtX products and lime kiln decarbonization are compared with CCS. The assessment of abatement cost are country specific as the cost for grid electricity and emissions of grid electricity (especially for the 150 MW_{el} plants) can differ.

The milled wood combustion with abatement cost of 46 €/t CO_2 would be the most cost effective option followed by CCS with abatement cost below 100 €/t CO_2 as derived from literature. The next most viable option is the air blown gasification showing abatement cost of 179 €/t CO_2. MeOH and AA would then be the next options with abatement cost between roughly 300 to 400 €/t CO_2. Above these values you find the H_2 based processes for lime kiln decarbonization and the PtX processes for FT syncrude and SNG.

However, besides the most cost effective measure, the scale of CO_2 reduction changes massively between lime kiln decarbonization, PtX processes and CCS. The lime kiln decarbonization is limited to the emissions of the lime kiln which account only for a small part of the pulp mill's emissions. CCS can be implemented in the largest scale which is limited by heat availability, and the required infrastructure for storage and transportation. PtX routes are limited by the availability of electricity or H_2 supply. Nevertheless, carbon based chemicals and fuels are needed in case of a phase out of fossil resources and therefore the production of these PtX products are not seen in competition with CCS but with other production processes for renewable products. Furthermore, most processes need steam from the pulp mill other than for the CO_2 capture process which reduces the amount of captured CO_2 compared to CCS. This is however not limiting for the processes which are net steam exporters. Unfortunately, H_2O_2 as a very promising product in terms of economics and emissions does not fix CO_2 and can therefore not reduce the direct CO_2 emissions of a pulp mill.

The plant size impacts the emission factor of the product, the economics and the integrability. For larger plant sizes, more electricity has to be imported from the grid which can lead depending on the emission factor of the imported electricity to a high emission factor of the product. For example the German grid mix leads to higher emissions than the fossil comparator except for H_2O_2. With increasing plant size the benefit of low carbon electricity provided by the pulp mill decreases. Furthermore, reaching high full load hours of the electrolysis is reduced for larger plant sizes if only fluctuating renewable energies are acquired. Furthermore, the integrability in terms of utilities like heat, waste water treatment or deionized water supply reaches a limit for larger plant sizes.

The results of the thesis are tailored to a non-integrated reference pulp mill. However, results can give a general indication for other pulp mills. One major concern is if the pulp mill is integrated with a paper production which immensely reduces the energy availability for the PtX processes. Furthermore, retrofitting of the processes requires a site specific assessment. Especially for the supply of fuel to the lime kiln, the rerouting of biomass streams and the flue gas flow must be considered.

Bibliography

[1] International Energy Agency. CO2 Emissions in 2022, (https://iea.blob.core.windows.net/assets/3c8fa115-35c4-4474-b237-1b00424c8844/CO2Emissionsin2022.pdf), 2023.

[2] Rainer Küngas, Peter Blennow, Thomas Heiredal-Clausen, Tobias Holt, Jeppe Rass-Hansen, Søren Primdahl, and John Bøgild Hansen. eCOs - A Commercial CO2 Electrolysis System Developed by Haldor Topsoe. *ECS Transactions*, 78(1):2879–2884, 2017.

[3] Pekka Ehtonen, Markku Hurme, and Martti Järveläinen. Integrating chemical plants at the pulp mill, 1995.

[4] Anna-Karin Jannasch, Hjalmar Pihl, Jens Wolf, Rolf Lindström, Mikael Ahlroth, Johan Schönström, Kalle Pelin, Johan Isaksson, Linda Rudén, and Sven Hermansson. Integration of the electro-fuel concept in pulp and paper industry for a future electricity system in balance and a sustainable energy system with minimal carbon foot print, 2019.

[5] D. T. Pio, A.C.M Vilas-Boas, v.d. Araújo, N.F.C. Rodrigues, and A. Mendes. Decarbonizing the aviation sector with Electro Sustainable Aviation Fuel (eSAF) from biogenic CO2 captured at pulp mills. *Chemical Engineering Journal*, 463:142317, 2023.

[6] D. T. Pio, A. C. M. Vilas-Boas, N. F. C. Rodrigues, and A. Mendes. Carbon neutral methanol from pulp mills towards full energy decarbonization: an inside perspective and critical review. *Green Chem*, 24(14):5403–5428, 2022.

[7] Confederation of European Paper Industries. Key statistics 2020: European pulp & paper industry, 2021.

[8] Pedro. Fardim. *Papermaking science and Technolog - Book 6. Chemical pulping. Part 1, Fibre chemistry and technology*. Finnish Paper Engineers' Association, Helsinki, 2nd edition, 2011.

[9] Jürgen Blechschmidt. *Taschenbuch der Papiertechnik*. Carl Hanser Fachbuchverlag, 1. edition, 2010.

[10] B. R. Blackwell, W. B. MacKay, F. E. Murry, and W. K. Oldham. Review of kraft foul condensates — sources, quantities, chemical composition and environmental effects. *TAPPI*, 62:33–40, 1979.

[11] J. Y. Zhu, S.-H Yoon, Pi-Hsin Liu, and Xin-Sheng Chai. Methanol formation during alkaline wood pulping. *TAPPI Journal*, 83, 2000.

[12] Thomas W. Joyce. Significance of methanol recovery to kraft mill total energy budget. *IPC Technical Paper Series*, (71), 1979.

[13] Sabrina Francey, Honghi Tran, and Niklas Berglin. Global survey on lime kiln operation, energy consumption, and alternative fuel usage. *TAPPI Journal*, 10(8):19–26, 2011.

[14] Sabrina Francey, Honghi Tran, and Andrew Jones. Current status of alternative fuel use in lime kilns. *TAPPI Journal*, 8:33–39, 2009.

[15] Peter W. Hart. Alternative "Green" Lime Kiln Fuels: Part II. Woody Biomass, Bio-Oils, Gasification, and Hydrogen. *TAPPI Journal*, 19(5):271–279, 2020.

[16] Peter W. Hart. Alternative "Green" Lime Kiln Fuels: Part I. Pulping/Recovery By-Products. *TAPPI Journal*, 19(5):263–269, 2020.

[17] Richard Manning and Honghi Tran. Impact of cofiring biofuels and fossil fuels on lime kiln operation. *TAPPI Journal*, 14(7):474–480, 2015.

[18] Per Ulmgren. Non-process elements in a bleached kraft pulp mill with a high degree of system closure - state of the art. *Nordic Pulp & Paper Research Journal*, 12(1):32–41, 1997.

[19] Jean Taillon, A. Horvath, and A. Oksman. Replacement of fossil fuel with biomass in pulp mill lime kilns. *O Papel*, 79:85–89, 2018.

[20] Valmet AB. Using wood powder as fuel in lime kilns ($https$: $//www.valmet.com/globalassets/media/downloads/white - papers/power - and - recovery/wood_powder_in_lime_kilns_whitepaper.pdf$), 2018.

[21] Volker Schneider, Rob van der Meer, and Jan Hammes. Hydrogen as fuel in the manufacture of concrete. EP3196177A1, 2017.

[22] Mårten Larsson, Mikael Jansson, Stefan Grönkvist, and Per Alvfors. Techno-economic assessment of anaerobic digestion in a typical kraft pulp mill to produce biomethane for the road transport sector. *Journal of Cleaner Production*, 104:460–467, 2015.

[23] Lalitha Devi Gottumukkala, Kate Haigh, François-Xavier Collard, Eugéne van Rensburg, and Johann Görgens. Opportunities and prospects of biorefinery-based valorisation of pulp and paper sludge. *Bioresource technology*, 215:37–49, 2016.

[24] Elina Mäki, Heidi Saastamoinen, Kristian Melin, Doris Matschegg, and Hanna Pihkola. Drivers and barriers in retrofitting pulp and paper industry with bioenergy for more efficient production of liquid, solid and gaseous biofuels: A review. *Biomass and Bioenergy*, 148:106036, 2021.

[25] Katja Kuparinen and Esa Vakkilainen. Green pulp mill: Renewable alternatives to fossil fuels in lime kiln operations. *BioResources*, 12(2):4031–4048, 2017.

[26] LimeArc process. $https$: $//limearcprocess.se/$ accessed on 01.01.2024.

[27] Elin Svensson, Holger Wiertzema, and Simon Harvey. Potential for negative emissions by carbon capture and storage from a novel electric plasma calcination process for pulp and paper mills. *Frontiers in Climate*, 3:83, 2021.

[28] Alfons Mersmann, Matthias Kind, and Johann Stichlmair. *Thermal separation technology*. EBL-Schweitzer. Springer, Dordrecht, 2011.

[29] Johann Stichlmair, Harald Klein, and Sebastian Rehfeldt. *Distillation*. Wiley, 2021.

[30] Wikipedia User:mbeychok. McCabe-Thiele diagram ($https$: $//de.m.wikipedia.org/wiki/datei$: $mccabe - thiele_diagram.svg$ accessed on 01.01.2024), 2008.

[31] Reiner Keller, Jürgen; Staudt. *Gas Adsorption Equilibria*. Kluwer Academic Publishers, Boston, 2005.

[32] Jayant K. Singh and Nishith Verma, editors. *Aqueous phase adsorption: Theory, simulations and experiments*. CRC Press, 2019.

[33] J. R. Perrich. *Activated Carbon Adsorption For Wastewater Treatment*. Taylor & Francis, 2017.

[34] Hans-Jörg Bart and Ulrich von Gemmingen. Adsorption. In *Ullmann's encyclopedia of industrial chemistry*. Wiley-VCH, 2010.

[35] Vimal Chandra Srivastava. An evaluation of desulfurization technologies for sulfur removal from liquid fuels. *RSC Adv*, 2(3):759–783, 2012.

[36] Minh-Viet Nguyen and Byeong-Kyu Lee. Removal of dimethyl sulfide from aqueous solution using cost-effective modified chicken manure biochar produced from slow pyrolysis. *Sustainability*, 7(11):15057–15072, 2015.

[37] Svetlana Bashkova, Andrey Bagreev, and Teresa J. Bandosz. Effect of surface characteristics on adsorption of methyl mercaptan on activated carbons. *Industrial & Engineering Chemistry Research*, 41(17):4346–4352, 2002.

[38] José A.F. Gamelas, Sofia M. Rebola, Margarita G. Evtyugina, Valdemar I. Esteves, and Dmitry V. Evtuguin. Purification of pulp mill condensates by an adsorptive process on activated carbon. *Holzforschung*, 73(6):589–597, 2019.

[39] Masoume Mollaei, Mazaher Moeinaddini, Nematollah Khorasani, Mohammad Azadfallah, and Amirhooman Hemmasi. Feasibility of removal S^{2-} from Kraft black liquor recovery cycle with synthetic adsorbents (Cu-PAC and Cu-GAC). *Nordic Pulp & Paper Research Journal*, 35(3):309–324, 2020.

[40] Qinglin Zhang and Karl T. Chuang. Adsorption of organic pollutants from effluents of a kraft pulp mill on activated carbon and polymer resin. *Advances in Environmental Research*, 5(3):251–258, 2001.

[41] Yong Tao, Chang-Yu Wu, and David W. Mazyck. Removal of methanol from pulp and paper mills using combined activated carbon adsorption and photocatalytic regeneration. *Chemosphere*, 65(1):35–42, 2006.

[42] Christian Frilund, Ilkka Hiltunen, and Pekka Simell. Activated Carbons for Syngas Desulfurization: Evaluating Approaches for Enhancing Low-Temperature H2S Oxidation Rate. *ChemEngineering*, 5(2):23, 2021.

[43] Peter Häussinger, Reiner Lohmüller, and Allan M. Watson. Hydrogen, 2. production. In *Ullmann's encyclopedia of industrial chemistry*. Wiley-VCH, 2010.

[44] Pedro J. Megía, Arturo J. Vizcaíno, José A. Calles, and Alicia Carrero. Hydrogen production technologies: From fossil fuels toward renewable sources. a mini review. *Energy & Fuels*, 35(20):16403–16415, 2021.

[45] International Energy Agency. Technology Roadmap - Hydrogen and Fuel Cells, 2015.

[46] Jacob A. Moulijn, Michiel Makkee, and Annelies E. van Diepen. *Chemical process technology*. John Wiley & Sons Inc, Chichester, West Sussex, 2nd edition, 2013.

[47] Matthias Binder, Michael Kraussler, Matthias Kuba, and Markus Luisser. Hydrogen from biomass gasification, 2018.

[48] Irena. Green hydrogen cost reduction: Scaling up electrolysers to meet the 1.5°c climate goal, 2020.

[49] Alexander Buttler and Hartmut Spliethoff. Current status of water electrolysis for energy storage, grid balancing and sector coupling via power-to-gas and power-to-liquids: A review. *Renewable and Sustainable Energy Reviews*, 82:2440–2454, 2018.

[50] Cong Chao, Yimin Deng, Raf Dewil, Jan Baeyens, and Xianfeng Fan. Post-combustion carbon capture. *Renewable and Sustainable Energy Reviews*, 138:110490, 2021.

[51] Friday O. Ochedi, Jianglong Yu, Hai Yu, Yangxian Liu, and Arshad Hussain. Carbon dioxide capture using liquid absorption methods: a review. *Environmental Chemistry Letters*, 19(1):77–109, 2021.

[52] Eric Favre. Carbon dioxide recovery from post-combustion processes: Can gas permeation membranes compete with absorption? *Journal of Membrane Science*, 294(1-2):50–59, 2007.

[53] Xiang Zhang, Zhen Song, Rafiqul Gani, and Teng Zhou. Comparative economic analysis of physical, chemical, and hybrid absorption processes for carbon capture. *Industrial & Engineering Chemistry Research*, 59(5):2005–2012, 2020.

[54] Dennis Y.C. Leung, Giorgio Caramanna, and M. Mercedes Maroto-Valer. An overview of current status of carbon dioxide capture and storage technologies. *Renewable and Sustainable Energy Reviews*, 39:426–443, 2014.

[55] David Kearns, Harry Liu, and Chris Consoli. Technology readiness and cost of CCS, 2021.

[56] Arthur L. Kohl and Richard B. Nielson. *Gas Purification*. Elsevier, 1997.

[57] Heinz-Wolfgang Häring, editor. *Industrial gases processing*. Wiley-VCH, Weinheim, 2008.

[58] M. Wang, A. Lawal, P. Stephenson, J. Sidders, and C. Ramshaw. Post-combustion CO2 capture with chemical absorption: A state-of-the-art review. *Chemical Engineering Research and Design*, 89(9):1609–1624, 2011.

[59] Paul H. M. Feron. *Absorption-based post-combustion capture of carbon dioxide*. Elsevier, Duxford, UK, 2016.

[60] A. Cousins, L. T. Wardhaugh, and P.H.M. Feron. A survey of process flow sheet modifications for energy efficient CO2 capture from flue gases using chemical absorption. *International Journal of Greenhouse Gas Control*, 5(4):605–619, 2011.

[61] Wilhelm Kuckshinrichs and Jürgen-Friedrich Hake. *Carbon Capture, Storage and Use*. Springer International Publishing, Cham, 2015.

[62] Zhaohui Zheng, Chuguang; Liu, editor. *Oxy-Fuel Combustion*. Elsevier, 2018.

[63] Maja B. Toftegaard, Jacob Brix, Peter A. Jensen, Peter Glarborg, and Anker D. Jensen. Oxy-fuel combustion of solid fuels. *Progress in Energy and Combustion Science*, 36(5):581–625, 2010.

[64] Rohan Stanger, Terry Wall, Reinhold Spörl, Manoj Paneru, Simon Grathwohl, Max Weidmann, Günter Scheffknecht, Denny McDonald, Kari Myöhänen, Jouni Ritvanen, Sirpa Rahiala, Timo Hyppänen, Jan Mletzko, Alfons Kather, and Stanley Santos. Oxyfuel combustion for CO2 capture in power plants. *International Journal of Greenhouse Gas Control*, 40:55–125, 2015.

[65] Johanna Jönsson and Thore Berntsson. Analysing the potential for implementation of CCS within the European pulp and paper industry. *Energy*, 44(1):641–648, 2012.

[66] Katja Kuparinen, Esa Vakkilainen, and Tero Tynjälä. Biomass-based carbon capture and utilization in kraft pulp mills. *Mitigation and Adaptation Strategies for Global Change*, 24(7):1213–1230, 2019.

[67] Sebastian Karlsson, Anders Eriksson, Fredrik Normann, and Filip Johnsson. Large-scale implementation of bioenergy with carbon capture and storage in the swedish pulp and paper industry involving biomass supply at the regional level. *Frontiers in Energy Research*, 9:29, 2021.

[68] Erik Hektor and Thore Berntsson. Reduction of greenhouse gases in integrated pulp and paper mills: possibilities for CO2 capture and storage. *Clean Technologies and Environmental Policy*, 11(1):59–65, 2009.

[69] Erik Hektor and Thore Berntsson. Future CO2 removal from pulp mills – Process integration consequences. *Energy Conversion and Management*, 48(11):3025–3033, 2007.

[70] Kristin Onarheim, Petteri Kangas, Sakari Kaijaluoto, Ville Hankalin, and Stanley Santos. Techno-Economic Evaluation of Retrofitting CCS in a Market Pulp Mill and an Integrated Pulp and Board Mill, 2016.

[71] Kristin Onarheim, Stanley Santos, Petteri Kangas, and Ville Hankalin. Performance and cost of CCS in the pulp and paper industry part 2: Economic feasibility of amine-based post-combustion CO2 capture. *International Journal of Greenhouse Gas Control*, 66:60–75, 2017.

[72] Kristin Onarheim, Stanley Santos, Petteri Kangas, and Ville Hankalin. Performance and costs of ccs in the pulp and paper industry part 1: Performance of amine-based post-combustion co 2 capture. *International Journal of Greenhouse Gas Control*, 59:58–73, 2017.

[73] Stefania Osk Gardarsdottir, Fredrik Normann, Klas Andersson, and Filip Johnsson. Process Evaluation of CO2 Capture in three Industrial case Studies. *Development of Integrated High Temperature and Low Temperature Fischer-Tropsch System for High Value Chemicals Coproduction*, 63:6565–6575, 2014.

[74] Ragnhild Skagestad, Stefania Osk Gardarsdottir, Fredrik Normann, Marie Anheden, and Jens Wolf. A Case Study of Partial Capture of CO2 from a Pulp Mill – the Effect on CO2 Capture Cost. *SSRN Electronic Journal*, 2019.

[75] Chikezie Nwaoha and Paitoon Tontiwachwuthikul. Carbon dioxide capture from pulp mill using 2-amino-2-methyl-1-propanol and monoethanolamine blend: Techno-economic assessment of advanced process configuration. *Applied Energy*, 250(1):1202–1216, 2019.

[76] Katja Kuparinen, Satu Lipiäinen, and Esa Vakkilainen. Can carbon capture be a new revenue opportunity for the pulp and paper sector? *TAPPI Journal*, 20(8):527–540, 2021.

[77] Amod Parkhi, Selen Cremaschi, and Zhihua Jiang. Techno-Economic Analysis of CO2 Capture from Pulp and Paper Mill Lime kiln. *IFAC-PapersOnLine*, 55(7):284–291, 2022.

[78] Katja Kuparinen, Satu Lipiäinen, Esa Vakkilainen, and Timo Laukkanen. Effect of biomass-based carbon capture on the sustainability and economics of pulp and paper production in the nordic mills. *Environment, Development and Sustainability*, 40(1):84, 2022.

[79] F. Yang, J. C. Meerman, and A.P.C. Faaij. Carbon capture and biomass in industry: A techno-economic analysis and comparison of negative emission options. *Renewable and Sustainable Energy Reviews*, 144(11):111028, 2021.

[80] W. J. Sagues, H. Jameel, D. L. Sanchez, and S. Park. Prospects for bioenergy with carbon capture & storage (BECCS) in the United States pulp and paper industry. *Energy & Environmental Science*, 13(8):2243–2261, 2020.

[81] Adrian Lefvert and Stefan Grönkvist. Smarter ways to capture carbon dioxide – exploring alternatives for small to medium-scale carbon capture in kraft pulp mills. *International Journal of Greenhouse Gas Control*, 127:103934, 2023.

[82] Jussi Saari, Petteri Peltola, Katja Kuparinen, Juha Kaikko, Ekaterina Sermyagina, and Esa Vakkilainen. Novel beccs implementation integrating chemical looping combustion with oxygen uncoupling and a kraft pulp mill cogeneration plant. *Mitigation and Adaptation Strategies for Global Change*, 28(4), 2023.

[83] Mónica P.S. Santos, Vasilije Manovic, and Dawid P. Hanak. Unlocking the potential of pulp and paper industry to achieve carbon-negative emissions via calcium looping retrofit. *Journal of Cleaner Production*, 280:124431, 2021.

[84] Muhammad Usman Khan, Jonathan Tian En Lee, Muhammad Aamir Bashir, Pavani Dulanja Dissanayake, Yong Sik Ok, Yen Wah Tong, Mohammad Ali Shariati, Sarah Wu, and Birgitte Kiaer Ahring. Current status of biogas upgrading for direct biomethane use: A review. *Renewable and Sustainable Energy Reviews*, 149:111343, 2021.

[85] Rainer Küngas. Review—Electrochemical CO2 Reduction for CO Production: Comparison of Low-and High-Temperature Electrolysis Technologies. *Journal of The Electrochemical Society*, 167(4):044508, 2020.

[86] Yolanda A. Daza and John N. Kuhn. CO2 conversion by reverse water gas shift catalysis: comparison of catalysts, mechanisms and their consequences for CO2 conversion to liquid fuels. *RSC Advances*, 6(55):49675–49691, 2016.

[87] Miriam González-Castaño, Bogdan Dorneanu, and Harvey Arellano-García. The reverse water gas shift reaction: a process systems engineering perspective. *Reaction Chemistry & Engineering*, 6(6):954–976, 2021.

[88] R. Matthew Bown, Miriam Joyce, Qi Zhang, Tomas Ramirez Reina, and Melis S. Duyar. Identifying commercial opportunities for the reverse water gas shift reaction. *Energy Technology*, 9(11), 2021.

[89] Sandra Adelung, Simon Maier, and Ralph-Uwe Dietrich. Impact of the reverse water-gas shift operating conditions on the power-to-liquid process efficiency. *Sustainable Energy Technologies and Assessments*, 43:100897, 2021.

[90] Jürgen Bierhals. Carbon monoxide. In *Ullmann's encyclopedia of industrial chemistry*. Wiley-VCH, 2010.

[91] J. D. Medrano-García, R. Ruiz-Femenia, and J. A. Caballero. Optimal carbon dioxide and hydrogen utilization in carbon monoxide production. *Journal of CO2 Utilization*, 34:215–230, 2019.

[92] Franz Fischer and Hans Tropsch. Über die reduktion des kohlenoxyds zu methan am eisenkontakt unter druck. *Brennst.-Chem.*, (4):193–197, 1923.

[93] Anthony N. Stranges. A History of the Fischer-Tropsch Synthesis in Germany 1926–45. In *Fischer-Tropsch Synthesis, Catalyst and Catalysis*, volume 163 of *Studies in Surface Science and Catalysis*, pages 1–27. Elsevier, 2007.

[94] Paul F. Schubert, Charles A. Bayens, Larry Weick, and Michael O. Haid. Expanding Markets for GTL Fuels and Specialty Products. In *Natural Gas Conversion VI*, volume 136 of *Studies in Surface Science and Catalysis*, pages 459–464. Elsevier, 2001.

[95] Vincent Dieterich, Alexander Buttler, Andreas Hanel, Hartmut Spliethoff, and Sebastian Fendt. Power-to-liquid via synthesis of methanol, DME or Fischer–Tropsch-fuels: a review. *Energy & Environmental Science*, 13(10):3207–3252, 2020.

[96] Martin Kaltschmitt, Hans Hartmann, and Hermann Hofbauer. *Energie aus Biomasse*. Springer Berlin Heidelberg, 2016.

[97] J. van de Loosdrecht, F. G. Botes, I. M. Ciobica, A. Ferreira, P. Gibson, D. J. Moodley, A. M. Saib, J. L. Visagie, C. J. Weststrate, and J. W. Niemantsverdriet. Fischer–tropsch synthesis: Catalysts and chemistry. In Jan Reedijk, editor, *Comprehensive inorganic chemistry II*, pages 525–557. Elsevier, Amsterdam, 2013.

[98] Arno de Klerk. *Fischer-Tropsch Refining*. John Wiley & Sons Incorporated, Weinheim, 1st edition, 2011.

[99] A. P. Steynberg, M. E. Dry, B. H. Davis, and B. B. Breman. Fischer-tropsch reactors. In *Fischer-Tropsch Technology*, volume 152 of *Studies in Surface Science and Catalysis*, pages 64–195. Elsevier, 2004.

[100] R. Guettel, U. Kunz, and T. Turek. Reactors for fischer-tropsch synthesis. *Chemical Engineering & Technology*, 31(5):746–754, 2008.

[101] Arno de Klerk. Environmentally friendly refining: Fischer–Tropsch versus crude oil. *Green Chem*, 9(6):560–565, 2007.

[102] Dieter Leckel. Diesel Production from Fischer−Tropsch: The Past, the Present, and New Concepts. *Energy & Fuels*, 23(5):2342–2358, 2009.

[103] Arno de Klerk. Fischer–Tropsch fuels refinery design. *Energy & Environmental Science*, 4(4):1177, 2011.

[104] Jörg Ott, Veronika Gronemann, Florian Pontzen, Eckhard Fiedler, Georg Grossmann, D. Burkhard Kersebohm, Günther Weiss, and Claus Witte. Methanol. In *Ullmann's Encyclopedia of Industrial Chemistry*, volume 16. Wiley-VCH, Weinheim, Germany, 2000.

[105] John Bgdil Hansen and Poul Erik Hjlund Nielsen. Methanol synthesis. In Gerhard Ertl, Helmut Knzinger, Ferdi Schth, and Jens Weitkamp, editors, *Handbook of heterogeneous catalysis*. Wiley-VCH and John Wiley distributor, 2008.

[106] Martin Bertau, Heribert Offermanns, Ludolf Plass, Friedrich Schmidt, and H. J. Wernicke. *Methanol: The Basic Chemical and Energy Feedstock of the Future*. 2014.

[107] Kenji Ushikoshi, Kouzou Moria, Taiki Watanabe, Masami Takeuchi, and Masahiro Saito. A 50 kg/day class test plant for methanol synthesis from CO2 and H2. In T. Inui, M. Anpo, K. Izui, S. Yanagida, and T. Yamaguchi, editors, *Studies in Surface Science and Catalysis : Advances in Chemical Conversions for Mitigating Carbon Dioxide*, volume 114, pages 357–362. Elsevier, 1998.

[108] Florian Pontzen, Waldemar Liebner, Veronika Gronemann, Martin Rothaemel, and Bernd Ahlers. CO2-based methanol and DME – Efficient technologies for industrial scale production. *Catalysis Today*, 171(1):242–250, 2011.

[109] Jan Kopyscinski, Tilman J. Schildhauer, and Serge M.A. Biollaz. Production of synthetic natural gas (SNG) from coal and dry biomass – A technology review from 1950 to 2009. *Fuel*, 89(8):1763–1783, 2010.

[110] Stefan Rönsch, Jens Schneider, Steffi Matthischke, Michael Schlüter, Manuel Götz, Jonathan Lefebvre, Praseeth Prabhakaran, and Siegfried Bajohr. Review on methanation – from fundamentals to current projects. *Fuel*, 166:276–296, 2016.

[111] Saeed Sahebdelfar and Maryam Takht Ravanchi. Carbon dioxide utilization for methane production: A thermodynamic analysis. *Journal of Petroleum Science and Engineering*, 134:14–22, 2015.

[112] Jiajian Gao, Yingli Wang, Yuan Ping, Dacheng Hu, Guangwen Xu, Fangna Gu, and Fabing Su. A thermodynamic analysis of methanation reactions of carbon oxides for the production of synthetic natural gas. *RSC Advances*, 2(6):2358, 2012.

[113] Patrizia Frontera, Anastasia Macario, Marco Ferraro, and PierLuigi Antonucci. Supported Catalysts for CO2 Methanation: A Review. *Catalysts*, 7(12):59, 2017.

[114] Halder Topsoe. From solid fuels to substitute natural gas (SNG) using TREMP™.

[115] Gustaaf Goor, Jürgen Glenneberg, Sylvia Jacobi, Jal Dadabhoy, and Elize Candido. Hydrogen peroxide. In *Ullmann's Encyclopedia of Industrial Chemistry*, pages 1–40. Wiley-VCH Verlag GmbH & Co. KGaA, 2000.

[116] Jose M. Campos-Martin, Gema Blanco-Brieva, and Jose L. G. Fierro. Hydrogen peroxide synthesis: an outlook beyond the anthraquinone process. *Angewandte Chemie (International ed. in English)*, 45(42):6962–6984, 2006.

[117] HPNow. On-site generation of hydrogen peroxide ($https://www.hpnow.eu/$), 2023.

[118] Samuel C. Perry, Dhananjai Pangotra, Luciana Vieira, Lénárd-István Csepei, Volker Sieber, Ling Wang, Carlos Ponce de León, and Frank C. Walsh. Electrochemical synthesis of hydrogen peroxide from water and oxygen. *Nature Reviews Chemistry*, 3(7):442–458, 2019.

[119] Sungeun Yang, Arnau Verdaguer-Casadevall, Logi Arnarson, Luca Silvioli, Viktor Čolić, Rasmus Frydendal, Jan Rossmeisl, Ib Chorkendorff, and Ifan E. L. Stephens. Toward the Decentralized Electrochemical Production of H2O2 : A Focus on the Catalysis. *ACS Catalysis*, 8(5):4064–4081, 2018.

[120] C. Oloman and A. P. Watkinson. Hydrogen peroxide production in trickle-bed electrochemical reactors. *Journal of Applied Electrochemistry*, 9(1):117–123, 1979.

[121] P. C. Foller and R. T. Bombard. Processes for the production of mixtures of caustic soda and hydrogen peroxide via the reduction of oxygen. *Journal of Applied Electrochemistry*, 25(7), 1995.

[122] Carole Le Berre, Philippe Serp, Philippe Kalck, and G. Paull Torrence. Acetic acid. In *Ullmann's Encyclopedia of Industrial Chemistry*, volume 68, pages 1–34. Wiley-VCH, 2000.

[123] Alexandre C. Dimian and Anton A. Kiss. Novel energy efficient process for acetic acid production by methanol carbonylation. *Chemical Engineering Research and Design*, 159:1–12, 2020.

[124] Jane H. Jones. The cativa™ process for the manufacture of acetic acid - iridium catalyst improves productivity in an established industrial process. *Platinum Metals Rev.*, (44 (3)):94–105, 2000.

[125] Glenn J. Sunley and Derrick J. Watson. High productivity methanol carbonylation catalysis using iridium. *Catalysis Today*, 58(4):293–307, 2000.

[126] Nathan Kirk Powell. Method and apparatus for making acetic acid with improved purification. US7619113, 2009.

[127] Raimon Marin. Power-to-X integration, the methanol case. *Decarbonisation Technology*, pages 61–65, 2022.

[128] Engelbert Schrapp. How can you make more out of your biogenic CO2? *Paper Technology International*, 2023.

[129] Engelbert Schrapp. How can you make more out of your biogenic CO2? Episode 2. *Paper Technology International*, 2023.

[130] Hannu Karjunen, Tero Tynjälä, Katja Kuparinen, Esa Vakkilainen, and Tero Joronen. Value creation by converting pulp mill flue gas streams to green fuels. *TAPPI Journal*, 22(3):193–205, 2023.

[131] Kátia D. Oliveira, Pedro H. G. Cademartori, Graciela I. B. Muniz, Luiz F. L. Luz-Junior, and Cícero N. Ávila-Neto. Biorefineries in kraft pulp mills for biofuels production: A critical review. *The Canadian Journal of Chemical Engineering*, 2022.

[132] Marcelo Hamaguchi, Marcelo Cardoso, and Esa Vakkilainen. Alternative technologies for biofuels production in kraft pulp mills—potential and prospects. *Energies*, 5(7):2288–2309, 2012.

[133] Valmet AB. Methanol, from waste byproduct to valuable fuel, 2018.

[134] K. Niemelä. Sulfur and nitrogen compounds in rectified methanol from foul condensate stripping. *International Chemical Recovery Conference*, 1:471–482, 2004.

[135] Tiina Räsänen, Katja Viljamaa, Jukka-Pekka Isoaho, Raimo Juhani Alén, and Hannu Pakkanen. A process for preparing purified methanol from a condensate of sulphate pulp cooking. EP2670908B1.

[136] Jan Warnqvist, Johan Olsson Slager, and Anders Eliasson. Process for removal of sulphur from raw methanol. CA2926589A1.

[137] Naceur Jemaa and Michael Paleologou. Method for producing bio-methanol at pulp mills. WO2014201555A1, 2014.

[138] Johan Olsson. A method of purifying raw methanol. WO2022003237A1, 2022.

[139] Olle Wennberg, David Blomberg Saitton, and Thomas Nordlander. A method and a system for obtaining methanol from foul condensate of a pulping process. US20210087745A1.

[140] Allan Jensen, Trevor Ip, and Jamie Percy. Methanol purification system. pages 2145–2152, 2012.

[141] Bruce Der and Allan Stewart Jensen. Methanol purification method and apparatus. EP2396105B1.

[142] Chang Geun Yoo and Arthur Ragauskas. *Lignin Utilization Strategies: From Processing to Applications*, volume 1377. American Chemical Society, 2021.

[143] A. Toledano, A. García, I. Mondragon, and J. Labidi. Lignin separation and fractionation by ultrafiltration. *Separation and Purification Technology*, 71(1):38–43, 2010.

[144] Marcus R. Olsson, Erik Axelsson, and Thore Berntsson. Exporting lignin or power from heat-integrated kraft pulp mills: A techno-economic comparison using model mills. *Nordic Pulp & Paper Research Journal*, 21(4):476–484, 2006.

[145] Marlene Kienberger, Silvia Maitz, Thomas Pichler, and Paul Demmelmayer. Systematic review on isolation processes for technical lignin. *Processes*, 9(5):804, 2021.

[146] Clara Lisseth Mendoza Martinez, Ekaterina Sermyagina, and Esa Vakkilainen. Hydrothermal carbonization of chemical and biological pulp mill sludges. *Energies*, 14(18):5693, 2021.

[147] Anna Hämäläinen, Marika Kokko, Viljami Kinnunen, Tuomo Hilli, and Jukka Rintala. Hydrothermal carbonization of pulp and paper industry wastewater treatment sludges - characterization and potential use of hydrochars and filtrates. *Bioresource technology*, 355:127258, 2022.

[148] Hanne Wikberg, Taina Ohra-aho, Mari Honkanen, Heimo Kanerva, Ali Harlin, Minnamari Vippola, and Christiane Laine. Hydrothermal carbonization of pulp mill streams. *Bioresource technology*, 212:236–244, 2016.

[149] Shimin Kang, Xianglan Li, Juan Fan, and Jie Chang. Solid fuel production by hydrothermal carbonization of black liquor. *Bioresource technology*, 110:715–718, 2012.

[150] Stora Enso Oyj. From hard-to-handle waste to pure bioenergy (*https://www.storaenso.com/en/newsroom/news/2019/12/from-hard-to-handle-waste-to-pure-bioenergy*).

[151] Saqib Sohail Toor, Lasse Aistrup Rosendahl, Jessica Hoffmann, Thomas Helmer Pedersen, Rudi Pankratz Nielsen, and Erik Gydesen Søgaard. Hydrothermal liquefaction of biomass. In Fangming Jin, editor, *Application of Hydrothermal Reactions to Biomass Conversion*, Green Chemistry and Sustainable Technology Series, pages 189–217. Springer Berlin / Heidelberg, 2014.

[152] Benjamin H. Y. Ong, Timothy G. Walmsley, Martin J. Atkins, and Michael R. W. Walmsley. A kraft mill-integrated hydrothermal liquefaction process for liquid fuel co-production. *Processes*, 8(10):1216, 2020.

[153] Benjamin H.Y. Ong, Timothy G. Walmsley, Martin J. Atkins, Petar S. Varbanov, and Michael R.W. Walmsley. A heat- and mass-integrated design of hydrothermal liquefaction process co-located with a kraft pulp mill. *Energy*, 189:116235, 2019.

[154] LiLu T. Funkenbusch, Michael E. Mullins, Lennart Vamling, Tallal Belkhieri, Nattapol Srettiwat, Olumide Winjobi, David R. Shonnard, and Tony N. Rogers. Technoeconomic assessment of hydrothermal liquefaction oil from lignin with catalytic upgrading for renewable fuel and chemical production. *WIREs Energy and Environment*, 8(1), 2019.

[155] Yawer Jafri, Elisabeth Wetterlund, Sennai Mesfun, Henrik Rådberg, Johanna Mossberg, Christian Hulteberg, and Erik Furusjö. Combining expansion in pulp capacity with production of sustainable biofuels – techno-economic and greenhouse gas emissions assessment of drop-in fuels from black liquor part-streams. *Applied Energy*, 279:115879, 2020.

[156] P. Bajpai. *Black liquor gasification*. Elsevier, 2014.

[157] M. Naqvi, J. Yan, and E. Dahlquist. Black liquor gasification integrated in pulp and paper mills: A critical review. *Bioresource technology*, 101(21):8001–8015, 2010.

[158] D. T. Pio, L.A.C. Tarelho, and P.C.R. Pinto. Gasification-based biorefinery integration in the pulp and paper industry: A critical review. *Renewable and Sustainable Energy Reviews*, 133:110210, 2020.

[159] Lara Carvalho, Joakim Lundgren, Elisabeth Wetterlund, Jens Wolf, and Erik Furusjö. Methanol production via black liquor co-gasification with expanded raw material base – techno-economic assessment. *Applied Energy*, 225:570–584, 2018.

[160] Jonas M. Joelsson and Leif Gustavsson. Reductions in greenhouse gas emissions and oil use by DME (di-methyl ether) and FT (Fischer-Tropsch) diesel production in chemical pulp mills. *Energy*, 39(1):363–374, 2012.

[161] Elzimar Tadeu de Freitas Ferreira and José Antonio Perrella Balestieri. Black liquor gasification combined cycle with CO2 capture – Technical and economic analysis. *Applied Thermal Engineering*, 75:371–383, 2015.

[162] Rickard Fornell, Thore Berntsson, and Anders Åsblad. Techno-economic analysis of a kraft pulp-mill-based biorefinery producing both ethanol and dimethyl ether. *Energy*, 50(1):83–92, 2013.

[163] Maryam Akbari, Adetoyese Olajire Oyedun, and Amit Kumar. Ammonia production from black liquor gasification and co-gasification with pulp and waste sludges: A techno-economic assessment. *Energy*, 151:133–143, 2018.

[164] E. Andersson and S. Harvey. Comparison of pulp-mill-integrated hydrogen production from gasified black liquor with stand-alone production from gasified biomass. *Energy*, 32(4):399–405, 2007.

[165] M. Naqvi, J. Yan, and M. Fröling. Bio-refinery system of DME or CH4 production from black liquor gasification in pulp mills. *Bioresource technology*, 101(3):937–944, 2010.

[166] Karin Pettersson and Simon Harvey. Comparison of black liquor gasification with other pulping biorefinery concepts – Systems analysis of economic performance and CO2 emissions. *Energy*, 37(1):136–153, 2012.

[167] Meire Ellen Gorete Ribeiro Domingos, Daniel Flórez Orrego, Moisés Teles Dos Santos, Hector Ivan Velásquez, and Silvio De Oliveira Junior. Exergy and environmental analysis of black liquor upgrading gasification in an integrated kraft pulp and ammonia production plant. *International Journal of Exergy*, 35(1):35, 2021.

[168] Meire Ellen Gorete Ribeiro Domingos, Daniel Flórez-Orrego, Moisés Teles Dos Santos, and Silvio De Oliveira Junior. Comparative assessment of black liquor upgraded gasification in integrated kraft pulp, methanol and dimethyl ether production plants. In *31st European Symposium on Computer Aided Process Engineering*, volume 50 of *Computer Aided Chemical Engineering*, pages 25–30. Elsevier, 2021.

[169] Meire Ellen Gorete Ribeiro Domingos, Daniel Flórez-Orrego, Moisés Teles dos Santos, Silvio de Oliveira, and François Maréchal. Techno-economic and environmental analysis of methanol and dimethyl ether production from syngas in a kraft pulp process. *Computers & Chemical Engineering*, 163:107810, 2022.

[170] Meire Ellen Gorete Ribeiro Domingos, Daniel Flórez-Orrego, Moisés Teles dos Santos, Silvio de Oliveira Junior, and François Maréchal. Modeling and simulation analysis on the process integration of hydrogen and synthetic natural gas production in a kraft pulp mill via black liquor gasification. *Renewable Energy*, 2023.

[171] Arif Darmawan, Flabianus Hardi, Kunio Yoshikawa, Muhammad Aziz, and Koji Tokimatsu. Enhanced process integration of black liquor evaporation, gasification, and combined cycle. *Applied Energy*, 204:1035–1042, 2017.

[172] March Linnhoff. *Introduction to Pinch Technology*. 1998.

[173] Ray Sinnott and Gavin Towler. Costing and project evaluation. In *Chemical Engineering Design*, pages 275–369. Elsevier, 2020.

[174] Richard Turton. *Analysis, synthesis, and design of chemical processes*. Prentice Hall international series in the physical and chemical engineering sciences. Prentice Hall, Upper Saddle River, NJ, 4th edition, 2012.

[175] J. M. Fox, B. D. Degen, G. Cady, F. D. Deslate, R. L. Summers, A. Akgerman, and J. M. Smith. Slurry reactor design studies.

[176] *CO2-Verminderung in Deutschland: Endbericht*. FfE, München, 2nd edition, 2009.

[177] Friedrich L. Boschke, Wilhelm Fresenius, J. F. K. Huber, Ernö Pungor, Garry A. Rechnitz, Wilhelm Simon, Thomas S. West, and Eugen Scholz. *Karl-Fischer-Titration*, volume 20. Springer Berlin Heidelberg, 1984.

[178] *Perry's chemical engineers' handbook*. McGraw-Hill chemical engineering series. McGraw-Hill, New York, 6. edition, 1988.

[179] IEAGHG. Towards Zero Emissions CCS in Power Plants Using Higher Capture Rates or Biomass, 2019.

[180] Mai Bui, Claire S. Adjiman, André Bardow, Edward J. Anthony, Andy Boston, Solomon Brown, Paul S. Fennell, Sabine Fuss, Amparo Galindo, Leigh A. Hackett, Jason P. Hallett, Howard J. Herzog, George Jackson, Jasmin Kemper, Samuel Krevor, Geoffrey C. Maitland, Michael Matuszewski, Ian S. Metcalfe, Camille Petit, Graeme Puxty, Jeffrey Reimer, David M. Reiner, Edward S. Rubin, Stuart A. Scott, Nilay Shah, Berend Smit, J. P. Martin Trusler, Paul Webley, Jennifer Wilcox, and Niall Mac Dowell. Carbon capture and storage (CCS): the way forward. *Energy & Environmental Science*, 11(5):1062–1176, 2018.

[181] Hyungwoong Ahn, Mauro Luberti, Zhengyi Liu, and Stefano Brandani. Process configuration studies of the amine capture process for coal-fired power plants. *International Journal of Greenhouse Gas Control*, 16(1):29–40, 2013.

[182] F. Vega, F. M. Baena-Moreno, Luz M. Gallego Fernández, E. Portillo, B. Navarrete, and Zhien Zhang. Current status of CO2 chemical absorption research applied to CCS: Towards full deployment at industrial scale. *Applied Energy*, 260(2):114313, 2020.

[183] Mari Voldsund, Stefania Gardarsdottir, Edoardo de Lena, José-Francisco Pérez-Calvo, Armin Jamali, David Berstad, Chao Fu, Matteo Romano, Simon Roussanaly, Rahul Anantharaman, Helmut Hoppe, Daniel Sutter, Marco Mazzotti, Matteo Gazzani, Giovanni Cinti, and Kristin Jordal. Comparison of Technologies for CO2 Capture from Cement Production–Part 1: Technical Evaluation. *Energies*, 12(3):559, 2019.

[184] W. J. Tiktak. Heat Management of PEM Electrolysis-A study on the potential of excess heat from medium to large scale PEM electrolyisis and the performance analysis of a dedicated cooling system, 2019.

[185] Haldor Topsoe. Tailored to your business - ecos™ (*https* : *//www.topsoe.com/processes/carbon − monoxide*).

[186] Matthew Jouny, Wesley Luc, and Feng Jiao. General Techno-Economic Analysis of CO2 Electrolysis Systems. *Industrial & Engineering Chemistry Research*, 57(6):2165–2177, 2018.

[187] Phil de Luna, Christopher Hahn, Drew Higgins, Shaffiq A. Jaffer, Thomas F. Jaramillo, and Edward H. Sargent. What would it take for renewably powered electrosynthesis to displace petrochemical processes? *Science*, 364(6438):eaav3506, 2019.

[188] Marta Moreno-Gonzalez, Angelina Berger, Tory Borsboom-Hanson, and Walter Mérida. Carbon-neutral fuels and chemicals: Economic analysis of renewable syngas pathways via CO2 electrolysis. *Energy Conversion and Management*, 244(7675):114452, 2021.

[189] Régis Anghilante, David Colomar, Annabelle Brisse, and Mathieu Marrony. Bottom-up cost evaluation of SOEC systems in the range of 10–100 MW. *International Journal of Hydrogen Energy*, 43(45):20309–20322, 2018.

[190] International Methanol Producers & Consumers Association. Impca methanol reference specifications, 2021.

[191] K.M.Vanden Bussche and G. F. Froment. A Steady-State Kinetic Model for Methanol Synthesis and the Water Gas Shift Reaction on a Commercial Cu/ZnO/Al2O3Catalyst. *Journal of Catalysis*, 161(1):1–10, 1996.

[192] Dimitri Mignard and Colin Pritchard. On the use of electrolytic hydrogen from variable renewable energies for the enhanced conversion of biomass to fuels. *Chemical Engineering Research and Design*, 86(5):473–487, 2008.

[193] Marle de Jong, Mark Bunse, and Carlo Hamelinck. Methanol carbon footprint and certification, 2022.

[194] Seungwoo Kang, Francisco Boshell, Alain Goeppert, Surya G. Prakash, Ingvar Landälv, and Deger Saygin. *Innovation outlook: Renewable methanol*. International Renewable Energy Agency, Abu Dhabi, 2021.

[195] Judit Nyári, Mohamed Magdeldin, Martti Larmi, Mika Järvinen, and Annukka Santasalo-Aarnio. Techno-economic barriers of an industrial-scale methanol CCU-plant. *Journal of CO2 Utilization*, 39(November (3)):101166, 2020.

[196] Hanfei Zhang, Ligang Wang, Jan van herle, François Maréchal, and Umberto Desideri. Techno-Economic Optimization of CO2-to-Methanol with Solid-Oxide Electrolyzer. *Energies*, 12(19):3742, 2019.

[197] Steffen Schemme, Janos Lucian Breuer, Maximilian Köller, Sven Meschede, Fiona Walman, Remzi Can Samsun, Ralf Peters, and Detlef Stolten. H2-based synthetic fuels: A techno-economic comparison of alcohol, ether and hydrocarbon production. *International Journal of Hydrogen Energy*, 45(8):5395–5414, 2020.

[198] Tomas Cordero-Lanzac, Adrian Ramirez, Alberto Navajas, Lieven Gevers, Sirio Brunialti, Luis M. Gandía, Andrés T. Aguayo, S. Mani Sarathy, and Jorge Gascon. A techno-economic and life cycle assessment for the production of green methanol from CO2: catalyst and process bottlenecks. *Journal of Energy Chemistry*, 68:255–266, 2022.

[199] Muflih A. Adnan and Md Golam Kibria. Comparative techno-economic and life-cycle assessment of power-to-methanol synthesis pathways. *Applied Energy*, 278:115614, 2020.

[200] Patrizio Battaglia, Giulio Buffo, Domenico Ferrero, Massimo Santarelli, and Andrea Lanzini. Methanol synthesis through CO2 capture and hydrogenation: Thermal integration, energy performance and techno-economic assessment. *Journal of CO2 Utilization*, 44:101407, 2021.

[201] Chao Chen, Yangsiyu Lu, and Rene Banares-Alcantara. Direct and indirect electrification of chemical industry using methanol production as a case study. *Applied Energy*, 243:71–90, 2019.

[202] Yu Gu, Danfeng Wang, Qianqian Chen, and Zhiyong Tang. Techno-economic analysis of green methanol plant with optimal design of renewable hydrogen production: A case study in china. *International Journal of Hydrogen Energy*, 47(8):5085–5100, 2022.

[203] Yaser Khojasteh-Salkuyeh, Omid Ashrafi, Ehsan Mostafavi, and Philippe Navarri. CO2 utilization for methanol production; Part I: Process design and life cycle GHG assessment of different pathways. *Journal of CO2 Utilization*, 50(5):101608, 2021.

[204] Nicolas Meunier, Remi Chauvy, Seloua Mouhoubi, Diane Thomas, and Guy de Weireld. Alternative production of methanol from industrial CO2. *Renewable Energy*, 146:1192–1203, 2020.

[205] Harri Nieminen, Arto Laari, and Tuomas Koiranen. CO2 Hydrogenation to Methanol by a Liquid-Phase Process with Alcoholic Solvents: A Techno-Economic Analysis. *Processes*, 7(7):405, 2019.

[206] Davide Parigi, Emanuele Giglio, Alicia Soto, and Massimo Santarelli. Power-to-fuels through carbon dioxide re-utilization and high-temperature electrolysis: A technical and economical comparison between synthetic methanol and methane. *Journal of Cleaner Production*, 226:679–691, 2019.

[207] Stefano Sollai, Andrea Porcu, Vittorio Tola, Francesca Ferrara, and Alberto Pettinau. Renewable methanol production from green hydrogen and captured CO2: A techno-economic assessment. *Journal of CO2 Utilization*, 68:102345, 2023.

[208] Ligang Wang, Ming Chen, Rainer Küngas, Tzu-En Lin, Stefan Diethelm, François Maréchal, and Jan van herle. Power-to-fuels via solid-oxide electrolyzer: Operating window and techno-economics. *Renewable and Sustainable Energy Reviews*, 110:174–187, 2019.

[209] Muhammad Yousaf, Asif Mahmood, Ali Elkamel, Muhammad Rizwan, and Muhammad Zaman. Techno-economic analysis of integrated hydrogen and methanol production process by CO2 hydrogenation. *International Journal of Greenhouse Gas Control*, 115:103615, 2022.

[210] EU. DIRECTIVE (EU) 2018/2001 OF THE EUROPEAN PARLIAMENT AND OF THE COUNCIL.

[211] Michael Neubert, Jonas Widzgowski, Stefan Rönsch, Peter Treiber, Marius Dillig, and Jürgen Karl. Simulation-based evaluation of a two-stage small-scale methanation unit for decentralized applications. *Energy & Fuels*, 31(2):2076–2086, 2017.

[212] Jie Zhang, Nouria Fatah, Sandra Capela, Yilmaz Kara, Olivier Guerrini, and Andrei Y. Khodakov. Kinetic investigation of carbon monoxide hydrogenation under realistic conditions of methanation of biomass derived syngas. *Fuel*, 111:845–854, 2013.

[213] Stefan Rönsch, Jakob Köchermann, Jens Schneider, and Steffi Matthischke. Global Reaction Kinetics of CO and CO2 Methanation for Dynamic Process Modeling. *Chemical Engineering & Technology*, 39(2):208–218, 2016.

[214] Remi Chauvy, Lionel Dubois, Paul Lybaert, Diane Thomas, and Guy de Weireld. Production of synthetic natural gas from industrial carbon dioxide. *Applied Energy*, 260:114249, 2020.

[215] Kristina Juhrich. CO2 Emission Factors for Fossil Fuels, 2022.

[216] Emanuele Giglio, Andrea Lanzini, Massimo Santarelli, and Pierluigi Leone. Synthetic natural gas via integrated high-temperature electrolysis and methanation: Part I–Energy performance. *Journal of Energy Storage*, 1:22–37, 2015.

[217] Emanuele Giglio, Andrea Lanzini, Massimo Santarelli, and Pierluigi Leone. Synthetic natural gas via integrated high-temperature electrolysis and methanation: Part II–Economic analysis. *Journal of Energy Storage*, 2:64–79, 2015.

[218] William L. Becker, Michael Penev, and Robert J. Braun. Production of synthetic natural gas from carbon dioxide and renewably generated hydrogen: A techno-economic analysis of a power-to-gas strategy. *Journal of Energy Resources Technology*, 141(2), 2019.

[219] Remi Chauvy, Damien Verdonck, Lionel Dubois, Diane Thomas, and Guy de Weireld. Techno-economic feasibility and sustainability of an integrated carbon capture and conversion process to synthetic natural gas. *Journal of CO2 Utilization*, 47:101488, 2021.

[220] Myriam de Saint Jean, Pierre Baurens, and Chakib Bouallou. Parametric study of an efficient renewable power-to-substitute-natural-gas process including high-temperature steam electrolysis. *International Journal of Hydrogen Energy*, 39(30):17024–17039, 2014.

[221] Myriam de Saint Jean, Pierre Baurens, Chakib Bouallou, and Karine Couturier. Economic assessment of a power-to-substitute-natural-gas process including high-temperature steam electrolysis. *International Journal of Hydrogen Energy*, 40(20):6487–6500, 2015.

[222] Valerie Eveloy. Hybridization of solid oxide electrolysis-based power-to-methane with oxyfuel combustion and carbon dioxide utilization for energy storage. *Renewable and Sustainable Energy Reviews*, 108:550–571, 2019.

[223] Emanuele Giglio, Fabio Alessandro Deorsola, Manuel Gruber, Stefan Raphael Harth, Eduard Alexandru Morosanu, Dimosthenis Trimis, Samir Bensaid, and Raffaele Pirone. Power-to-gas through high temperature electrolysis and carbon dioxide methanation: Reactor design and process modeling. *Industrial & Engineering Chemistry Research*, 57(11):4007–4018, 2018.

[224] F. Gutiérrez-Martín and L. M. Rodríguez-Antón. Power-to-SNG technology for energy storage at large scales. *International Journal of Hydrogen Energy*, 41(42):19290–19303, 2016.

[225] Dimitris Ipsakis, Georgios Varvoutis, Athanasios Lampropoulos, Spiros Papaefthimiou, George E. Marnellos, and Michalis Konsolakis. Techno-economic assessment of industrially-captured CO2 upgrade to synthetic natural gas by means of renewable hydrogen. *Renewable Energy*, 179:1884–1896, 2021.

[226] Mahdi Momeni, M. Soltani, M. Hosseinpour, and Jatin Nathwani. A comprehensive analysis of a power-to-gas energy storage unit utilizing captured carbon dioxide as a raw material in a large-scale power plant. *Energy Conversion and Management*, 227:113613, 2021.

[227] Eduard Alexandru Morosanu, Andrés Saldivia, Massimiliano Antonini, and Samir Bensaid. Process Modeling of an Innovative Power to LNG Demonstration Plant. *Energy & Fuels*, 32(8):8868–8879, 2018.

[228] Alessandra Perna, Linda Moretti, Giorgio Ficco, Giuseppe Spazzafumo, Laura Canale, and Marco Dell'Isola. Sng generation via power to gas technology: Plant design and annual performance assessment. *Applied Sciences*, 10(23):8443, 2020.

[229] Ralf Peters, Maxana Baltruweit, Thomas Grube, Remzi Can Samsun, and Detlef Stolten. A techno economic analysis of the power to gas route. *Journal of CO2 Utilization*, 34:616–634, 2019.

[230] Fabio Salomone, Paolo Marocco, Daniele Ferrario, Andrea Lanzini, Debora Fino, Samir Bensaid, and Massimo Santarelli. Process simulation and energy analysis of synthetic natural gas production from water electrolysis and CO2 capture in a waste incinerator. *Applied Energy*, 343:121200, 2023.

[231] Meng Qi, Jinwoo Park, Robert Stephen Landon, Jeongdong Kim, Yi Liu, and Il Moon. Continuous and flexible Renewable-Power-to-Methane via liquid CO2 energy storage: Revisiting the techno-economic potential. *Renewable and Sustainable Energy Reviews*, 153:111732, 2022.

[232] Mats Nystrom and Christina Jarnvik. Chemical process and composition. US 7,425,316 B2, 2008.

[233] W. Eul, A. Moeller, and N. Steiner. Hydrogen peroxide. In *Kirk-Othmer Encyclopedia of Chemical Technology*. Wiley, 2001.

[234] Database Ecoinvent 3.8.

[235] Rosaria Ciriminna, Lorenzo Albanese, Francesco Meneguzzo, and Mario Pagliaro. Hydrogen peroxide: A key chemical for today's sustainable development. *ChemSusChem*, 9(24):3374–3381, 2016.

[236] Svetlana van Bavel, Sumit Verma, Emanuela Negro, and Maarten Bracht. Integrating CO2 Electrolysis into the Gas-to-Liquids–Power-to-Liquids Process. *ACS Energy Letters*, 5(8):2597–2601, 2020.

[237] Daniel Klüh and Matthias Gaderer. Integrating a fischer tropsch process into a pulp mill - a techno-economic assessment. *Energy*, 285:129015, 2023.

[238] Daniel Klüh and Matthias Gaderer. Integrating a fischer-tropsch fuel production process into pulp mills. *Chemical Engineering Transactions*, 94:13–18, 2022.

[239] H. J. Grabke. Metal dusting. *Materials and Corrosion*, 54(10):736–746, 2003.

[240] Sandra Adelung and Ralph-Uwe Dietrich. Impact of the reverse water-gas shift operating conditions on the Power-to-Liquid fuel production cost. *Fuel*, 317:123440, 2022.

[241] David Vervloet, Freek Kapteijn, John Nijenhuis, and J. Ruud van Ommen. Fischer–Tropsch reaction–diffusion in a cobalt catalyst particle: aspects of activity and selectivity for a variable chain growth probability. *Catalysis Science & Technology*, 2(6):1221–1233, 2012.

[242] Daniel H. König, Marcel Freiberg, Ralph-Uwe Dietrich, and Antje Wörner. Techno-economic study of the storage of fluctuating renewable energy in liquid hydrocarbons. *Fuel*, 159:289–297, 2015.

[243] Daniel H. König, Nadine Baucks, Ralph-Uwe Dietrich, and Antje Wörner. Simulation and evaluation of a process concept for the generation of synthetic fuel from CO2 and H2. *Energy*, 91:833–841, 2015.

[244] Ilkka Hannula, Noora Kaisalo, and Pekka Simell. Preparation of Synthesis Gas from CO2 for Fischer–Tropsch Synthesis—Comparison of Alternative Process Configurations. *C*, 6(3):55, 2020.

[245] Friedemann G. Albrecht, Daniel H. König, Nadine Baucks, and Ralph-Uwe Dietrich. A standardized methodology for the techno-economic evaluation of alternative fuels – a case study. *Fuel*, 194:511–526, 2017.

[246] Ralph-Uwe Dietrich, Friedemann G. Albrecht, Simon Maier, Daniel H. König, Stefan Estelmann, Sandra Adelung, Zoé Bealu, and Antje Seitz. Cost calculations for three different approaches of biofuel production using biomass, electricity and CO2. *Biomass and Bioenergy*, 111:165–173, 2018.

[247] Guiyan Zang, Pingping Sun, Amgad Elgowainy, Adarsh Bafana, and Michael Wang. Life Cycle Analysis of Electrofuels: Fischer-Tropsch Fuel Production from Hydrogen and Corn Ethanol Byproduct CO2. *Environmental science & technology*, 55(6):3888–3897, 2021.

[248] Christoph Markowitsch, Markus Lehner, and Markus Maly. Evaluation of process structures and reactor technologies of an integrated power-to-liquid plant at a cement factory. *Journal of CO2 Utilization*, 70:102449, 2023.

[249] Diego Freire Ordóñez, Nilay Shah, and Gonzalo Guillén-Gosálbez. Economic and full environmental assessment of electrofuels via electrolysis and co-electrolysis considering externalities. *Applied Energy*, 286:116488, 2021.

[250] Xuping Li, Paul Anderson, Huei-Ru Molly Jhong, Mark Paster, James F. Stubbins, and Paul J. A. Kenis. Greenhouse Gas Emissions, Energy Efficiency, and Cost of Synthetic Fuel Production Using Electrochemical CO2 Conversion and the Fischer–Tropsch Process. *Energy & Fuels*, 30(7):5980–5989, 2016.

[251] Konstantinos Atsonios, Jun Li, and Vassilis J. Inglezakis. Process analysis and comparative assessment of advanced thermochemical pathways for e-kerosene production. *Energy*, 278:127868, 2023.

[252] Ioanna Dimitriou, Pelayo García-Gutiérrez, Rachael H. Elder, Rosa M. Cuéllar-Franca, Adisa Azapagic, and Ray W. K. Allen. Carbon dioxide utilisation for production of transport fuels: process and economic analysis. *Energy & Environmental Science*, 8(6):1775–1789, 2015.

[253] Ruxing Gao, Chundong Zhang, Ki-Won Jun, Seok Ki Kim, Hae-Gu Park, Tiansheng Zhao, Lei Wang, Hui Wan, and Guofeng Guan. Green liquid fuel and synthetic natural gas production via CO2 hydrogenation combined with reverse water-gas-shift and Co-based Fischer-Tropsch synthesis. *Journal of CO2 Utilization*, 51:101619, 2021.

[254] Hannah Kirsch, Ulrich Sommer, Peter Pfeifer, and Roland Dittmeyer. Power-to-fuel conversion based on reverse water-gas-shift, Fischer-Tropsch Synthesis and Hydrocracking: Mathematical modeling and simulation in Matlab/Simulink. *Chemical Engineering Science*, 227:115930, 2020.

[255] Marco Marchese, Emanuele Giglio, Massimo Santarelli, and Andrea Lanzini. Energy performance of power-to-liquid applications integrating biogas upgrading, reverse water gas shift, solid oxide electrolysis and fischer-tropsch technologies. *Energy Conversion and Management: X*, 6:100041, 2020.

[256] Maria Fernanda Rojas-Michaga, Stavros Michailos, Evelyn Cardozo, Muhammad Akram, Kevin J. Hughes, Derek Ingham, and Mohamed Pourkashanian. Sustainable aviation fuel (SAF) production through power-to-liquid (PtL): A combined techno-economic and life cycle assessment. *Energy Conversion and Management*, 292:117427, 2023.

[257] Steffen Schemme. *Techno-economic Assessment of Processes for the Production of Fuels from H2 and CO2*. RWTH Aachen University, 2020.

[258] Daniel H. König. Techno-ökonomische Prozessbewertung der Herstellung synthetischen Flugturbinentreibstoffes aus CO2 und H2, 2016.

[259] C. St. Teuner, P. Neumann, and F. von Linde. CO through CO2 Reforming - The Calcor Standard and Calcor Economy Processes. *OIL Gas European Magazine*, (3):44–46, 2001.

[260] Evert Jan Ditzel, John Glenn Sunley, and Robert John Watt. Iridium catalyzed carbonylation process for the production of acetic acid. US5877347, 1997.

[261] Paul Torrence, Brian W. Hokkanen, Michael O. Nutt, Tianshu Pan, and Ronald David Shaver. Production of acetic acid with high conversion rate. US 8,394.988 B2, 2010.

[262] Anthony Haynes. Acetic acid synthesis by catalytic carbonylation of methanol. In Matthias Beller, editor, *Catalytic carbonylation reactions*, volume 18 of *Topics in Organometallic Chemistry*, pages 179–205. Springer, 2006.

[263] Evert Jan Ditzel, Howden John, and Robert John Watt. Iridium-catalyzed carbonylation process for the production of acetic acid. US 5877348, 1999.

[264] Falko Ueckerdt, Christian Bauer, Alois Dirnaichner, Jordan Everall, Romain Sacchi, and Gunnar Luderer. Potential and risks of hydrogen-based e-fuels in climate change mitigation. *Nature Climate Change*, 11(5):384–393, 2021.

[265] Deger Saygin and Dolf Gielen. Zero-emission pathway for the global chemical and petrochemical sector. *Energies*, 14(13):3772, 2021.

[266] Hans Böhm, Markus Lehner, and Thomas Kienberger. Techno-economic assessment of thermally integrated co-electrolysis and methanation for industrial closed carbon cycles. *Frontiers in Sustainability*, 2, 2021.

[267] Sebastian Gärtner, Thomas Marx-Schubach, Matthias Gaderer, Gerhard Schmitz, and Michael Sterner. Techno-economic analysis of carbon dioxide separation for an innovative energy concept towards low-emission glass melting. *Energies*, 16(5):2140, 2023.

[268] Kristoffer Svedin, Christofer Ivarsson, and Rickard Lundborg. Lime kiln modeling - CFD & one-dimensional simulations, 2009.

[269] Arafat Aloqaily, David C.S. Kuhn, Pierre Sullivan, and Honghi Tran. Flame length in lime kilns with a separate noncondensible gas burner. *TAPPI Journal*, 6(12):21–26, 2008.

[270] Arafat Aloqaily, David C.S. Kuhn, Pierre Sullivan, and Honghi Tran. Numerical prediction of flame length in lime kilns. *International Chemical Recovery Conference, Quebec City*, 2007.

[271] Kamyar Mohammadpour. *CFD Simulation of Reactive Flow in Lime Shaft Kilns using Porous Media - Model and Experimental Validation*. 2019.

[272] Linda Tegehall. *Combined systems and detailed model of the lime kiln*. 2017.

[273] Stefanía Ósk Garðarsdóttir, Fredrik Normann, Klas Andersson, and Filip Johnsson. Postcombustion CO2 Capture Using Monoethanolamine and Ammonia Solvents: The Influence of CO2 Concentration on Technical Performance. *Industrial & Engineering Chemistry Research*, 54(2):681–690, 2015.

[274] Ilkka Hannula. Co-production of synthetic fuels and district heat from biomass residues, carbon dioxide and electricity: Performance and cost analysis. *Biomass and Bioenergy*, 74:26–46, 2015.

[275] Santanu De, Avinash Kumar Agarwal, V. S. Moholkar, and Bhaskar Thallada, editors. *Coal and Biomass Gasification*. Springer Singapore, 2018.

[276] Ian Narváez, Alberto Orío, Maria P. Aznar, and José Corella. Biomass gasification with air in an atmospheric bubbling fluidized bed. effect of six operational variables on the quality of the produced raw gas. *Industrial & Engineering Chemistry Research*, 35(7):2110–2120, 1996.

[277] Javier Gil, Jose Corella, Maria P. Aznar, and Miguel A. Caballero. Biomass gasification in atmospheric and bubbling fluidized bed: Effect of the type of gasifying agent on the product distribution. *Biomass and Bioenergy*, 17(5):389–403, 1999.

[278] Reinhard Rauch, Jitka Hrbek, and Hermann Hofbauer. Biomass gasification for synthesis gas production and applications of the syngas. *WIREs Energy and Environment*, 3(4):343–362, 2014.

[279] M. Mozaffarian and R. W. R. Zwart. *Feasibility of biomass/waste-related SNG production technologies*. 2003.

[280] J.R.C. Rey, D. T. Pio, and L.A.C. Tarelho. Biomass direct gasification for electricity generation and natural gas replacement in the lime kilns of the pulp and paper industry: A techno-economic analysis. *Energy*, 237:121562, 2021.

[281] LEILAC. Leilac technology roadmap to 2050: A cost-effective path to carbon neutral industrial production (*https://www.leilac.com/wp-content/uploads/2022/09/leilac-roadmap.pdf*), 2021.

[282] Roope Hellgrén. Review of bark gasification via aspen plus pseudo-equilibrium model: Master's thesis, 2023.

[283] Cepi. Key statistics 2022: European pulp & paper industry, 2023.

[284] Abdul M. Petersen, Kate Haigh, and Johann F. Görgens. Techno-economics of integrating bioethanol production from spent sulfite liquor for reduction of greenhouse gas emissions from sulfite pulping mills. *Biotechnology for biofuels*, 7(1):169, 2014.

[285] Kristian Melin, Harri Nieminen, Daniel Klüh, Arto Laari, Tuomas Koiranen, and Matthias Gaderer. Techno-economic evaluation of novel hybrid biomass and electricity-based ethanol fuel production. *Frontiers in Energy Research*, 10, 2022.

[286] Thanh Khoa Phung and Guido Busca. Selective bioethanol conversion to chemicals and fuels via advanced catalytic approaches. In Sonil Nanda, Dai-Viet N. Vo, and Prakash Kumar Sarangi, editors, *Biorefinery of Alternative Resources: Targeting Green Fuels and Platform Chemicals*, pages 75–103. Springer Singapore, Singapore, 2020.

[287] Robert A. Dagle, Austin D. Winkelman, Karthikeyan K. Ramasamy, Vanessa Lebarbier Dagle, and Robert S. Weber. Ethanol as a renewable building block for fuels and chemicals. *Industrial & Engineering Chemistry Research*, 59(11):4843–4853, 2020.

[288] Germán Giner-Santonja, Michael Suhr, Gabriele Klein, Ioanna Kourti, Miguel Gonzalo, Serge Roudier, and Luis Sancho. *Best Available Techniques (BAT) Reference Document for the Production of Pulp, Paper and Board*. 2015.

[289] Matthias Rehfeldt, Tobias Fleiter, and Felipe Toro. A bottom-up estimation of the heating and cooling demand in european industry. *Energy Efficiency*, 11(5):1057–1082, 2018.

[290] Jorge Perpiñán, Manuel Bailera, Begona Peña, Luis M. Romeo, and Valerie Eveloy. High oxygen and SNG injection in blast furnace ironmaking with Power to Gas integration and CO2 recycling. *Journal of Cleaner Production*, 405:137001, 2023.

[291] Michael Zier, Peter Stenzel, Leander Kotzur, and Detlef Stolten. A review of decarbonization options for the glass industry. *Energy Conversion and Management: X*, 10:100083, 2021.

[292] Methanol Institute. Methanol Price and Supply/Demand (*https* : *//www.methanol.org/methanol − price − supply − demand/*), 2023.

[293] BP. bp statistical review of world energy (*https* : *//www.bp.com/content/dam/bp/business − sites/en/global/corporate/pdfs/energy − economics/statistical − review/bp − stats − review* − 2022 − *full − report.pdf*), 2022.

[294] Chemanalyst. Decode the future of acetic acid (*https* : *//www.chemanalyst.com/industry − report/acetic − acid − market* − 609), 2023.

[295] Open Grid Europe. Erdgas - Orientierunswerte 2021.

[296] Petra Icha and Gunter Kuhs. Entwicklung der spezifischen Kohlendioxid-Emissionen des deutschen Strommix in den Jahren 1990 - 2019, 2020.

[297] Wilhelm Kuckshinrichs, Thomas Ketelaer, and Jan Christian Koj. Economic analysis of improved alkaline water electrolysis. *Frontiers in Energy Research*, 5, 2017.

[298] Max Stone Peters, Klaus Dieter Timmerhaus, and Ronald Emmett West. *Plant design and economics for chemical engineers*. McGraw-Hill chemical engineering series. McGraw-Hill, Boston, 5. edition, 2004.

[299] Simon Roussanaly, Rahul Anantharaman, Karl Lindqvist, and Brede Hagen. A new approach to the identification of high-potential materials for cost-efficient membrane-based post-combustion CO2 capture. *Sustainable Energy & Fuels*, 2(6):1225–1243, 2018.

[300] J. Olsson and G. Zacchi. Simulation of the condensate treatment process in a kraft pulp mill. *Chemical Engineering & Technology*, 24(2):195, 2001.

[301] Roberts Edward, Jean-Francois Larive, David Rickeard, and Werner Weindorf. WELL-TO-TANK Appendix 1 - Version 4a Conversion factors and fuel properties, 2014.

[302] Per Lundqvist. *Mass and energy balances over the lime kiln in a kraft pulp mill*. 2009.

[303] Sabrina Francey. *Impacts of burning alterantive fuels in lime kilns at kraft pulp mills*. 2009.

[304] Geoffrey D. Silcox, John C. Kramlich, and David W. Pershing. A mathematical model for the flash calcination of dispersed calcium carbonate and calcium hydroxide particles. *Industrial & Engineering Chemistry Research*, 28(2):155–160, 1989.

A Technologies

A.1 CO_2 electrolysis

Figure A.1 shows the flowsheet of the CO_2 electrolysis process.

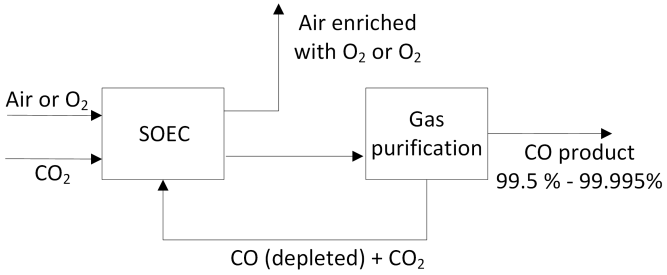

Figure A.1 Schematic of the eCOs system, according to [2]

A.2 Sulfite pulp mill

Figure A.2 shows the flow diagram of a sulphite pulp mill. In contrast to the sulphate pulp mill, the sulphite pulp mill has only one chemical recycle loop for magnesium and sulphur. Wood chips and cooking liquor are fed to the digester where the cooking process takes place at temperatures of 125 °C to 140 °C [8]. After the separation of pulp and spent liquor, the spent liquor is evaporated and incinerated under oxidative combustion conditions in the recovery boiler [8, 9]. The mean heating value of the spent liquor is 6.97 MJ/kg [9]. MgO is recoverd from flue gas dust in the cyclone and filters [8, 9]. The SO_2 is scrubbed from the flue gas [8, 9].

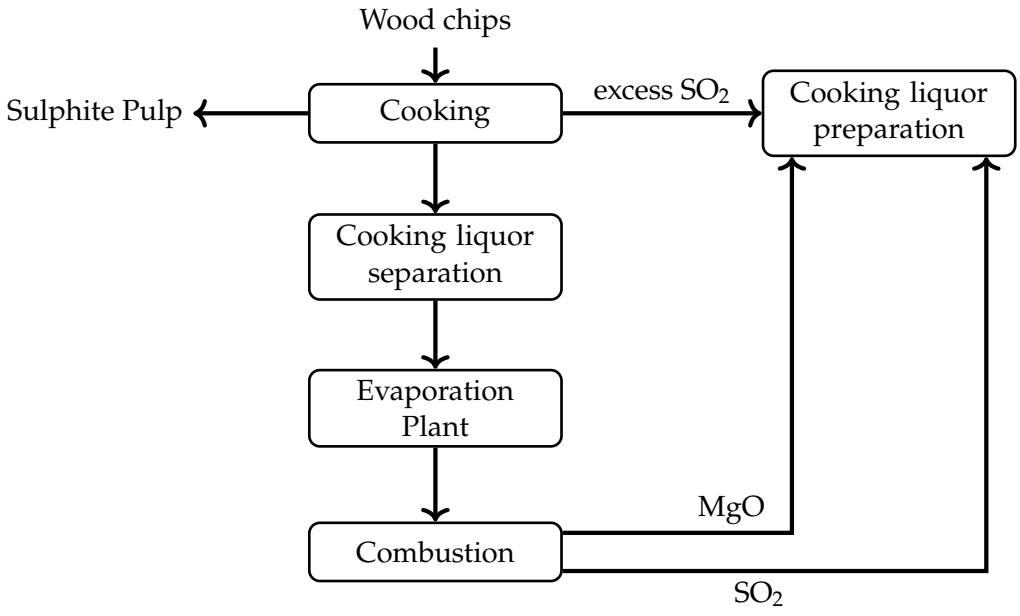

Figure A.2 Flow diagram of the sulfite pulping process with one cycle for chemical recycling [9]

B Methods

B.1 Composition of natural gas and air

The composition of natural gas is based on high calorific natural gas. Table B.1 shows the assumed composition which is based on [295].

Table B.1 Molar composition of high calorific natural gas

Component	mol%	wt.%
CH_4	92	84.7
C_2H_6	5	8.6
C_3H_8	1	2.5
N_2	1	1.6
CO_2	1	2.5

Table B.2 shows the assumed composition of air.

Table B.2 Molar composition of air

component	mole fraction
N_2	78 %
O_2	21 %
Ar	1 %

B.2 Composition of biomass

Table B.3 shows the composition and properties of bark and wood residues from the pulp mill. The samples were grinded in a mill to reduce particle size and analyzed in the laboratory for elemental composition, ash content and water content. The sulphur and chlorine content, and LHV was taken from an analysis available from the pulp mill. Oxygen content was calculated.

Table B.3 Composition and properties of bark and other residual biomass (values in wt.%, [a] comprises of rejected material from the cooking process and fine particles from wood chipping

Property	bark	wood residues[a]	Source
C	50.89 %	49.91 %	measured, triple
H	3.74 %	1.40 %	measured, triple
N	0.39 %	0.09 %	measured, triple
S	0.04 %	0.02 %	available analysis by pulp mill
O	40.89 %	48.04 %	calculated
Cl	0.02 %	0.03 %	available analysis by pulp mill
Ash content	4.04 %	0.51 %	measured, triple
Water content	38.2 %	36.1 %	measured, triple
LHV	19.0 MJ/kg_{dry}	20.1 MJ/kg_{dry}	available analysis by pulp mill

B.3 Emission factors

The used emission factors are shown in the following table. They are used for the calculation of the CO_2 balance and CO_2 abatement cost.

Table B.4 Emission factors ([a] Strominlandsverbrauch 2019)

	EF	Unit	Source
Electricity pulp mill	0	kg CO_2/MWh	own assumption
Electricity german gid mix	380[a]	kg CO_2/MWh	[296]
Natural gas	201	kg CO_2/MWh	[215]
MeOH	97.1	g CO_2/MJ	[193]
AA	1.31	t CO_2/t AA	[234]
FT syncrude	94	g CO_2/MJ	[210]
H_2O_2	1.12	t CO_2/t H_2O_2	[234]

B.4 Heat integration

Table B.5 shows the available steam and hot water streams in the pulp mill which are used for the heat integration. The lower temperatures of the steam are derived from the saturation temperature at the given pressure. The temperature difference for hot water is set to 10 °C.

Table B.5 Inlet and outlet temperatures (in °C) of thermal energy carriers in the pulp mill either for generation or for supply

Medium	Pressure in bar	T_{in} in °C	T_{out} in °C
HP Steam generation	85	299	485
MP1 Steam generation	36	244	250
MP2 Steam generation	12	188	200
LP Steam generation	3.6	140	150
Hot water 1 generation	-	50	60
Hot water 2 generation	-	80	90
HP Steam supply	85	485	299
MP1 Steam supply	36	250	244
MP2 Steam supply	12	200	188
LP Steam supply	3.6	150	140
Hot water 1 supply	-	60	50
Hot water 2 supply	-	90	80

After heat integration, the supplied or generated steam is assessed regarding the change in electricity generation. With the first law of thermodynamics, the impact on electricity production is calculated. The electrical power output from the turbine is calculated as shown in the following equation. The mechanical efficiency of the turbine and the generator efficiency are neglected. The enthalpies are derived from the steam table. The values are reported in Table B.6. Steam is assumed to be expanded to 0.12 bar and 50 °C with a steam fraction of 90 % at the turbine outlet.

$$W_{el} = \dot{m}_{steam} \cdot (h_{in} - h_{out}) \tag{B.1}$$

Table B.6 Enthalpies used in power plant calculations ([1] @ 50 °C and an assumed steam fraction of 90 wt. %, [2] Enthalpy difference @ 50 °C for the full condensation of the steam starting at a steam fraction of 90 wt.%)

	Enthalpy in kJ/kg
HP Steam	3,356
MP2 Steam	2,816
LP Steam	2,756
Turbine outlet[1]	2,353
Condensation[2]	2,144

C Cost Calculation

C.1 Operating cost

The O_2 produced by electrolysis substitutes O_2 generated with the PSA plant onsite. The economic calculation considers only the capital cost of the plant as the electricity used for the plant is already incorporated in the electricity balance. The surplus O_2 is sold for a low price as the economic value of not liquefied O_2 is questionable. The production of deionized water is also incorporated in the electricity balance. Therefore, the cost assumption is lower than in other publications (10 €/t [297]). The electricity is either supplied by the surplus electricity of the pulp mill or imported from the grid. As the pulp mill receives a reimbursement based on the Renewable Energy Act, the electricity price of 83 €/MWh is assumed which is the lower threshold for reimbursement. In case of higher electricity prices on the market, the electricity is sold for the market price. The electricity from the grid, biomass and natural gas price is based on a reasonable assumption. The price of CaO is provided by the pulp mill.

All other cost components are derived from relations found in literature. For the maintenance of the electrolyzers no special cost assumptions were made.

Table C.1 Assumptions for operating cost ([a] Reimbursement based on the Renewable Energy Source Act Germany, [b] data from pulp mill)

Price category	Value and unit	Reference
O_2 substitution $C_{O2,sub}$	31.5 €/t	based on ACC[b]
O_2 surplus sale price $C_{O2,sale}$	10 €/t	own assumption
Deionized water C_{DW}	2 €/t	own assumption
Electricity from pulp mill $C_{E,Pulp}$	83 €/MWh	[a,b]
Grid electricity $C_{E,Grid}$	60 €/MWh	own assumption
CO_2 capture cost C_{CO2}	50 €/t	see C.1.2
Natural gas C_{NG}	25 €/MWh	own assumption
Maintenance cost C_M	7 % of FCI	[298]
Labor cost C_L	-	see C.1.1
Laboratory charges C_{LC}	15 % of C_L	[298]
Operating supervision and clerical assistance $C_{S\&C}$	15 % of C_L	[298]
Insurance and taxes $C_{I\&T}$	3 % of FCI	[298]
Plant overhead cost C_{PO}	60 % of (C_L + $C_{S\&C}$ +C_M)	[298]
Administration cost C_A	20 % of C_L	[298]
Calcium oxide C_{CaO}	280 €/t	[b]
Biomass $C_{Biomass}$	20 €/MWh	own assumption
H_2O_2 substituted $C_{H2O2,sub}$	750 €/$t_{H2O2,\ pure}$	[b]
Makeup anthraquinone C_{AQ}	5000 €/t_{AQ}	own assumption

C.1.1 Labor cost

We are considering an average of 5.19 employees per workplace, derived from 1095 annual shifts and accounting for 50 days of absence per year (due to sick leave, vacation, and holidays). The assumed annual cost per employee, including wages and all taxes, is set at 70,000 €. The calculation

of the required number of operators per shift (N_{OL}) follows Equation C.1, as outlined in Alkhayat and Gerrard's work [174]. N_{OL} is not subject to rounding. N_{np} denotes the count of nonparticulate processing steps, with the assumption that both water electrolysis, CO_2 electrolysis, and the CO_2 capture process constitute one process step each.

$$N_{OL} = (6.29 + 0.23 \cdot N_{np})^{0.5} \tag{C.1}$$

C.1.2 CO_2 capture cost

The literature presented in Section 2.5.4 shows the range of capture cost in pulp mills. The assumed cost in this study is established at 50 €/t. A breakdown of costs reveals that approximately 60 to 75 % of the capture cost for a MEA absorption process is attributable to energy consumption, justifying the assumed capture cost [299]. Unlike in literature, the capture cost in this thesis excludes the steam cost of the reboiler as heat will be sourced from other processes via heat integration. If steam extraction from the turbine is necessary, the associated cost will be factored into a reduced electricity generation of the turbine.

C.2 Investment cost

C.2.1 CEPCI

The prices for equipment are based on different years. With the chemical engineering plant index (CEPCI), the equipment cost is normalized to the same year. The base year of this work is 2021. Cost data from the Aspen Energy Analyzer is based on cost data of 2019. Equation C.2 gives the relation of the purchased equipment cost C for year b based on the ratio of the CEPCI of year b and a multiplied by the purchased equipment cost for year a.

$$C_b = C_a \frac{CEPCI_b}{CEPCI_a} \tag{C.2}$$

C.2.2 Currency conversion

Most of the cost data is given in dollar. The resulting product prices are reported in Euro. Therefore, the cost data has to be converted The conversion of equipment cost was done according to Equation C.3.

$$C_{Euro} = C_{Dollar} \cdot 0.85 \tag{C.3}$$

D PtX Process simulations

In this chapter additional information related to Chapter 4 is presented.

D.1 Methanol

D.1.1 Technical parameters

Table D.1 shows the settings of the distillation columns in the MeOH models.

Table D.1 Settings of columns for MeOH models

Case	$50/150MW_{el}$	$50MW_{el}$-FC		$150MW_{el}$-FC	
Column	C1	C1	FC-C1	C1	FC-C1
Reflux ratio (mole)	1.025	2	-	1.134	-
D:F ratio (mole)	0.497	0.496	0.1	0.497	0.1
Number of stages	30	30	10	30	10
Feed stage	on 24	on 24	above 1	on 24	above 1

The composition of the SOG is shown in Table D.2. The composition is partially based on [300] and on information by industry. The S and N concentration is adjusted to 2.5 and 1 wt. % which is close to the mean values of the measurements shown in Figure 3.6. The MeOH content was reported by the pulp mill. The sulphur components and terpentines are inspired by [300]. Ammonia was selected as the main N component.

Table D.2 Composition of foul condensate in wt.%

component	mass fraction
MeOH	0.6
Water	0.3511
Methylmercaptan	0.01465
NH_3	0.0123
Dimethyl sulfide	0.01
H_2S	0.01
Dimethyl disulfide	0.001
Guaiacol	0.0004
α terpineol	0.00035
α pinene	0.0002

The mass balance of the MeOH processes is given in Table D.3.

Table D.3 Mass balance of the MeOH processes in t/h

Case	50 MW_{el}	150 MW_{el}	50 MW_{el}-FC	150 MW_{el}-FC
		Input		
Water	9.4	28.2	9.4	28.2
CO_2	7.6	22.9	7.6	22.9
FC	0.0	0.0	0.7	0.7
		Internal		
Recycle	64.9	194.8	64.9	194.8
H_2	1.1	3.2	1.1	3.2
		Output		
O_2	8.3	25.0	8.3	25.0
MeOH	5.3	16.0	5.7	16.4
Waste water	3.0	9.1	3.3	9.3
Purge	0.3	1.0	0.4	1.0

Table D.4 gives the mass balance with focus on the contaminants introduced by the foul condensate. The mass flows for the sulphur and nitrogen compounds are broken down in total sulphur and nitrogen content. The removal of sulphur species in the stripper column is very efficient removing 98 % of the sulphur. For ammonia the removal is only at 59 %. No terpenes are removed in this step. However, the terpenes are then mostly removed from the MeOH product as the bottom product of the distillation column. Contrary, the sulphur and nitrogen species all end up in the MeOH product after distillation.

Table D.4 Mass balance for the contaminants introduced with the FC for 50 MW_{el}-FC and 150 MW_{el}-FC

	Feed	Purge	MeOH	Waste water	Unit
S	16.26	15.95	0.31	0.00	kg S/h
N	6.58	3.90	2.67	0.00	kg N/h
Terpenes	0.62	0.00	0.13	0.49	kg Terpenes/h

D.1.2 Economics

Table D.5 gives the detailed cost breakdown for the production of MeOH.

Table D.5 Cost breakdown for MeOH processes in M€

Case	50 MW_{el}	150 MW_{el}	50 MW_{el}-FC	150 MW_{el}-FC
OPEX	50.2	124.0	50.4	124.2
Labor	1.1	1.1	1.1	1.1
Laboratory	0.2	0.2	0.2	0.2
Operating supervision	0.2	0.2	0.2	0.2
Water	0.1	0.4	0.1	0.4
Electricity Pulp Mill	32.8	37.4	32.8	37.4
Electricity Grid	-	45.4	-	45.5
Natural gas	-0.3	-0.8	-0.3	-0.9
O_2	-1.3	-2.5	-1.3	-2.5
CO_2	2.9	8.6	2.9	8.6
Maintenance	6.7	16.4	6.7	16.4
Insurance + Taxes	2.9	7.0	2.9	7.0
Plant overhead	4.8	10.6	4.8	10.6
Administration	0.2	0.2	0.2	0.2
FCI	95.8	233.8	96.2	234.5
Water electrolysis	60.0	180.0	60.0	180.0
Chemical plant	35.8	53.8	36.2	54.5
ACC	9.8	23.8	9.8	23.9
TAC	60.0	147.9	60.2	148.1

Figures D.1 show the impact of various parameters on the levelized cost of MeOH.

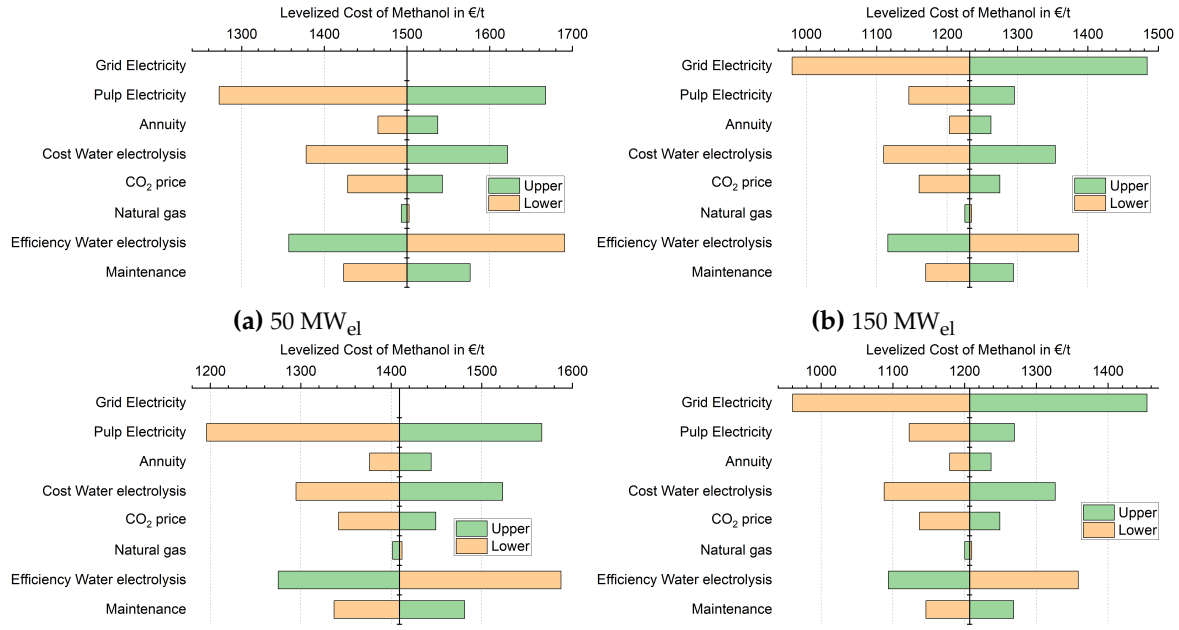

(a) 50 MW_{el} **(b)** 150 MW_{el}

(c) 50 MW_{el}-FC **(d)** 150 MW_{el}-FC

Figure D.1 Sensitivity analysis on the levelized cost of MeOH

D.1.3 Heat integration

Table D.6 shows the heat flows as derived from pinch analysis for the integration of the MeOH plants with the energy system of the pulp mill.

Table D.6 Heat flows in MW_{th} for MeOH plant integration

Case	50 MW_{el}	150 MW_{el}	50 MW_{el}-FC	150 MW_{el}-FC
HP Steam generation	-	-	-	-
MP1 Steam generation	-	-	-	-
MP2 Steam generation	-	-	-	-
LP Steam generation	-	-	-	-
Hot water 1 generation	13.0	39.1	13.0	39.0
Hot water 2 generation	2.8	8.4	2.8	8.4
HP Steam supply	-	-	-	-
MP1 Steam supply	-	-	-	-
MP2 Steam supply	6.4	19.3	6.4	19.3
LP Steam supply	3.4	10.2	3.7	11.0
Hot water 1 supply	-	-	-	-
Hot water 2 supply	-	-	-	-
Steam generation (greenfield)	-	-	-	-
Steam supply (greenfield)	9.8	29.5	10.1	30.3

Figures D.2 to D.5 show the composite curves for the integrated MeOH plants.

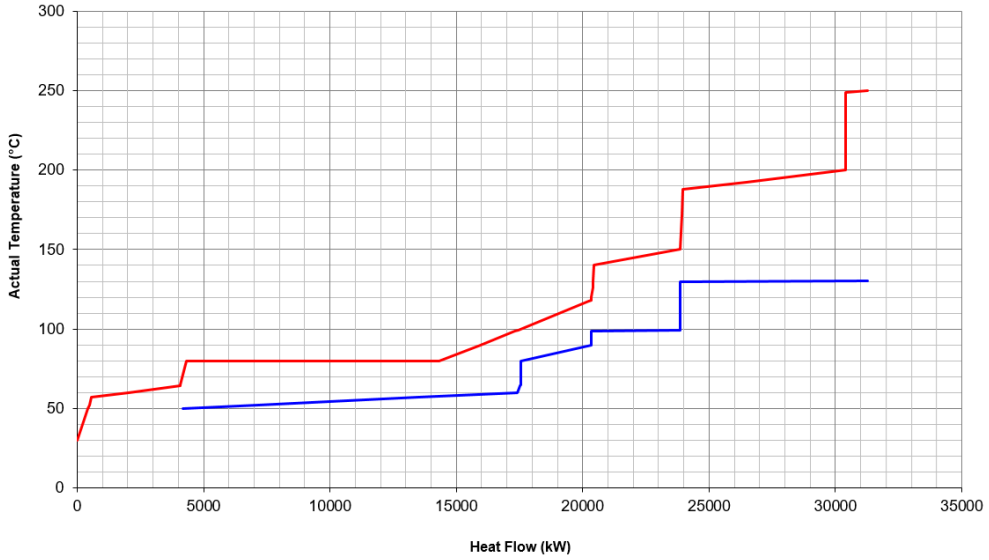

Figure D.2 Composite curve for the 50 MW_{el} MeOH plant

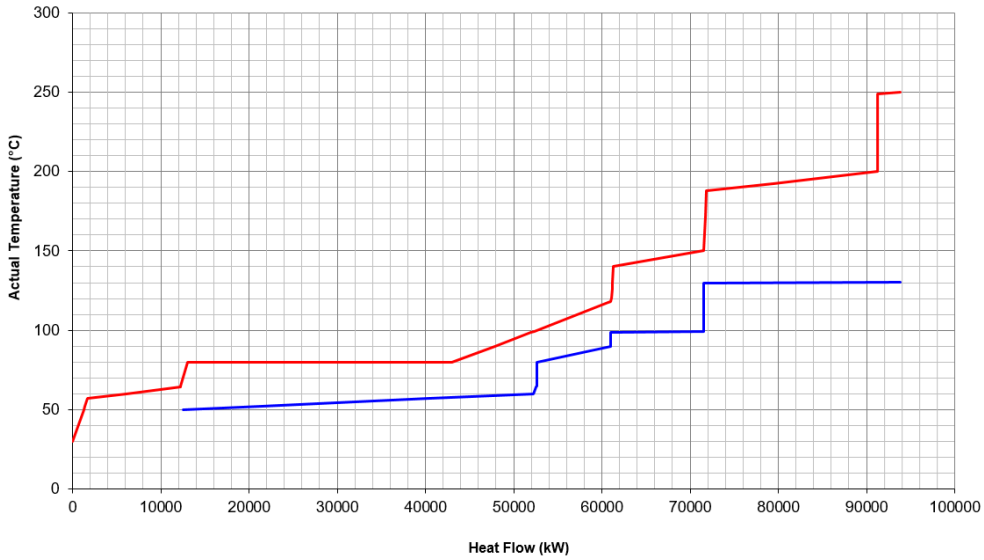

Figure D.3 Composite curve for the 150 MW_{el} MeOH plant

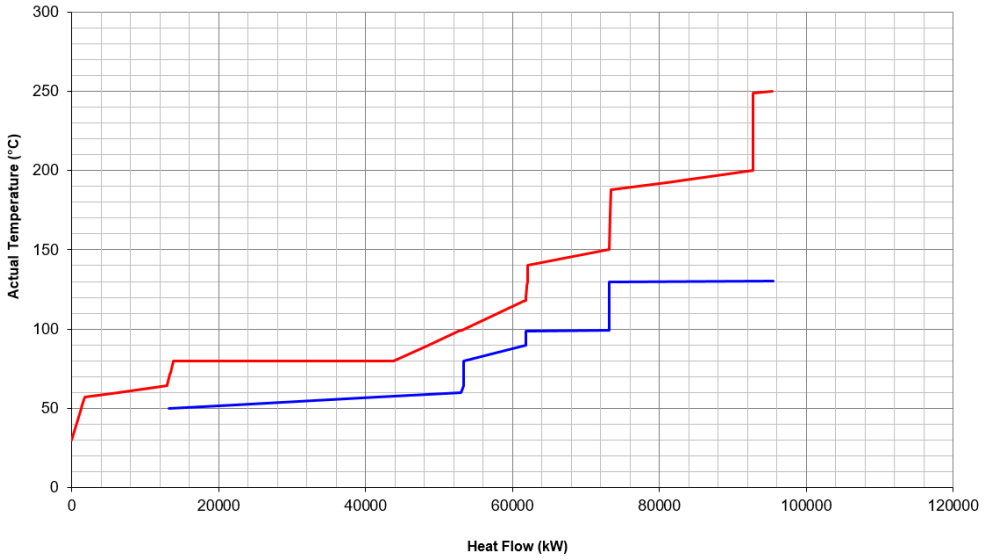

Figure D.4 Composite curve for the 50 MW_{el}-FC MeOH plant

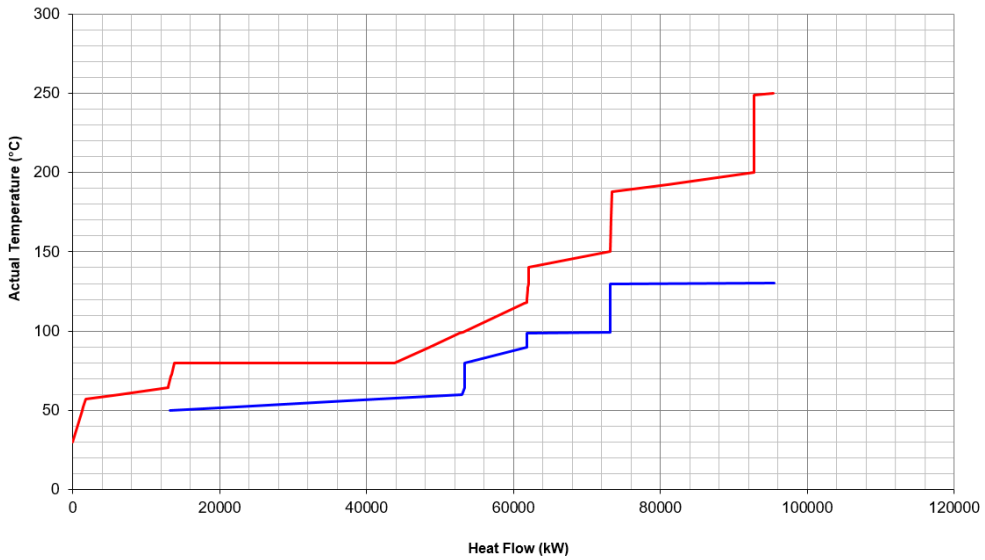

Figure D.5 Composite curve for the 150 MW_{el}-FC MeOH plant

D.1.4 CO_2 emissions

Figure D.6 and D.7 show the annual CO_2 emissions of the MeOH production process over the carbon intensity of the imported grid electricity.

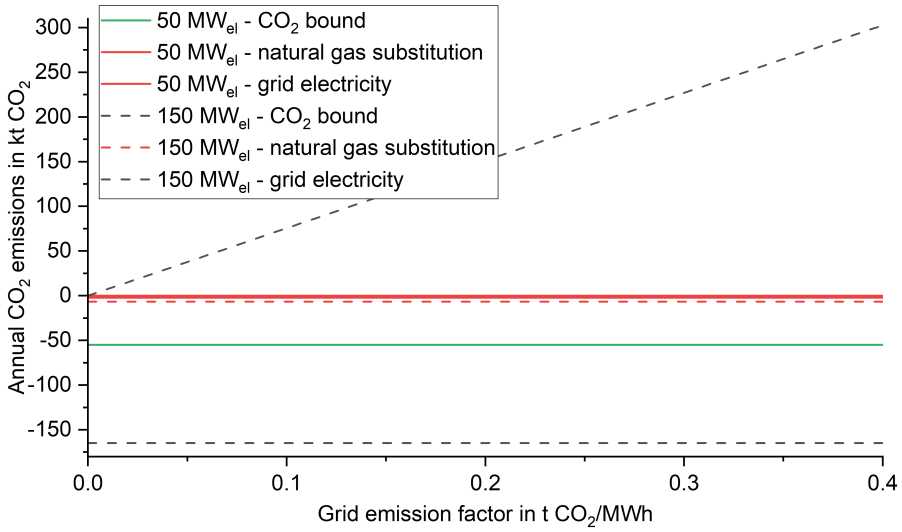

Figure D.6 Annual CO_2 emissions over the emission factor of grid electricity for 50 and 150 MW_{el} plants

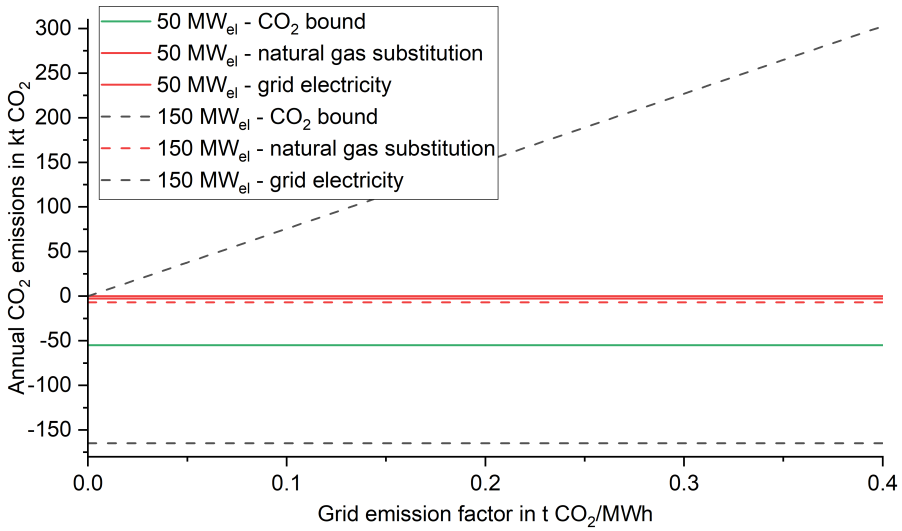

Figure D.7 Annual CO_2 emissions over the emission factor of grid electricity for $50MW_{el}$-FC and $150MW_{el}$-FC plants

D.2 SNG

In this section you find additional information on the SNG process.

D.2.1 Technical parameters

Table D.7 shows the mass balance of the SNG process.

Table D.7 Mass balance SNG in t/h

Plant size in MW_{el}	50	150
Input		
Water	9.4	28.2
CO_2	5.7	17.2
Internal		
Recycle	12.6	37.8
H_2 (water electrolysis)	1.1	3.2
Output		
O_2 (water electrolysis)	8.3	25.0
SNG	2.1	6.3
Waste water	4.7	14.0

D.2.2 Economics

Table D.8 gives the LCOSNG in €/t and €/MWh. The LCOSNG is shown without electricity cost and capital cost. Table D.9 summarizes the cost breakdown of all cost categories included in the economic assessment.

Table D.8 Levelized cost of SNG expressed in different units

Plant size	50 MW_{el}	150 MW_{el}	Unit
Levelized cost of SNG	3315	2833	€/t
	241	206	€/MWh
Levelized cost of SNG w/o electricity	1376	1185	€/t
	100	86	€/MWh
Levelized cost of SNG w/o ACC	2833	2398	€/t
	206	174	€/MWh

Table D.9 Yearly cost in M€for SNG production

Plant size in MW_{el}	50	150
OPEX	44.7	113.4
Labor	1.1	1.1
Laboratory	0.2	0.2
Operating supervision	0.2	0.2
Water	0.1	0.4
Electricity Pulp Mill	30.6	37.4
Electricity Grid	-	40.6
O_2	-1.3	-2.5
CO_2	2.1	6.4
Maintenance	5.2	14.1
Insurance + Taxes	2.2	6.1
Plant overhead	3.9	9.3
Administration	0.2	0.2
FCI	74.7	202.0
Water electrolysis	60.0	180.0
Chemical plant	14.7	22.0
ACC	7.6	20.6
TAC	52.3	134.0

Figure D.8 shows the sensitivity analysis for the SNG plant. Parameters are varied according to Table 3.2.

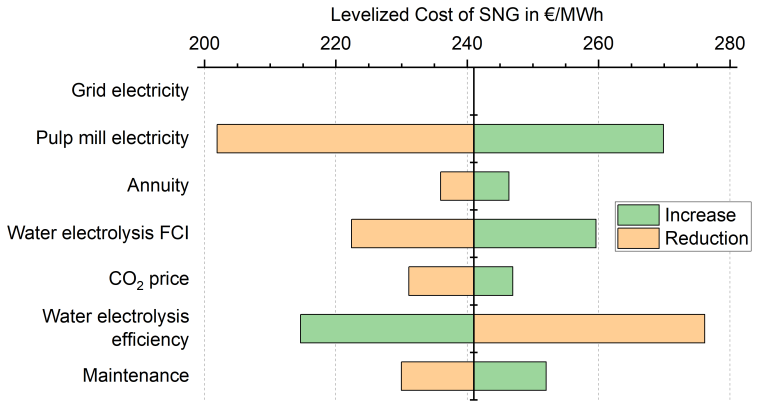

(a) 50 MW_{el}

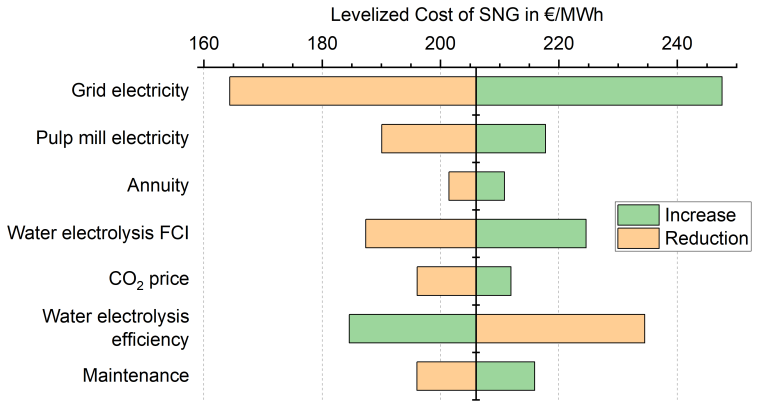

(b) 150 MW_{el}

Figure D.8 Sensitivity analysis on the levelized cost of SNG for the (a) 50 MW_{el} and (b) 150 MW_{el} plant size

D.2.3 Heat integration

Table D.10 shows the heat flows as derived from pinch analysis for the integration of the SNG plant with the energy system of the pulp mill.

Table D.10 Heat flows in MW_{th} for SNG plant integration

	integrated		greenfield	
Plant size	50	150	50	150
HP Steam generation	2.4	7.2	-	-
MP1 Steam generation	-	-	-	-
MP2 Steam generation	-	-	-	-
LP Steam generation	-	-	-	-
Hot water 1 generation	11.2	33.7	-	-
Hot water 2 generation	-	-	-	-
HP Steam supply	-	-	-	-
MP1 Steam supply	-	-	-	-
MP2 Steam supply	-	-	-	-
LP Steam supply	-	-	-	-
Hot water 1 supply	-	-	-	-
Hot water 2 supply	-	-	-	-
Steam generation (greenfield)	-	-	2.4	7.2
Steam supply (greenfield)	-	-	-	-

The composite curves for the integrated SNG plants are shown in the following.

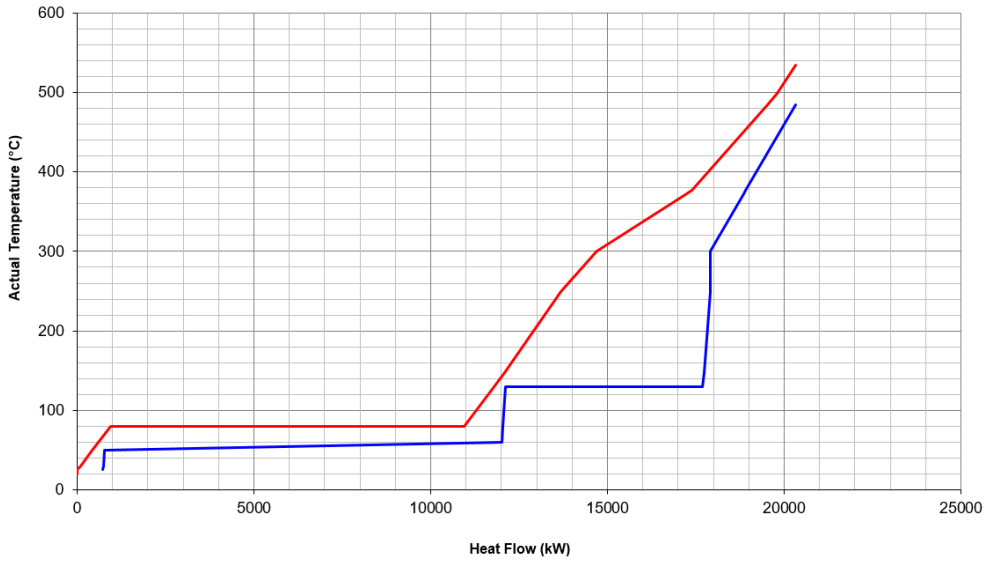

Figure D.9 Composite curve for the 50 MW_{el} SNG plant

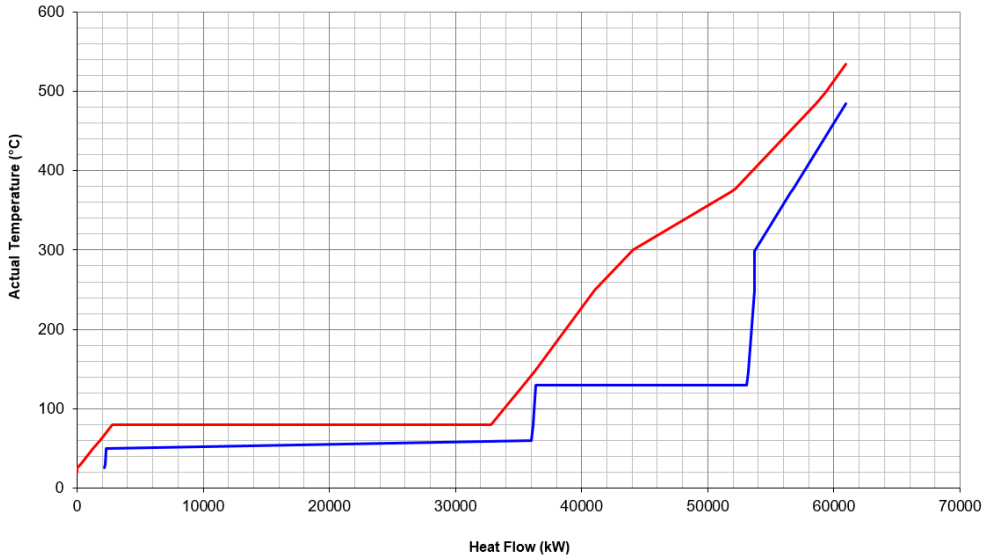

Figure D.10 Composite curve for the 150 MW_{el} SNG plant

D.2.4 CO_2 emissions

Figure D.11 shows the annual CO_2 emissions of the 50 and 150 MW_{el} plant. The CO_2 fixed in the SNG is refered to as bound CO_2.

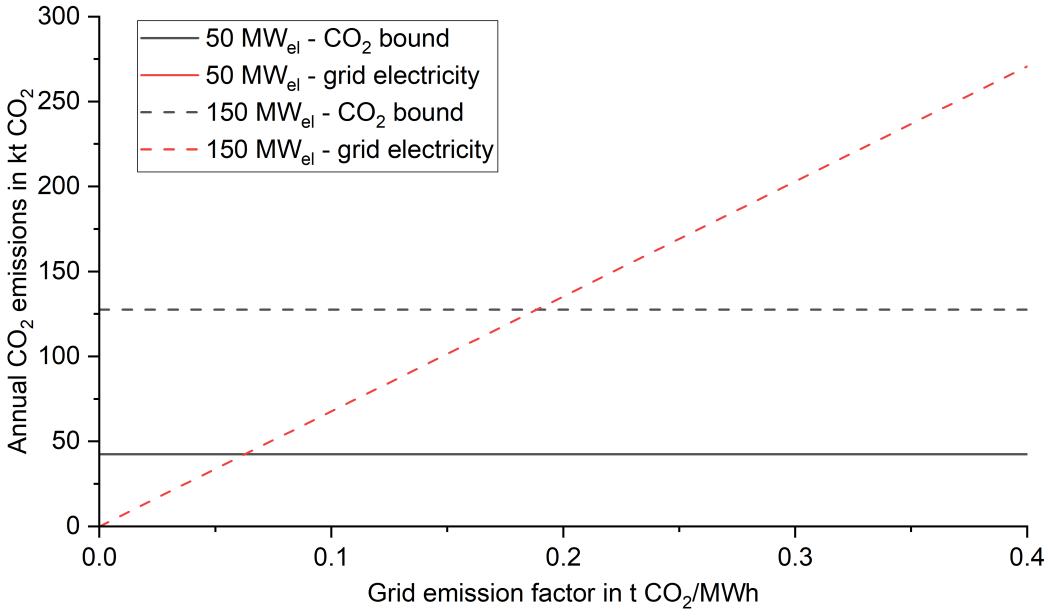

Figure D.11 Annual CO_2 emissions over the emission factor of grid electricity

D.3 H_2O_2

D.3.1 Technical parameters

The energy balance is shown in Table D.11.

Table D.11 Energy balance of the H_2O_2 processes in MW

Plant size in MW_{el}	6	50	150
Input			
Electricity total	5.4	50.9	155.5
-Water electrolysis	5.5	50.0	150.0
-Compression and pumping	0.2	1.5	4.5
-Integration	-0.3	-0.6	1.0
Heat	0.0	14.5	47.3
Output			
Heat	5.0	60.1	184.0

D.3.2 Economics

Table D.12 shows the breakdown of the total annual cost by each category.

Table D.12 Cost breakdown of the H_2O_2 process in M€

Plant size in MW_{el}	6	50	150
OPEX	8.9	51.9	159.9
Labor	1.1	1.2	1.2
Laboratory	0.2	0.2	0.2
Operating supervision	0.2	0.2	0.2
Electricity Pulp Mill	3.4	31.7	37.4
Electricity Grid	-	-	43.0
Water	0.1	0.5	1.6
H_2O_2 replaced	-	- 11.0	- 11.0
Makeup	1.2	10.7	31.9
O_2	- 0.2	- 1.3	- 2.5
Maintenance	1.0	9.2	28.1
Insurance + Taxes	0.4	4.0	12.0
Plant overhead	1.4	6.3	17.7
Administration	0.2	0.2	0.2
FCI	14.5	131.8	401.5
Water electrolysis	6.6	60.0	180.0
Chemical plant	7.9	71.8	221.5
ACC	1.5	13.4	40.9
TAC	10.3	65.3	200.8

The following Figure shows the results of the sensitivity analysis.

In Table D.13 the bare equipment cost of the reactors and extraction column are shown. The cost are assumptions. Since the reactors are complex, high cost are assumed here.

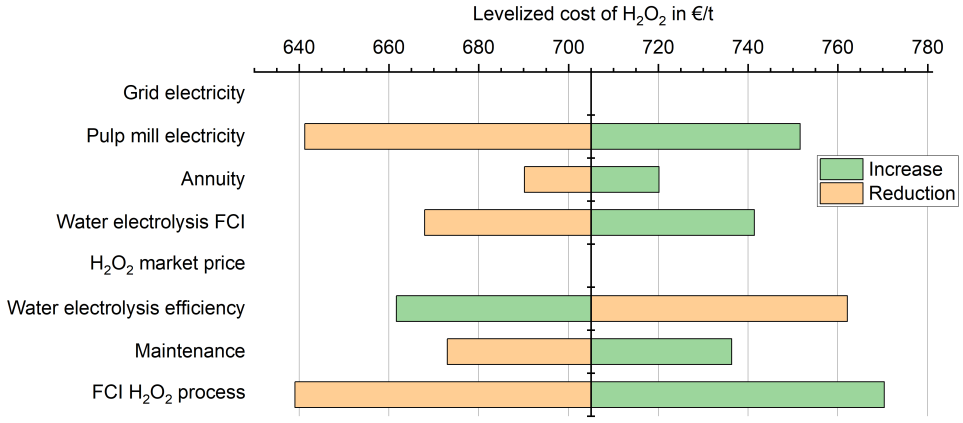

(a) 6 MW_{el} plant

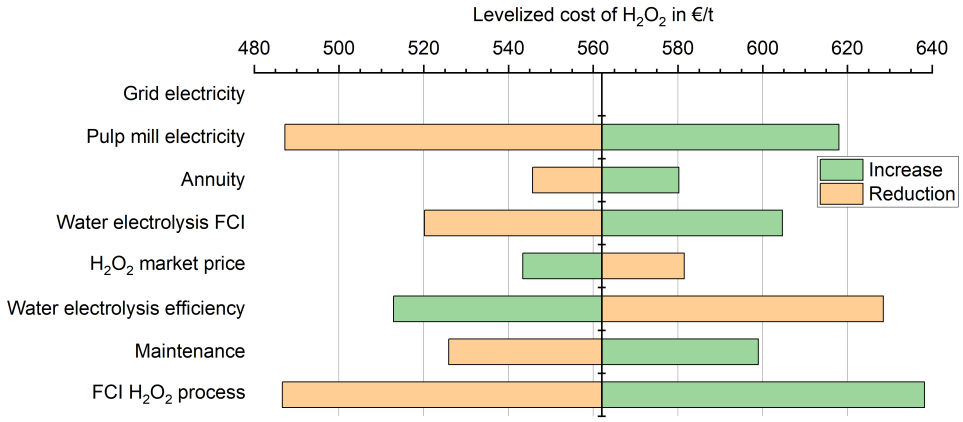

(b) 50 MW_{el} plant

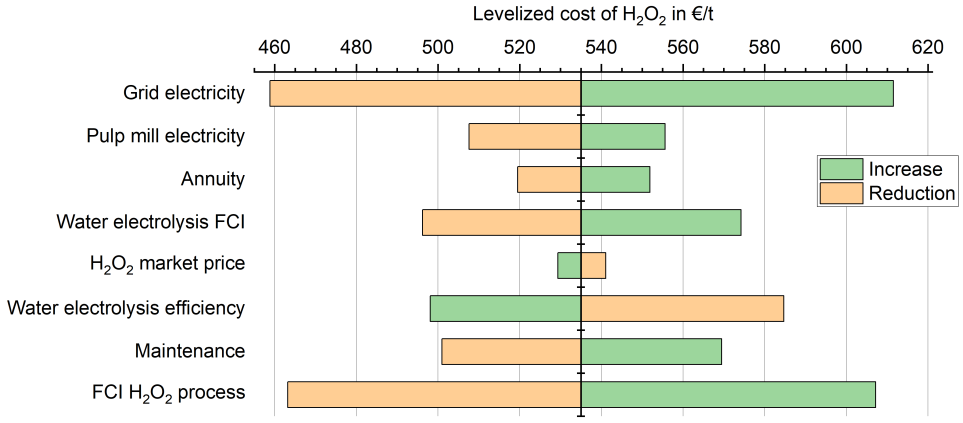

(c) 150 MW_{el} plant

Figure D.12 Sensitivity analysis on the levelized cost of H_2O_2

Table D.13 Assumed bare equipment cost for reactors and extraction column in M€

Plant size in MW_{el}	6	50	150
Hydrogenation reactor	0.2	2	6
Oxidation reactor	0.2	2	6
Extraction column	0.1	1	3

D.3.3 Heat integration

Table D.14 shows the results of heat integration. Only hot water is needed as utility. For the greenfield plants, the heat is supplied by a heating fluid heated by natural gas.

Table D.14 Heat flows in MW_{th} for H_2O_2 plant integration

Plant size	6	50	150
HP Steam generation	-	-	-
MP1 Steam generation	-	-	-
MP2 Steam generation	-	-	-
LP Steam generation	-	-	-
Hot water 1 generation	1.1	4.4	11.6
Hot water 2 generation	-	-	-
HP Steam supply	-	-	-
MP1 Steam supply	-	-	-
MP2 Steam supply	-	-	-
LP Steam supply	-	-	-
Hot water 1 supply	-	-	-
Hot water 2 supply	-	7.9	25.8
Steam generation (greenfield)	-	-	-
Steam supply (greenfield)	-	7.9	25.8

Figures D.13 to D.15 show the composite curves.

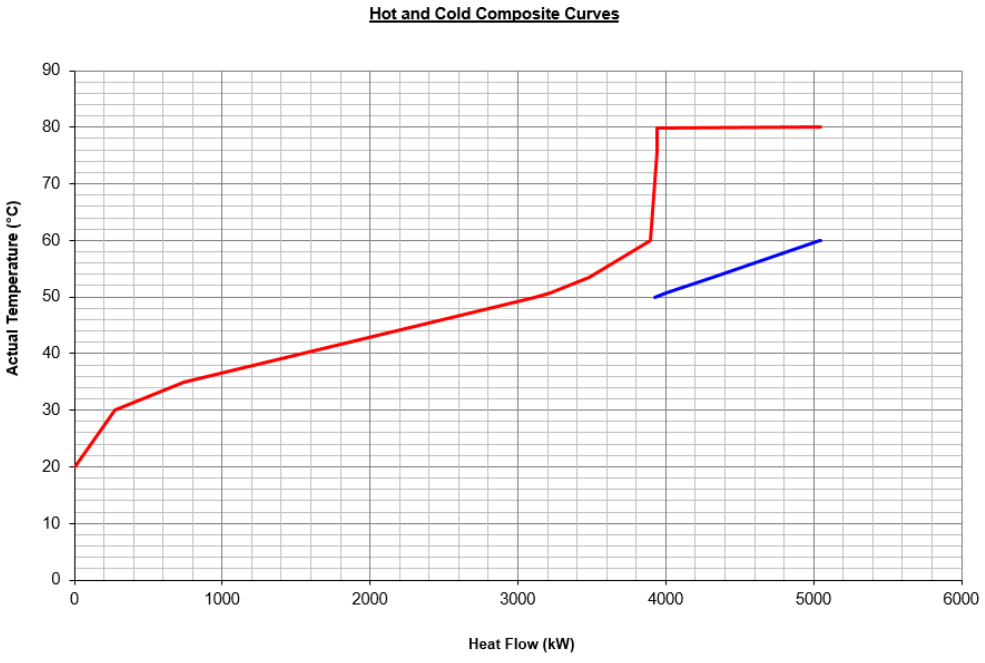

Figure D.13 Composite curve for the 6 MW_{el} H_2O_2 plant

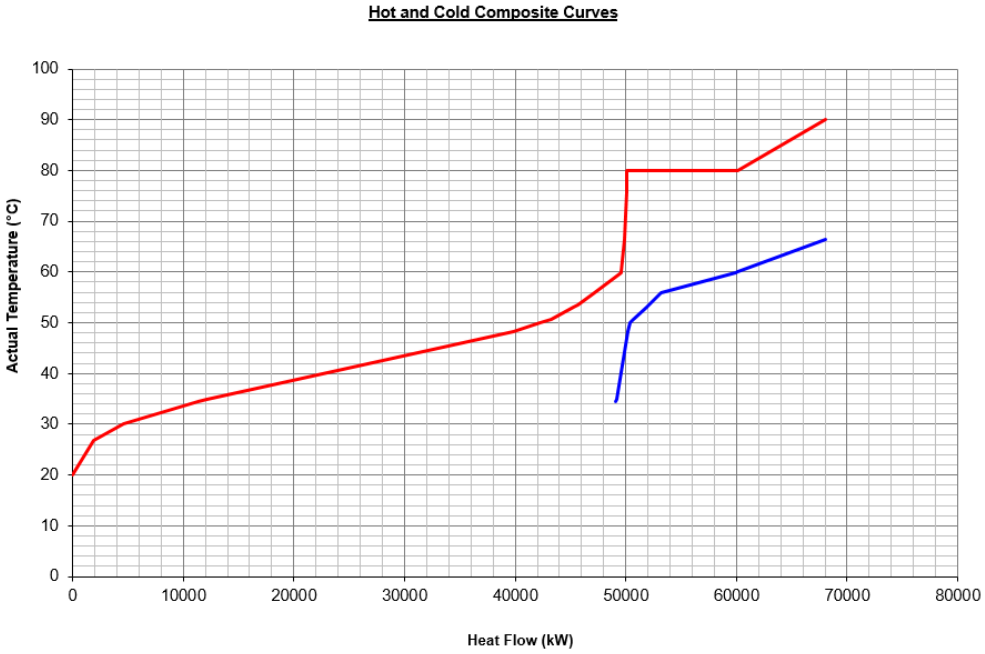

Figure D.14 Composite curve for the 50 MW_{el} H_2O_2 plant

Figure D.15 Composite curve for the 150 MW_{el} H_2O_2 plant

D.4 Acetic acid

D.4.1 Technical parameters

Table D.15 shows the mass balance of the AA production process.

Table D.15 Mass balance AA in t/h

CO generation	RWGS		CO2E	
Plant size in MW_{el}	50	150	50	150
Input				
Water	9.4	28.2	6.1	18.4
CO_2	11.4	34.1	9.9	29.6
Internal				
H_2	1.1	3.2	0.7	2.1
CO (total)	3.6	10.7	3.1	9.3
MeOH	4.0	12.0	3.5	10.5
Output				
O_2 (water electrolysis)	8.3	25.0	5.5	16.4
O_2 (CO_2 electrolysis)	0.0	0.0	1.8	5.3
Waste water	4.6	13.7	2.0	5.9
Purge	0.4	1.2	0.3	0.9
AA	7.4	22.2	6.5	19.4
AA total	7.4	22.3	6.5	19.5

The settings for the membrane separation in the RWGS process is depicted in Table D.16. The split fractions are equal in both stages of the separation process. The split fractions are based on an educated guess based on the permeability of the components. The resulting mole fraction after the membrane separation are in line with the commercial process described by Teuner et al. [259].

Table D.16 Split fractions in membrane stages

	split ratio to permeate
H_2	0.99
CH_4	0.05
H_2O	1
CO_2	0.95
CO	0.15

D.4.2 Economics

The following Figure shows the results of the sensitivity analysis.

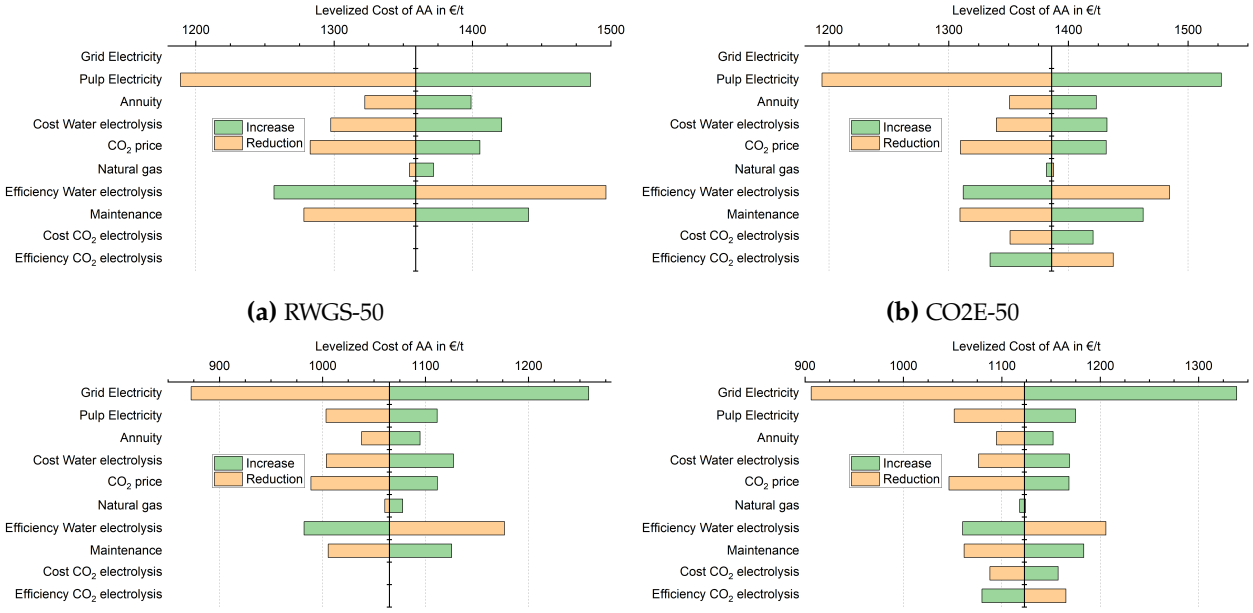

(a) RWGS-50 **(b)** CO2E-50

(c) RWGS-150 **(d)** CO2E-150

Figure D.16 Sensitivity analysis on the levelized cost of AA

Table D.17 gives the detailed cost breakdown for the production of AA.

Table D.17 Cost breakdown AA in M€

CO generation	RWGS		CO2E	
Plant size	50	150	50	150
OPEX	61.3	146.0	55.6	135.5
Labor	1.5	1.5	1.4	1.4
Laboratory	0.2	0.2	0.2	0.2
Operating supervision	0.2	0.2	0.2	0.2
Water	0.1	0.4	0.1	0.3
Electricity Pulp Mill	34.2	37.4	33.7	37.4
Electricity Grid	-	48.3	-	47.3
O_2	-1.3	-2.5	-1.2	-2.3
Natural gas	0.7	2.1	-0.2	-0.6
CO_2	4.3	12.8	3.7	11.1
Maintenance	9.9	21.9	8.1	19.4
Insurance + Taxes	4.2	9.4	3.5	8.3
Plant overhead	6.9	14.1	5.8	12.6
Administration	0.3	0.3	0.3	0.3
FCI	141.1	312.7	116.4	277.5
Water electrolysis	60.0	180.0	39.2	117.7
CO_2 electrolysis	-	-	27.7	83.0
Chemical plant	81.1	132.7	49.4	76.7
ACC	14.4	31.9	11.9	28.3
TAC	75.6	177.9	67.4	163.8

D.4.3 Heat integration

Table D.18 shows the heat streams derived from pinch analysis. The composite curves for the integrated processes are shown in Figure D.17 to D.20.

Table D.18 Heat flows in MW_{th} for AA plant integration

CO generation	RWGS		CO2E	
Plant size	50	150	50	150
HP Steam generation	-	-	-	-
MP1 Steam generation	-	-	-	-
MP2 Steam generation	-	-	-	-
LP Steam generation	-	-	-	-
Hot water 1 generation	19.6	58.7	12.9	38.6
Hot water 2 generation	7.1	18.4	4.5	13.6
HP Steam supply	-	-	-	-
MP1 Steam supply	-	-	-	-
MP2 Steam supply	1.6	4.7	5.3	16.1
LP Steam supply	13.7	38.2	12.2	36.5
Hot water 1 supply	-	-	-	-
Hot water 2 supply	-	-	-	-
Steam generation (greenfield)	-	-	-	-
Steam supply (greenfield)	15.3	42.8	17.5	52.6

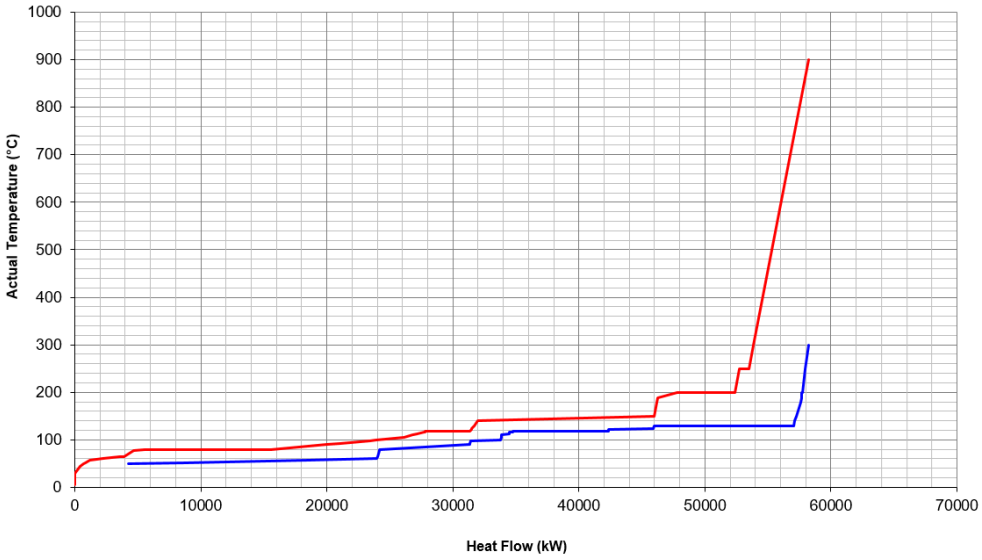

Figure D.17 Composite curve for the RWGS-50 AA plant

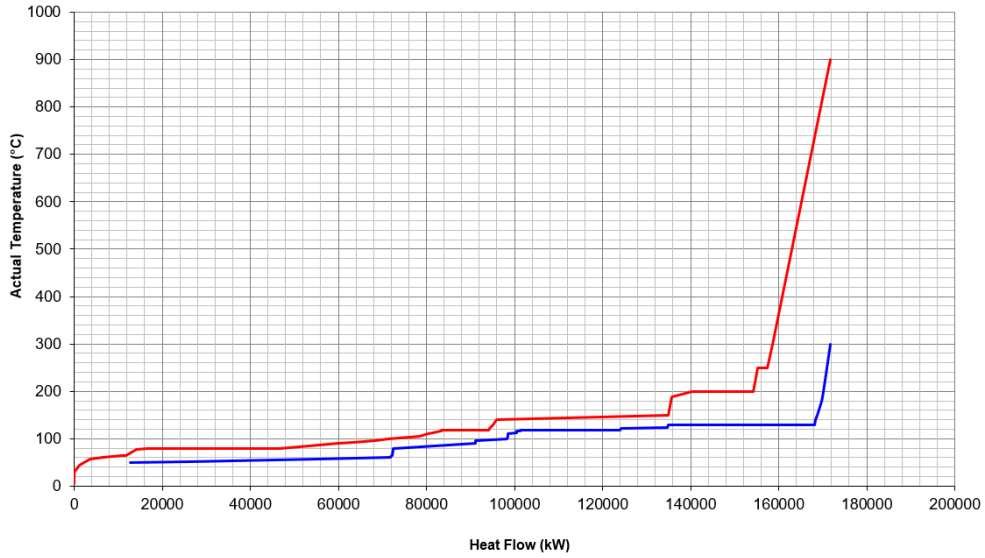

Figure D.18 Composite curve for the RWGS-150 AA plant

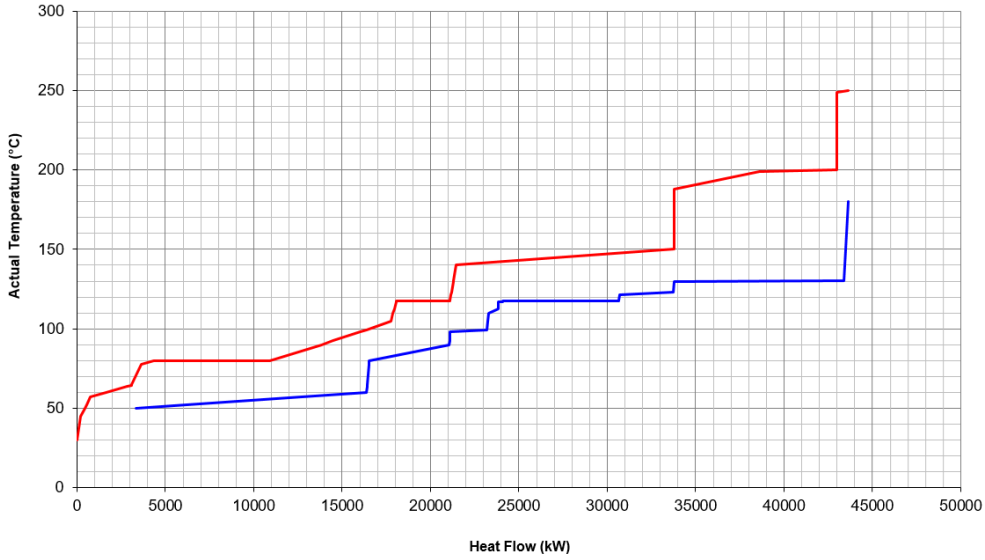

Figure D.19 Composite curve for the CO2E-50 AA plant

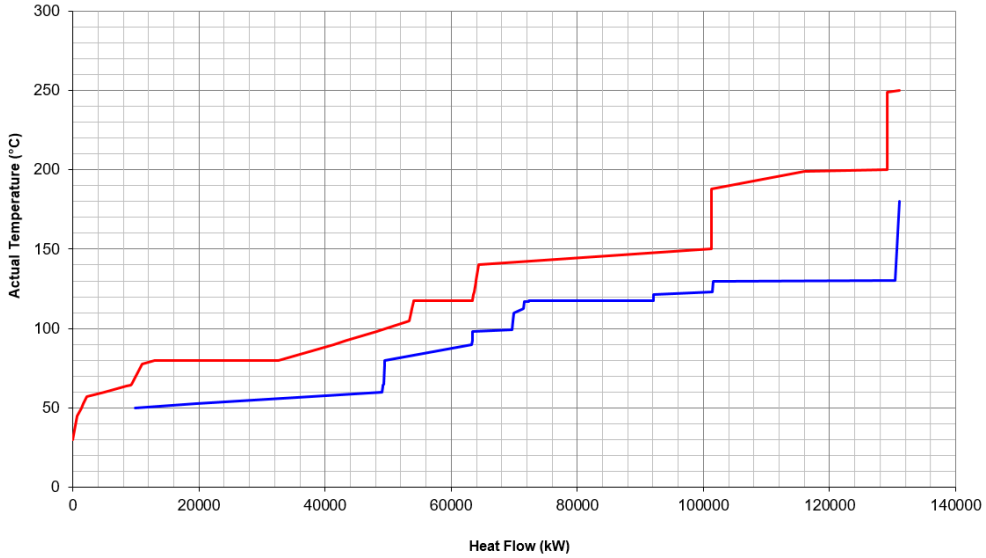

Figure D.20 Composite curve for the CO2E-150 AA plant

D.4.4 CO_2 emissions

Figure D.21 and D.22 show the annual CO_2 emissions (fossil and biogenic) of the AA production process.

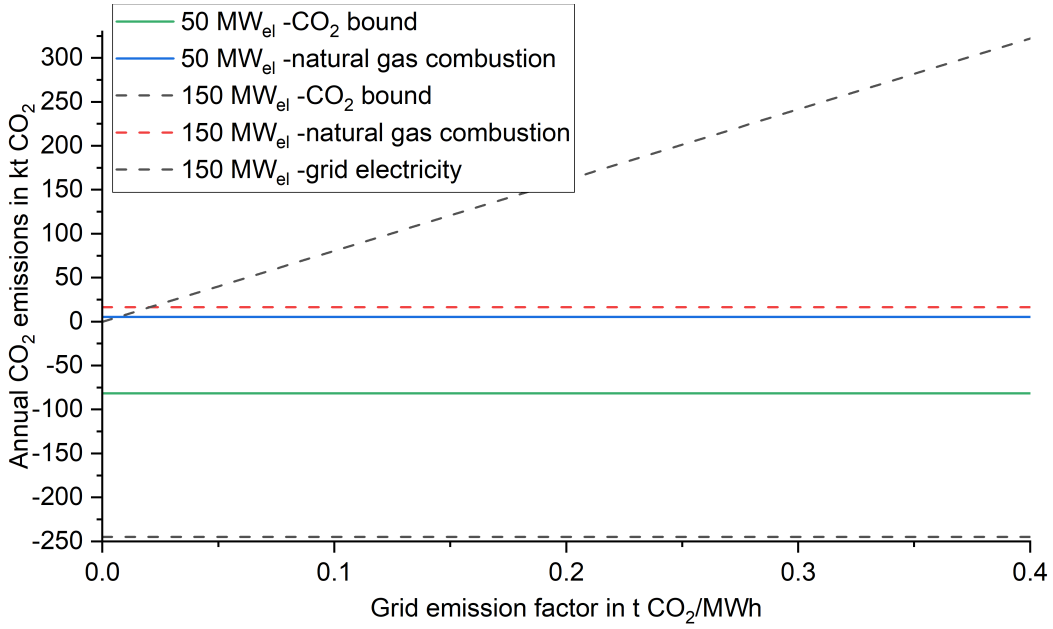

Figure D.21 Annual CO_2 emissions over the emission factor of grid electricity for RWGS

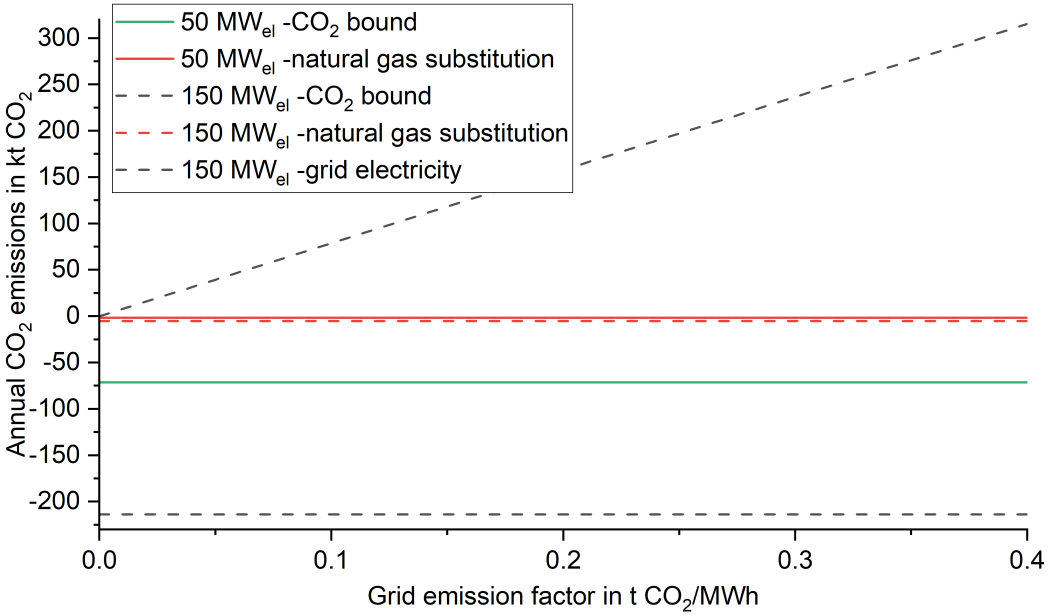

Figure D.22 Annual CO_2 emissions over the emission factor of grid electricity for CO2E

D.5 Fischer Tropsch

D.5.1 Syncrude

Figure D.23 shows the chain length distribution of the syncrude. The ASF distribution for $\alpha = 0.84$ is represented by the line for comparison. The syncrude has a heating value of 34.3 to 35.4 MJ/kg.

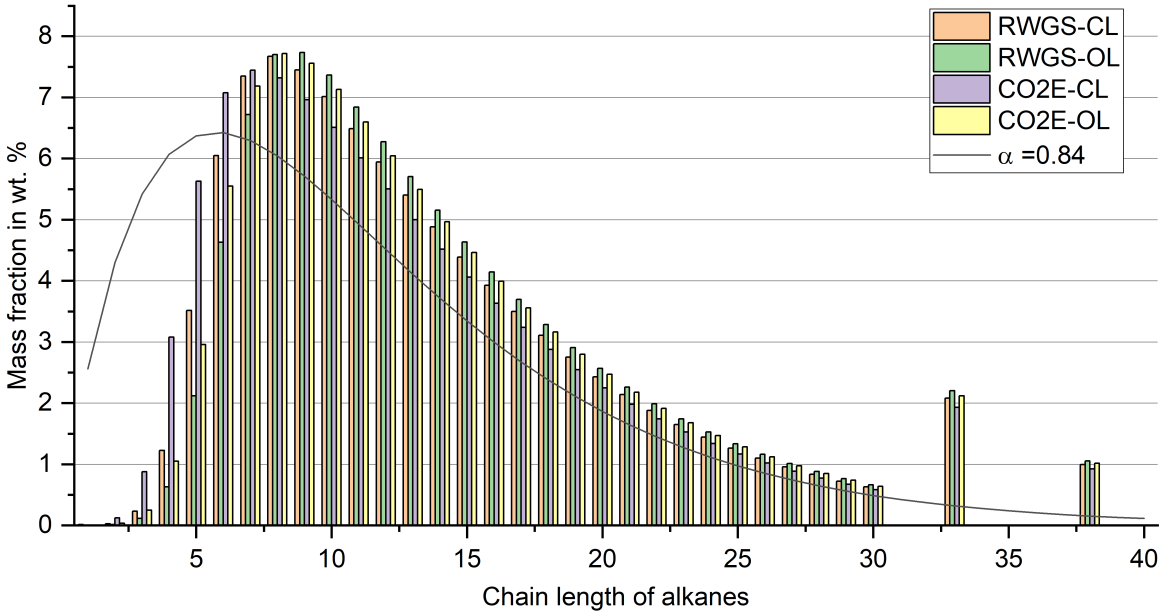

Figure D.23 Chain length distribution of syncrude

D.5.2 Economics

Table D.19 shows the levelized cost of syncrude of the scenarios expressed in different units to foster a better understanding of the values. The density for syncrude is derived from Aspen Plus. The diesel and gasoline equivalent calculation is based on the LHV of diesel (35.9 MJ/l) and gasoline (32.3 MJ/l) [301].

Table D.19 Levelized cost of syncrude in different units (DE: diesel equivalent, GE: gasoline equivalent)

Syngas preparation and gas loop design	RWGS-CL		RWGS-OL		CO2E-CL		CO2E-OL	
Plant size in MW_{el}	50	150	50	150	50	150	50	150
in €/kg	3.96	3.35	7.84	6.60	4.77	4.01	7.46	6.45
in €/l	5.71	4.83	11.30	9.51	6.87	5.78	10.75	9.30
in €/MJ	0.11	0.10	0.23	0.19	0.14	0.12	0.22	0.19
in €/l_{DE}	4.12	3.48	8.15	6.86	4.95	4.17	7.75	6.71
in €/l_{GE}	3.69	3.12	7.31	6.15	4.44	3.74	6.96	6.02

Figures D.24 and D.25 show the impact of various parameters on the levelized cost of FT syncrude.

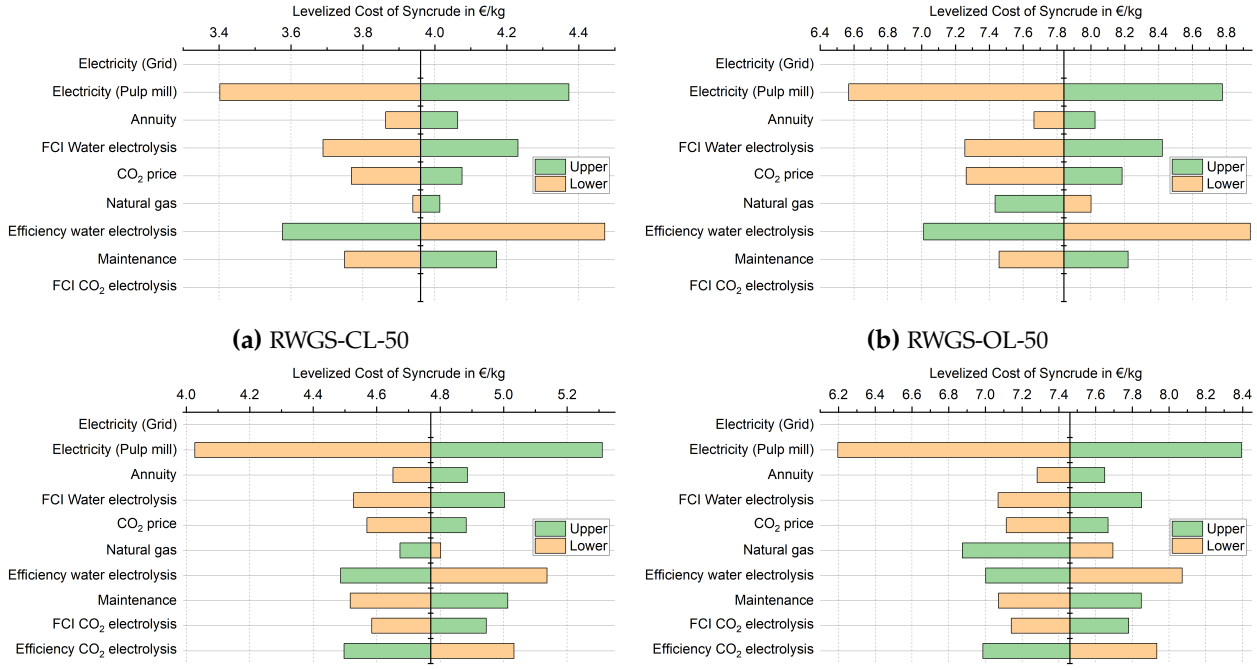

(a) RWGS-CL-50

(b) RWGS-OL-50

(c) CO2E-CL-50

(d) CO2E-OL-50

Figure D.24 Sensitivity analysis on the levelized cost of FT syncrude for the 50 MW_{el} plant size

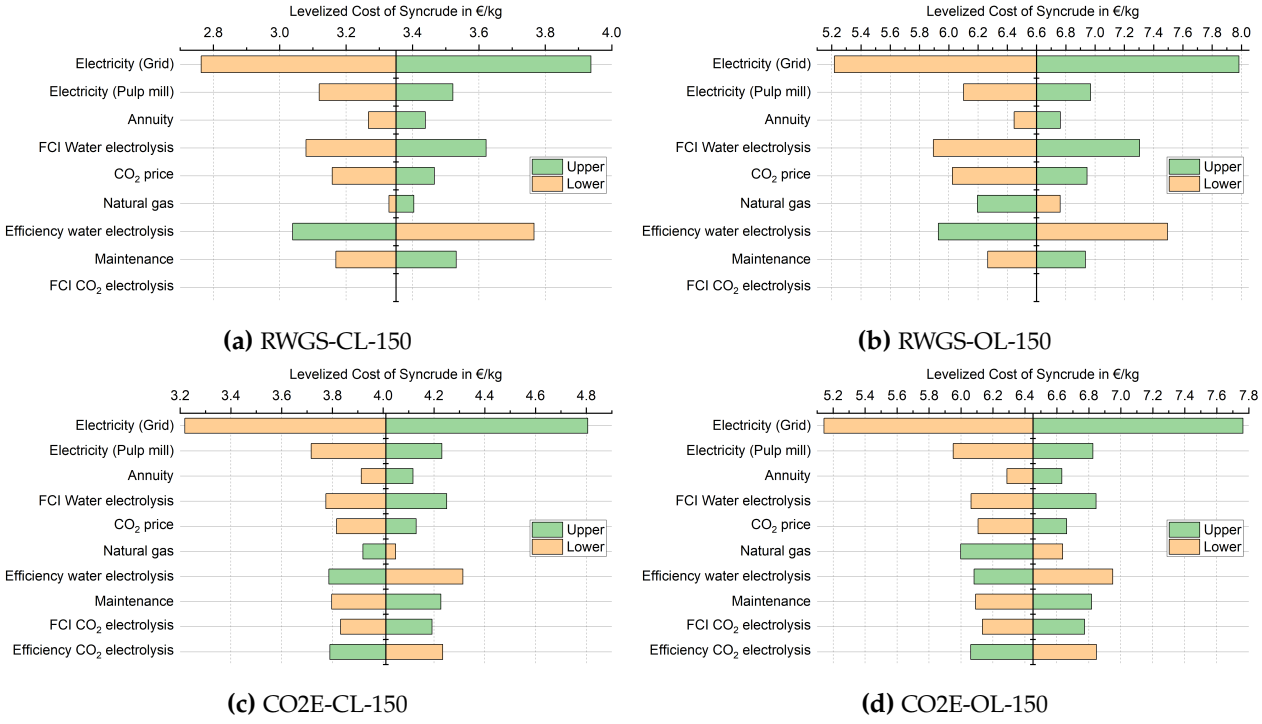

(a) RWGS-CL-150 **(b)** RWGS-OL-150

(c) CO2E-CL-150 **(d)** CO2E-OL-150

Figure D.25 Sensitivity analysis on the levelized cost of FT syncrude for the 150 MW_{el} plant size

Table D.20 Cost breakdown for FT process in M€

Scenarios	RWGS-CL		RWGS-OL		CO2E-CL		CO2E-OL	
Plant size	50	150	50	150	50	150	50	150
OPEX	49.0	123.9	45.8	114.9	46.3	116.4	42.7	109.1
Labor	1.1	1.1	1.1	1.1	1.1	1.1	1.1	1.1
Laboratory	0.2	0.2	0.2	0.2	0.2	0.2	0.2	0.2
Operating supervision	0.2	0.2	0.2	0.2	0.2	0.2	0.2	0.2
Water	0.1	0.4	0.1	0.4	0.1	0.2	0.1	0.2
Electricity	30.0	37.4	31.7	37.4	31.0	37.4	31.3	37.4
O_2	-1.3	-2.5	-1.3	-2.5	-1.2	-2.2	-1.2	-2.2
Natural gas	0.8	2.4	-2.8	-8.4	-1.1	-3.2	-4.0	-9.4
CO_2	2.9	8.6	4.0	11.9	2.3	6.8	2.4	7.1
Maintenance	6.9	17.7	5.8	15.1	6.3	16.5	5.8	16.3
Insurance + Taxes	3.0	7.6	2.5	6.5	2.7	7.1	2.5	7.0
Plant overhead	4.9	11.4	4.2	9.8	4.5	10.6	4.2	10.5
Administration	0.2	0.2	0.2	0.2	0.2	0.2	0.2	0.2
FCI	98.4	252.9	82.3	216.3	90.4	235.2	83.4	233.6
Water electrolysis	60.0	180.0	60.0	180.0	34.1	102.4	33.0	99.0
CO_2 electrolysis	-	-	-	-	34.5	103.5	36.0	107.9
Chemical plant	38.4	72.9	22.3	36.3	21.8	29.3	14.4	26.7
ACC	10.0	25.8	8.4	22.0	9.2	24.0	8.5	23.8
TAC	59.0	149.7	54.2	136.9	55.6	140.3	51.2	132.9

D.5.3 Heat integration

Table D.21 shows the heat flows derived by pinch analysis for the integration with the pulp mill.

Table D.21 Heat flows in MW_{th} for FT plant integration

Scenario	RWGS-CL		RWGS-OL		CO2E-CL		CO2E-OL	
Plant size	50	150	50	150	50	150	50	150
HP Steam generation	6.6	19.9	-	-	-	-	-	12.9
MP1 Steam generation	-		-	-	-	-	-	-
MP2 Steam generation	-		-	-	0.7	2.1	-	-
LP Steam generation	1.8	5.3	-	-	-	-	-	-
Hot water 1 generation	11.5	34.6	11.5	34.6	6.6	19.7	6.2	18.6
Hot water 2 generation	-	-	-	-	-	-	-	-
HP Steam supply	-	-	-	-	-	-	-	-
MP1 Steam supply	-	-	-	-	-	-	-	-
MP2 Steam supply	-	-	-	-	-	-	1.7	5.0
LP Steam supply	-	-	-	-	-	-	-	-
Hot water 1 supply	-	-	-	-	-	-	-	-
Hot water 2 supply	-	-	-	-	-	-	-	-
Steam generation (greenfield)	8.40	25.20	0.22	0.66	0.70	2.10	-	-
Steam supply (greenfield)	-	-	-	-	-	-	1.70	5.10

The following figures show the composite curves of the integrated plants.

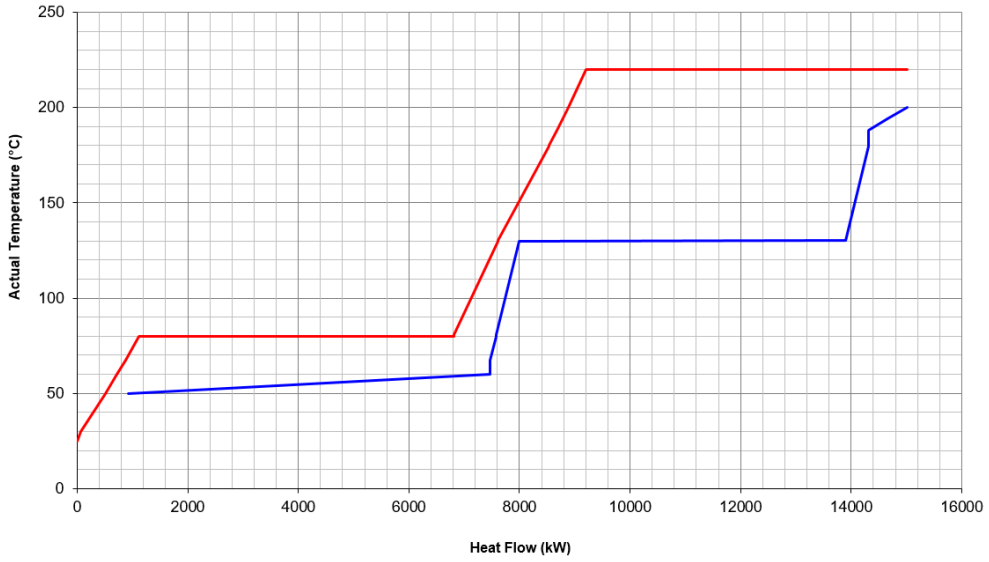

Figure D.26 Composite curve for the 50 MW_{el} CO2E-CL plant

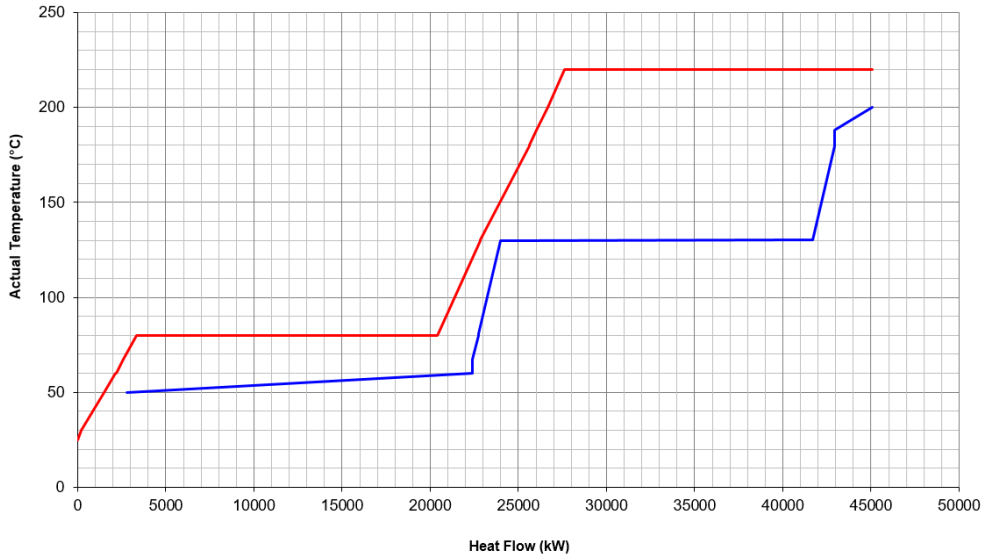

Figure D.27 Composite curve for the 150 MW_{el} CO2E-CL plant

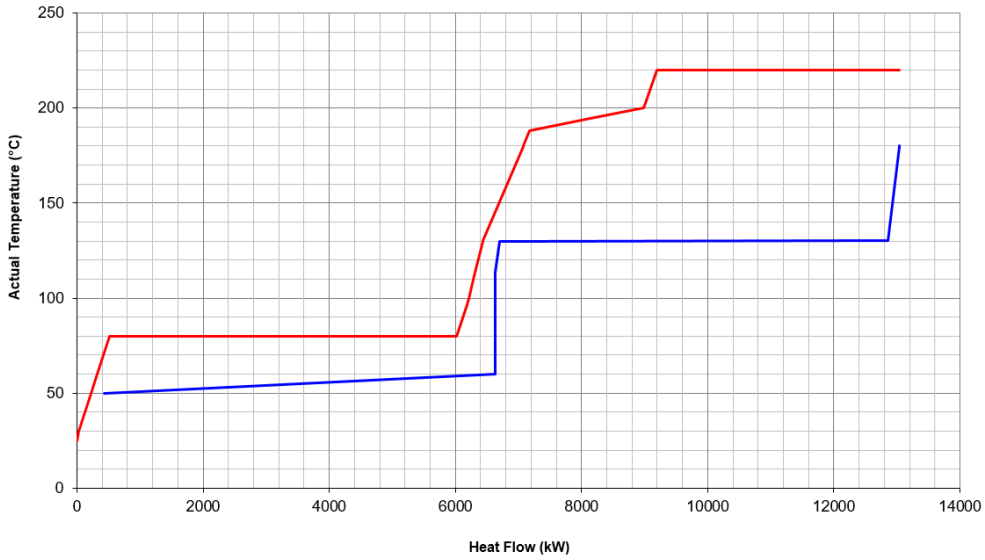

Figure D.28 Composite curve for the 50 MW_{el} CO2E-OL plant

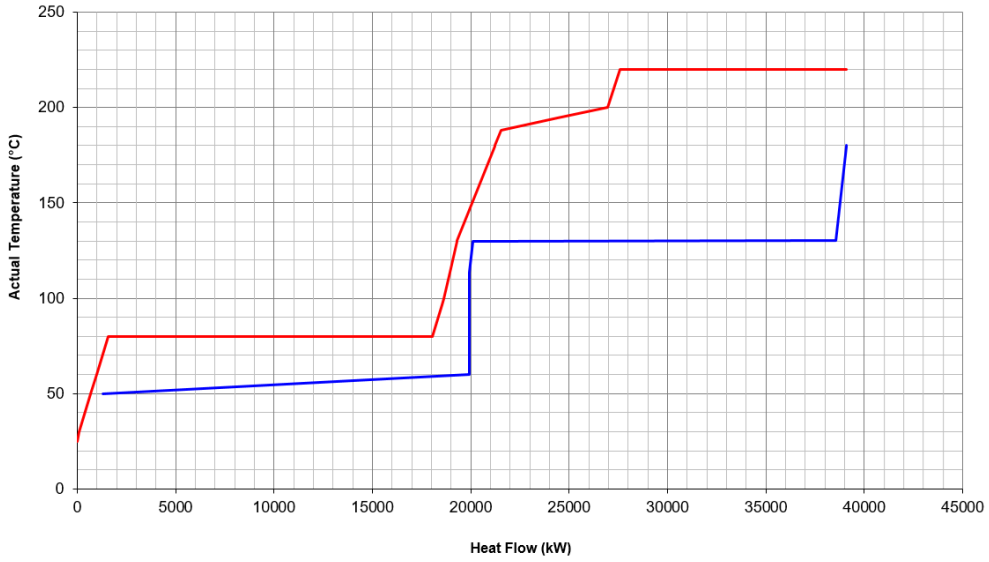

Figure D.29 Composite curve for the 150 MW_{el} CO2E-OL plant

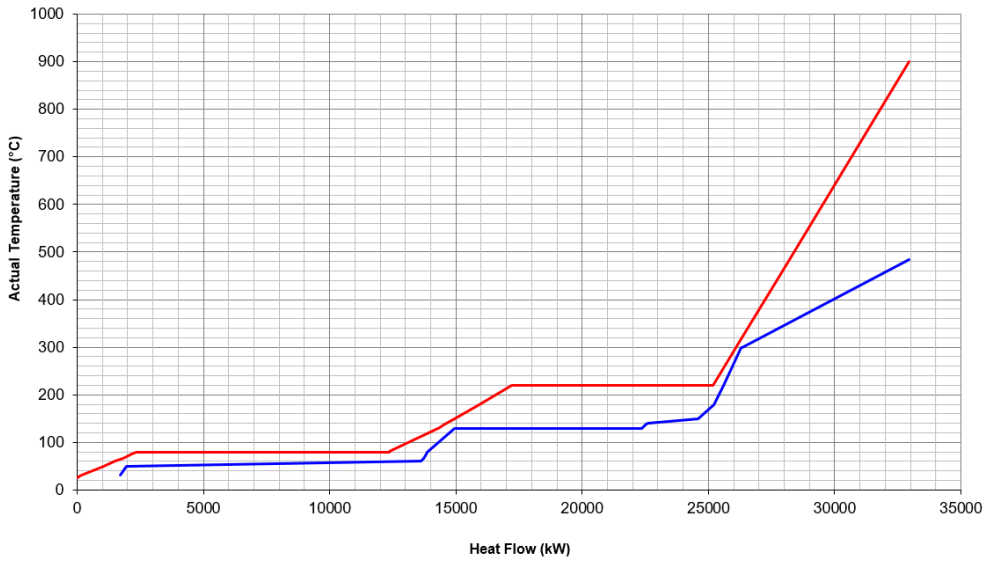

Figure D.30 Composite curve for the 50 MW_{el} RWGS-CL plant

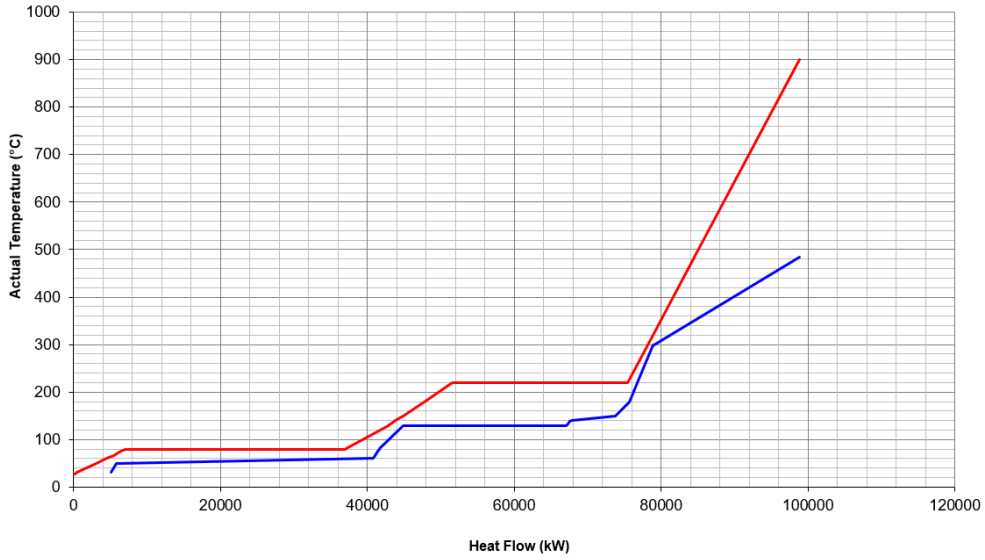

Figure D.31 Composite curve for the 150 MW_{el} RWGS-CL plant

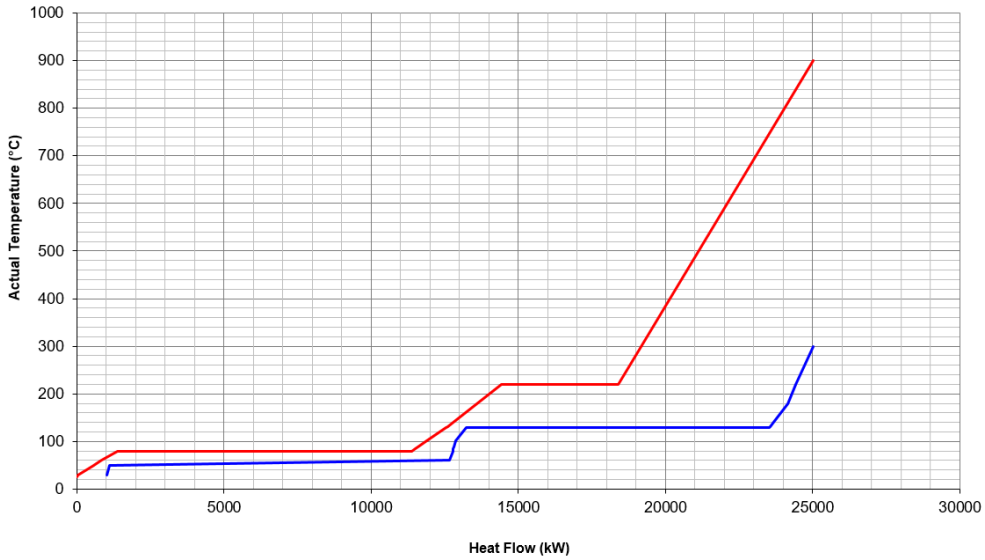

Figure D.32 Composite curve for the 50 MW_{el} RWGS-OL plant

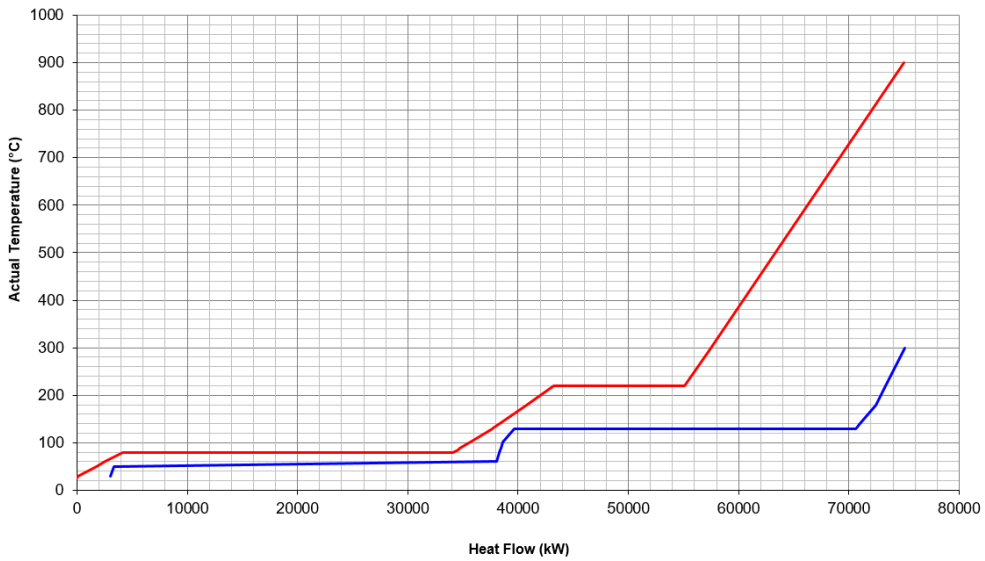

Figure D.33 Composite curve for the 150 MW_{el} RWGS-OL plant

D.5.4 CO_2 emissions

The following figures show the annual CO_2 emissions for the four scenarios. Reported are biogenic emissions bound in the FT syncrude, additional emissions for natural gas combustion, substituted natural gas and emissions from grid electricity.

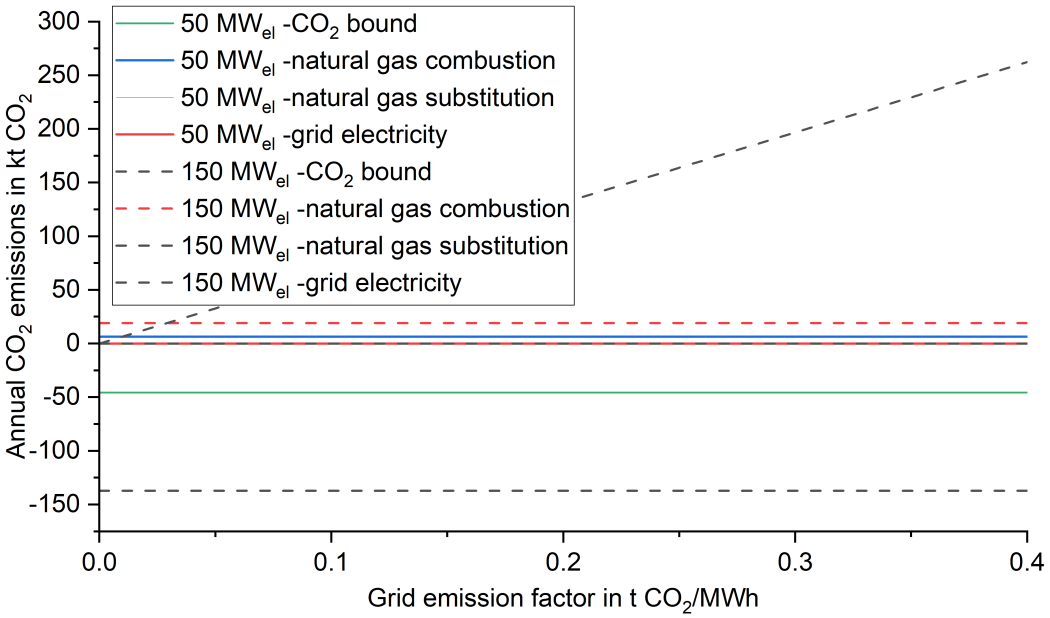

Figure D.34 Annual CO_2 emissions over the emission factor of grid electricity for RWGS-CL

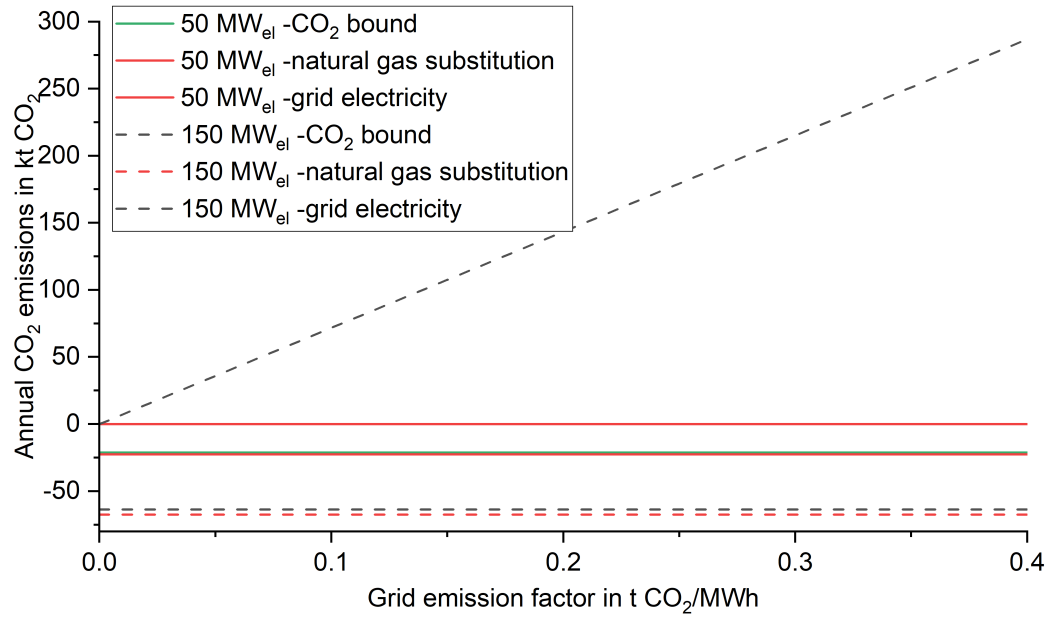

Figure D.35 Annual CO_2 emissions over the emission factor of grid electricity for RWGS-OL

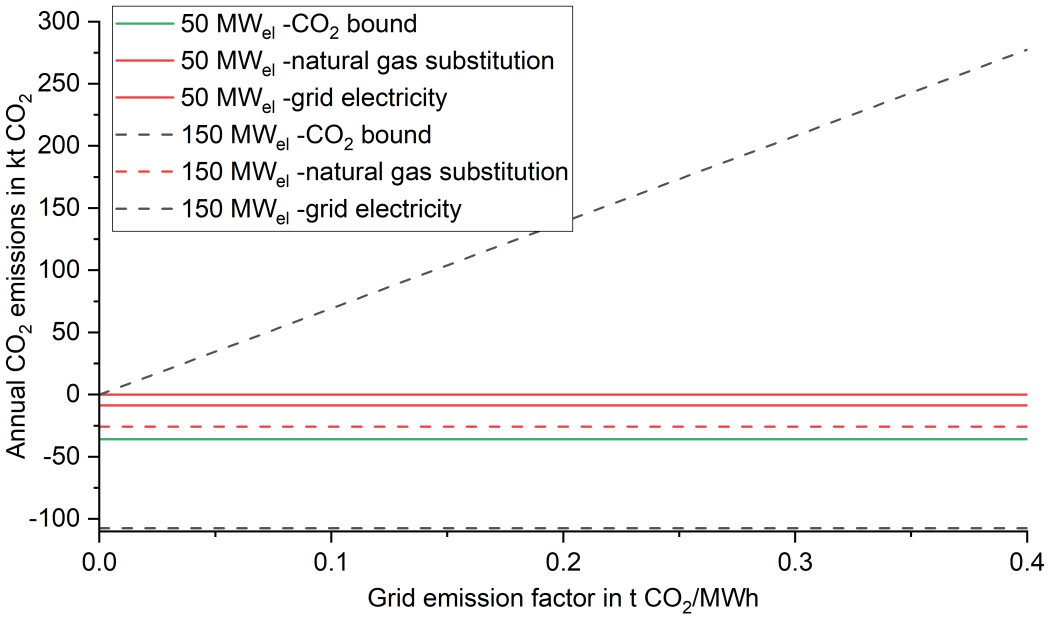

Figure D.36 Annual CO_2 emissions over the emission factor of grid electricity for CO2E-CL

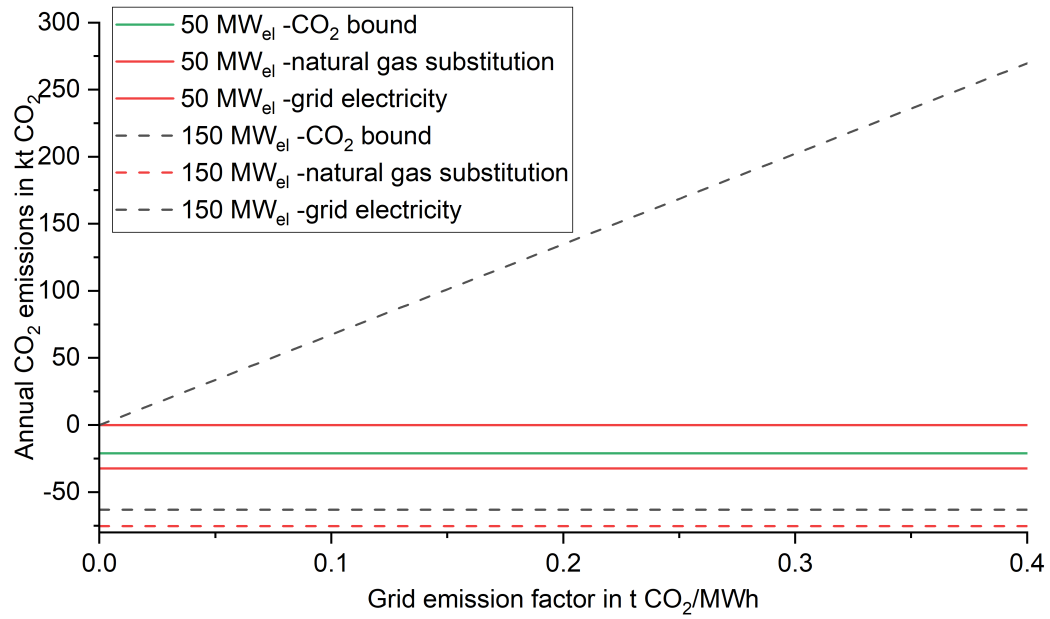

Figure D.37 Annual CO_2 emissions over the emission factor of grid electricity for CO2E-OL

D.6 Comparison CO_2 emissions

Figure D.38 shows the same data than Figure 4.28 but with a focus on the zeros of the curves.

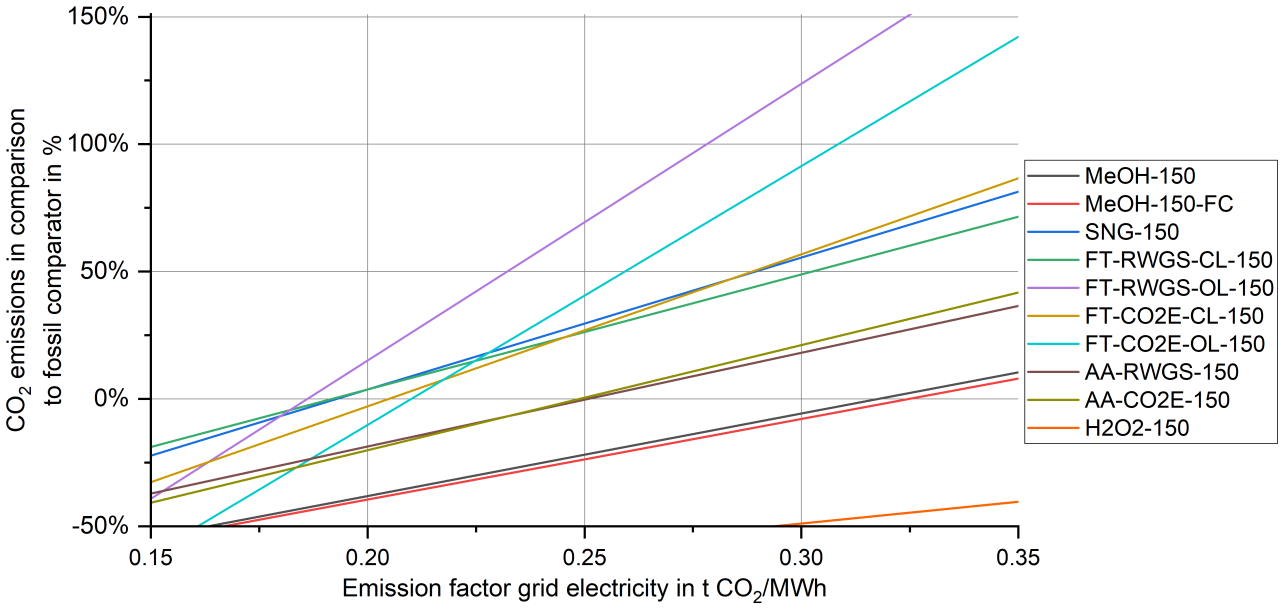

Figure D.38 Comparison of emission factor over the emission factor of the grid electricity

D.7 CO_2 electrolysis vs. RWGS

Figure D.39 shows the comparison of efficiencies for the process routes using CO_2 electrolysis or RWGS process.

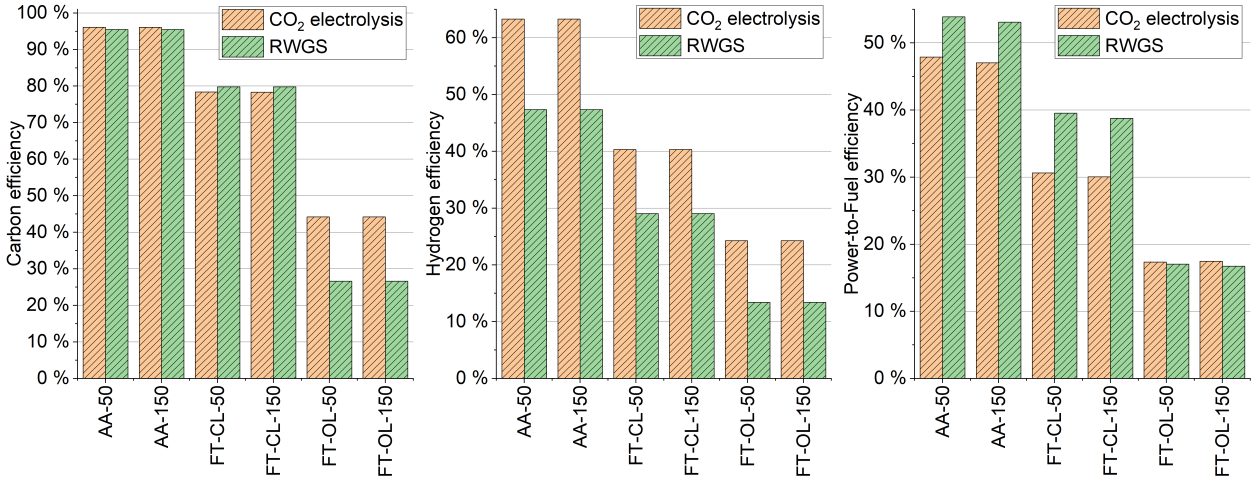

(a) Carbon efficiency **(b)** Hydrogen efficiency **(c)** Power-to-Fuel efficiency

Figure D.39 Carbon, hydrogen and Power-to-Fuel efficiency of the investigates scenarios for comparison

The LCOP is shown in Figure D.40 for the process routes using CO_2 electrolysis or the RWGS process. The cost are normalized for AA or FT syncrude to the respective RWGS case.

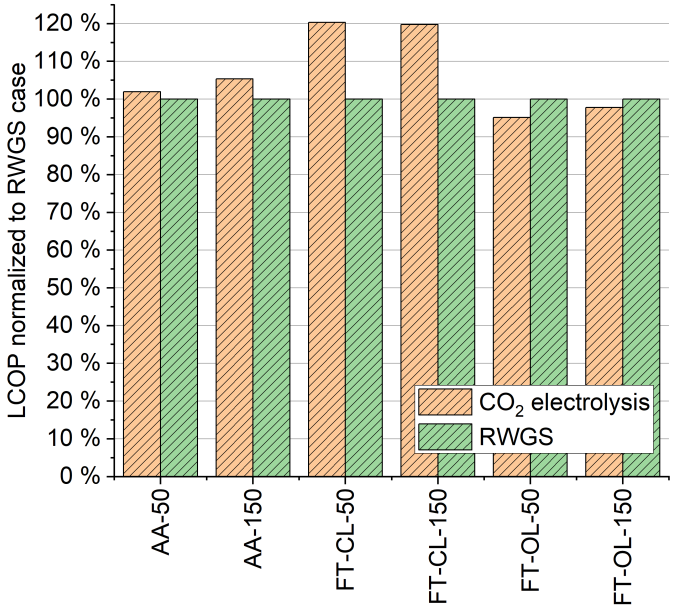

Figure D.40 LCOP normalized to RWGS case

Figure D.41 shows the CO_2 emissions compared to the fossil equivalent. The dashed lines represent the curves for cases with CO_2 electrolysis and the full lines the curves with RWGS unit. The emissions are normalized to the fossil comparator.

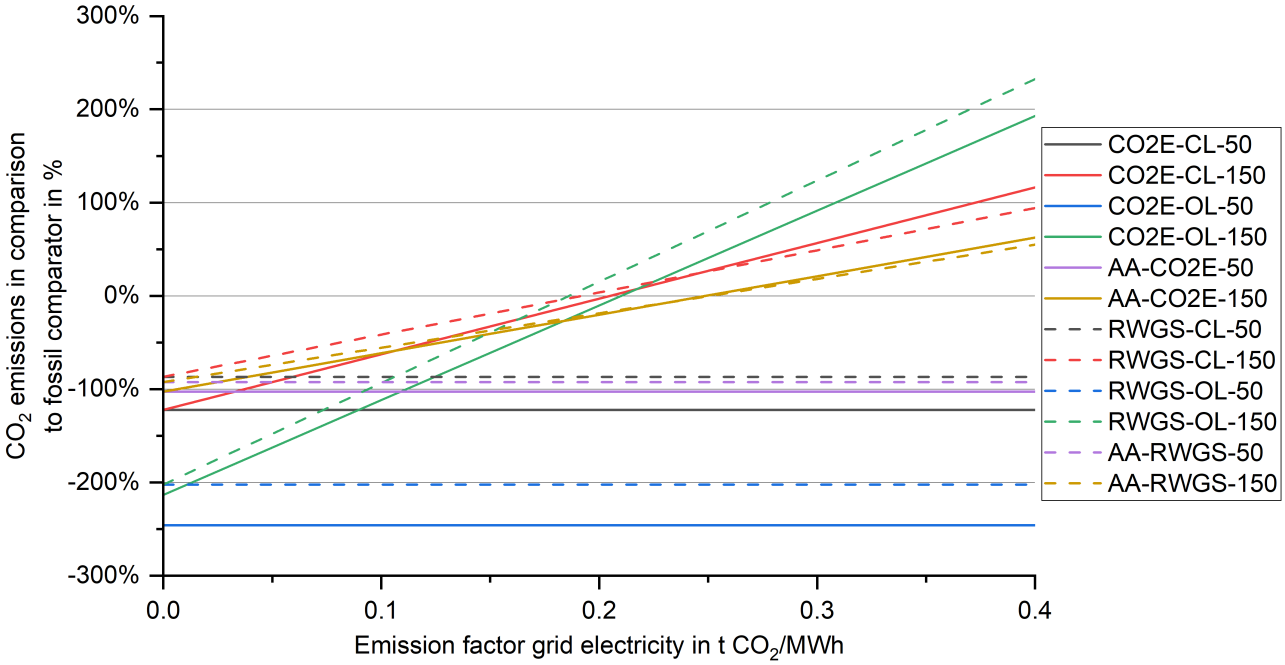

Figure D.41 CO_2 emissions compared to fossil equivalent for the cases utilizing CO_2 electrolysis and RWGS process

E Lime Kiln

E.1 Modeling

The following molecules were considered in the Aspen simulations: CO_2, O_2, CO, H_2O, CH_4, C_2H_6, C, H_2, N_2, CL_2, S, NO, NO_2, H_2S, HCL, HCN, SO_2 and NH_3. Bark and Ash were implemented as non-conventional components.

E.1.1 Mass and energy balance fuel preparation

Table E.1 shows the energy balance of the fuel preparation excluding the PtX process. The mass balance is depicted in Table E.2.

Table E.1 Energy balance of fuel preparation in MW

	BC	FO	Wood	H2-NG	H2-SNG-partial	H2-SNG-full	G-Air	G-Air + H2	G-H2	G-O2
Input										
Electricity total	0.0	0.0	0.3	33.8	75.8	75.8	0.6	37.5	50.9	0.4
-Electrolysis	0.0	0.0	0.0	33.8	74.8	74.8	0.0	37.2	50.7	0.0
-Compression and Pumping	0.0	0.0	0.0	0.0	1.0	1.0	0.2	0.1	0.0	0.0
-Dryer	0.0	0.0	0.3	0.0	0.0	0.0	0.5	0.2	0.2	0.4
H_2	0.0	0.0	0.0	23.7	33.9	33.9	0.0	26.0	35.5	0.0
Wood/Bark	0.0	0.0	50.2	0.0	0.0	0.0	81.6	38.1	26.5	72.8
Heat Dryer	0.0	0.0	6.4	0.0	0.0	0.0	8.9	4.1	2.9	7.6
Heat Gasifier	0.0	0.0	0.0	0.0	0.0	0.0	0.0	0.0	1.4	1.5
Output										
Wood	0.0	0.0	50.2	0.0	0.0	0.0	0.0	0.0	0.0	0.0
Natural gas	50.0	0.0	0.0	23.7	0.0	0.0	0.0	0.0	0.0	0.0
Fuel oil	0.0	49.2	0.0	0.0	0.0	0.0	0.0	0.0	0.0	0.0
H_2	0.0	0.0	0.0	23.7	23.7	23.7	0.0	26.0	0.0	0.0
Syngas	0.0	0.0	0.0	0.0	0.0	0.0	55.8	26.0	49.0	49.0
Heat Gasifier	0.0	0.0	0.0	0.0	0.0	0.0	0.0	0.0	6.9	9.4
Heat Electrolysis	0.0	0.0	0.0	6.8	6.8	6.8	0.0	7.4	10.1	0.0

Table E.2 Mass balance of fuel preparation in t/h

	BC	FO	Wood	H2-NG	H2-SNG-partial	H2-SNG-full	G-Air	G-Air + H2	G-H2	G-O2
					Input					
H_2O to Electrolysis	0.0	0.0	0.0	6.3	6.3	24.5	0.0	7.0	9.5	0.0
H_2O to Gasifier	0.0	0.0	0.0	0.0	0.0	0.0	0.0	0.0	0.0	1.2
Wood	0.0	0.0	14.4	0.0	0.0	0.0	0.0	0.0	0.0	0.0
Bark	0.0	0.0	0.0	0.0	0.0	0.0	25.0	11.7	8.1	15.5
Air	0.0	0.0	0.0	0.0	0.0	0.0	24.8	11.6	0.0	0.0
					Internal demand					
H_2 to lime kiln	0.0	0.0	0.0	0.0	0.0	0.0	0.0	0.0	1.1	0.0
O_2	0.0	0.0	0.0	0.0	0.0	0.0	0.0	0.0	0.0	4.4
					Output					
Waste water	0.0	0.0	0.0	0.0	3.8	3.8	0.0	0.0	0.0	2.3
H_2	0.0	0.0	0.0	0.7	0.7	0.7	0.0	0.8	0.0	0.0
Producer gas/Syngas	0.0	0.0	0.0	0.0	0.0	0.0	42.7	19.9	3.5	18.5
Ash+Char	0.0	0.0	0.0	0.0	0.0	0.0	0.4	0.2	0.7	0.3
O_2	0.0	0.0	0.0	5.6	12.4	21.7	0.0	6.2	8.4	28.3
Fuel oil	0.0	4.1	0.0	0.0	0.0	0.0	0.0	0.0	0.0	0.0
Natural gas/SNG	3.8	0.0	0.0	1.8	1.7	1.7	0.0	0.0	0.0	0.0
Wood powder	0.0	0.0	9.5	0.0	0.0	0.0	0.0	0.0	0.0	0.0

E.1.2 Mass balance PtX processes

The following table shows the mass balance of the PtX processes for the production of SNG and MeOH.

Table E.3 Mass balance of PtX process in t/h

	H2-SNG-partial	H2-SNG-full	G-O2
Input			
H_2O	7.7	18.1	36.8
CO_2	4.7	11.1	30.0
H_2	0.9	2.0	4.1
Output			
Waste water	3.8	9.1	11.9
O_2	6.8	16.1	32.6
Purge	0.0	0.0	1.4
Product	1.7	4.1	20.9

E.1.3 Fuel composition

Table E.4 shows the fuel composition as fed to the lime kiln.

Table E.4 Composition of liquid and gaseous fuels as delivered to lime kiln in wt.% and LHV in MJ/kg

	BC	FO	H2-NG	H2-SNG	G-Air	G-Air + H2	G-H2	G-O2
N_2	1.6%	-	1.2%	-	44.1%	42.8%	0.5%	0.3%
O_2	-	-	-	-	-	-	-	-
Ar	-	-	-	-	0.7%	0.7%	-	-
CO_2	2.5%	-	1.8%	1.0%	23.9%	23.1%	11.1%	49.8%
H_2	-	-	28.4%	29.6%	0.8%	4.6%	12.0%	2.3%
H_2O	-	-	-	0.2%	4.5%	4.4%	0.2%	2.1%
CO	-	-	-	0.0%	22.2%	21.5%	5.7%	38.4%
CH_4	84.7%	-	60.6%	69.2%	3.0%	2.9%	70.3%	6.7%
C_2H_6	8.6%	-	6.2%	-	-	-	0.0%	-
C15	-	100.0%	-	-	-	-	-	-
MeOH	-	-	-	-	-	-	-	0.5%
Others	2.5%	-	1.8%	-	0.8%	-	0.1%	-
LHV	47.66	43.00	68.22	70.10	4.71	9.11	50.12	10.03

E.1.4 Adiabatic flame temperature

The calculation model presented in Section 3.6 yields the AFT as shown in Table E.5. The calculation is based on the fuel composition and the fuel temperature. The table shows literature data which mostly compare very well to the own calculations. However, the literature sources generally do not give the full data like fuel composition, moisture and fuel temperature needed for a valid comparison.

Table E.5 Adiabatic flame temperature including literature data and own calculations

Fuel	[25]	[16]	[302]	[303]	own calculation
BC	2050	-	2053	2055	2039
FO	-	2068	2139	2118	2069
NG + H2	-	-	-	-	2141
SNG + H2	-	-	-	-	2139
Wood	1950	1982	2085	-	2306[a]
Bark	-	2005	2056	1947	2306
G-Air	1870	-	-	-	1815
G-Air + H2	-	-	-	-	1959
G-H2	-	-	-	-	2077
G-O2	-	2226	-	-	1846

[a]: calculation gives 3006 °C, AFT of wood from [16] used instead

E.2 Economics

Table E.6 shows the change in TAC if electricity prices are 0 €/MWh and ACC are neglected.

Table E.6 Annual cost in M€with no cost for electricity or ACC in absolute (M€) and relative numbers (%)

		BC	FO	Wood	H2-NG	H2-SNG-partial	H2-SNG-full	G-Air	G-Air + H2	G-H2	G-O2
w/o electricity	absolut	9.4	29.5	6.4	15.4	28.1	41.1	11.0	16.5	19.7	-37.9
	relative		215%	-32%	64%	200%	339%	17%	76%	110%	-504%
w/o ACC	absolut	9.4	29.5	12.0	32.3	61.1	92.4	20.1	38.8	46.5	43.7
	relative		215%	28%	245%	552%	885%	114%	314%	396%	367%

E.2.1 Sensitivity analysis on total annual cost

Figures E.1 to E.10 show the tornado diagrams for the sensitivity analysis of the investigated cases. The altered parameters are shown in Table 3.2.

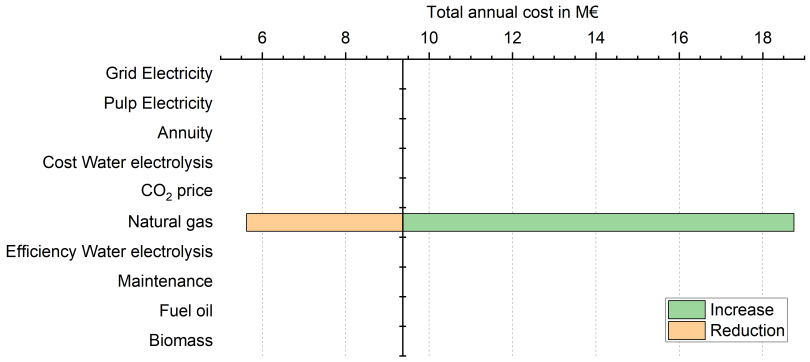

Figure E.1 Sensitivity analysis on the total annual cost for case BC

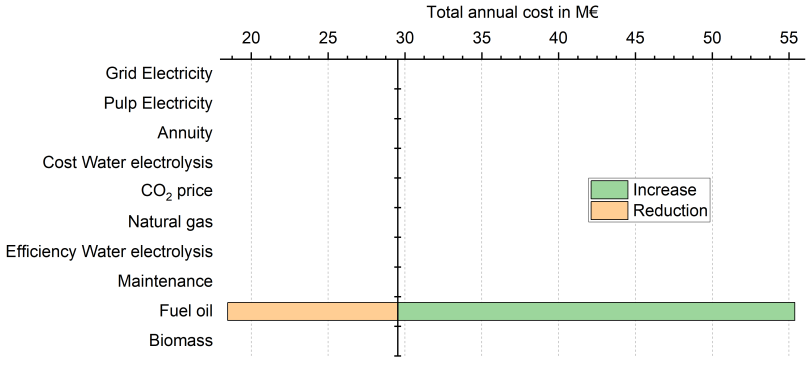

Figure E.2 Sensitivity analysis on the total annual cost for case FO

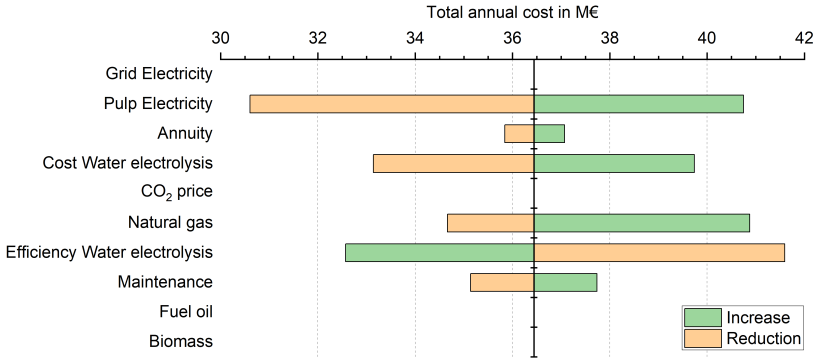

Figure E.3 Sensitivity analysis on the total annual cost for case H2-NG

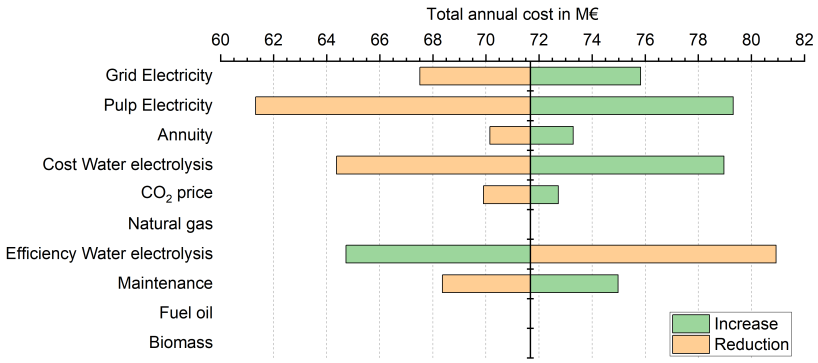

Figure E.4 Sensitivity analysis on the total annual cost for case H2-SNG-partial

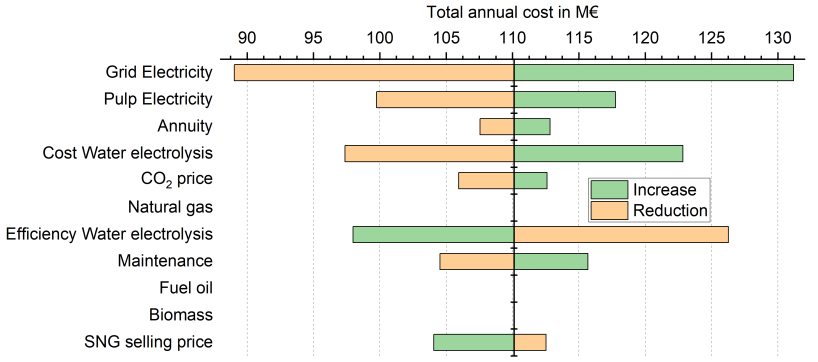

Figure E.5 Sensitivity analysis on the total annual cost for case H2-SNG-full

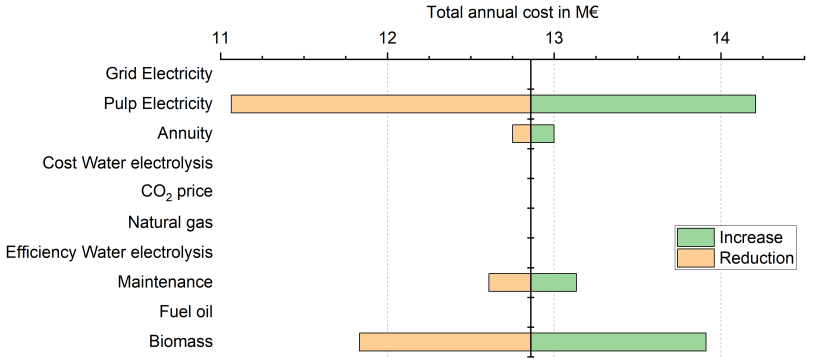

Figure E.6 Sensitivity analysis on the total annual cost for case Wood

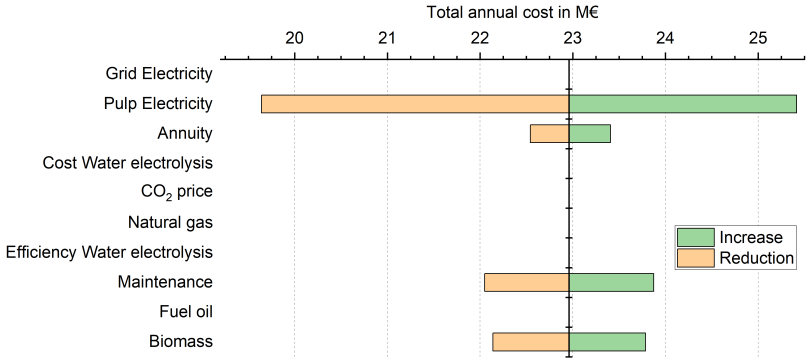

Figure E.7 Sensitivity analysis on the total annual cost for case G-Air

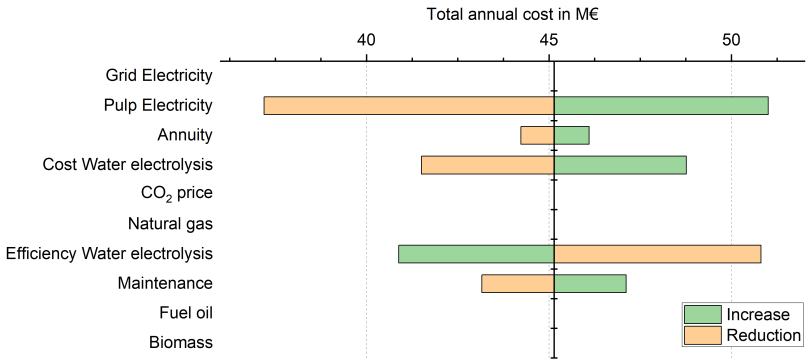

Figure E.8 Sensitivity analysis on the total annual cost for case G-Air+H2

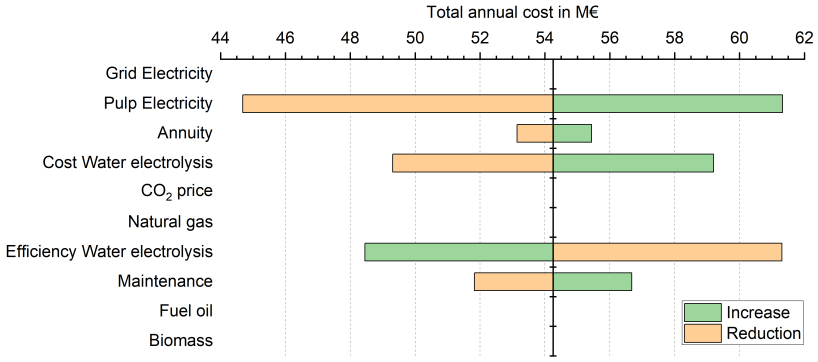

Figure E.9 Sensitivity analysis on the total annual cost for case G-H2

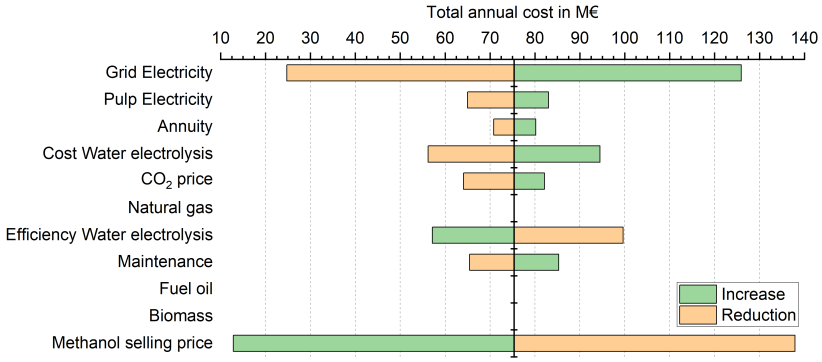

Figure E.10 Sensitivity analysis on the total annual cost for case G-O2

E.2.2 Sensitivity analysis on CO_2 abatement cost

Figures E.11 to E.16 show the tornado diagrams for the sensitivity analysis of the investigated cases. The altered parameters are shown in Table 3.2.

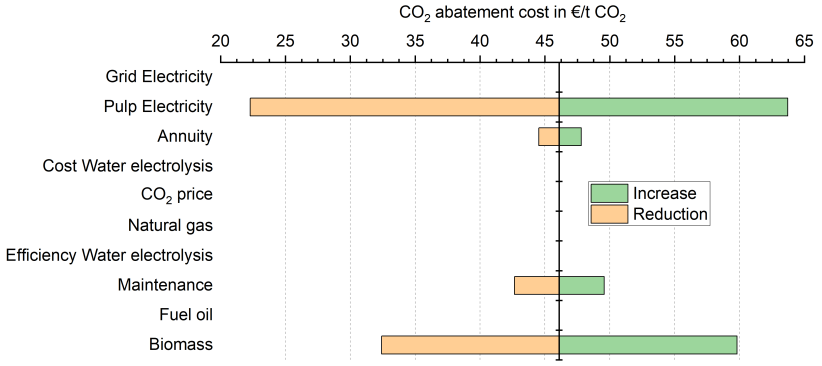

Figure E.11 Sensitivity analysis on the CO_2 abatement cost for case Wood

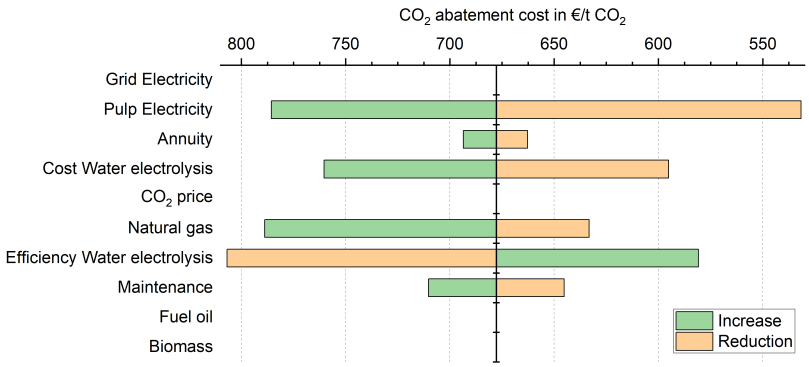

Figure E.12 Sensitivity analysis on the CO_2 abatement cost for case H2-NG

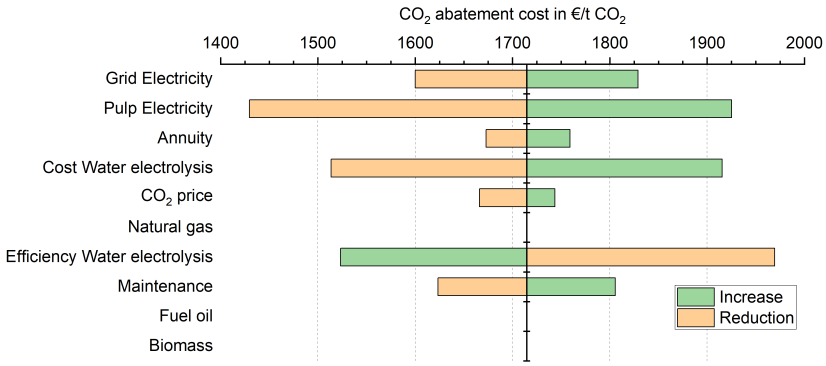

Figure E.13 Sensitivity analysis on the CO_2 abatement cost for case H2-SNG-partial

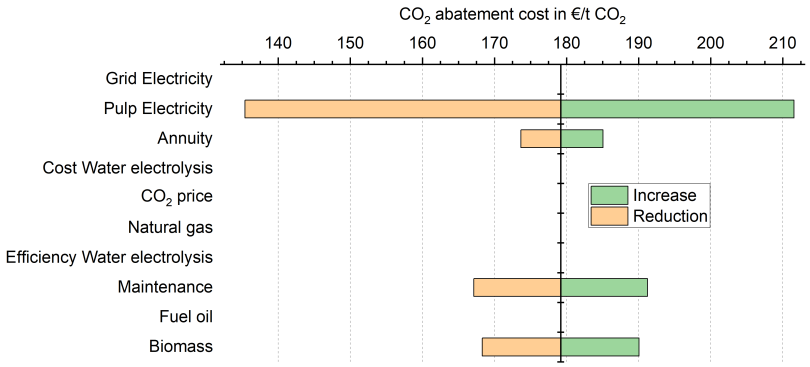

Figure E.14 Sensitivity analysis on the CO_2 abatement cost for case G-Air

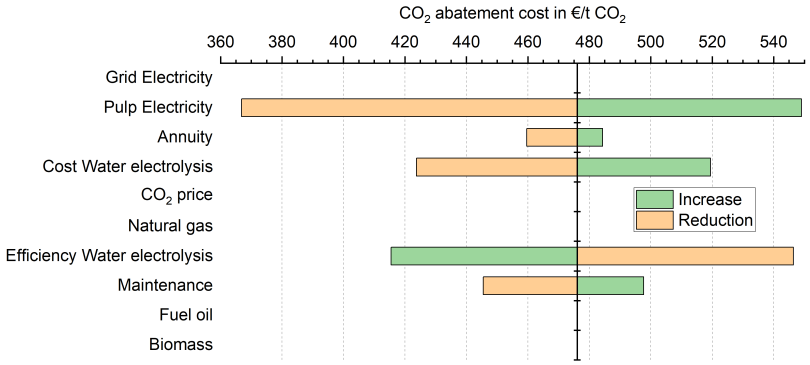

Figure E.15 Sensitivity analysis on the CO_2 abatement cost for case G-Air+H2

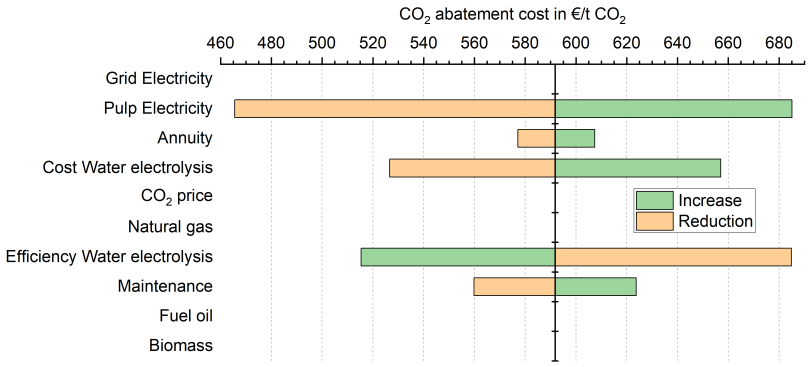

Figure E.16 Sensitivity analysis on the CO_2 abatement cost for case G-H2

E.3 Heat integration

Figures E.17 to E.24 shows the composite curves for the assessment of heat integration.

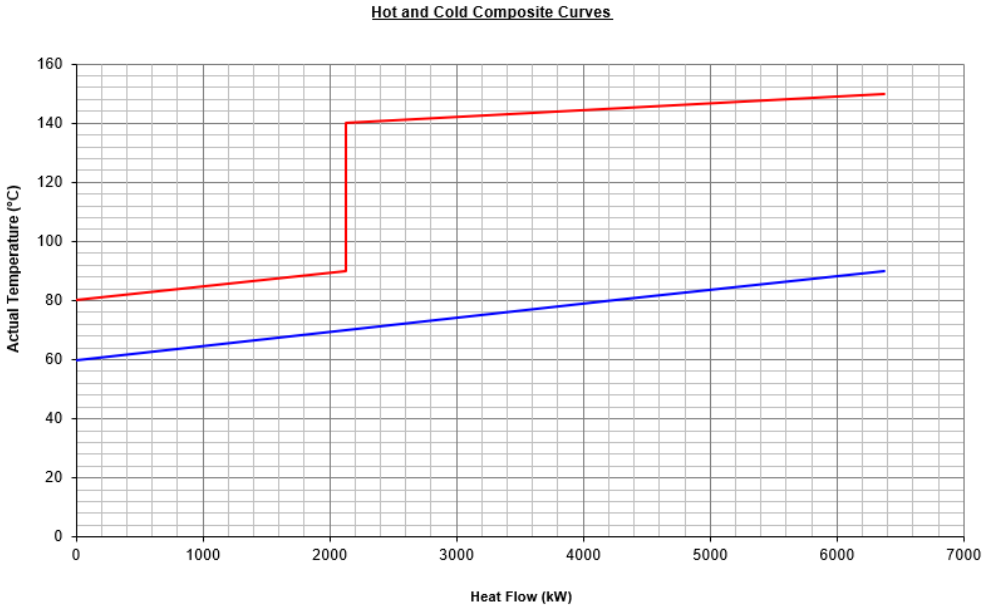

Figure E.17 Composite curve for Wood

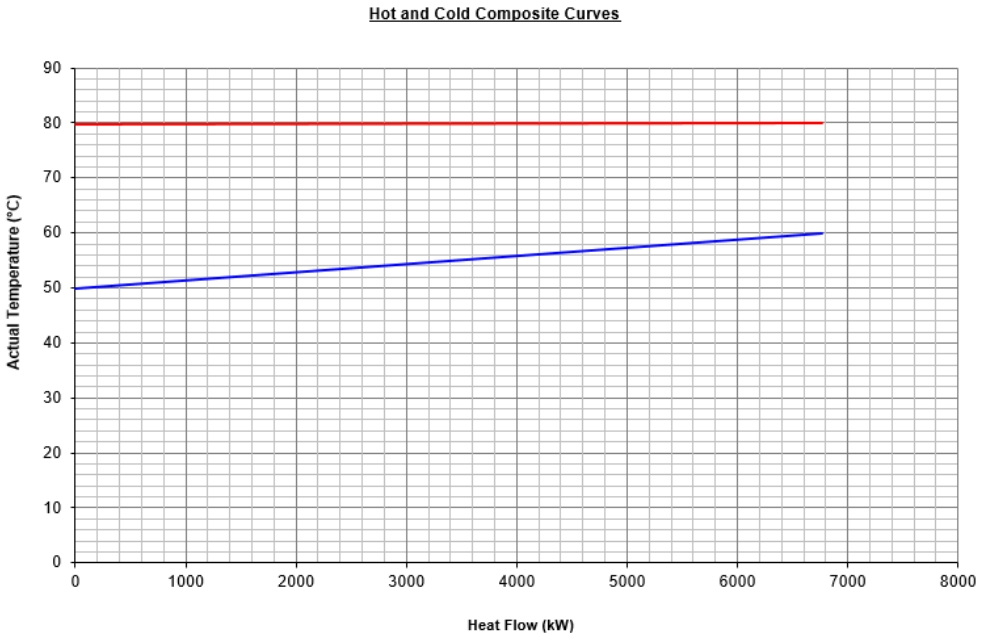

Figure E.18 Composite curve for H2-NG

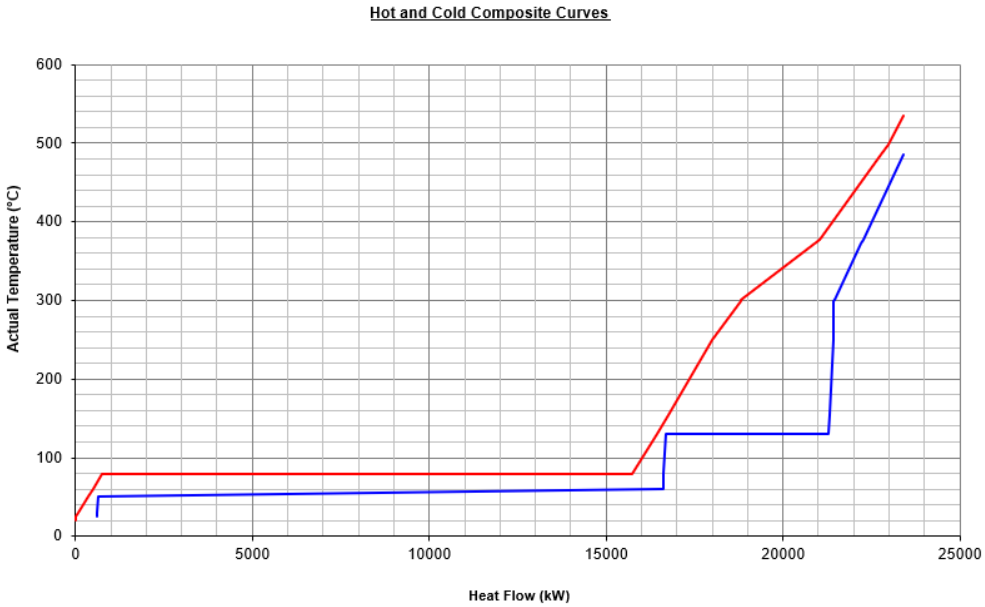

Figure E.19 Composite curve for H2-SNG-partial

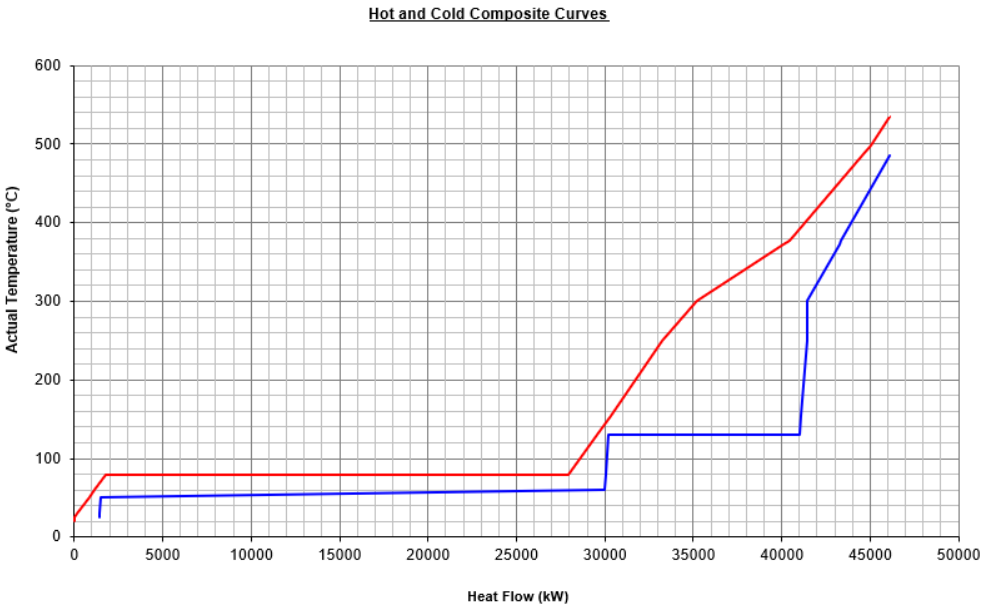

Figure E.20 Composite curve for H2-SNG-full

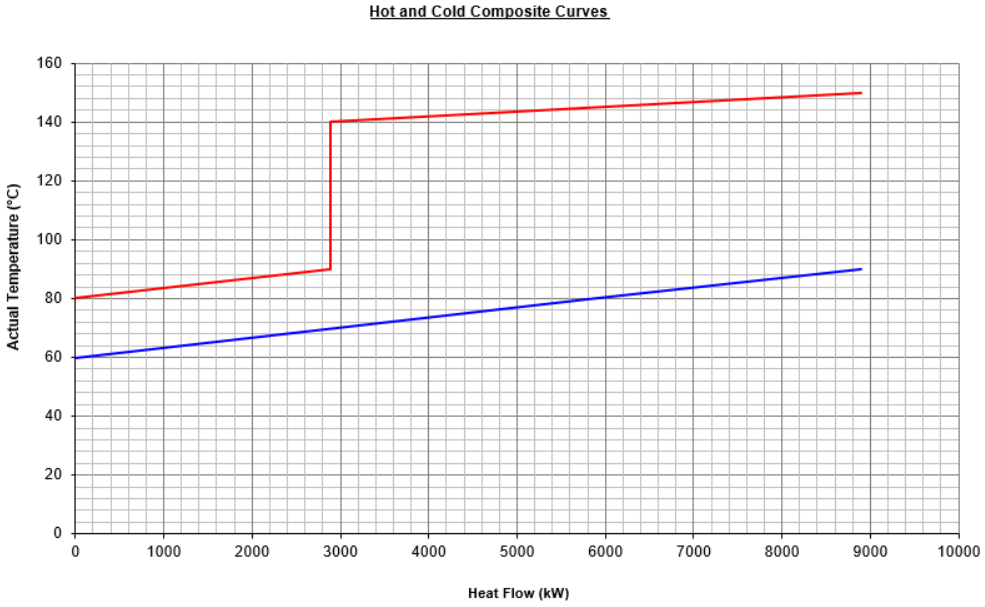

Figure E.21 Composite curve for G-Air

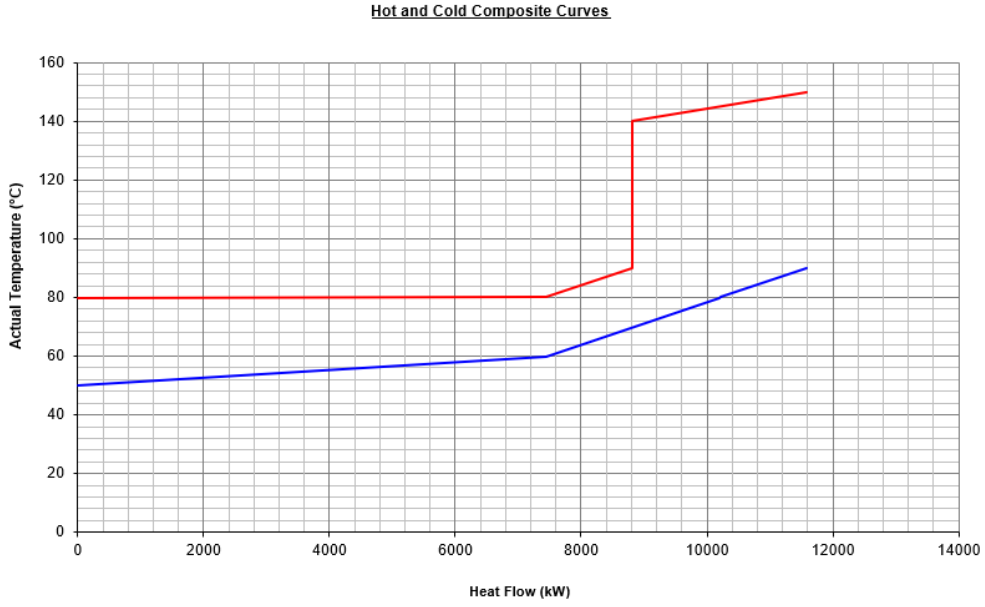

Figure E.22 Composite curve for G-Air+H2

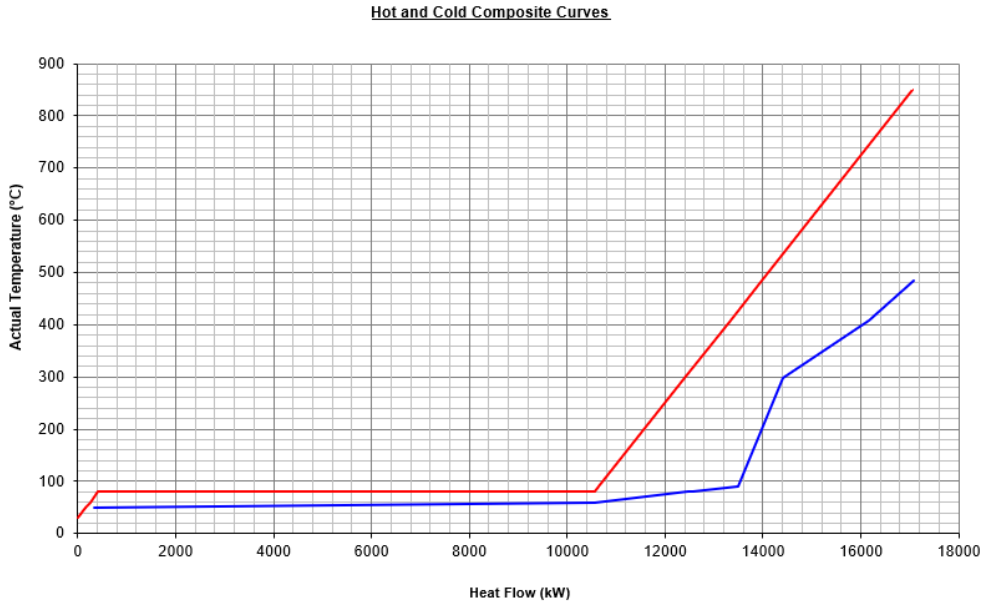

Figure E.23 Composite curve for G-H2

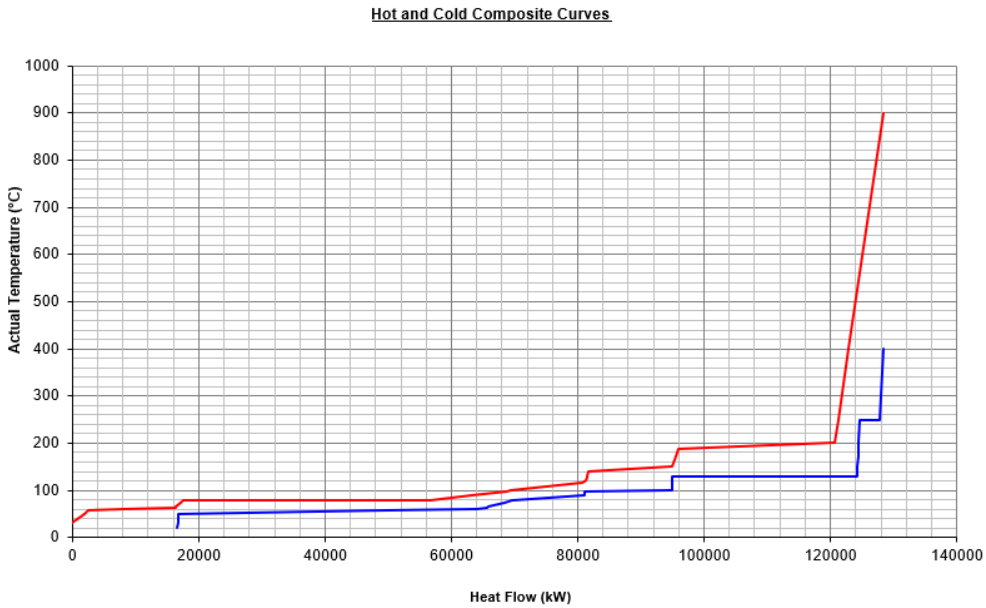

Figure E.24 Composite curve for G-O2

E.4 Calcination temperature

The required reaction temperature for calcination is dependent on the partial pressure of CO_2 in the gas phase. For the different simulated scenarios, the partial pressure in the flue gas will change significantly depending on the used fuel. A relation between reaction temperature, reaction rate and partial pressure is available in literature (Eq. E.1-E.3) [304]. The reaction rate R_D (in kmol m^{-2} s^{-1}) depends on a rate constant k_D (in kmol m^{-2} s^{-1} atm^{-1}) and the pressure difference between the equilibrium dissociation pressure P_e (in atm) and the partial pressure of CO_2 at the CaO-$CaCO_3$ interface (in atm) [304].

$$R_D = k_D(P_e - P) \tag{E.1}$$

with

$$k_D = 0,00122exp(-4026/T) \tag{E.2}$$

$$P_e = exp(17,74 - 0,00108T + 0,332ln(T) - \frac{22020}{T}) \tag{E.3}$$

With this relation, the reaction rate was plotted over the temperature ranging from 850 to 950 °C (Figure E.25). For a typical reaction temperature of 900 °C at 0.2 atm, the reaction temperature for the same reaction rate at 0.1 atm or 0.3 atm is roughly increased or decreased by 5 °C. Therefore, the impact of CO_2 partial pressure is neglectable on the reaction temperature. Therefore, changing the combustion temperature will only slightly impact the conversion in the lime kiln.

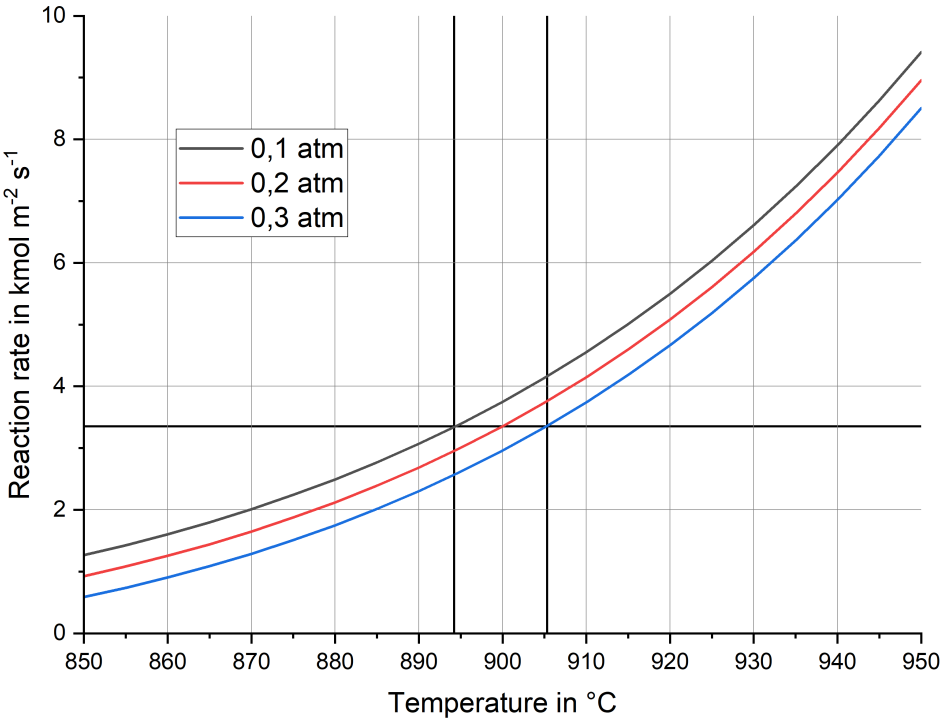

Figure E.25 Reaction rate vs. temperature for different CO_2 partial pressures

F Methanol purification

F.1 Calibration curve of pump

The pump was characterized by measuring the mass flow feed to the column (after E303) for a known time period on the level of the feed port. The pump was running at a certain power before the measurement was started. Deionized water was used as medium. The time of measurement ranges from 5 to 10 min depending on the power of the pump as higher flow rates exceed the used vessel capacity faster than for lower flow rates. The pump power was changed in 10 % increments between 20 and 80 %. Each pump power was measured three times leading to the curve shown in Figure F.1.

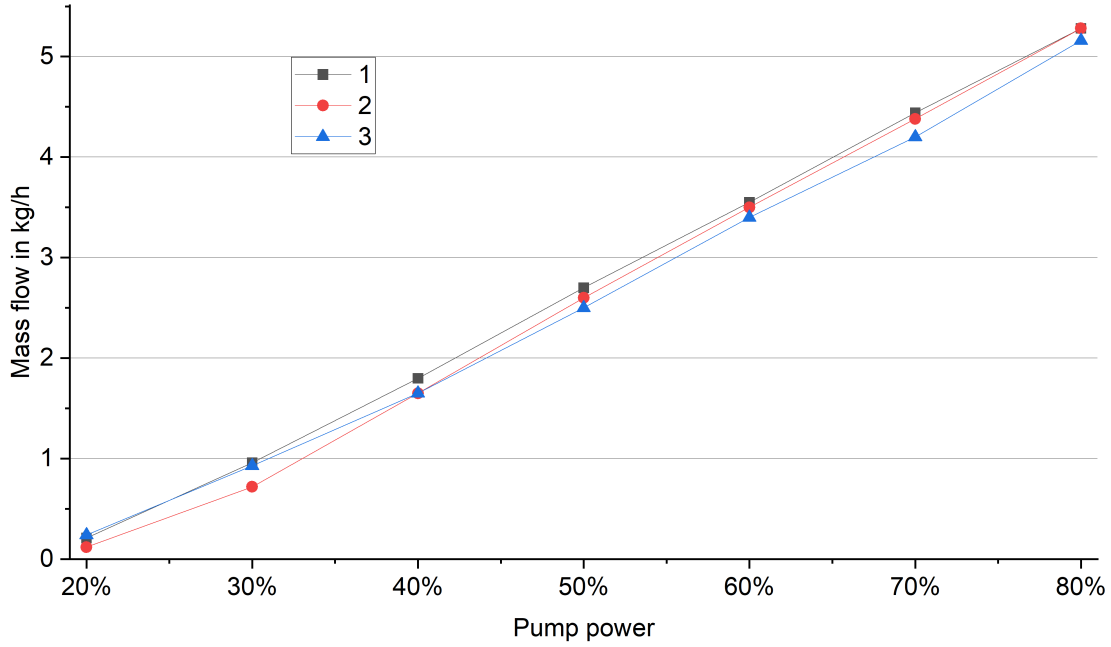

Figure F.1 Calibration curve for water (3 measurements are performed for each pump power setting. Data points are connected for better visualization.)

Based on this data the linear relation between mass flow $\dot{m}$ in kg/h and pump power (in %) based on the mean value of the mass flow can be established as shown in the following equation.

$$\dot{m} = (8.5262 \cdot \frac{P_{Pump}}{\%} - 1.6312)\frac{kg}{h} \tag{F.1}$$

F.2 Temperature of feed stream

Figure F.2 shows the temperature of the feed after heat exchanger E303 measured by T311. The mean values and standard deviation of the values during the times of the experiment are shown. The feed temperature was set to 65 °C. The data shows that this values was reliably held constant over the time of the experiment.

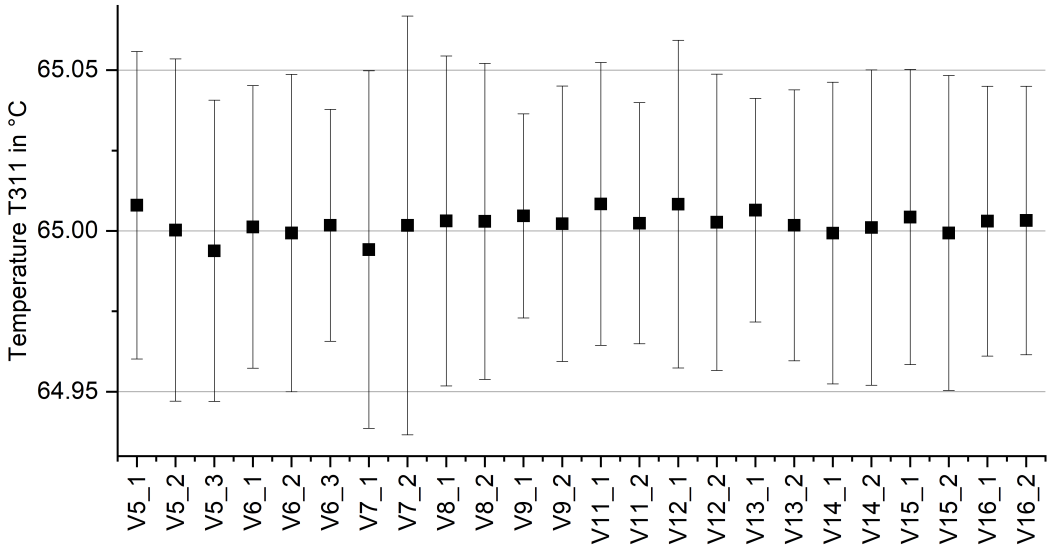

Figure F.2 Mean and standard deviation of the feed temperature T311

F.3 Pressure drop

The pressure drop is measured by PD301. The mean value and standard deviation is shown in Figure F.3. The pressure drop was set to 2.0, 2.2 and 2.4 mbar. In V6, the pressure drop was altered. V9_2 is again due to the missed end of the experiment an outliner in terms of deviation of the mean value from the set value and high standard variation. Higher standard variations are a sign for a more instable operation.

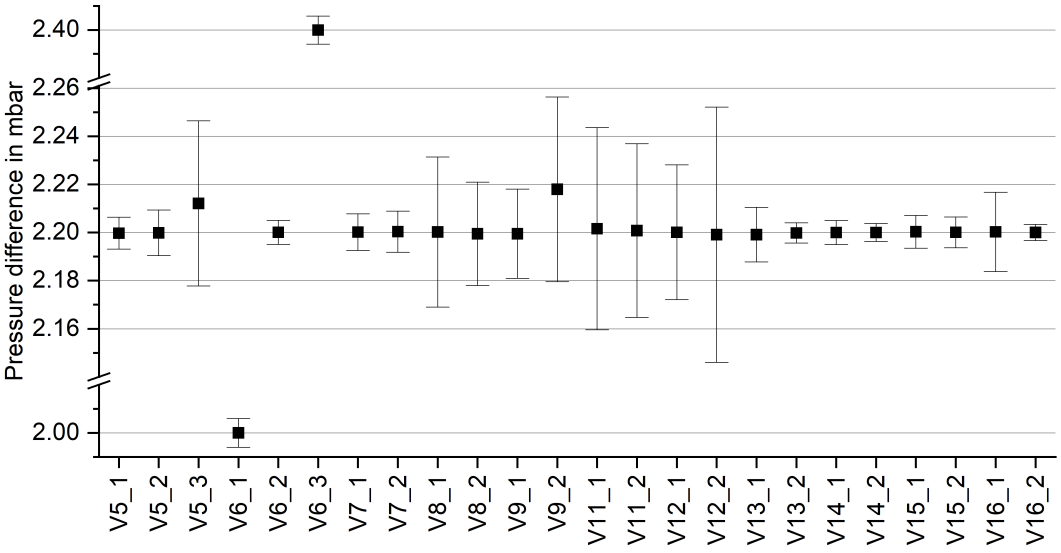

Figure F.3 Mean and standard deviation of the pressure drop PD301

F.4 Feed preparation

Figure F.4 shows the MeOH and S/N concentration in the feed stream dreived from laboratory measurements. The resulting concentration of the contaminants in the top product are usually higher than in the feed stream. Additionally the pFC cases reveal that the water content in the FC might be higher than assumed in the model FC stream.

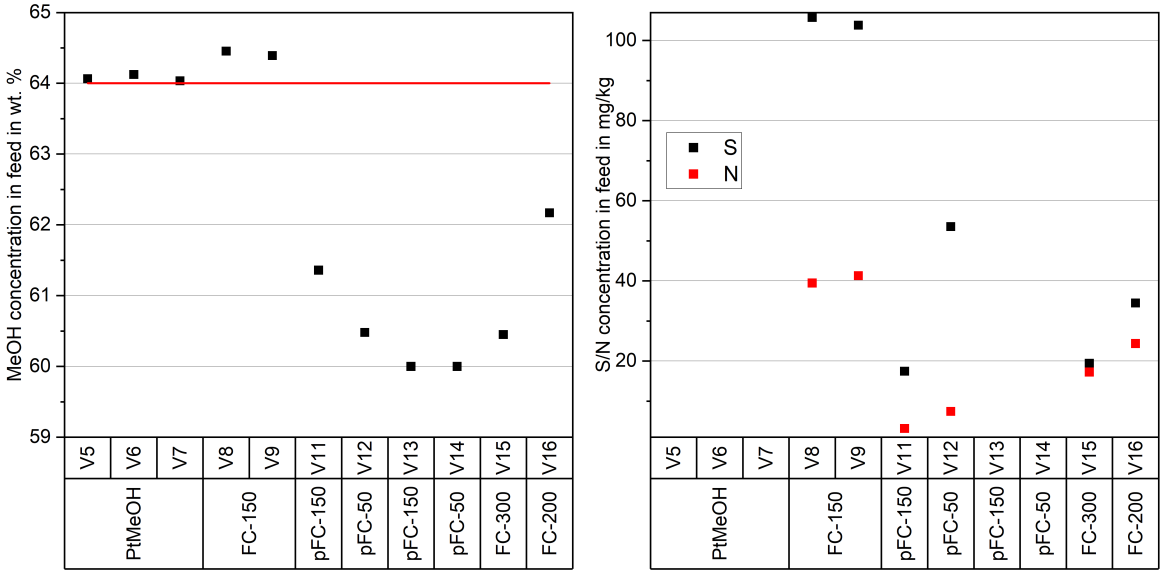

(a) MeOH **(b)** S+N

Figure F.4 Concentration of MeOH, S and N in the feed stream